

University of Southampton Research Repository

Copyright © and Moral Rights for this thesis and, where applicable, any accompanying data are retained by the author and/or other copyright owners. A copy can be downloaded for personal non-commercial research or study, without prior permission or charge. This thesis and the accompanying data cannot be reproduced or quoted extensively from without first obtaining permission in writing from the copyright holder/s. The content of the thesis and accompanying research data (where applicable) must not be changed in any way or sold commercially in any format or medium without the formal permission of the copyright holder/s.

When referring to this thesis and any accompanying data, full bibliographic details must be given, e.g.

Thesis: Author (Year of Submission) "Full thesis title", University of Southampton, name of the University Faculty or School or Department, PhD Thesis, pagination.

Data: Author (Year) Title. URI [dataset]

University of Southampton

Faculty of Environmental & Life Sciences

School of Biological Sciences

Multi-omics studies of Zika virus infection in nervous system cells to investigate novel oncolytic virotherapy for childhood cancer

by

Matthew Lewis Sherwood

MRes, BSc

ORCID ID <u>0000-0002-1912-9758</u>

Thesis for the degree of Doctor of Philosophy

November 2025

University of Southampton Abstract

Faculty of Environmental and Life Sciences

School of Biological Sciences

Doctor of Philosophy

Multi-omics studies of Zika virus infection in nervous system cells to investigate novel oncolytic virotherapy for childhood cancer

by

Matthew Lewis Sherwood

Paediatric nervous system tumours account for a third of all childhood cancer cases, and survival is disproportionately poor. Aggressive treatment regimens significantly impair quality of life and subject survivors to socio-economic challenges. Novel immunotherapies, such as oncolytic viruses (OVs), that harness the patient's immune system to eradicate the tumour with minimal adverse effects are desperately needed. Zika virus (ZIKV) is efficacious against paediatric nervous system tumours in vitro and in vivo; however, how this efficacy is achieved and the molecular mechanisms involved are virtually unknown. To address this, I generate an array of large data and omics datasets of ZIKV-infected nervous system cells to investigate infection across the host cell transcriptome, global proteome, immunopeptidome and secretome. I integrate these datasets with publicly available resources to enhance the scope of my research by yielding additional molecular and functional insights, which also help validate my findings. I primarily analyse ZIKV infection of paediatric neuroblastoma and brain tumour cells. However, I also investigate infection of neural precursor cells (NPCs) derived from congenital Zika syndrome (CZS)-affected patients to further our understanding of ZIKV neuropathology. In my thesis, I first present a comprehensive re-analysis of publicly available datasets and literature concerning ZIKV-infected neuroblastoma cells. This led to the cancer cell ZIKV life cycle being mapped out for the first time, creating an instrumental reference tool for future research. I identify a conserved TNF and cytokine response of ZIKV-infected nervous system tumour cells at the transcriptome level. Following these observations, I demonstrate that TNF-alpha is implicated in brain tumour cell oncolysis and highlight it as a potential prognostic marker for oncolytic ZIKV (oZIKV) therapy. A highly relevant finding is that I demonstrate ZIKV infection to induce a clinically relevant and diverse pro-inflammatory brain tumour cell secretome. Through modelling responses of the medulloblastoma tumour microenvironment (TME) and the immune system to this secretome in silico, I shed significant insight into the anti-tumoural immune response evoked by oZIKV infection. I present evidence that ZIKV infection of brain tumour cells engages the HLA class I pathway and I document brain tumour cell surface presented ZIKV epitopes for the first time. I identify the ZIKV non-structural (NS) protein 3 helicase as a rich source of immunogenic peptides, highlighting its potential utility as an immunotherapy or vaccine candidate. Collectively, my thesis describes multiple host mechanisms and pathways involved in neuropathogenic and oncolytic ZIKV infection of nervous system cells, and my work delivers a unique collection of multi-omics datasets to the research community. My research significantly contributes to the growing body of evidence supporting the progression of oZIKV therapy towards clinical trials.

Table of	Contents	. 3
Table of	Tables	. 9
Table of	Figures	10
Researc	h Thesis: Declaration of Authorship	12
Acknowl	edgements	13
Abbrevia	ations	14
Chapter	1 Introduction	21
1.1 Pa	ediatric cancer biology	21
1.1.1	Medulloblastoma	22
1.1.2	2 Atypical teratoid rhabdoid tumour (ATRT)	24
1.1.3	Neuroblastoma	25
1.2 Pa	ediatric cancer therapy and the immune system	26
1.2.1	Standard-of-care therapy	26
1.2.2	? The immune system and cancer	28
1.2.3	Immunotherapy	29
1.2.4	Oncolytic virotherapy	31
1.3 Zik	a virus (ZIKV)	35
1.3.1	Viral biology	35
1.3.2	2 Viral transmission and life cycle	36
1.3.3	3 ZIKV epidemiology	37
1.3.4	Infection of CNS cells	38
1.3.5	Congenital infection	40
1.3.6	Postnatal infection	41
1.4 ZIK	(V oncolytic virotherapy	42
1.4.1	Advantages and limitations for paediatric cancer patients	42
1.4.2	2 Oncolysis	43
	1.4.2.1 Paediatric nervous system tumours	43

		1.4.2.2 Adult nervous system tumours	.40
	1.4.3	Anti-tumoural immune response	.47
	1.4.4	Safety and practicality for paediatric patients	.48
1.5	5 Lar	ge data and omics as powerful tools to investigate cellular and viral	
	bio	ogy	.50
1.6	6 Res	earch hypothesis, aims and objectives	.51
	1.6.1	Research Hypothesis	.51
	1.6.2	Chapter 2 aims and objectives	.51
	1.6.3	Chapter 3 aims and objectives	.52
	1.6.4	Chapter 4 aims and objectives	.52
1.7	7 Figu	ıres	.54
1.8	3 Tab	les	.63
Cha	apter 2	Integrated re-analysis of transcriptomic and proteomic datase	ts
	•	reveals potential mechanisms for Zika viral-based oncolytic	
		therapy in neuroblastoma	68
2.1	1 Aut	horship Statement	.68
2.2	2 Abs	A A	
2.3		tract	.69
	3 Intr	τracτoduction	.69 .70
2.4			.70
2.4	4 Met	oduction	.70 .72
2.4	4 Met 2.4.1	oductionhods	. 70 . 72
2.4	4 Met 2.4.1 2.4.2	hodsRNA sequencing data source and processing	. 70 . 72 72
2.4	4 Met 2.4.1 2.4.2 2.4.3	hodsRNA sequencing data source and processing	. 7072 7272
2.4	2.4.1 2.4.2 2.4.3 2.4.4	hodsRNA sequencing data source and processing	7072 727272
	2.4.1 2.4.2 2.4.3 2.4.4 Res	hods RNA sequencing data source and processing Differential gene expression and pathway analysis ZIKV interactome source and analysis ZIKV dependency factor source and analysis	7072 72727272
	2.4.1 2.4.2 2.4.3 2.4.4 5 Res 2.5.1	hods	7072 72727272
	2.4.1 2.4.2 2.4.3 2.4.4 5 Res 2.5.1	hods RNA sequencing data source and processing. Differential gene expression and pathway analysis ZIKV interactome source and analysis ZIKV dependency factor source and analysis ults and Discussion	7072 72727273 74
	2.4.1 2.4.2 2.4.3 2.4.4 5 Res 2.5.1 2.5.2	hods RNA sequencing data source and processing Differential gene expression and pathway analysis ZIKV interactome source and analysis ZIKV dependency factor source and analysis ults and Discussion ZIKV displays strong oncolytic properties against neuroblastoma cells ZIKV strains present with differential therapeutic potential against	70 7272727374

	2.5.4	ZIKV infection upregulates TNF and cytokine gene signatures in
		neuroblastoma cells75
	2.5.5	ZIKV infection upregulates lipid metabolism gene signatures in
		neuroblastoma cells76
	2.5.6	ZIKV infection upregulates the ER stress response in neuroblastoma cells.78
	2.5.7	ZIKV infection is dependent on the ER Membrane Protein Complex (EMC)79
	2.5.8	ZIKV infection is dependent on the V-ATPase in neuroblastoma cells79
	2.5.9	ZIKV NS4B protein-protein interactions may explain its apoptotic capability against neuroblastoma cells
	2.5.10	ZIKV NS4B interacts with the Mammalian Translocon in neuroblastoma cells
2.6	6 Cor	nclusions82
2.7	' Dat	a Availability83
2.8	B Ack	nowledgements83
2.9) Cor	npeting interests83
2.1	0 Figu	ıres84
2.1	1 Tab	les98
Cha	pter 3	Multi-omics analysis reveals key immunogenic signatures
		induced by oncolytic Zika virus infection of paediatric brain
		tumour cells103
3.1	Aut	horship Statement104
3.2	2 Abs	tract104
3.3	3 Intr	oduction105
3.4	l Met	hods108
	3.4.1	Cell and Viral Culture
	3.4.2	Confocal Microscopy108
	3.4.3	RNA Sequencing109
	3.4.4	Recombinant TNF Assays109
	3.4.5	Medulloblastoma Patient Survival Analysis110

	3.4.6	ProcartaPlex Multiplex ELISA Assay110
	3.4.7	Paracrine Signalling Analysis110
	3.4.8	Endocrine Signalling Analysis111
3.5	Res	ults111
	3.5.1	ZIKV infection induces cell type-specific transcriptome responses111
	3.5.2	TNF-alpha is a potential prognostic marker for brain tumour oZIKV therapy 113
	3.5.3	ZIKV infection stimulates a diverse pro-inflammatory cytokine secretome
		from brain tumour cell lines114
	3.5.4	In silico modelling predicts the medulloblastoma tumour immune
		microenvironment (TIME) is primed to respond to pro-inflammatory ZIKV
		secretome paracrine signalling115
	3.5.5	In silico modelling predicts the pro-inflammatory ZIKV secretome to
		stimulate diverse immune cell polarisations through endocrine signalling
		116
3.6	Disc	cussion118
3.7	Dat	a Availability121
3.8	Ack	nowledgements121
3.9	Figu	ıres123
3.10) Tab	les137
Cha	pter 4	Identification of natural Zika virus peptides presented on the
•		surface of paediatric brain tumour cells by HLA class I138
4.1	Aut	horship Statement139
4.2	Abs	tract139
4.3	Aut	hor Summary140
4.4	Intr	oduction141
4.5	Met	hods143
	4.5.1	Cell Culture and ZIKV infection143
	452	Transcriptomics 143

		4.5.2.1	HLA typing	143
		4.5.2.2	Adult glioma RNA sequencing data mining	143
	4.5.3	Proteon	nics	144
		4.5.3.1	Global proteome sample preparation	144
		4.5.3.2	LC-MS/MS analysis of global proteome	144
		4.5.3.3	Data analysis for global proteome	144
	4.5.4	Immund	opeptidome analysis	145
		4.5.4.1	Purification of HLA immunopeptides	145
		4.5.4.2	LC-MS/MS analysis of HLA immunopeptides	145
		4.5.4.3	Data analysis for immunopeptidome	146
4.6	Res	sults		147
	4.6.1	ZIKV infe	ection enriches HLA Class I presentation pathways in brain tu	mour
		cell line	·s	147
	4.6.2	USP7 br	rain tumour cells predominantly present HLA-A*02:01 peptide	s147
	4.6.3	USP7 br	rain tumour cells present ZIKV HLA-I immunopeptides, and	
		present	ation corresponds with protein abundance in the HLA-I pathw	ay .148
	4.6.4	ZIKV NS	3 helicase is a rich source of immunopeptides	149
4.7	' Dis	cussion.		150
4.8	Dat	ta Availak	bility	153
4.9	Acl	knowledg	gments	153
4.1	0 Fig	ures		154
4.1	1 Tab	oles		158
Cha	pter	5 Gene	ral discussion and future directions	163
5.1	Ove	erview		163
5.2	. Cha	apter 2 D	iscussion	163
	5.2.1	Summa	ry of results	163
	5.2.2	Strength	ns and relevance of findings	164
	5.2.3	Limitatio	ons	165
	524	Future v	work	166

5.3	Cha	apter 3 Discussion	167
	5.3.1	Summary of results	.167
	5.3.2	Strengths and relevance of findings	.168
	5.3.3	Limitations	.169
	5.3.4	Future work	.170
5.4	Cha	apter 4 Discussion	.171
	5.4.1	Summary of results	.171
	5.4.2	Strengths and relevance of findings	.172
	5.4.3	Limitations	.173
	5.4.4	Future work	.174
5.5	Col	lective summary and insight	175
5.6	Crit	ical analysis of omics techniques	178
5.7	Rec	commended future directions of the oZIKV research field	181
5.8	Cor	ncluding remarks	183
5.9	Ach	ievements and additional research contributions	184
aa/	endix	A Chapter 2 supplementary material	185
		B Chapter 3 supplementary material	
		CChapter 4 supplementary material	
		es202	

Table of Tables

Table 1. 1. Medulloblastoma and ATRT brain tumour molecular subgroups and	l subtypes .63
Table 1. 2. Molecular markers for neuroblastoma stratification into INRGSS an	
groups	65
Table 1. 3. Oncolytic virotherapy clinical trials for paediatric brain tumour and	
neuroblastoma patients	66
Table 2. 1. ZIKV infects and reduces cell viability of paediatric neuroblastoma	cell lines98
Table 2. 2. Different ZIKV strains demonstrate varying clinical potential agains	t paediatric
neuroblastoma cells	100
Table 2. 3. ZIKV infection in neuroblastoma cells can be regulated through mo	difying lipid
abundance, composition and localisation.	102
Table 3. 1. Differentially expressed genes (DEGs) observed following ZIKV infe	ction in all
four cell lines.	137
Table 4. 1. USP7 cell HLA allotypes and their expression across the human po	pulation 158
Table 4. 2. Number of USP7 cell-presented ZIKV immunopeptides	159
Table 4. 3. Number of USP7 cell-presented ZIKV immunopeptides per protein .	160
Table 4. 4. USP7 cell-presented ZIKV immunopeptides and their predicted pro	perties 161
Table 4. 5. ZIKV : human peptide homology	162

Table of Figures

Figure 1. 1. Primary anatomical locations of medulloblastoma, ATRT and neuroblastoma
development54
Figure 1. 2. Immunotherapeutic strategies to target the immune system against cancer 56
Figure 1. 3. Oncolytic virotherapy dual mechanism of action
Figure 1. 4. Oncolytic viruses (OVs) heat up the Tumour immune microenvironment (TIME).
59
Figure 1. 5. ZIKV structure and genome organisation60
Figure 1. 6. ZIKV Infection Life Cycle62
Figure 2. 1. Differential gene expression, GO biological process and pathway analysis of
ZIKV infection in SH-SY5Y cells85
Figure 2. 2. Pathway mapping of ZIKV infection in SH-SY5Y cells
Figure 2. 3. ZIKV infection upregulates TNF and cytokine signalling gene signatures in
neuroblastoma cells89
Figure 2. 4. ZIKV infection upregulates lipid metabolism gene signatures in neuroblastoma cells
Figure 2. 5. ZIKV infection upregulates UPR gene signatures in neuroblastoma cells93
Figure 2. 6. ZIKV dependency factors95
Figure 2. 7. ZIKV NS4B interacts with host proteins and known ZIKV dependency factors in
neuroblastoma cells96
Figure 2. 8. ZIKV life cycle in neuroblastoma cells
Figure 3. 1. ZIKV infection dynamics in brain tumour and neural precursor cells
Figure 3. 2. Differential biological processes and pathways following ZIKV infection 126
Figure 3. 3. Cell type-specific responses in the highest ranked DEGs following ZIKV
<i>infection.</i> 128
Figure 3. 4. TNF signalling pathways during ZIKV infection of brain tumour cells
Figure 3. 5. ZIKV-infected brain tumour cell secretome

Table of Figures

$\textbf{\textit{Figure 3. 6. The pro-inflammatory ZIKV} secretome \ and its \ predicted \ medulloblastometric processors and the pro-inflammatory \textit{\textit{ZIKV}} secretome \ and \textit{\textit{its predicted medulloblastometric processors}.}$	
paracrine signalling	134
Figure 3. 7. Modelling of ZIKV-induced secretome endocrine signalling to lymph node	
immune cells.	136
Figure 4. 1. ZIKV infection enriches the HLA Class I pathway in brain tumour cells	154
Figure 4. 2. The immunopeptidomes of USP7 brain tumour cells	155
Figure 4. 3. ZIKV immunopeptides binding affinity and viral protein abundance	156
Figure 4. 4. ZIKV polyprotein with mapped immunopeptides	157

Research Thesis: Declaration of Authorship

Research Thesis: Declaration of Authorship

Print name: Matthew Lewis Sherwood

Title of thesis: Multi-omics studies of Zika virus infection in nervous system cells to investigate

novel oncolytic virotherapy for childhood cancer

I declare that this thesis and the work presented in it are my own and has been generated by me

as the result of my own original research.

I confirm that:

1. This work was done wholly or mainly while in candidature for a research degree at this

University;

2. Where any part of this thesis has previously been submitted for a degree or any other

qualification at this University or any other institution, this has been clearly stated;

3. Where I have consulted the published work of others, this is always clearly attributed;

4. Where I have quoted from the work of others, the source is always given. With the exception

of such quotations, this thesis is entirely my own work;

5. I have acknowledged all main sources of help;

6. Where the thesis is based on work done by myself jointly with others, I have made clear

exactly what was done by others and what I have contributed myself;

7. Parts of this work have been published as:

Sherwood M, Zhou Y, Sui Y, Wang Y, Skipp P, Kaid C, et al. Integrated re-analysis of

transcriptomic and proteomic datasets reveals potential mechanisms for Zika viral-based

oncolytic therapy in neuroblastoma. F1000Res. 2024 May 21;12:719.

Sherwood M, Mitsugi TG, Kaid C, Coke B, Zatz M, Maringer K, et al. Multi-omics analysis reveals

key immunogenic signatures induced by oncolytic Zika virus infection of paediatric brain tumour

cells. Sci Rep. 2025 Apr 16;15(1):13090.

Sherwood M, Nicholas B, Bailey A, Mitsugi TG, Kaid C, Okamoto OK, et al. Identification of

natural Zika virus peptides presented on the surface of paediatric brain tumour cells by HLA

class I | PLOS One. 2025 Nov 6.

Signature	

Acknowledgements

I would like to take this opportunity to acknowledge and thank my Southampton supervisory team (**Rob Ewing** and **Paul Skipp**), who worked extensively with me to initially secure the funding for this candidature and who have aided me throughout the years of research. A special thanks to **Rob Ewing**, who has been a critical enabler in helping me pursue many academic and non-academic endeavours throughout my candidature.

I would like to thank my collaborators at the University of São Paulo (USP), principally **Keith Okamoto**, **Thiago Mitsugi** and **Carolini Kaid**, for helping to build the foundations for this PhD project, and for their continued collaboration and support. Notable thanks to **Steve John** and **Magdalena Castellano-Vidalle**, who made the research laboratory at the University of Southampton (UoS) a fun and enjoyable place to work during the first half of the PhD. The final stages of my PhD research have significantly benefited from the opportunity to work at The Pirbright Institute (TPI). For this, I thank **Kevin Maringer** for welcoming me into the research group and supporting me through the final stages of my laboratory research.

I would like to thank my parents, **John Sherwood** and **Tina Sherwood**, my brother, **Will Sherwood**, and my grandmother, **Mavis Bleasdale**; I owe a lot of what I have achieved in life down to having such a strong family support network. Your support, dedication, and love have been instrumental in helping me throughout the long journey of first securing a PhD and then completing it. I would like to thank my partner, **Abi Goddess**, for bringing such joy to my life since we met and for being dedicated to doing your utmost to support me; I couldn't have completed this PhD without you and Yuki. Finally, I owe my mental and physical health and a whole lot more to my incredible group at the gym (**Ash Yates**, **Janice Chow**, **James Cottrell**, **Thomas Todeschini**, **Nick Chandler**, **Richard Cook** and **Helen Roberts**).

I would like to dedicate this PhD to **June Sherwood** (1940-2012) and **Derek Bleasdale** (1940 - 2024), who always supported me and who would be proud of me for the research I have achieved during my PhD.

Abbreviations

AP-1 Activator protein 1

padj Adjusted p-value

aa Amino acid

ADCC Antibody-dependent cellular cytotoxicity

APC Antigen-presenting cell

ATRT Atypical teratoid rhabdoid tumour

AGC Automatic gain control

MCPH Autosomal recessive primary microcephaly

BBB Blood-brain barrier

BM Bone marrow

CREB cAMP response element-binding protein

CSC Cancer stem-like cell

C Capsid protein

CCL C-C motif chemokine ligand

T4 CD4+Tcell

CD8T CD8+Tcell

T8 CD8+Tcell

CNS Central nervous system

CAR Chimeric antigen receptor

CDC Complement-dependent cytotoxicity

CZS Congenital Zika syndrome

cDC Conventional dendritic cell

cDC1 Conventional dendritic cell type 1

cDC2 Conventional dendritic cell type 2

CDK Cyclin-dependent kinase

CHIM Controlled human infection model

DAMP Damage-associated molecular pattern

DAVID Database for annotation, visualization and integrated discovery

DC Dendritic cell

DENV Dengue virus

DEG Differentially expressed gene

DGC Differentiated glioma cell

DIPG Diffuse intrinsic pontine glioma

DMG Diffuse midline glioma

DDR DNA damage response

DNMT DNA methyltransferase

DHA Docosahexaenoic acid

DSB Double-strand break

ER Endoplasmic reticulum

EMC Endoplasmic reticulum membrane protein complex

E Envelope protein

ENA European nucleotide archive

FDR False discovery rate

FACS Fluorescence-activated cell sorting

GEO Gene expression omnibus

GO Gene ontology

GSEA Gene set enrichment analysis

GBM Glioblastoma

GSC Glioma stem cell

GO_BP Gene ontology biological process

GCP Granule cell precursor

GBS Guillain-barré syndrome

HR Hazard rate

HSV Herpes simplex virus

HCD Higher-energy collisional dissociation

HGG High-grade glioma

HIC High-income country

HLA-I Human leukocyte antigen class I

HLA-II Human leukocyte antigen class II

hpi Hours post-infection

HUG-CELL Human genome and stem-cell center

hiPSC Human induced pluripotent stem cell

HLA Human leukocyte antigen

hPSC Human pluripotent stem cell

ID Identifier

IDA Immune dictionary application

IEDB Immune epitope database

ICD Immunogenic cell death

INRGSS INRG staging system

IFN Interferon

ISG Interferon-stimulated gene

INRG International neuroblastoma risk group

INSS International neuroblastoma staging system

SIOP International society for paediatric oncology

IT Intratumoural

IV Intravenous

iTRAQ isobaric tags for relative and absolute quantitation

JEV Japanese encephalitis virus

KEGG Kyoto encyclopedia of genes and genomes

LFQ Label free quantitation

LXR Liver X receptor

LFC Log2(Fold Change)

LMIC Low and middle-income country

LLOQ Lower limit of quantification

LP Lumbar puncture

MHC Major histocompatibility complex

M Membrane protein

MSC Mesenchymal stem cell

Mono/Macro Monocyte/Macrophage

MOI Multiplicity of infection

MDSC Myeloid-derived suppressor cell

mTNFSF9 Membrane TNFSF9

mTNFRSF9 Membrane TNFRSF9

NK Natural killer

NKT Natural killer T

NPC Neural precursor cell

NP Neural progenitor

NSC Neural stem cell

NB Neuroblastoma

Neu Neutrophil

Neutro Neutrophil

Non-amp Non-amplified

NHP Nonhuman primate

NS Non-structural protein

NES Normalised enrichment score

NA Not applicable

ND Not detected

N3 NPC-763-1

N7 NPC-788-1

OPC Oligodendrocyte progenitor cell

OST Oligosaccharyl transferase

OV Oncolytic virus

OS Overall survival

oZIKV Oncolytic Zika virus

PAMP Pathogen-associated molecular pattern

PBMC Peripheral blood mononuclear cell

PNS Peripheral nervous system

PEA Proximity extension assay

PFU Plaque-forming unit

prM Pre-membrane protein

PNET Primitive neuro-ectodermal tumour

PC Principal component

PCA Principal component analysis

PFS Progression-free survival

PPI Protein-protein interaction

RGC Radial glial cell

Treg Regulatory T cell

RNA-Seq RNA -Ssequencing

RT Room temperature

SHH Sonic hedgehog

SD Standard deviation

lfcSE Standard error of the Log2(Fold Change) estimate

SNaP Stem cell-derived NGN2-accelerated progenitor cell

SREBP Sterol regulatory element binding protein

sfRNA Subgenomic flavivirus RNA

SVZ Subventricular zone

sTNFRSF9 Soluble TNFRSF9

Stable isotope labelling by amino acids in cell culture

TCR T cell receptor

TMZ Temozolomide

IMEx The international molecular exchange consortium

TRAP Translocon-associated protein

TNF Tumor necrosis factor

TIME Tumour immune microenvironment

TME Tumour microenvironment

TAM Tumour-associated macrophage

TPI The Pirbright Institute

TMT Tandem mass tag

UPR Unfolded protein response

UTR Untranslated region

UoS University of Southampton

USP University of São Paulo

P13 USP13

USP13 USP13-Med

P7 USP7

USP7 USP7-ATRT

WNV West nile virus

WHO World health organisation

YFV Yellow fever virus

ZIKV Zika virus

>ULOQ Above limit of quantification

+ssRNA Positive-sense single-stranded RNA

Chapter 1 Introduction

1.1 Paediatric cancer biology

Cancer is a principal cause of death in children under the age of 15 worldwide, accounting for approximately 290,000 new diagnoses and nearly 100,000 deaths per year (1). Incidence and mortality are most prevalent in children aged one to four years old, with males at slightly greater risk than females (1). Considering health system capability and the increasing global population, approximately seven million diagnosed cases, six million undiagnosed cases, and eleven million childhood cancer-related deaths are predicted to occur by 2050 (2). To combat this, the Global Initiative for Childhood Cancer aims to improve global childhood cancer survival to at least 60% by 2030 (3). Geographical location is the primary determinant of paediatric cancer survival. Shockingly, 90% of children reside in low and middle-income countries (LMICs), where cancer five-year survival rate of 40% is half that of high-income countries (HICs) (4,5). This stark difference is due to LMICs having inadequate diagnosis, follow-up, treatment accessibility, financing, supportive care, and insurance, in addition to more malnutrition, therapy abandonment, and therapy toxicity (4,5).

Childhood cancer commonly arises during fetal development from immature progenitor cells with blocked normal maturation which drive oncogenic transformation (6). The origins, biology and diversity of childhood cancer are quite distinct from those of adult tumours. Most paediatric tumours arise from the mesoderm or neuroectoderm during defined stages of postnatal development, where they frequently resemble fetal tissue (7). In contrast, adult cancer is inherently linked to age, and most tumours arise from the epithelium through the accumulation of somatic mutations. Compared to adult cancers, childhood cancers possess low levels of somatic mutations but present with high levels of germline or *de novo* mutations (8). Epigenetic dysregulation and genetic abnormalities, such as chromosomal rearrangements, are associated with an elevated risk of childhood cancer development (8).

In 2021 the World Health Organisation (WHO) independently classified paediatric cancers for the first time (9). Paediatric cancers are categorised into four broad families: (i) leukaemias and lymphomas, (ii) soft-tissue and bone tumours, (iii) central nervous system (CNS) tumours, and (iv) other solid tumours (9). Nervous system tumours account for approximately one-third of all childhood cancer diagnoses, primarily consisting of CNS tumours (20%) and neuroblastoma (6-10%) (1,10). CNS tumours disproportionately affect children and are the largest cause of paediatric cancer-related deaths, with approximately 40,000 new cases and 20,000 deaths worldwide per year (1,11). The WHO categorises paediatric brain and CNS tumours as high- or

low-grade glioma, medulloblastoma, ependymoma, or other CNS tumours such as atypical teratoid rhabdoid tumour (ATRT), each having within-tumour-type grading from Grade I (low) to Grade IV (high) (9). The WHO classifies neuroblastoma as a paediatric solid tumour within the peripheral neuroblastic tumour category, alongside ganglioneuroma and forms of ganglioneuroblastoma (9). CNS tumours (e.g. medulloblastoma and ATRT) and neuroblastoma share neural features, and as they collectively account for a significant number of all childhood cancer cases, an investigation into therapeutic approaches which jointly address these different nervous system tumours is warranted. The following sections describe in detail the three embryonal nervous system tumours, medulloblastoma, ATRT and neuroblastoma, which are the focus of the current thesis.

1.1.1 Medulloblastoma

Medulloblastoma (WHO Grade IV) accounts for the largest number of childhood brain tumours and primarily arises in the cerebellum of the posterior fossa of patients with an average age of nine (Figure 1.1) (12,13). The stages of medulloblastoma diagnosis include pre- and postoperative neuraxis imaging (principally by MRI), surgery, molecular profiling, and lumbar cerebrospinal fluid (CSF) analysis. Medulloblastoma is composed of the four principal molecular subgroups WNT-activated, SHH-activated and non-WNT/SHH medulloblastoma (Group 3 and Group 4) (Table 1.1), each respectively contributing to approximately 10%, 30%, and 60% (22% and 38%) of cases (14). These subgroups are further subtyped based on distinct molecular and clinicopathological factors. WNT signalling pathway-activated medulloblastoma arises in the lower rhombic lip of the dorsal brainstem from progenitors in the mossy fiber neuron lineage (15,16). WNT medulloblastoma is divided into only two subtypes (WNTα and β) based on age and chromosome 6 (17). This molecular subgroup is most frequently characterised by CTNNB1 mutation, with mutations occurring to a lesser extent in APC, CSNK2B, EPHA7, and components of the SWI/SNF nucleosome-remodelling complex (18). Sonic Hedgehog (SHH) signalling pathway-activated medulloblastoma arises in the external granular layer from cells within the granule cell precursor (GCP) lineage and is divided into four subtypes (SHH1-4) by the WHO classification system and a concordant four subtypes (SHH α - δ) by Cavalli (9,14,17). Disruptions to RNA processing and the cAMP-dependent pathway both contribute to SHH medulloblastoma. This molecular subgroup is most frequently characterised by mutations in PTCH1 across all subtypes or by subtype-specific gene alterations in the SHHa (TP53 and ELP1), SHHβ-γ (SUFU), and SHHδ (SMO and TERT promoter) subtypes (14,18–20). Groups 3 and 4 (Non-WNT/SHH) medulloblastoma are believed to arise from stem and progenitor cells in the right lateral (sub)ventricular zones of the cerebrum; however, their biology remains relatively unclear compared to subgroups WNT and SHH (21,22). Group 3 and 4

medulloblastomas are separated into eight subtypes (I-VIII) by the WHO and into three subtypes each (G3α-γ and G4α-γ) by Cavalli (9,17). Subtype-specific gene or chromosome alternations within the different subtypes are G3α (chromosome 8q), G3β (OTX2, GFI1 and GFI1B), G3γ (MYC), G4α (MYCN), G4β (SNCAIP and GFI), and G4γ (CDK6, chromosomes 8p and 7q) (23).

Medulloblastoma prognostic markers include patient age, degree of tumour dissemination at diagnosis, molecular profile, extent of tumour resection, and histopathology. The extent of tumour resection is classed as gross-total, near-total, and sub-total resection, with $0 \text{ cm}^2 \le 1.5$ cm² and > 1.5 cm² of detectable residual disease, respectively. Tumour dissemination staging ranges from no dissemination (M0) to extraneural metastasis (M4). Medulloblastoma prognosis varies drastically depending on the subgroup, from 41.8% to 100% five-year survival for G3y and WNTB, respectively (13). The morphologic differences observed in medulloblastoma are histologically classified as classic, desmoplastic/nodular, medulloblastoma with extensive nodularity, and large cell/anaplastic (24). Medulloblastoma prognosis and risk stratification are governed by molecular classification and multiple clinicopathological factors: age, disease stage, dissemination, residual disease, CSF cytology, histological classification, and haematological markers (25). Patients are categorised into two risk and treatment groups based on the probability of tumour recurrence: average and high-risk. Average-risk patients are over three years old, have gross-total or near-total resection and do not have tumour dissemination. High-risk patients are all those under three years old or those over three years with tumour dissemination, sub-total resection, large cell/anaplastic histology, or specific molecular features such as MYC or MYCN amplification (26).

Treatment paradigms are informed by assessing the histologic classification alongside the molecular classification. A large-scale risk-adapted Phase III clinical trial (SJMB03) reported a five-year progression-free survival (PFS) of 83.2% for average-risk and 58.7% for high-risk patients (27). Medulloblastoma patient treatment is risk-adapted, and there is no internationally agreed consensus on patient standard-of-care therapy. Multimodal therapy includes maximal safe surgical resection with varying chemotherapy and radiotherapy strategies depending on risk stratification: high-risk patients receive greater and more intense doses than average-risk patients. Children over three years old tend to receive postoperative craniospinal radiotherapy; however, due to an elevated propensity of children under three years old to develop late effects, radiotherapy is omitted from their treatment regimen (28). The International Society for Paediatric Oncology (SIOP) is currently performing the first biomarker-driven large-scale international randomised Phase III clinical trial to determine an international consensus for high-risk treatment based on achieving maximal efficiency with minimal late effects (26).

1.1.2 Atypical teratoid rhabdoid tumour (ATRT)

ATRT (WHO Grade IV) is a rare neoplasm that disproportionately affects young children aged under three years and is the prevailing malignant brain tumour in infants (9). ATRT is highly aggressive, and patients frequently succumb within 6-18 months (29). These tumours predominantly occur in the posterior fossa and the brainstem but can arise in regions throughout the CNS, such as the diencephalon and cerebrum (**Figure 1.1**) (30,31). The median age of patients is one year eight months, and nearly a third have disseminated disease at diagnosis (32,33). Despite a low level of genetic mutations, ATRT is a highly heterogeneous disease at the molecular and clinical levels due to aberrant epigenetics that drive tumorigenesis. ATRT tumours frequently harbour loss-of-function mutations of the tumour suppressor gene and epigenetic regulator SMARCB1 or, to a lesser extent, SMARCA4 (34). Approaches for diagnosing ATRT include craniospinal and full-body MRI screening, lumbar CSF cytology, and biopsies to assess SMARCB1 and for DNA methylation molecular subgrouping (29).

The WHO splits ATRT into three (epi)genetically and clinically defined subgroups: Sonic Hedgehog (ATRT-SHH), Tyrosinase (ATRT-TYR), and Myelocytomasis Oncogene (ATRT-MYC) (Table 1.1) (24). ATRT-SHH, ATRT-TYR, and ATRT-MYC comprise approximately half, a third, and a fifth of all ATRT cases, respectively (32). The average survival of ATRT-SHH, ATRT-TYR and ATRT-MYC patients is 16, 37, and 13 months, respectively (35). ATRT-SHH is a highly heterogeneous subgroup that can be split into 2-3 subtypes, but a WHO consensus has not yet been established (36,37). The ATRT-SHH subgroup is thought to arise from early neuroectodermal lineage progenitors, and these tumours form in the posterior fossa or basal ganglia (15,29). ATRT-SHH is characterised by heterozygous SMARCB1 point mutation, MYCN overexpression, and subtype-dependent gene overexpression: SHH-1A (GSX1, FOXG1, OLIG2, and GFAP), SHH-1B (ASCL1, NEUDOD6, CACNG3, OLIG2, and GFAP), and SHH-2 (EN2) (36,38). The ATRT-TYR subgroup is thought to arise from a non-neuroectodermal lineage, and these tumours are commonly found in the cerebellopontine angle (15,29). ATRT-TYR is characterised by inactivating SMARCB1 point mutations, chromosome 22 loss, high levels of euchromatin, and overexpression of melanosome pathway (TYR, TYRP and MITF) and mesenchymal (BMP4, OTX2 and PDGFRB) genes (38,39). The ATRT-MYC subgroup arises from a non-neuroectodermal lineage and is commonly found in the posterior fossa or supratentorial region (15,29). This molecular subgroup is characterised by homozygous SMARCB1 deletion and MYC and HOX cluster gene overexpression (38,40).

To date, there is no evidence-based staging or internationally agreed treatment consensus for ATRT patients. Prognosis is principally governed by molecular subgroup classification, age, and

extent of resection, but tumour location and dissemination also influence prognosis. Due to the rarity of ATRT tumours, how these factors contribute to overall survival (OS) is unclear. A combination of age and molecular classification has been shown to heavily influence prognosis, as ATRT-non-TYR patients under one year old have a five-year OS of 0% whilst ATRT-TYR patients over one year old have 71.5% (32,41). Current trimodal treatment approaches include maximal safe surgical resection, local or craniospinal radiotherapy, and conventional or high-dose chemotherapy. Intensive multimodal therapy can increase survival (42,43). Radiotherapy improves ATRT patient survival; however, it is used in an age-dependent manner due to the high probability of late effects in children under three years old (29,44). Alternatives to radiotherapy include intraventricular chemotherapy (conventional chemotherapy replacement) and proton beam therapy, which are associated with reduced late effects in ATRT patients (45). Additional components of multimodal therapy approaches include high-dose chemotherapy with autologous stem cell rescue. Two-thirds of ATRT patients experience tumour relapse or progression. As there is no consensus on how to treat these patients, they are usually included in early-phase clinical trials or undergo individualised targeted therapy, which is frequently unsuccessful (32).

1.1.3 Neuroblastoma

Neuroblastoma is the most common extracranial solid paediatric cancer, accounting for 6-10% of all childhood cancers and disproportionately causing 12-15% of paediatric cancer-related deaths (10). Neuroblastoma is predominantly a paediatric tumour, with 95% of diagnoses occurring in the first ten years of life (46). During the fifth week of embryonic development, neural crest cells migrate along the spinal cord and contribute to the development of the sympathetic ganglia. In the lumbar region, neural crest cells give rise to the sympathetic chain, and in the thoracic region, they produce the adrenal medulla. Oncogenic transformation dysregulates neural crest cell differentiation to form neuroblastoma. Defined as a small blue round cell tumour, neuroblastoma most commonly arises along the sympathetic chain in the abdomen and the adrenal gland; however, these primary tumours arise throughout the sympathetic nervous system and, in rare cases, are observed within the CNS (Figure 1.1) (47). Neuroblastoma tumour biology is highly heterogeneous, ranging from tumours which do not require treatment and spontaneously regress to highly aggressive, metastatic, and therapyresistant tumours. Whilst most patients are diagnosed by age five, the median age of patients is 18 months.

Prognosis is highly heterogeneous and can be predicted by several factors, including metastatic disease, age, chromosomal aberrations, and molecular signatures such as MYCN amplification (48). Instead of molecular subgrouping, as used for medulloblastoma and ATRT patients,

neuroblastoma patients are categorised according to internationally agreed risk groups (Table **1.2**). The International Neuroblastoma Risk Group (INRG) Task Force developed a classification system using clinical criteria and tumour imaging. This system defined seven prognostic factors (stage, age, histological category, grade of tumour differentiation, MYCN oncogene, chromosome 11q aberration, and DNA ploidy) to produce 16 pre-treatment groups, which were simplified into four risk groups: very low-, low-, intermediate- and high-risk (49). In 2019, a study sought to validate the INRG classification system and showed that for the very low through to high-risk groups, the five-year event-free survival was 95.8%, 80.8%, 50.0%, and 45.9%, respectively (50). Neuroblastoma staging is determined by the INRG Staging System (INRGSS) and the International Neuroblastoma Staging System (INSS). The INRGSS stages (L1, L2, M, and MS) are deduced from imaging results to inform treatment strategies, whereas the INSS stages (1, 2A, 2B, 3, 4, and 4S) are based on tumour biopsy results following surgery. The outcome for patients with very low- to intermediate-risk neuroblastoma is good, with some patients requiring little or no treatment. However, approximately 50% of patients have high-risk disease, for which prognosis is poor, with less than 60% OS (51). High-risk patients are defined and distinguished from the other risk groups by the presence of MYCN amplification and/or if they are ≥ 18 months old with metastatic disease or Stage 4. Treatment regimens to combat low- and middle-risk neuroblastoma have improved; however, high-risk patients have significantly lower OS and account for approximately half of all neuroblastoma cases. Their treatment comprises induction chemotherapy, tumour resection, myeloablative chemotherapy, autologous stem cell transplantation, and post-consolidation therapy (52).

1.2 Paediatric cancer therapy and the immune system

1.2.1 Standard-of-care therapy

Despite decades of research, standard-of-care therapy for paediatric oncology still predominantly relies on surgery, radiotherapy, and systemic use of cytotoxic chemotherapeutic agents. As a direct result of therapy-related late effects or disease-related morbidities, by the age of 45, 95% of childhood cancer survivors have impaired quality of life or suffer from life-threatening morbidities (53). This is particularly prominent for high-risk cancer survivors who suffer severe late effects following their intensive therapy regimens. Childhood cancer survivors suffer from a plethora of socio-economic challenges that impair their self-sufficiency as adults, thus limiting their integration and contribution to society (54–58). Consequently, there is a strong need for the development of novel childhood cancer therapies with increased efficacy and reduced toxicity to improve their quality of life. Many hurdles limit this development, including low incidence rate, low patient age, unclear tumour developmental origins, lack of

targeted therapies, cancer stem-like cells (CSCs), organ-specific factors, and the immune system.

Childhood tumour biology is distinct from adult cancer. Despite this, testing novel therapies in adults before children is ethically favoured. Novel therapies reaching paediatric patients are slow and are often limited to only therapies that show efficacy in adults (59). Due to low incidence rates and within-tumour type subgrouping, small patient cohort sizes elevate the complexity of paediatric clinical trials. International collaboration is required to enrol enough patients, and these trials struggle to recruit drug-naïve paediatric patients due to the high cure rate of standard-of-care therapy. These constraints and the concurrent limitation to collecting patient samples and data for research make assessing new paediatric treatment strategies incredibly challenging. This is further compounded by low interest from industry to develop novel treatments for relatively rare diseases, such as paediatric nervous system cancers. Compared to adult cancers that frequently harbour targetable oncogenic somatic mutations, childhood cancer genetic mutational burden is 14 times lower and, as such, there are substantially less effective targeted therapies for paediatric patients (6,60). The vast obscurity surrounding the dysregulated developmental origin of many paediatric tumours complicates and impairs our ability to accurately model them *in vivo* using animal models.

Aggressive tumours harbour cancer stem-like cells (CSCs), which are correlated with worse prognosis in medulloblastoma, ATRT, and neuroblastoma patients (61–63). CSCs are transformed cells with stem-like properties that are proposed to initiate tumour development by producing the various proliferating and differentiated transformed cell types that constitute the tumour (64). CSCs are thought to primarily arise from perturbations (i.e. oncogenic mutations) that affect the self-renewal, proliferation, or differentiation of stem and progenitor cells (64). CSCs can also arise from the dedifferentiation of differentiated cells; however, this is less common. Normal multi-potent stem cells utilise quiescence, symmetric and asymmetric cell division, multi-potency, and plasticity to environmental cues, to give rise to an organ's highly diverse and complex cellular architecture (65). When these stem-like properties are co-opted and utilised by CSCs, highly aggressive and heterogeneous tumours with high metastatic potential and therapeutic resistance arise (66–68). CSCs primarily escape standard-of-care therapy through their quiescence and plasticity (69). Many standard-of-care therapies (i.e. chemotherapy) target highly proliferative cells, so their efficacy against CSCs, which are quiescent, is low (69). Additionally, following challenge by a drug, plastic CSCs upregulate (i) drug transporters to pump the drug back out of the cell and (ii) DNA damage repair processes to repair drug-induced genomic damage (69). Consequently, CSCs persist and are enriched following standard-of-care therapy, and frequently then drive fatal tumour recurrence.

Brain tumours, such as medulloblastoma and ATRT, arise within the most complex organ in the human body during crucial stages of development. This adds enormous complexity to therapeutically targeting the brain, and there are many unique clinical barriers to brain tumour therapy, including surgical limitations, the blood-brain barrier (BBB), and the immune system. The surgical inaccessibility of specific brain regions makes tumours that arise within them inoperable. For accessible tumours, their frequent invasion into functional brain regions makes complete tumour resection to capture local invasion unachievable. The bioavailability of the brain is heavily regulated by the BBB, which prevents approximately 98% of small-molecule and 100% of large-molecule therapies from accessing the brain (70,71). The brain also possesses an immunologically distinct status, which can complicate the application of cancer therapy that co-opts the immune system (72).

1.2.2 The immune system and cancer

The human immune system is an intricate system composed of proteins, cells, tissues, and organs which collectively function to protect the body from infection and disease (73). The immune system is classified into two subsystems: innate and adaptive. The former is a nonspecific and rapid response that doesn't generate immunological memory, while the latter is specific and generates immunological memory, but experiences a delay between initial exposure (e.g. to a pathogen) and response (74). Once acquired, immunological memory allows rapid induction of a specific and potent immune response upon subsequent exposure (75).

Following exposure to a pathogen, cells release cytokines, viral antigens, pathogen-associated molecular patterns (PAMPs) and damage-associated molecular patterns (DAMPs) to initiate the innate immune response (73). Innate immune system cells, such as monocytes, macrophages, dendritic cells (DCs), neutrophils, and natural killer (NK) cells, respond to cytokines through their cognate receptors and to DAMPs and PAMPs through pattern recognition receptors (73). These cells respond rapidly via a few principal mechanisms to clear the pathogen, including: (i) phagocytosis (i.e. monocytes, macrophages, DCs and neutrophils), (ii) cytotoxicity (i.e. NK cells), and (iii) antigen processing and presentation to stimulate adaptive immune responses (i.e. DCs and macrophages) (76).

Lymphocytes (i.e. B cells and T cells) are the primary constituents of the adaptive immune system (77). Whilst B cells respond to extracellular antigens, T cells require antigen processing and presentation on the cell surface of antigen-presenting cells (APCs) by human leukocyte antigen (HLA) complexes (73). B cells mediate the adaptive humoral immune response through the production of antibodies and cytokines in response to pathogen exposure. B cells can be subcategorised based on (i) their prior pathogen exposure status (naïve vs. memory B cells), (ii)

whether they support other immune cells (regulatory B cells), or (iii) following the process of activation, proliferation and differentiation into antibody-producing effector cells (plasma cells) (78). T cells mediate the adaptive cellular immune response by binding to HLA-presented antigens on APCs via their T cell receptor (TCR) (79). TCR binding specificity is dictated by the CD4 and CD8 co-receptors, which specify binding to antigen-bound HLA class II and I complexes, respectively (77). This categorises T cells into two main subtypes: CD4+ T helper cells and cytotoxic CD8+ T cells. Following activation, CD4+ T helper cells promote pathogen clearance by facilitating the activity of both innate (i.e. DCs and NK cells) and adaptive (i.e. cytotoxic CD8+ T cells) immune cells (77,79). Following activation, cytotoxic CD8+ T cells specifically induce the lysis of pathogen-exposed cells through the secretion of cytotoxic cytokines and granules, as well as direct interactions between the cells via Fas/FasL interactions (77,79).

Solid tumours present with differing immunological states based on the amount, composition and phenotype of infiltrated immune cells, and these tumour states are classified as immunologically hot, cold or desert (80). Tumour cells help shape these immunophenotypes through intrinsic factors, such as tumour mutational burden, and by modulating tumour antigen presentation, immune checkpoint blockade and immunoregulatory cytokine secretion (81). Infiltration of cytotoxic cells of the innate (i.e. NK cells) and adaptive (i.e. CD8+ T cells) immune system is a key feature of hot tumours (Figure 1.4B), and this infiltration is associated with greater immunotherapy efficacy (Section 1.2.3) (80). In contrast, cold tumours present with limited cytotoxic immune cells, which are commonly exhausted and restricted to the tumour periphery, and instead harbour immunosuppressive immune cells (i.e. regulatory T cells (Treg), tumour-associated macrophages (TAMs), and myeloid-derived suppressor cells (MDSC)) (82) (Figure 1.4A). Immune desert tumours are a subcategory of cold tumours with very low immunogenicity and are virtually barren of immune cells (83). Medulloblastoma, ATRT, and neuroblastoma are generally immunologically cold tumours; however, patients with increased tumoural immune-cell content can present with positive features such as reduced tumour grade and improved survival (84–87). As such, leveraging the immune system against a patient's tumour may hold therapeutic merit. Immunotherapy employs this approach and can mitigate many of the biological hurdles discussed for treating paediatric nervous system tumours.

1.2.3 Immunotherapy

Since its discovery in 1891 by the Father of Immunotherapy, William Coley, who stimulated the human immune system against sarcoma, lymphoma, and testicular carcinoma using bacteria, a multitude of immunotherapies have been generated that leverage the immune system to recognise and eradicate cancer (88). They have had varying degrees of success to date, with

only subsets of patients responding to treatment due to the heterogeneous and complex nature of the TME (89). Immunotherapeutic strategies include monoclonal antibodies (principally immune checkpoint inhibitors), cancer vaccines, chimeric antigen receptor (CAR) T cells, oncolytic viruses (OVs), and cytokine therapies (**Figure 1.2**). There are currently five FDA-approved immunotherapies for nervous system tumours, including three for neuroblastoma. These include two monoclonal antibodies targeting the GD2 pathway (Dinutuximab and Naxitamab), a monoclonal antibody targeting the VEGF/VEGFR pathway (Bevacizumab), an immune checkpoint inhibitor targeting the PD-1/PD-L1 pathway (Pembrolizumab), and a cytokine therapy (GM-CSF) (90).

Immunotherapeutic monoclonal antibodies are a form of targeted therapy designed for specific antigen binding to promote anti-tumour immune responses (**Figure 1.2A**). Their two main mechanisms of action are those that (i) act on immune cells to bolster the immune response and (ii) specifically target and flag cancer cells to the immune system. A key example of the former is Pembrolizumab, which targets the co-inhibitory PD-1/PD-L1 pathway to potentiate CD8+ T cell responses against aggressive brain or nervous system cancer (91). Key examples of the latter are Dinutuximab and Naxitamab, which bind neuroblastoma cell surface GD2 and trigger antibody-dependent cellular cytotoxicity (ADCC) and complement-dependent cytotoxicity (CDC) in high-risk patients (92,93). Both ADCC and CDC are initiated by antibodies binding to cell-surface pathogen or tumour antigens. For ADCC, the recognition of cell surface-bound antibodies by Fc receptors on effector immune cells (e.g. NK cells) triggers effector immune cell cytotoxicity to lyse the target cell (e.g. perforin and granzyme-containing cytotoxic granule release) (94). For CDC, the recognition of cell surface-bound antibodies by the first classical complement component triggers the recruitment and assembly of the membrane attack complex, which forms pores in the cell membrane and induces cell death (95).

Cancer vaccines co-opt the tumour antigen presentation capabilities of APCs to primarily stimulate cytotoxic CD8+ T cell responses against the patient's tumour (**Figure 1.2B**). DCs are the preferred APCs as they prime CD4+ and CD8+ T cells through antigen recognition and promote T cell responses through cytokine secretion. Two main strategies are used to activate DCs: (i) tumour antigen administration in the form of nucleic acids, peptides, or viruses to stimulate patient DCs *in vivo*, or (ii) the DCs are stimulated and loaded with the tumour antigens ex *vivo* before administration. To date, the only FDA-approved cancer vaccines are the DC vaccine Sipuleucel-T for metastatic prostate cancer and the historical bacteria-based vaccine Bacillus Calmette-Guérin, which is the standard-of-care therapy for non-muscle-invasive bladder cancer (96,97). Cancer vaccines are in early-stage clinical trials for paediatric patients and are associated with reduced side effects (98). Interestingly, a clinical trial demonstrated a

better response of ATRT patients over medulloblastoma patients to autologous tumour-lysate-loaded DCs, highlighting that response can depend on tumour type (99).

In chimeric antigen receptor (CAR) T cell therapy, T cells are genetically engineered to express a chimeric receptor that recognises and binds tumour cell antigens (**Figure 1.2C**). This activates an intracellular signalling domain, stimulating the CAR T cell and eliciting an anti-tumoural immune response. Following treatment, the CAR T cell population can potentially expand within the patient to ensure long-term immunity against the tumour (100). The FDA has approved the CAR T cell therapy Tisagenlecleucel for the treatment of paediatric B-cell acute lymphoblastic leukaemia (101). Multiple Phase I clinical trials against paediatric nervous system cancers are underway using CAR T cells to target antigens such as GD2 (NCT05298995), HER2 (NCT03500991), B7-H3 (NCT04185038) and EGFR (NCT02442297). Completed trials have thus far shown limited success of GD2-targeting CAR T cells against neuroblastoma (102,103).

Specific pro-inflammatory cytokines have potent anti-tumoural effects by acting as anti-proliferative or pro-apoptotic factors to impair cancer cell growth or bolster immune cell activity (**Figure 1.2E**). The clinical application of cytokine therapy is often restricted by their small half-life, limited efficacy and off-target toxicity; however, the FDA has approved two cytokine therapies (IL-2 and IFN alpha) for the treatment of various adult cancers (104). Additionally, GM-CSF cytokine therapy is employed as an adjuvant to anti-GD2 immunotherapy for high-risk neuroblastoma patients as it stimulates neutrophils to augment the anti-GD2 ADCC (93,105).

A constraint to antigen-targeting immunotherapies (e.g. monoclonal antibodies, CART cells, and cancer vaccines) is that the low mutational burden of childhood cancers results in low amounts of neoantigens. Neoantigens are cancer-specific antigens that arise from genetic mutations and aberrant protein production (splicing and post-translational modification), and are ideal targets for antigen-targeting immunotherapies as they are unique to cancer cells (106). The efficacy of these single-modality immunotherapies is frequently hampered by multiple factors that collectively produce a suppressive tumour immune microenvironment (TIME). One approach to overcoming these constraints is to remodel the TIME in a multimodal fashion. OVs are capable of such remodelling and are associated with reduced side effects compared to monoclonal antibodies, checkpoint inhibitors, and CART cell therapy (98).

1.2.4 Oncolytic virotherapy

During oncogenic transformation, cells dysregulate antiviral responses such as interferon (IFN) signalling, thus increasing their susceptibilities to viral infection (107). Oncolytic virotherapy utilises this and hijacks the natural characteristics of some viruses to preferentially infect and kill tumour cells with minimal damage to healthy cells. The therapeutic efficacy of OVs arises

from their dual mechanism of action, where they induce targeted cancer cell death (oncolysis) and an anti-tumoural immune response (**Figure 1.3**). OVs infect, replicate within, and lyse cancer cells, releasing fresh progeny for continual cycles of infection and oncolysis. OV-induced cell death is immunogenic and cell death occurs through several mechanisms, including apoptosis, necrosis, necroptosis, pyroptosis, and autophagic cell death (108). The specificity for destruction of cancer cells over normal cells in children minimises treatment-related damage to developing tissues and generally has reduced acute side effects compared to standard-of-care therapy. Many paediatric tumours are immunologically "cold" (**Figure 1.4A**), and OVs overcome this by stimulating the immune system to recognise and attack the infected tumour, leading to robust long-term tumour immunity.

Clinical trials investigating OVs for the treatment of solid tumours started in the 2000s and have generally reported low toxicity and minimal adverse effects in patients (109,110). The year 2004 saw the first breakthrough in oncolytic virotherapy when the State Agency of Medicines of the Republic of Latvia approved the unmodified picornavirus Rigvir (ECHO-7) for the treatment of melanoma, the first ever OV (111). The following year, China's State Food and Drug Administration approved the modified form of adenovirus Oncorine (H101) for treating head and neck squamous cell carcinoma (112). Little progress in the OV research field was then made until 2015, when the first FDA OV approval was granted for a modified form of herpes simplex virus (HSV) type 1 (T-VEC) for the treatment of recurrent adult melanoma (113). Six years later, a significant breakthrough in brain tumour therapy was made when the Japanese Ministry of Health, Labor and Welfare approved the oncolytic herpes virus Delytact (G47 Δ) as the first brain tumour oncolytic virotherapy (114). The clinical trial demonstrated the safety and efficacy of Delytact against residual or recurrent adult glioblastoma, resulting in a 1-year survival rate of 84.2% and significantly improved OS and PFS (115).

To date, 15 clinical trials have employed OVs against paediatric brain tumours or neuroblastoma (**Table 1.3**). Ten trials employ DNA-based OVs (adenovirus, HSV, and vaccinia virus), and five employ RNA-based OVs (measles virus, Newcastle disease virus, poliovirus, reovirus, and Seneca Valley virus). Eight trials are complete, and they all document a tolerable level of OV-related adverse events, predominantly Grade 1 or 2, with only rare instances of Grade 3 (none of which impaired patient quality of life) (**Table 1.3**) (116–122). The OV-related late effects, if any, will be identified in the coming years as sufficient time elapses post-treatment. Apparent increases in survival were observed compared to historical data for diffuse midline glioma (DMG) and high-grade glioma (HGG) patients following treatment with the oncolytic viruses DNX-2401 and G207, respectively (116,117).

Certain OVs can infect and destroy CSCs, thus eradicating the most aggressive population of cancer cells responsible for resistance to standard-of-care therapy and tumour relapse (123,124). Refer to **Section 1.2.1** for an explanation of CSCs. These OVs can reduce late effects in patients due to sensitising the tumour to lower doses of standard-of-care therapy. CSC destruction has been demonstrated in a preclinical trial for G207 in Group 3 and 4 medulloblastoma xenograft models (125). The universal sensitivity of the medulloblastoma models highlighted it as a better target for G207 therapy than adult glioblastoma (125). Additionally, DNX-2401 has been shown to induce autophagic cell death in glioma stem cells (GSCs) and to sensitise paediatric HGG and diffuse midline glioma (DMG) xenograft mouse tumours to radiotherapy by downregulating DNA damage repair proteins (126,127).

An inherent constraint of OV therapy is achieving a clinically potent and beneficial anti-tumoural immune response whilst minimising antiviral responses, which limit OV efficacy. To date, twothirds of paediatric trials employed intratumoural OV administration, with the remaining trials favouring intravenous administration (Table 1.3). One trial incorporated OV administration into the CSF via lumbar puncture for disseminated recurrent medulloblastoma or ATRT (NCT02962167). Intratumoural OV administration maximises tumour OV levels and mitigates clearance by the immune system. This approach is limited to operable tumours, cannot target metastatic disease, and is associated with a toxicity risk to normal tissue surrounding the tumour due to the large viral load. Systemic OV delivery through intravenous administration is less invasive, easy to administer on multiple occasions, and can target disseminated disease (128). However, the primary constraint to this approach is OV clearance by the immune system before established tumour infection. Systemic delivery approaches that try to mitigate OV clearance in paediatric nervous system patients include combination therapy with the immunosuppressive agent cyclophosphamide to limit neutralising antibody production (NCT01048892) and concealing the OV within tumour-targeting mesenchymal stem cells (NCT04758533 and NCT01844661) (121,128).

Genetically modifying OVs can improve their clinical efficacy and safety. Modifications that elevate the tropism of OVs specifically for cancer cells can lead to improved viral binding and entry into cancer cells (e.g. tumour-surface antigen receptors), enhanced replication in cancer cells (e.g. tumour-specific promoters), or reduced replication in normal cells (e.g. miRNA response elements). Modifying OVs to express transgenes can enhance oncolysis (e.g. proapoptotic proteins), augment the anti-tumoural immune response (e.g. pro-inflammatory cytokines) or impede the tumour through remodelling the TME (e.g. anti-angiogenics). The hematopoietic growth factor GM-CSF is a well employed transgene and is expressed and delivered as a payload by both Pexa-Vec and T-VEC (113,122). These OVs infect the cancer cell,

and viral replication drives GM-CSF expression, which promotes an anti-tumoural immune response by remodelling the TIME through NK cell and T cell recruitment (122).

OV-induced remodelling of the TIME is multifactorial. Following OV-induced ICD, innate immune cells are recruited and stimulated by the cytokines, DAMPs, viral PAMPs, tumour antigens, and viral antigens released into the TME (108). Cytotoxic NK cells are activated by OVinduced Type I IFNs, which also stimulate macrophage pro-inflammatory cytokine secretion (129). NK cells employ perforin and granzyme-mediated cytolysis to kill tumour cells that lack HLA complexes or portray signatures of virus-induced stress (130,131). Macrophages and DCs bridge innate and adaptive immunity by processing and presenting tumour and viral antigens on their cell surface. Upon translocation of DCs to the lymph node, tumour or viral antigen presentation by HLA class I and II complexes on their surface primes CD8+ and CD4+ T cells, respectively. The T cell population expands and migrates along chemokine and molecular gradients to locate, infiltrate and drive an adaptive immune response against the infected tumour. Tumour-infiltrating CD8+ cytotoxic T cells specifically target and kill cancer cells presenting tumour or viral antigens via HLA class I. CD4+ Thelper cells assist in the activation of DCs and cytotoxic T cells, and secrete cytokines (e.g. IFN gamma) to assist other immune cells (e.g. NK cells). B cells raise humoral immunity against the OV by producing neutralising antibodies. Following clearance by the immune system, long-term immunological memory remains due to the maintenance of small populations of antigen-specific memory B and T cells, thus protecting against recurrence.

In paediatric brain tumour and neuroblastoma patients that respond to OV therapy, immune cell recruitment to the tumour is observed alongside a concomitant improvement in survival (116,117,119,120,122,128). It is predominantly a T cell anti-tumoural immune response that is observed. DNX-2401 induces CD4+ and CD8+ T cell recruitment and upregulation of viral and immune response-related pathways in tumour-infiltrating macrophages in DMG patients (NCT03178032) (116). G207 significantly increases CD4+ and CD8+ T cell infiltration into paediatric HGG, which is sustained following OV clearance, indicating a lasting anti-tumoural immune response (NCT02457845) (117). Additionally, G207 increased the number of plasma and B cells in certain paediatric HGG patients (117). Monocyte and CD8+T cell infiltration were documented in paediatric HGG tumours following Pelareorep and PVSRIPO treatment, respectively (NCT02444546 and NCT03043391) (119,120). However, it is unclear if this immune cell recruitment was due to the Pelareorep and PVSRIPO OV therapy or due to pre-treatment with GM-CSF or inactivated poliovirus vaccine, respectively. Interestingly, the ability of paediatric patients with advanced solid tumours to respond to mesenchymal stem cells (MSCs) carrying ICOVIR-5 (Celyvir) correlates with the number of circulating B and T lymphocytes, indicating a clinical dependency on an active immune system for Celyvir efficacy

(NCT01844661) (128). Paediatric patients with non-CNS solid tumours demonstrate a robust antigen-specific effector T cell response specifically after Pexa-Vec treatment (NCT01169584) (122).

The pro-inflammatory TIME that OVs generate presents a unique opportunity to augment tumour destruction by coupling oncolytic virotherapy with additional immunotherapy. Interestingly, in a paediatric glioblastoma patient, G207 upregulated immune checkpoint proteins on tumour cells (PD-L1 and IDO) and T cells (PD-1 and CTLA-4), identifying potential targets for combinational immunotherapy (132). Upregulation of PD-1 is also observed in a preclinical glioblastoma mouse model following DNX-2401 treatment (133). This observation led to an adult glioblastoma clinical trial combining DNX-2401 and the immune checkpoint blockade anti-PD-1 antibody pembrolizumab, where synergistic effects and improved survival were observed (NCT02798406) (91).

In summary, OVs pose real clinical potential as novel therapies against paediatric nervous system cancers. An optimal OV for these patients would be easily made, modifiable, BBB penetrable, systemically deliverable, CSC targetable, nervous system cancer cell targetable, and tolerable by the developing body (regarding adverse events and late effects). Zika virus (ZIKV) is one such virus that largely meets, or is capable of meeting, these criteria.

1.3 Zika virus (ZIKV)

1.3.1 Viral biology

ZIKV (Orthoflavivirus zikaense) is a positive-sense single-stranded RNA virus (+ssRNA) in the *Orthoflavivirus* genus (*Flaviviridae* family), which includes multiple pathogenic human viruses such as dengue virus (DENV), Japanese encephalitis virus (JEV), West Nile virus (WNV), and yellow fever virus (YFV) (134,135). ZIKV virions are approximately 40 nm in diameter and are composed of an outer lipid membrane containing 180 densely packed envelope (E) and membrane (M) proteins that surround the nucleocapsid (*Figure 1.5*) (136). The +ssRNA genome encodes ten viral proteins flanked by untranslated regions (UTRs) to produce a single polyprotein of 3,424 amino acids (aa) that is processed by viral and host proteases (*Figure 1.5*) (137). The 5' UTR is highly conserved and contains a cap that protects the genome from host 5'-3' exonucleases and also initiates translation along with stem-loop structures for genome replication by the viral RNA-dependent RNA polymerase (RdRp) (138). The 3' UTR consists of three domains, lacks a poly(A) tail, and has variability that assists in host adaption. The subgenomic flavivirus RNA (sfRNA) is produced from the 3' UTR, which aids productive infection and affects ZIKV pathogenesis (139).

The cleaved viral products include three structural proteins (capsid, C, pre-membrane, prM, and envelope, E), which drive viral assembly, cell attachment, and cell entry, and seven nonstructural (NS) proteins (NS1-5) that regulate the viral life cycle and allow evasion of host antiviral responses (140,141). An additional small peptide, 2K, is produced, which affects NS4A and NS4B functions. The 122 aa C protein is critical to virion assembly, as multiple copies interact and encapsulate a single copy of the ZIKV +ssRNA genome to form the nucleocapsid (142,143). The 168 aa prM protein interacts with the E protein to encase the nucleocapsid and is fundamental for viral maturation through cleavage into its M form in the Golgi apparatus as the virion egresses from the cell (144). The 504 aa E protein is the viral binding protein responsible for attaching and fusing the viral membrane with the host cell membrane (145). The 352 aa NS1 protein primarily localises to the endoplasmic reticulum (ER) lumen and assists replication compartment formation, or it can cause tissue hyperpermeability and vascular leakage following secretion from the cell as a hexamer (146,147). The 226 aa NS2A transmembrane protein localises to the ER, recruits the viral NS2B/3 protease and structural polyprotein to replication compartments, and presents the newly synthesised viral genome to C protein for nucleocapsid assembly (148,149). The 130 aa NS2B transmembrane protein localises to the ER to recruit, stabilise, and stimulate the NS3 protease domain to produce the active NS2B/3 protease (150,151). The 617 aa NS3 protein consists of an N-terminal serine protease domain responsible for processing the viral polyprotein and a C-terminal helicase domain to unwind viral RNA during replication (152). The 127 aa NS4A and 251 aa NS4B transmembrane proteins mediate the remodelling of the ER membrane into replication compartments (153,154). The 903 aa NS5 protein localises to the nucleus and consists of an N-terminal methyltransferase domain to cap the ZIKV genome and a C-terminal RdRp domain for genome replication (155). The ZIKV genome and protein sizes referenced are of the historical MR766 strain (137).

1.3.2 Viral transmission and life cycle

ZIKV transmission primarily occurs through the *Aedes aegypti* or *Aedes albopictus* mosquito (156). Human-to-human transmission routes include blood and semen, or vertically from mother to fetus (157,158). The ZIKV infection life cycle is well established in human cells (**Figure 1.6**). Following E protein recognition and binding to host cell receptors, ZIKV is internalised by receptor-mediated endocytosis. Viral particles travel through the endosomal-lysosomal system until the V-ATPase-driven drop in pH drives the fusion of the viral membrane with the host membrane to release the viral nucleocapsid into the cytosol (159). Following degradation of the nucleocapsid, the +ssRNA ZIKV genome interacts with host cell translational machinery and is targeted to the ER. The positive-sense nature of the ZIKV genome results in rapid *de novo* synthesis of ZIKV proteins into the ER membrane and lumen. ZIKV increases the proliferation

and cellular abundance of ER and vesicles and induces intracellular reorganisation of the ER and other host organelle structures to create viral replication and assembly compartments (160,161). The rapid ZIKV protein synthesis and host membrane remodelling trigger the host ER stress response, principally the unfolded protein response (UPR), to deal with the elevated stress. Immature virions are produced in the ER-derived membrane and mature as they are transported through the Golgi, where a host furin-like protease cleaves the prM protein to M protein to form mature infectious viral particles (162). The virions egress from the cell and are released into the surrounding microenvironment for subsequent infection. Cells capable of mounting an antiviral response curb ZIKV infection by inhibiting viral replication, degrading the viral particles and inducing apoptosis to prevent the local spread of fresh virions.

1.3.3 ZIKV epidemiology

ZIKV was first isolated from a rhesus macaque monkey in the Zika Forest in Uganda in 1947 (strain MR766), and its ability to infect humans was first identified in 1952 (163). Throughout the next 55 years, only sporadic ZIKV cases were reported until 2007, when the first major ZIKV outbreak occurred in the Yap Islands (164). The next major outbreak hit French Polynesia in 2013. These outbreaks were the first indications of the emergence of the Asian ZIKV lineage (165). In 2015, an Asian ZIKV lineage outbreak in Brazil was quickly accompanied by an approximate four times increase in Guillain-Barré syndrome (GBS) incidence, with incidence increasing with age and a nearly ten times increase in congenital microcephaly incidence (166,167). In February 2016, the World Health Organisation (WHO) issued a Public Health Emergency of International Concern following evidence indicating that intrauterine ZIKV infection causes congenital neurodevelopmental disorders (168). Since the identification of Asian ZIKV lineage neuropathology, extensive research efforts have been made to elucidate how this lineage acquired this potential and the molecular biology through which it inflicts its catastrophic effects on the fetus.

As ZIKV spread geographically, it underwent evolutionary adaptation, resulting in approximately 12% nucleotide and 4% as divergence between the Asian and African lineages (169). Through this divergence, Asian ZIKV acquired neurovirulence and neuroinvasiveness. Genetic alterations, primarily within the E and prM coding regions and in the 3' UTR, have all been indicated to contribute to increased virulence, intrauterine transmission, or the neuropathology of the Asian lineage (170–174). Additionally, differential E protein glycosylation and NS1 mutation of the Asian lineage have been connected to elevated neurovirulence and *Aedes aegypti* mosquito infection, respectively (175,176).

1.3.4 Infection of CNS cells

It is well documented that the Asian ZIKV lineage primarily causes microcephaly through direct effects on fetal radial glial (RGCs) and neural precursor (NPCs) cells (177–180). RGCs are elongated bipolar cells that span from the ventricular zone to the pial surface and undergo interkinetic nuclear migration and asymmetric cell division. They arise from neuroepithelial cells early during neurodevelopment, produce NPCs, and ultimately give rise to neurons that migrate along the RGC processes to populate the cerebral cortex (181). RGCs also produce astrocytes and oligodendrocytes, which are central to fetal neurodevelopment. In primary human brain slices, ZIKV infects RGCs and disrupts centrosomes and mitosis, leading to cell death (177,182). Infection of RGCs and signs of the development of microencephaly have been reported in mouse models as early as 24 hours post forebrain intraventricular ZIKV administration (183). Vertical transmission of ZIKV during mouse pregnancy leads to fetal RGC infection, a reduced pool of proliferative RGCs, and an accompanying disruption to cortex development (184). ZIKV NS2A was specifically found to disrupt adherens junctions to dysregulate and deplete RGCs, which impairs cortical neurogenesis of the fetal mouse brain (185).

NPCs are multipotent cells found in the subventricular zone (SVZ) that arise from RGCs and give rise to neuronal and glial cells (186). Direct infection and depletion of fetal NPCs are hallmarks of ZIKV pathogenesis and ZIKV-induced microcephaly. Fetal NPCs are ill-equipped to combat ZIKV infection as they have limited functional IFN antiviral immunity and produce a suboptimal cytokine response to ZIKV infection (187,188). The ZIKV genome hijacks intracellular machinery, such as the RNA-binding protein MSI1, which regulates stem-like properties, to promote its replication within NPCs (189). Fetal NPC depletion leads to cortical thinning and the underdevelopment of the fetal brain due to a concomitant loss of NPC progeny. ZIKV infection dysregulates and depletes fetal NPCs by disrupting proliferation and inducing premature differentiation, cell-cycle arrest and cell death (178,190,191). ZIKV inflicts this by affecting a plethora of cellular mechanisms and structures, inducing the DNA damage response (DDR), innate immune response, UPR, mRNA regulation, lipid metabolism, organelle stress (ER stress, ribosomal stress, and mitochondrial fragmentation), and multiple forms of cell death (192). ZIKV dysregulates numerous signalling pathways in NPCs, and these are primarily pathways involved in neurodevelopment, such as mTOR, WNT, Notch, Toll-like-receptor, Ephrin Receptor, and PPAR signalling pathways (190,193–196). A caveat to these observations is that they predominantly arise from research using commercial NPCs or cancerous neural cells. An investigation into ZIKV infection of congenital Zika syndrome (CZS)-affected patient-derived NPCs to determine the molecular processes and pathways that are dysregulated during infection in these unique cells is deeply warranted.

ZIKV can also infect neurons, astrocytes, oligodendrocytes, and microglia to varying degrees, and understanding how these cells are affected by ZIKV infection is fundamental to understanding ZIKV neuropathogenesis (192). Neurons are nerve cells that employ action potentials to transmit signals and allow communication throughout the CNS and body to regulate all aspects of human life. Substantial loss of neurons, especially in the cortex, is a hallmark consequence of pathogenic intrauterine ZIKV infection. This loss mainly occurs indirectly through ZIKV-induced reduction of the RGCs and NPCs that generate neurons, rather than through direct infection and depletion of neurons themselves (197). However, there is limited evidence to show that ZIKV can infect neurons at low efficiency and that this may have some relevance for CZS (180).

Astrocytes are glial cells and are the predominant cells in the CNS. Astrocytes regulate CNS homeostasis, maintain BBB integrity, and heavily support neuronal function (198). ZIKV infection of astrocytes is mediated through the first identified ZIKV receptor, AXL (177,199). Astrocytes are the first cell type infected in neonate mice, which leads to astrogliosis and aberrant CNS development (200,201). Astrocytes may act as a ZIKV reservoir within the human CNS, as infection and viral shedding lasting over a month have been documented in primary human astrocytes (202). ZIKV infection induces a limited pro-inflammatory cytokine response in primary human astrocytes (203). This prolonged viral shedding and limited cytokine response, in cohort with the resistance of ZIKV-infected astrocytes to IFN signalling and apoptosis, collectively contribute to aberrant CNS development following ZIKV infection (202,204).

Oligodendrocytes are glial cells that arise from oligodendrocyte progenitor cells (OPCs). They insulate axons through myelination to support neuronal function in the CNS. Both OPCs and oligodendrocytes have been observed to be susceptible to ZIKV, and infection impairs cell viability (205,206). ZIKV infection of nonhuman primates (NHPs) has been shown to impair oligodendrocyte development, cause aberrant axonal myelination and dysfunction, and result in white matter hypoplasia in the fetal brain (207–209). This ZIKV-induced oligodendrocyte and axonal dysfunction is a potential explanation for neurodevelopmental delays in children who appeared asymptomatic at birth following maternal ZIKV infection (205,207).

Microglia are CNS-resident macrophages that arise from yolk sac primitive myeloid progenitors and are the principal CNS immune cell. Vertical transmission of ZIKV early during pregnancy leads to infection of the yolk sac progenitors, which produce infected microglia that migrate from the yolk sac and transport ZIKV in a Trojan horse-like manner into the developing CNS (210). Like astrocytes, microglia can serve as ZIKV reservoirs due to their anti-apoptotic phenotype following infection (211). Unlike astrocytes, microglia develop a robust pro-inflammatory cytokine response following ZIKV infection (212). Interestingly, ZIKV-infected

microglia-secreted cytokines impair NPC proliferation and their astrocytic differentiation, thus highlighting a potential inter-cellular mechanism contributing to the reduction in the fetal NPC pool (213).

1.3.5 Congenital infection

Maternal ZIKV infection during the first, second, and third trimesters of human pregnancy results in vertical transmission in 47%, 28% and 25% of cases, and CZS symptoms in 9%, 3% and 1% of cases, respectively (214). ZIKV is a teratogen and causes miscarriage or stillbirth in 4-7% of cases (215). The five unique abnormalities that are used to diagnose CZS are severe microcephaly, thin cerebral cortices, macular scarring and retinal mottling, congenital contractures, and early hypertonia (216). The main fetal CZS malformations include low birth weight, neurological complications (microcephaly, parenchymal or cerebellar calcifications, ventriculomegaly, CNS hypoplasia or atrophy), osteoskeletal complications (arthrogryposis), or ophthalmic complications (ocular findings in the posterior and anterior segments or abnormal visual function) (217). Longitudinal studies of infants born asymptomatic for congenital ZIKV infection are beginning to highlight that postnatal neurodevelopmental issues can arise for these patients (218–222). Additionally, some clinical interventions have started to demonstrate the capability to treat these postnatal neurodevelopmental issues (223).

Studies of non-identical (dizygotic) twins born discordant for CZS have indicated that both intrauterine environmental factors, such as the placenta, and genetics can govern the differential response to ZIKV infection (193,224,225). The former might be explained by trophoblast cells, one of the principal cell types constituting the placental barrier, from the CZSaffected twin having increased susceptibility to ZIKV infection than trophoblast cells from the unaffected twin (226). For the latter, two independent studies implicate the mTOR pathway in genetic susceptibility to CZS development (193,224). The mTOR pathway regulates neural stem cell (NSC) proliferation and differentiation, and disruption of the pathway leads to aberrant neurodevelopment (227). Induced pluripotent stem cell (iPSC)-derived NPCs from CZS-affected twins have differential expression of mTOR and WNT pathway regulators compared to their unaffected twin, and mTOR pathway activity affects ZIKV replication (193). Whole exome sequencing of blood from the CZS-affected twin identified a mutation affecting the mTOR gene (224). Additionally, ZIKV NS4A and NS4B suppress mTOR signalling within primary fetal neural stem cells (NSCs) and impair neurogenesis in vitro (228). Thus, the differential activity of the mTOR pathway through changes at the genetic or transcriptome level may predispose certain individuals to ZIKV-induced dysregulation of neurogenesis and CZS development, and this process likely involves ZIKV NS4A and NS4B.

Maternal ZIKV infection at later stages of pregnancy correlates with reduced CZS incidence, thus implying that the underdeveloped nature of the fetal CNS is an inherent risk factor that contributes to CZS development (214,229). Bulstrode et al. demonstrated that myeloid cell-secreted IFN beta could induce interferon-stimulated gene (ISG) expression in primary fetal brain progenitor cells and this significantly reduced their susceptibility to ZIKV infection (230). As myeloid cells are immature and scarce during the early stages of fetal brain development, this finding implies that the absence of myeloid cell-derived IFN beta may render the fetal brain susceptible to ZIKV (230). In summary, there is a complex interplay between the virus and many CNS cell types, and both the presence and absence of specific cell types in the fetal brain contribute to the development of CZS.

1.3.6 Postnatal infection

Most postnatal ZIKV infections are asymptomatic. One in five cases are symptomatic, and disease is generally self-limiting, with symptoms resolving within two to seven days (215). Both ZIKV-infected children and adults suffer from the same main acute symptoms: headache, fever, rash (exanthema), joint pain (arthralgia), conjunctivitis, and muscle pain (myalgia) (231,232). Postnatal ZIKV infection can cause severe conditions such as GBS, meningitis and encephalitis; however, these are rare and are more frequently observed in adults than children (215,233). Postnatal ZIKV infection results in neurological complications in 0.52% of children, which primarily consists of GBS (0.22%), encephalitis (0.09%), demyelinating diseases (0.04%) and CNS inflammatory diseases (0.02%) (232). ZIKV-related paediatric mortality is incredibly rare, and recorded cases are accompanied by comorbidities, including acute myeloid leukaemia, sickle cell disease, Evans syndrome, and bacterial meningitis (232). A caveat to these studies is that they predominantly consider children over 12 months old as surveillance of postnatal ZIKV infection in young human infants is scarce. The highly crucial and complex neurodevelopmental stages within the first 24 months of human life pose a potential vulnerability to neuropathogenic infections such as ZIKV (234,235). Longitudinal studies have begun to highlight that postnatal ZIKV infection in young infants can result in long-term neurodevelopment complications (236,237). From a cohort of 60 infants with symptomatic postnatal ZIKV infection during the first year of life, 15% had clinical neurodevelopmental manifestations by 20-30 months, causing them to underperform in neurologic or audio-visual assessments (237). Temporal and anatomical neurodevelopment in NHPs is highly similar to humans (238). NHP infants infected with ZIKV postnatally suffer from irregular neurodevelopment and physical brain differences that result in impaired behaviour and motor cognition (239,240). Notably, treating infant NHPs with sofosbuvir, an FDA-approved antiviral drug which inhibits the ZIKV NS5 RdRp, during peak ZIKV infection is neuroprotective against many ZIKV-associated neurodevelopmental and

behavioural complications (241,242). In summary, whilst acute adverse effects are rare following ZIKV infection in the paediatric population, there is an indication that infants infected with ZIKV before the age of one are particularly vulnerable to developing long-term neurodevelopmental complications.

1.4 ZIKV oncolytic virotherapy

1.4.1 Advantages and limitations for paediatric cancer patients

Penetration of the BBB, its neurotropism, and many additional attractive properties first drew the attention of researchers to investigate the oncolytic potential of the Asian ZIKV lineage against brain tumours. ZIKV can preferentially infect CSCs and sensitise these highly aggressive cells, which are frequently associated with poor prognosis and reduced survival, to standard-ofcare therapy (243). The ZIKV RNA genome presents certain benefits over that of DNA viruses. RNA OVs have greater delivery efficiency, better BBB penetration capability due to their smaller size, are more immunogenic, and pose a significantly lower host genome integration risk (244). One drawback of RNA viruses is that they lack a high-fidelity polymerase, which predisposes them to reduced genetic integrity (244). The young nature of paediatric patients with embryonal tumours inherently mitigates the risks of both sexual and vertical transmission. Blood transfusions from cancer patients to other individuals are not performed, thus mitigating this transmission route. Consequently, the risk of Asian ZIKV transmission by paediatric cancer patients is incredibly low where Aedes mosquitoes do not reside. Regarding clinical administration of ZIKV, the virus can be produced under cGMP compliance, and several different viable administration routes are available, including systemic delivery (245). Thus, ZIKV presents with many attractive characteristics that pose it as a potential candidate for OV development, including its neurotropism, BBB penetration, cGMP compliance, systemic delivery, RNA genome, CSC targeting, restricted transmission routes and its low incidence of severe pathology following postnatal infection.

Despite the numerous aforementioned attractive properties, there are significant concerns and limitations to developing ZIKV as an oncolytic virotherapy for use in a paediatric oncology setting where patients are still developing. As discussed in **Section 1.3.6**, significant stages of neurodevelopment occur during infancy, and the administration of a neurotropic and neurotoxic virus raises major concerns due to the potential for neurological complications (234,235). Additionally, ZIKV infection can induce acute side effects in children (**Section 1.3.6**) (215,231–233). These require careful consideration and must be weighed against the benefits ZIKV OV therapy may offer paediatric patients. This is particularly pertinent for brain tumour patients, as

some acute side effects are neurological (i.e. headaches and encephalitis), so could exacerbate current cancer symptoms (232). The immune system, especially the adaptive immune system, is immature and underdeveloped in infants (246,247). Additionally, the immune system and its development can be compromised in paediatric cancer patients (248). Both of these factors elevate patients' susceptibility to infectious diseases, posing a safety concern for the use of a viral-based immunotherapy. The unpredictable nature of the immune system in paediatric cancer patients means that a suboptimal response may result in excessive viral shedding, viremia, and off-target effects, while an excessive response may lead to systemic inflammatory syndromes such as cytokine storm (248). For details on how some of these limitations can be addressed to improve the safety profile of ZIKV as a potential therapy for paediatric patients, please refer to **Section 1.4.4**.

1.4.2 Oncolysis

ZIKV has demonstrated, with varying success, the ability to infect and destroy cells from paediatric (medulloblastoma, ATRT, DMG, ependymoma, and neuroblastoma) and adult (glioma and meningioma) nervous system tumours, with research into adult glioma dominating this research field to date (249–251). As ZIKV infection of non-nervous system tumours (prostate, colorectal, breast and testicular cancer) is highly variable and oncolysis is generally limited, only nervous system tumours will be discussed further (249,252–254).

1.4.2.1 Paediatric nervous system tumours

Medulloblastoma arises from various stem and progenitor cell types and predominantly forms in the cerebellum of the posterior fossa (**Section 1.1.1**). All six medulloblastoma cell lines (USP13-Med, DAOY, ONS-76, HDMB03, D283 and D341) assessed to date are susceptible to productive ZIKV infection and oncolysis (249,250,254). USP13-Med (USP13) cells are highly aggressive paediatric cells that aberrantly express NSC markers and have CSC properties such as elevated proliferation, invasion, drug resistance and high tumorigenicity *in vivo* (255). USP13 cells are of the non-WNT/SHH medulloblastoma (Group 3 or 4) molecular subgroup. USP13 and DAOY tumorspheres are significantly disrupted following ZIKV infection, with an approximate ten- and four-times reduction in tumorsphere area by 72 hours post-infection (hpi) (multiplicity of infection (MOI) 1), respectively (249). The WNT signalling pathway regulates ZIKV infection of USP13 cells but not DAOY cells (249). A single intracerebroventricular dose of 2 x 10³ plaqueforming units (PFU) ZIKV significantly reduces USP13 brain tumour growth two weeks after administration in xenograft mouse models (249). By week three, partial remission, complete remission, and tumour relapse occur in 89%, 67%, and 44% of infected mice, respectively. ZIKV inhibits metastatic spread in USP13 tumour-bearing mice. Despite these encouraging

observations, a single ZIKV administration did not significantly improve survival from USP13 tumours. Repeated intracerebroventricular ZIKV doses achieved complete destruction of USP13 tumours; however, this approach was toxic, with significant viral shedding, irregular parenchyma, reduced body weight, and reduced survival reported (256). DAOY xenograft tumour growth was unaffected by intracerebroventricular ZIKV and no survival improvement was observed (249).

ATRT has various embryonal cell origins and is primarily found in the posterior fossa, diencephalon, cerebrum, or midbrain (Section 1.1.2). Of the two ATRT cell lines assessed to date, by 72 hpi, ZIKV induces an approximate 80% reduction in CHLA06 cell viability (MOI 5) and induces complete USP7-ATRT (USP7) cell destruction (MOI 1) (249,254,256). USP7 cells are susceptible to ZIKV oncolysis at MOIs as low as 0.01. Like USP13 cells, USP7 cells are aggressive CSCs that are highly tumorigenic in vivo (249). ZIKV-infected USP7 tumorspheres undergo a more than 20 times reduction in tumorsphere area by 72 hpi (MOI 1) (249). The WNT signalling pathway strongly modulates ZIKV oncolysis of USP7 cells, with pathway activation and inhibition increasing and suppressing oncolysis, respectively (249). A single intracerebroventricular administration of 2 x 10³ PFU ZIKV to the right lateral ventricle significantly improved the survival of USP7 tumour-bearing xenograft mice (249). This significantly reduced brain tumour growth one-week following administration, and partial remission, complete remission, and tumour relapse occurred in 80%, 20%, and 0% of treated mice by week three, respectively. To assess ZIKV tropism for aggressive USP7 brain malignancies in vivo, three intraperitoneal (systemic) ZIKV injections were given which resulted in tumour infection, cell death, improved clinical features, and increased survival (256).

DMG, previously known as diffuse intrinsic pontine glioma (DIPG), is a paediatric-type diffuse HGG (WHO Grade IV) that mainly arises from oligodendrocyte progenitor cell (OPCs) and forms within the thalamus, brainstem, or spinal cord (24,257). They are highly aggressive, invasive, and predominantly inoperable, resulting in a very poor prognosis with a median survival of less than 24 months (258). Of the four paediatric DMG cell lines assessed to date (DMG 007, DMG 3752, DMG B117 and DMG B169), all are susceptible to productive ZIKV infection (230,250). Of the two ZIKV-infected cell lines assessed via cell death assays (DMG 007 and DMG 3752), both undergo a severe reduction in cell viability and a potent caspase 3-dependent apoptotic response (250).

Ependymoma is an ependymal cell glioma (WHO Grade I-III) that forms throughout the CNS, mainly in the supratentorial, infratentorial, or spinal regions. RGCs produce ependymal cells to line the ventricle and spinal cord cavities. Paediatric patients primarily develop intracranial ependymoma, the third most common paediatric brain, which has an OS rate of 40-75%

(13,259). ZIKV infection in USP21-EPE and EP1 ependymoma cells is productive and significantly reduces cell viability and number (250,260). Notably, USP21-EPE cells are aggressive and aberrantly express stem cell markers. USP21-EPE tumorspheres are highly susceptible to ZIKV infection and complete 3D structure destruction occurs by 72 hpi (MOI 1) (260).

Neuroblastoma arises from neural crest cell transformation, predominantly forming in the peripheral nervous system (PNS) and only in the CNS in rare cases (Section 1.1.3). Of the six neuroblastoma cell lines assessed to date (IMR-32, SK-N-AS, SMS-KAN, LA-N-6, SK-N-Be(1), and CHLA-42), four are highly receptive to productive ZIKV infection and oncolysis during prolonged monolayer culture (IMR-32, SMS-KAN, SK-N-Be(1), and CHLA-42) (MOI 10) (251). ZIKV-induced destruction of neuroblastoma cells is dependent on CD24 expression but independent of AXL expression and MYCN status. CD24 governs neuroblastoma susceptibility by negatively regulating responses to Type I IFNs and intracellular antiviral pathways (Type I IFN, NF-kappa B, and Ras signalling), thus permitting productive ZIKV infection and oncolysis (261). ZIKV infection of cell isolates from primary neuroblastoma tumours ex vivo results in approximately 20-40% cell death (262). Intratumoural administration of 2 x 106 PFU ZIKV to xenograft mice with hind flank IMR-32, SK-N-AS, SMS-KAN or SMS-KANR tumours caused necrosis and reduced tumour volume by 35-100%, whilst uninfected tumour volume increased by 188-857% (262). Interestingly, ZIKV significantly reduced the volume of xenograft tumours from treatment-naïve primary neuroblastoma cells (SMS-KAN, 80% reduction) and posttreatment metastasised neuroblastoma cells (SMS-KANR, 35% reduction) from the same patient. Notably, despite only one of four tumour models completely responding to ZIKV administration, a 90-100% survival was observed for all four models, while vehicle treatment resulted in 0% survival.

In summary, research into oncolytic Zika virus (oZIKV) therapy for paediatric cancers has demonstrated that ZIKV can infect and destroy DMG and ependymoma *in vitro* and medulloblastoma, ATRT and neuroblastoma in both *in vitro* and *in vivo*. With one-third of all paediatric cancer diagnoses being nervous system tumours, ZIKV proving efficacious against both CNS (medulloblastoma and ATRT) and PNS (neuroblastoma) tumours *in vivo* is particularly poignant, as this research field may yield a single treatment modality applicable to various nervous system tumours. A caveat to this current knowledge is that the molecular mechanisms governing these responses are grossly unknown for paediatric nervous system tumours and warrant investigation (**Chapters 2 and 3**).

1.4.2.2 Adult nervous system tumours

Adult-type diffuse gliomas (WHO Grade II-IV) consist of glioblastoma, oligodendroglioma and astrocytoma (263). These tumours are incredibly infiltrative, arising throughout the CNS from glial cells and resulting in highly variable patient survival. Since Zhu et al. first described ZIKV oncolysis of adult glioma in 2017, a multitude of studies have documented ZIKV efficacy against glioma in vitro (monolayer, tumorsphere, organoid, and patient explants) and in vivo (immunodeficient or immunocompetent rodents and canines) (230,243,250,264-267). ZIKV preferentially infects GSCs over glioma cells with a differentiated phenotype (DGCs) (250,265,268). ZIKV binds and enters GSCs through integrin ανβ5, and ZIKV selectively infects GSCs over DGCs because the stem cell marker SOX2 controls ITGAV expression (250,268). ZIKV also enters human glioma cells via AXL, Dynamin-II, Caveolin-1 and NCAM1, and can utilise both clathrin-dependent and clathrin-independent endocytosis (159,250,269,270). AXLmediated ZIKV entry into glioma cells is controversial, with independent studies publishing contrasting results (250,269). SOX2 also governs GSC sensitivity to ZIKV by downregulating ISG expression to produce a low basal Type I IFN signature and suppress GSC innate immunity (230,243,250). Following infection, ZIKV induces potent GSC inflammatory responses, including IFN signalling, TNF signalling, NF-κB signalling, and pro-inflammatory cytokine signalling (243,265,271). ZIKV infection induces GSC differentiation and various forms of glioma cell death. ZIKV-induced GSC differentiation occurs through miR34c upregulation, resulting in the subsequent downregulation of the stemness maintenance markers NOTCH and NUMB (272). Both ZIKV NS2B/3 and NS5 have been implemented in oncolysis of glioma cells. NS2B/3 cleaves Gasdermin D (GSDMD) to induce caspase-independent pyroptosis of glioma cells in vitro, and NS5 suppresses human glioma cell proliferation and invasion in vitro and reduces tumorigenesis of mouse glioma in vivo (273,274).

A preclinical canine study and a human case report are of particular importance for demonstrating the potential of ZIKV as an OV against adult glioma. In the canine study, two intrathecal ZIKV doses to an adult male with a naturally occurring oligodendroglioma halted tumour progression for four months and improved clinical symptoms (264). Oligodendroglioma infection led to significant necrosis, immune cell infiltration, and a reduced tumour volume. In the case report, a glioblastoma patient with oncogenic mutations suggestive of poor prognosis was naturally infected with ZIKV or DENV 3.5 weeks following surgical resection (275). The patient also received standard-of-care radiotherapy and temozolomide (TMZ) chemotherapy, which is often ineffective as glioblastoma patients have an average life expectancy of 15 months. Nevertheless, six years post-diagnosis, this patient is healthy with no signs of tumour recurrence and not taking cancer-related medicine. This retrospective study is heavily limited by not being able to demonstrate actual ZIKV infection and oncolysis. It is interesting to speculate,

however, that this unusually prolonged survival may be indicative of ZIKVs efficacious effects against human glioblastoma.

Meningioma is the most common adult primary CNS tumour (WHO Grade I-III), which predominantly affects older women, and only 1-5% of cases are children (276). Meningiomas are predominantly benign and low-grade tumours arising from meningeal cells within the meningeal tissue layers that encase and protect the CNS. ZIKV infection induces a significant but modest cell viability reduction (approximately 25%) in two adult meningioma cell lines (CH-157MN and IOMM-LEE) at 72 hpi (250). Despite this modest oncolytic response, intrathecal (spinal canal) ZIKV administration to an adult female canine with a naturally occurring intracranial meningioma led to tumour infection, reduced tumour volume, necrosis, immune cell infiltration, and clinical improvement (264).

1.4.3 Anti-tumoural immune response

In **Section 1.4.2**, a notable capability of ZIKV to infect and lyse nervous system tumour cells was discussed. Most of these studies, however, primarily assess direct oncolysis, whose efficacy is often inferior to that of the anti-tumoural immune response. ICD and the secretion of cytokines from OV-infected tumours recruit an array of immune cells to the tumour to orchestrate anti-tumour immunity. Intrathecal ZIKV administration to three canines with naturally occurring brain tumours elevated cytokine IL-8, CCL2 and KC-like levels in the CSF of all canines and in the serum of two canines (264). Additionally, ZIKV infection of canine glioblastoma cells *in vitro* significantly increased secretion of IL-2, IL-6, IL-7, IL-15 and CXCL10 (264). ZIKV-infected canines present with extensive immune cell infiltration and pseudoprogression, likely in response to ICD and this cytokine response, accompanied by reduced clinical symptoms and improved OS (264). ZIKV-induced tumoural immune cell infiltration has been documented to include lymphocytes, such as CD4+ and CD8+ T cells, and myeloid cells, such as monocytes/macrophages, DCs, and microglia.

In immunocompetent glioma mouse models, ZIKV infection induces a robust T cell immune response by stimulating the infiltration of cytotoxic CD8+ and CD4+ T cells (271,277). CD8+ and CD4+ T cells persist after ZIKV clearance from the brain, indicating a sustained immune response (271,277). Combining ZIKV infection with CD8+ or CD4+ T cell depletion demonstrated that (i) T cells moderate tumour ZIKV levels, (ii) CD4+ T cells stimulate CD8+ T cell activity, and importantly, (iii) ZIKV-induced tumour clearance is dependent on both CD8+ and CD4+ T cells (271,277). Additionally, long-term mouse glioma survivors present with memory CD8+ T cells or effector, effector memory and CD69-activated CD4+ T cells that protect against tumour rechallenge (266,277). Thus, CD8+ and CD4+ T cells are central to the ZIKV anti-tumoural

immune response and can generate long-term immunity. ZIKV infection also leads to reduced levels of tumour-associated Tregs and transient infiltration of NK and natural killer T (NKT) cells, but their involvement is unknown (271,277).

Myeloid cells such as monocytes/macrophages, DCs, and microglia play important roles in antitumoural immunity. ZIKV-infected mice and canine brain tumours present with monocyte/macrophage infiltration, with macrophages in a pro-inflammatory M1 state (264,277). Canine glioblastoma cells co-cultured with canine monocytes specifically secrete IL-8, CCL2, and KC-like cytokines and activate monocytes following ZIKV infection (264). This implies that a monocyte/macrophage-mediated immune response is raised against canine brain tumours following ZIKV administration. ZIKV infection in a glioma mouse model elevated DC maturation and activity levels, implying that DCs may contribute to ZIKV-induced tumour clearance through antigen presentation (271). Additionally, in long-term mouse glioma survivors treated with a combination of ZIKV and a tumour vaccine, increased DC levels were observed following tumour rechallenge, alongside increased microglia (266). Interestingly, whilst ZIKV infection of glioma-associated myeloid cells promotes a pro-inflammatory state, the myeloid cells secrete Type I IFN (IFN beta) to render glioma resistant to ZIKV infection by stimulating glioma cell JAK/STAT signalling (230). A mechanism through which ZIKV may combat this antiviral response in vivo is through decreasing tumour-associated MDSCs, as observed in immunocompetent mouse glioma models (271). Neutrophils do not appear to be involved in the mechanism of oZIKV therapy (277). Thus, myeloid cells are involved in oZIKV therapy but vary in their function and contributions to supporting or suppressing anti-tumoural immunity.

In summary, ZIKV is efficacious against both paediatric and adult nervous system tumours through direct tumour cell oncolysis and also for adult nervous system tumours through inducing anti-tumoural immune responses. It is entirely unknown if or how ZIKV may mediate an immune response against paediatric nervous system tumours. An investigation into the components that may orchestrate this immune response is deeply warranted (**Chapters 3 and 4**).

1.4.4 Safety and practicality for paediatric patients

The progression of any novel therapeutic into a clinical trial is governed by its safety profile demonstrated throughout preclinical research. A thorough assessment of off-target effects on cells and tissues informs approaches to modify the therapy to mitigate toxicity whilst maintaining efficacy. Due to ZIKV neurotoxicity, assessing infection of normal CNS cells, particularly NPCs, alongside tumour cells is fundamental for assessing and addressing potential safety concerns. Several studies report preferential targeting of ZIKV for tumour cells

over normal neural cells, and this is exemplified by the preferential tumour tropism over neurotoxicity documented in canines bearing natural brain tumours (249,250,256,264). Notably, ZIKV selectively infects and kills tumour cells with minimal toxicity to normal cells within human cerebral organoids infiltrated with four different brain tumour cell lines (250,256).

Cancer patients are frequently immunosuppressed following standard-of-care therapy, and several safety concerns arise regarding treatment with replication-competent OVs. The immunodeficient nature of xenograft mice model the patient's immunosuppressed nature to some degree. Intratumoural ZIKV administration to immunodeficient mouse models bearing medulloblastoma, ATRT, or neuroblastoma is asymptomatic with limited and non-permissive viral shedding and doesn't cause adverse effects or neurological damage (249,256,262). However, viral shedding and infection of normal cells and tissues in a murine model do not fully recapitulate that of the human body. Due to these reasons, the oZIKV safety profile needs to be improved, which can be achieved through genetic engineering. Flaviviral RNA genomes are generally resistant to large genetic modifications (278). As such, current genetic engineering approaches for oZIKV therapy predominantly employ small nucleotide changes. ZIKV infection of normal cells has been repressed by (i) ZIKV NS5 mutation to inhibit replication in Type I IFNresponsive cells, (ii) miRNA response element addition to sensitise ZIKV to non-tumour miRNA, and (iii) CpG-recoding to sensitive ZIKV to non-tumour antiviral proteins (243,254,279). Repurposed live attenuated vaccines, or ZIKV attenuation by gamma irradiation or inhibition of Envelope protein glycosylation, have proved viable methods to improve oZIKV safety (265– 267,277,280). Abolishing Aedes mosquito infection capability mitigates oZIKV transmission by cancer patients in regions where Aedes mosquitoes reside (265,281). Pseudotyped viruses reduce ZIKV pathology and circumvent genome size restriction by possessing a different viral core whilst retaining ZIKV prM/E envelope-mediated glioma tropism in vitro (282–284).

Efficacy can be bolstered through multimodal treatment of synergistic therapies. With its CSC targeting capability and ability to remodel the TIME, employing ZIKV as an adjuvant alongside standard therapy or immunotherapy holds great promise. ZIKV sensitises drug-resistant glioma cells to standard-of-care TMZ chemotherapy, AKT inhibitors and CDK4/6 inhibitors *in vitro*, and to immunotherapy *in vivo* (243,266,267,271,277,285). Interestingly, low SLFN11 expression confers resistance of GSCs to TMZ but also sensitises them to ZIKV oncolysis (286). ZIKV remodelling of the immunosuppressive TIME sensitises mouse glioma to PD-1 and PD-L1 immune checkpoint blockade and to tumour vaccination (266,271,277). All three combination immunotherapy regimens reported good safety profiles and significantly improved OS *in vivo*. Crucially, all three also generated adaptive anti-tumoural immune memory that protected survivors against tumour rechallenge. To conclude, ZIKV demonstrates acceptable safety in mouse models. While genetic engineering attempts to improve oZIKV safety are accompanied

by reduced anti-tumoural efficacy, ZIKV efficacy can be bolstered by combination with standard therapy or immunotherapy.

1.5 Large data and omics as powerful tools to investigate cellular and viral biology

The development of omics techniques has revolutionised our understanding of biological systems. The datasets they yield are invaluable tools for investigating and characterising the molecular foundations and building blocks that make up biological systems, principally DNA, RNA, proteins, or metabolites (287). Coupling these datasets with computational and bioinformatic approaches allows for the thorough exploration, analysis, integration, and visualisation of the datasets. Each omics technique allows an unbiased and in-depth analysis of that omics layer to inform the development of testable hypotheses. The response of a cell to a stimulus such as viral infection propagates throughout the cells, altering cellular behaviour through contributions made by multiple omics layers (288). Considering the global response of the cell at one of these layers allows comprehensive analysis of the response within that layer and can sometimes infer the response at other layers. Generating datasets that investigate different omics layers enables their integration to yield more extensive insight than can be achieved by analysing the individual datasets alone (289).

Since the 2015 Brazilian outbreak, a multitude of large data and omics datasets have been generated to assess ZIKV infection of NPCs, or to compare patients born with CZS against those without CZS. These datasets include but are not limited to, transcriptomics, expression proteomics, methylomics, metabolomics and whole genome CRISPR-Cas9 screens (193,290–295). These are but a few of the powerful datasets that have significantly contributed to our current knowledge and understanding of intracellular mechanisms and their complex interplay in orchestrating CZS development. A caveat to this current work is that, to my knowledge, not a single omics dataset exists to assess ZIKV infection in NPCs derived specifically from patients affected by CZS. Previous work by my collaborators at the University of São Paulo (USP) showed that genetics may, in part, contribute to the susceptibility for developing CZS following ZIKV infection (193). A more thorough understanding of how intracellular mechanisms may contribute to NPC susceptibility to ZIKV infection is required, and I address this in **Chapter 3** by generating the first RNA-Seq datasets of ZIKV-infected NPCs derived from CZS patients.

Since Zhu et al. first described ZIKV oncolysis of adult glioma in 2017, a small collection of omics datasets has been generated to investigate the differential responses of adult glioma cells to ZIKV infection to investigate its therapeutic potential (230,265,268). Despite ZIKV demonstrating a strong oncolytic potential against paediatric nervous system cancers, no such

omics datasets exist to investigate the molecular mechanisms involved in ZIKV oncolysis of paediatric nervous system cancers. In **Chapters 2 and 3**, I perform these investigations. ICD and consequential induction of an anti-tumoural immune response are essential contributors to oncolytic virotherapy efficacy. I investigate these by generating large data and omics datasets in **Chapters 3 and 4**.

1.6 Research hypothesis, aims and objectives

1.6.1 Research Hypothesis

I hypothesise that integrating omics techniques with bioinformatic approaches to investigate the response of nervous system tumour cells to ZIKV infection will support its development as an oncolytic virotherapy by revealing key molecular mechanisms, biological processes and pathways implemented in ZIKV-induced oncolysis and anti-tumoural immune responses.

1.6.2 Chapter 2 aims and objectives

Due to the vast information that can be drawn from a single omics dataset, its analysis is commonly tailored towards investigating a specific hypothesis. As such, omics datasets are frequently published with many biologically relevant and clinically interesting discoveries yet to be made. This permits computational biologists to employ *in silico* and systems-based approaches to re-analyse and integrate these datasets to yield novel discoveries (296). In neuroscience, neuroblastoma cell lines such as SH-SY5Y are frequently used to model neural cells *in vitro* because they are immortalised, they divide rapidly, and they possess neural characteristics (297,298). As such, neuroblastoma cells have been extensively used to model how ZIKV dysregulates neural cells and infer how infection leads to CZS. Multiple omics datasets have been generated for this purpose, but none have been analysed from an oncological perspective to investigate how ZIKV may dysregulate and lyse these cancer cells. To date, the therapeutic potential of ZIKV against neuroblastoma has drawn the attention of only one other group. This group demonstrated that ZIKV oncolysis of neuroblastoma occurs *in vitro* and *in vivo*, and its dependency on CD24 expression is the only molecular mechanism known to be involved in this response to date (251,261,262).

Research Aim 1. Re-analyse pre-existing resources and datasets from an oncological perspective to investigate ZIKV as an oncolytic virus in neuroblastoma cells and to identify the molecular mechanisms involved.

Objective 1.1. Assess ZIKV infection assay data in all relevant published literature to (i) determine susceptibility across neuroblastoma cell lines to ZIKV infection and (ii) identify which ZIKV strains present as top candidates for neuroblastoma oncolytic virotherapy.

Objective 1.2. Re-analyse RNA-Seq data of Mock and ZIKV-infected SH-SY5Y cells to identify ZIKV-induced differentially regulated genes and pathways.

Objective 1.3. Mine datasets and databases pertaining to ZIKV infection of neuroblastoma (interaction proteomics, CRISPR datasets and compound datasets) in an attempt to validate results drawn from Objective 1.2.

1.6.3 Chapter 3 aims and objectives

To date, oncolytic ZIKV research has been heavily dominated by adult glioma due to its high incidence and lethality. In contrast, very minimal research has sought to elucidate the biology governing paediatric brain tumour cell ZIKV oncolysis, and no omics datasets currently exist for this purpose (249). In the absence of these datasets, the only intracellular factor currently known to regulate ZIKV infection in paediatric brain tumour cells is WNT signalling (249,262). Additionally, it is unknown whether extracellular factors, such as the secretome, are involved in and contribute to ZIKV oncolysis of these cells.

Research Aim 2. Employ large data approaches to identify molecular mechanisms and investigate their involvement in oncolytic ZIKV infection of paediatric brain tumour cells.

Objective 2.1. Generate RNA-Seq data of ZIKV-infected brain tumour cells and employ bioinformatic approaches to identify ZIKV-induced differentially regulated genes and pathways of interest for validation in the brain tumour cells.

Objective 2.2. Validate key findings from Objective 2.1: (i) perform *in vitro* assays to determine how the TNF signalling pathway is involved in oZIKV infection, and (ii) perform a large multiplex ELISA assay to define the oZIKV-induced secretome from paediatric brain tumour cells.

Objective 2.3. Employ *in silico* approaches to re-analyse publicly available scRNA-Seq datasets to model and predict the responses of the human immune system to paracrine and endocrine signalling by the oZIKV-induced secretome from brain tumour cells.

1.6.4 Chapter 4 aims and objectives

ZIKV infection stimulates the infiltration of cytotoxic CD8+ T cells into adult glioma, which is central to the ZIKV anti-tumoural immune response and tumour destruction (271,277). A critical component that governs cytotoxic CD8+ T cell activity during OV therapy is the recognition of

Chapter 1

viral peptides presented on the surface of infected tumour cells by HLA class I complexes. It is currently unknown whether paediatric brain tumour cells present viral peptides following ZIKV infection. Identifying the components, such as HLA-presented antigens, that are involved in cytotoxic CD8+ T cell activation following ZIKV infection of brain tumour cells will provide molecular insights into how oZIKV therapy mounts an anti-tumoural immune response.

Research Aim 3. Investigate whether paediatric USP7 brain tumour cells present ZIKV peptides via HLA molecules on their cell surface.

Objective 3.1. Perform global proteomics mass spectrometry of Mock and ZIKV-infected USP7 brain tumour cells to determine whether antigen processing and presentation processes are enriched following infection.

Objective 3.2. Perform immunopeptidomics of Mock and ZIKV-infected USP7 cells to identify endogenous and ZIKV-derived peptides, and to determine from which ZIKV proteins the HLA-presented peptides arise.

Objective 3.3. Apply standardised bioinformatic techniques to predict (i) which HLA allotypes present the ZIKV peptides, (ii) which ZIKV peptides are strong binders, and (iii) which ZIKV peptides are immunogenic.

1.7 Figures

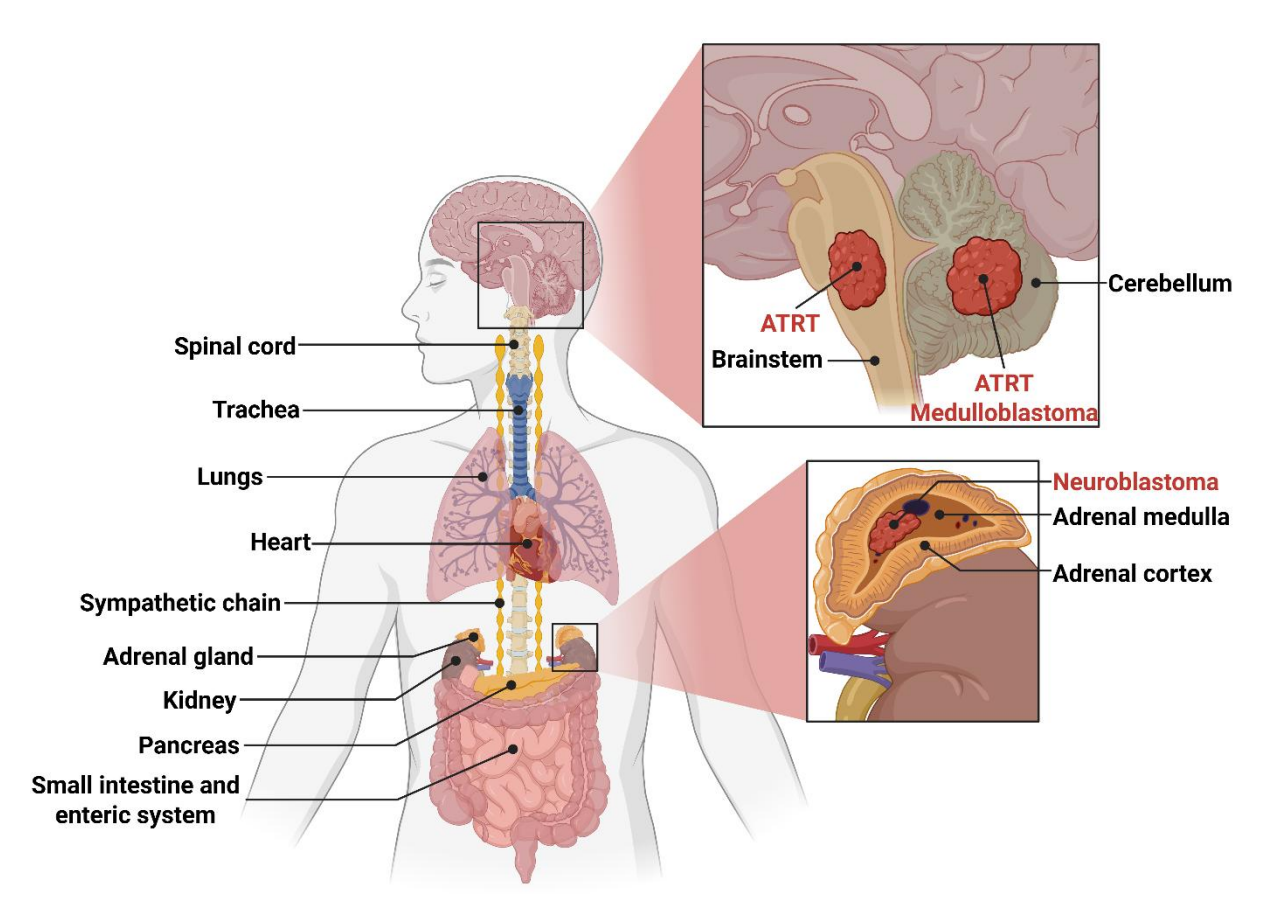


Figure 1. 1. Primary anatomical locations of medulloblastoma, ATRT and neuroblastoma development.

Figure depicting the general human anatomy with close-ups of the primary locations where medulloblastoma, ATRT and neuroblastoma develop. Neuroblastoma is a peripheral nervous system tumour and primarily forms in the adrenal glands. Medulloblastoma and ATRT are both central nervous system tumours, and both mainly form in the cerebellum of the posterior fossa. The brainstem is an additional key site of ATRT development. Figure created using BioRender. BioRender.com/u63c617. Abbreviations, atypical teratoid rhabdoid tumour (ATRT).

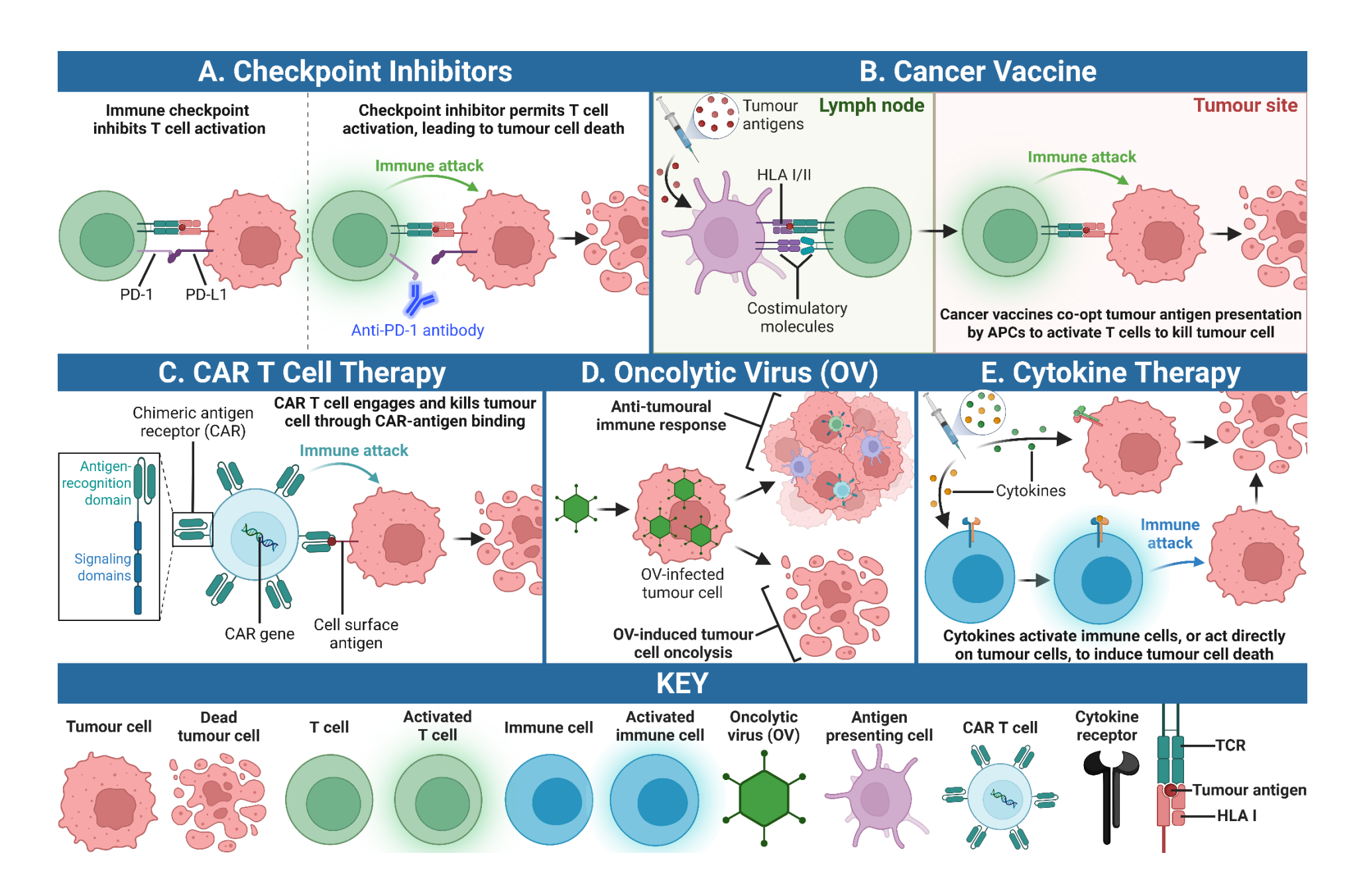


Figure 1. 2. Immunotherapeutic strategies to target the immune system against cancer.

Schematic of the five main forms of immunotherapy, showing how each targets the immune system against tumour cells. (A) PD-1 checkpoint protein targeting by anti-PD-1 demonstrates how immune checkpoint inhibitors specifically target antigen binding to promote anti-tumour immune responses. (B) Cancer vaccines co-opt the tumour antigen presentation capabilities of antigen-presenting cells (APCs) to induce T cell responses against tumour cells. (C) CAR T cells are modified to express a chimeric antigen receptor (CAR) that recognise and bind tumour cell antigens, leading to the induction of an anti-tumoural immune response. (D) Oncolytic viruses specifically infect and induce cancer cell oncolysis, in addition to raising an anti-tumoural immune response against the infected tumour. (E) Cytokine therapies directly employ anti-proliferative or pro-apoptotic properties on cancer cells to impair tumour growth, or they stimulate immune cell activity against tumour cells. Figure created using BioRender.

BioRender.com/u63c617. Abbreviations, Oncolytic virus (OV), Chimeric antigen receptor (CAR), antigen-presenting cells (APCs), T cell receptor (TCR), Human leukocyte antigens class I (HLA I).

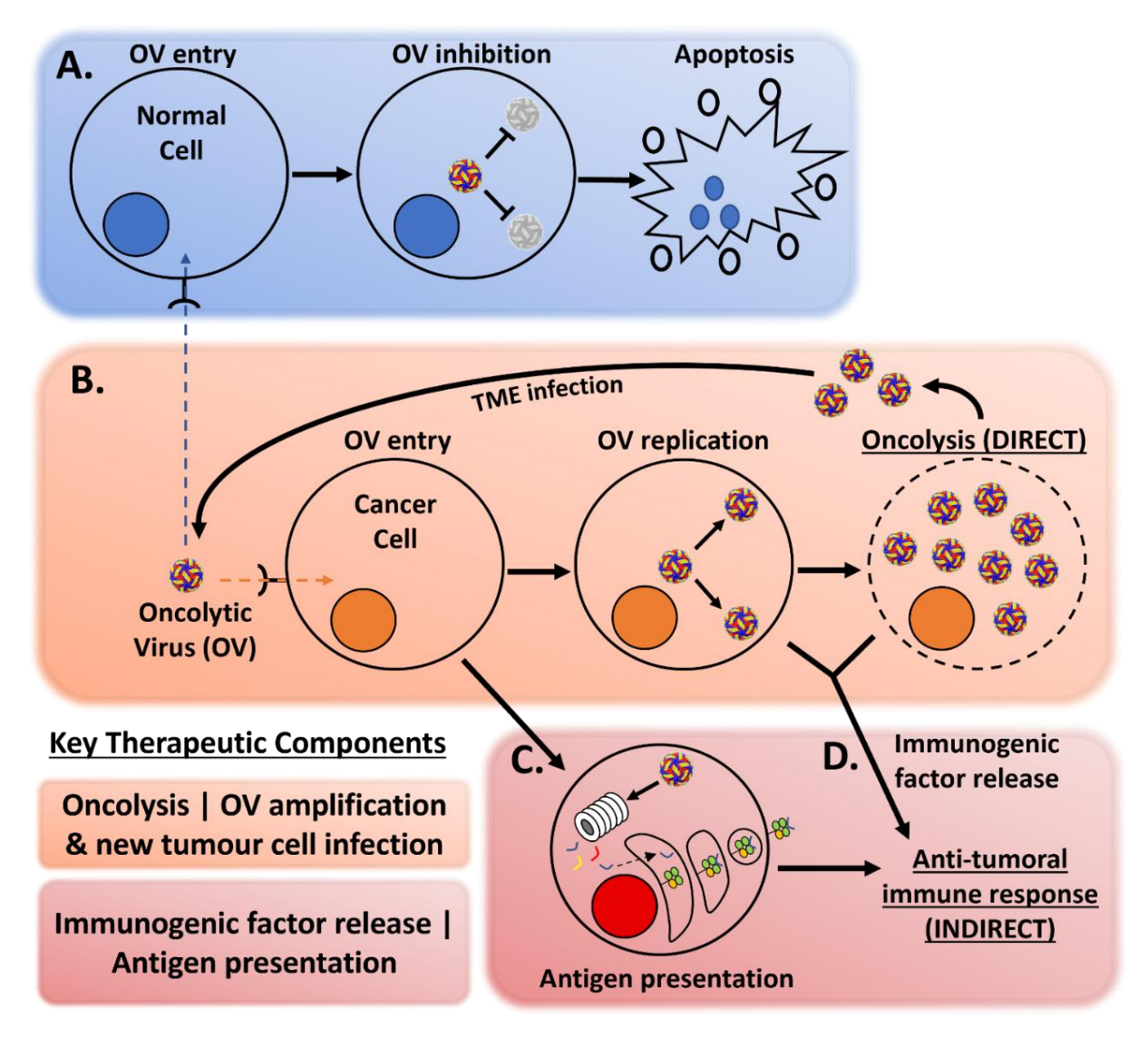
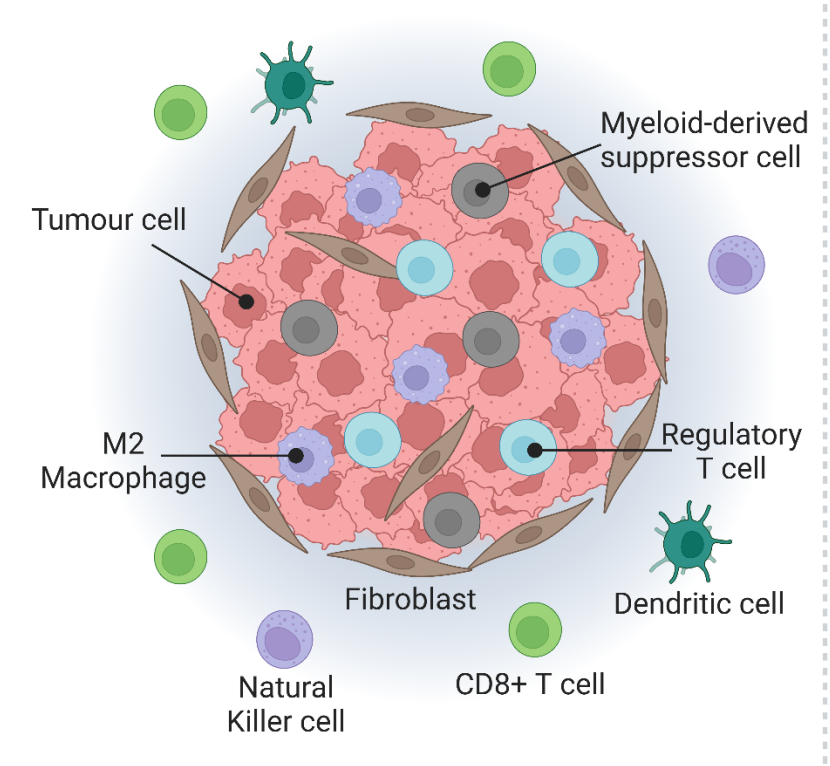


Figure 1. 3. Oncolytic virotherapy dual mechanism of action.

(A) Oncolytic virus infects a normal cell and cannot replicate due to the antiviral responses, leading to impaired cell growth and programmed cell death. (B) Oncolytic virus infects a cancer cell and, if able to replicate due to insufficient antiviral responses, will lead to oncolysis (direct cell death). Oncolysed cancer cells release fresh virions into the TME to infect neighbouring tumour cells. An anti-tumoural immune response (indirect cell death) will be raised against (C) the viral peptides presented by HLA complexes on the surface of infected cancer cells and (D) the immunogenic cellular factors released by infected and oncolysed cancer cells. Figure adapted from Kaid et al. 2021 (260). Abbreviations, Oncolytic virus (OV), Tumour microenvironment (TME), Human leukocyte antigens (HLA).

A Immunologically "Cold" Tumour



- Active anti-tumoural immune cells absent from tumour
- · Immunosuppressive immune cells present in tumour
- Poor response to standard-of-care therapy

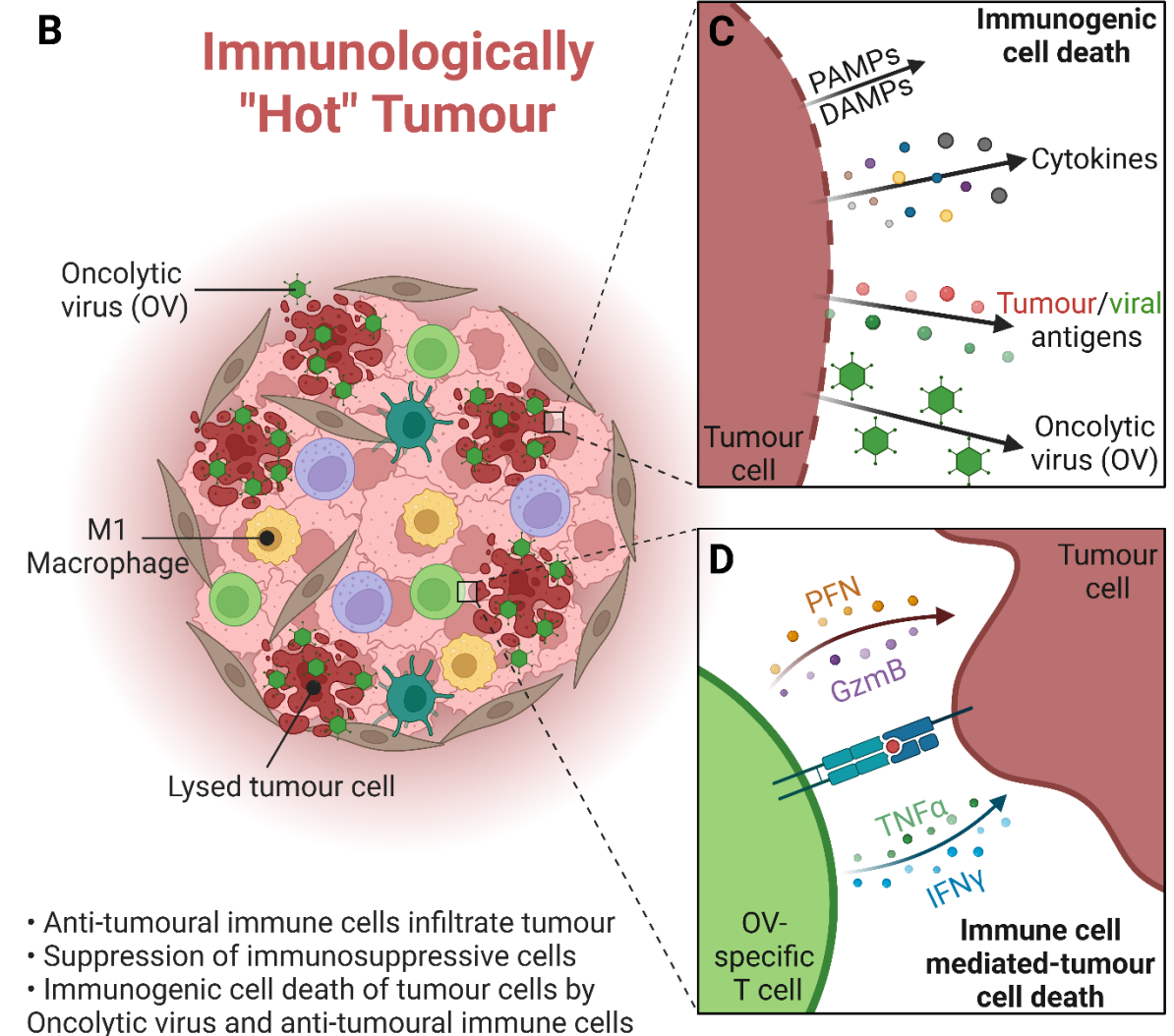


Figure 1. 4. Oncolytic viruses (OVs) heat up the Tumour immune microenvironment (TIME).

(A) Immunologically "cold" tumours present with immunosuppressive immune cells such as M2 Tumour-associated macrophages (TAMs), Myeloid-derived suppressor cells (MDSCs) and Regulatory T cells (Tregs), which promote a suppressed immune environment and reduce responsiveness to standard-of-care therapy. (B) OVs remodel and heat up the TIME by causing the release of multiple cellular factors, leading to the recruitment, infiltration and activation of immune cells. (C) OV-induced immunogenic tumour cell death releases immunogenic factors, which initially recruit and stimulate innate immune cells. (D) OVs generate adaptive immune responses, such as cytotoxic CD8+ T cell-induced tumour cell lysis in response to tumour/viral antigen presentation. OV-induced changes in immune cells phenotypes (M2 to M1 macrophage transition) and reductions in immunosuppressive immune cells contribute to the shift from a "cold" to a "hot" tumour state. Figure created using BioRender. BioRender.com/u63c617. Abbreviations, Oncolytic virus (OV), Tumour-associated macrophage (TAM), Myeloid-derived suppressor cell (MDSC), Regulatory T cell (Treg), Tumour immune microenvironment (TIME), Perforin (PFN), Granzyme B (GzmB), Tumour necrosis factor α (TNFα), Interferon γ (IFNγ), Damage-associated molecular patterns (DAMPs), Pathogen-associated molecular patterns (PAMPs).

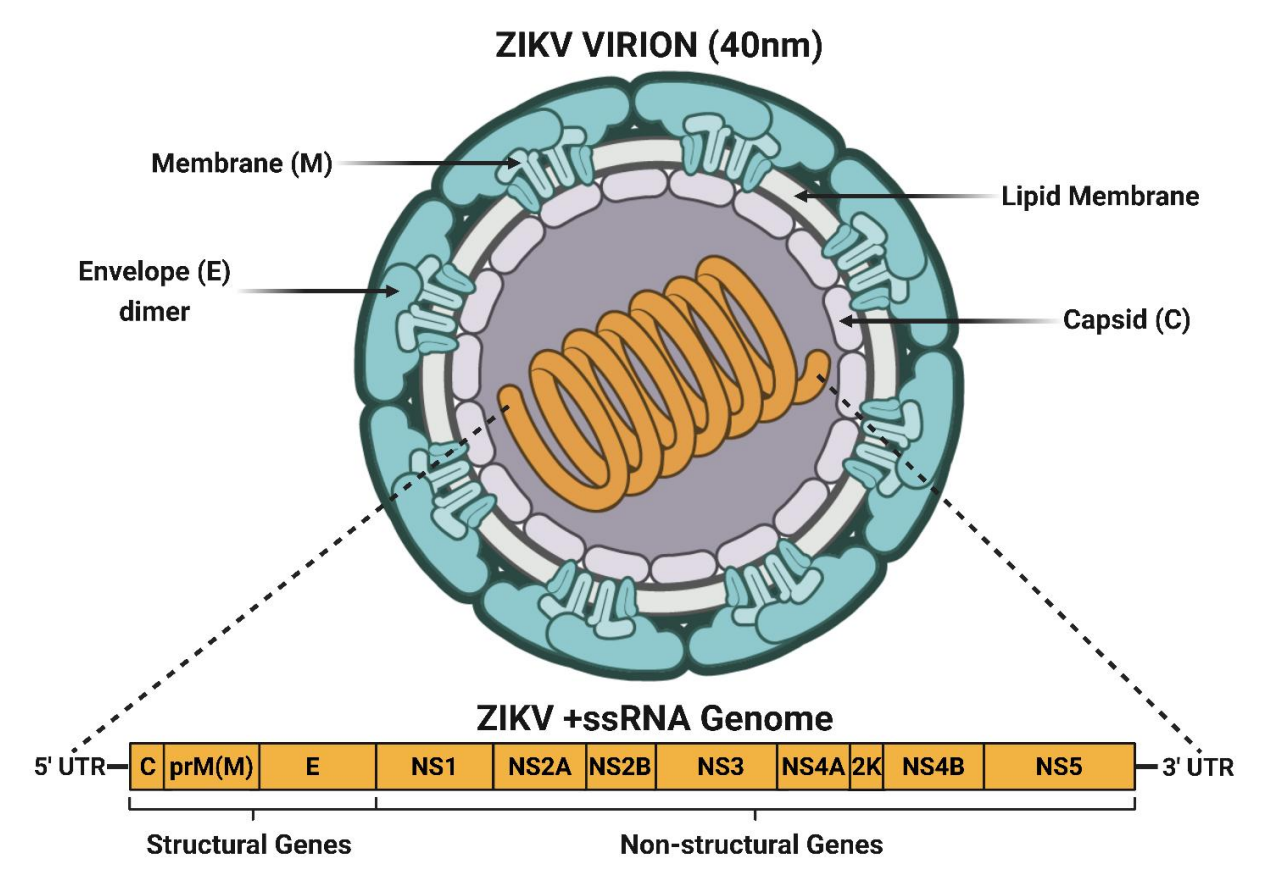


Figure 1. 5. ZIKV structure and genome organisation.

ZIKV virions comprise a nucleocapsid, surrounded by a lipid membrane densely packed with envelope (E) and membrane (M) proteins. Within the nucleocapsid, the +ssRNA genome encodes three structural viral proteins and seven non-structural viral proteins, flanked by untranslated regions (UTRs). ZIKV genome not to scale. Figure created using Bioart and BioRender. BioRender.com/u63c617. Abbreviations, Zika virus (ZIKV), positive-sense single-stranded RNA virus (+ssRNA), untranslated region (UTR), Capsid (C), Membrane (M), Envelope (E), non-structural (NS) proteins (NS1-5).

ZIKV Infection Life Cycle ZIKV Viral E protein recognition and binding to host membrane receptor New virion released into the microenvironment Host receptor Receptormediated endocytosis 8 Viral egress Internalisation into the 3 endosomal-lysosomal system pH-driven release of +ssRNA genome into cytosol Viral protein translation into ER membrane and lumen Viral Viral maturation assembly through prM to M cleavage Golgi Viral RNA Ribosome _ Endoplasmic reticulum (ER) Nucleus

Figure 1. 6. ZIKV Infection Life Cycle.

Viral E protein recognises and binds host cell receptors, leading to internalisation by receptor-mediated endocytosis into the endosomal-lysosomal system. A reduced pH drives membrane fusion, and following nucleocapsid degradation, the viral genome is released into the cytosol, where it is recruited to the ER by host cell translational machinery. Viral genome translation leads to rapid de novo ZIKV protein synthesis into the ER membrane and lumen, and immature virions form in viral replication and assembly compartments. Immature virions are transported through the Golgi, where the prM protein is cleaved to M protein to form mature infectious viral particles. Virions egress and are released into the microenvironment for subsequent infection. Figure created using Bioart and BioRender. BioRender.com/u63c617. Abbreviations, Zika virus (ZIKV), positive-sense single-stranded RNA virus (+ssRNA), Pre-membrane (preM), Membrane (M), Envelope (E), Endoplasmic reticulum (ER).

1.8 Tables

Table 1. 1. Medulloblastoma and ATRT brain tumour molecular subgroups and subtypes

		Subgroup				
Tumour Type	Name	Molecular Markers	Name	Molecular Markers	References	
		CTNNB1, DDX3X, SMARCA4,	WNTa	Monosomy 6		
	WNT	TP53APC, CSNK2B and EPHA7	WNTβ	No Monosomy 6		
			SHHα (SHH1)	TP53 and ELP1		
		PTCH1, TERT, TP53, SUFU, ELP1 and	SHHβ (SHH2)			
	SHH	U1 snRNA	SHHy (SHH3)	SUFU		
			SHHδ (SHH4)	SMO and TERT promoter		
Medulloblastoma	Group 3		Group 3a	Chromosome 8q	(14,17,19,20,23,29	
		MYC, GFI1, GFI1B, SMARCA4, OTX2 and KBTBD4	Group 3β	OTX2, GFI1 and GFI1B		
		and KBTBB4	Group 3γ	MYC		
	Group 4		Group 4a	MYCN		
		KDM6A, MYCN, CDK, PRDM6 and	Group 4β	SNCAIP and GFI		
		CBFA2T2	Group 4γ	CDK6, chromosome 8p and chromosome 7q		

		Subgroup		References	
Tumour Type	Name	Molecular Markers	Name		
	SHH		SHH-1A	N/A	
		SMARCB1 and MYCN	SHH-1B	N/A	
Atypical teratoid rhabdoid			SHH-2	N/A	(24,34,38,39)
tumour (ATRT)	TYR	SMARCB1, TYR, TYRP, MITF, BMP4, OTX2, PDGFRB and Chromosome 22		(= ,,= ,,= ,,= ,,	
	MYC	SMARCB1, MYC and HOX			

Abbreviations, atypical teratoid rhabdoid tumour (ATRT), wingless/integrase-1 (WNT), sonic hedgehog (SHH), tyrosinase (TYR), myelocytomasis oncogene (MYC), not applicable (N/A).

Table 1. 2. Molecular markers for neuroblastoma stratification into INRGSS and treatment groups

INRGSS Group	Treatment Group	Molecular Markers	References
	Low Risk	MYCN-	
L1	High Risk	MYCN+	
	Intermediate Risk	MYCN- WITH DI ≥ 1 AND/OR SCA±	
L2	High Risk	MYCN+	
		MYCN- (age < 12 months)	
	Intermediate Risk	MYCN- WITH DI > 1 AND SCA- (age 12-18 months)	
M		MYCN+	(51)
	High Risk	MYCN- WITH DI = 1 OR SCA+ (age 12-18 months)	
	Low Risk	MYCN- WITH DI > 1 AND SCA- (age < 12 months)	
		MYCN- WITH DI = 1 OR SCA+ (age < 12 months)	
MS	Intermediate Risk	MYCN- WITH DI > 1 AND SCA- (age 12-18 months)	
		MYCN+	
	High Risk	MYCN- WITH DI = 1 OR SCA+ (age 12-18 months)	

Molecular markers were extracted from Irwin et al., 2021, Figure 1 (51). Patient age is indicated where it is important for treatment group classification using molecular markers; however, other non-biomarker risk classifiers have not been included. Segmental chromosome aberrations (SCA) refer to alterations to chromosomes 1p and 11q. DNA Index (DI) refers to whether cancer cells are diploid (DI = 1) or hyperdiploid (DI > 1). Abbreviations, International Neuroblastoma Risk Group Staging System (INRGSS), MYCN amplified (MYCN+), MYCN non-amplified (MYCN-), segmental chromosomal aberration (SCA), DNA Index (DI).

Table 1. 3. Oncolytic virotherapy clinical trials for paediatric brain tumour and neuroblastoma patients

Viral Family	OV Name	Delivery Route	Trial Number	Trial Status	Trial Phase	Paediatric Tumour Type	Patient Number	Median OS	Adverse Events	References
/ taonoviriado	Ad-TD- nsIL12	IT	NCT05717712	Recruiting	1	DMG	18	NA	NA	
		IT	NCT05717699	Recruiting	1	DMG	18	NA	NA	
	DNX-2401	IT	NCT03178032	Completed	1	DMG	12	17.8 months	≤ Grade 3	(116)
(DNA)		IV	NCT04758533	Recruiting	1	Medulloblastoma or DMG	12	NA	NA	
	ICOVIR-5	IV	NCT01844661	Completed	1	Metastatic and Refractory Solid Tumours	15	NA	Grade 1	(128)
Herpesviridae (DNA)	G207	IT	NCT02457845	Completed	1	HGG	12	12.2 months	Grade 1	(117)
		IT	NCT03911388	Active, not recruiting	1	Cerebellar brain tumour (including Medulloblastoma or ATRT)	24	NA	NA	(300)
		IT	NCT04482933	Not yet recruiting	2	HGG	40	NA	NA	
	HSV1716	IT	NCT02031965	Terminated	1	HGG	2	NA	NA	
Paramyxoviridae (RNA)	MV-NIS	IT/LP	NCT02962167	Completed	1	Medulloblastoma or ATRT	34	NA	NA	

Viral Family	OV Name	Delivery Route	Trial Number	Trial Status	Trial Phase	Paediatric Tumour Type	Patient Number	Median OS	Adverse Events	References
Paramyxoviridae (RNA)	NDV-HJU	IV	NCT01174537	Withdrawn	1/2	Glioblastoma	14	7.4 months	≤ Grade 2	(118)
Picornaviridae (RNA)	PVSRIPO	IT	NCT03043391	Completed	1	Medulloblastoma, ATRT or WHO Grade III or IV Glioma	8	4.1 months	≤ Grade 3	(119)
Reoviridae (RNA)	Pelareorep	IV	NCT02444546	Completed	1	Medulloblastoma, ATRT, Glioma or PNET	6	3.6 months	≤ Grade 3	(120)
Picornaviridae (RNA)	NTX-010	IV	NCT01048892	Completed	1	Neuroblastoma, Rhabdomyosarcoma, or Rare Neuroendocrine Tumour	22	NA	≤ Grade 3	(121)
Poxviridae (DNA)	Pexa-Vec	IT	NCT01169584	Completed	1	Non-CNS Solid Tumour (including Neuroblastoma)	6	NA	≤ Grade 3	(122)

Abbreviations, oncolytic virus (OV), overall survival (OS), intratumoural (IT), intravenous (IV), lumbar puncture (LP), atypical teratoid rhabdoid tumour (ATRT), diffuse midline glioma (DMG), high-grade glioma (HGG), World Health Organisation (WHO), Primitive Neuro-Ectodermal Tumour (PNET), central nervous system (CNS) and not applicable (NA).

Chapter 2 Integrated re-analysis of transcriptomic

and proteomic datasets reveals potential

mechanisms for Zika viral-based oncolytic therapy

in neuroblastoma

Matt Sherwood¹, Yilu Zhou¹, Yi Sui¹, Yihua Wang¹, Paul Skipp¹, Carolini Kaid², Juliet Gray³, Keith Okamoto², Rob M. Ewing¹

Author affiliations:

¹ School of Biological Sciences, Faculty of Environmental and Life Sciences, University of

Southampton, Southampton, England, SO17 1BJ, UK

² Human Genome and Stem-Cell Center (HUG-CELL), Biosciences Institute, Universidade de

São Paulo, São Paulo, State of São Paulo, Brazil

³ Centre for Cancer Immunology, Faculty of Medicine, University of Southampton,

Southampton, England, UK

Contact Author

Professor Rob M. Ewing

B85, Life Sciences Building

University of Southampton

University Road

Highfield

Southampton, Hants.

SO17 1BJ

Tel No: +44(0)2380 59 5503

email: rob.ewing@soton.ac.uk

2.1 **Authorship Statement**

This chapter is the product of: Sherwood M, Zhou Y, Sui Y, Wang Y, Skipp P, Kaid C, et al.

Integrated re-analysis of transcriptomic and proteomic datasets reveals potential mechanisms

for Zika viral-based oncolytic therapy in neuroblastoma. F1000Res. 2024 May 21;12:719.

68

Matthew Sherwood initially conceptualised the study, and jointly planned it with Rob M. Ewing. Matthew Sherwood performed all aspects of literature searching, data mining and data analysis, apart from receiving assistance in downloading and processing the RNA sequencing (RNA-Seq) dataset from Yilu Zhou. Matthew Sherwood performed the investigation, created Figures 2.1-2.7, created all tables, and wrote the manuscript in its entirety. Matthew Sherwood drafted, and Yi Sui produced, Figure 2.8. Rob M. Ewing, Keith Okamoto and Juliet Gray supervised the study, and reviewed the finalised manuscript alongside Yihua Wang, Paul Skipp and Carolini Kaid. Matthew Sherwood, Rob M. Ewing, Oswaldo K. Okamoto and Juliet Gray acquired funding for the study.

Supplementary material for this chapter can be found in **Appendix A**.

2.2 Abstract

Paediatric neuroblastoma and brain tumours account for a third of all childhood cancer-related mortality. High-risk neuroblastoma is highly aggressive, and survival is poor despite intensive multimodal therapies. These therapies have significant toxicity, and novel treatments are desperately needed. Zika virus (ZIKV) can access the nervous system, and there is growing interest in employing ZIKV as a potential therapy against paediatric nervous system tumours, including neuroblastoma. Here, we perform extensive data mining, integration and re-analysis of ZIKV infection datasets to highlight molecular mechanisms that may govern the oncolytic response in neuroblastoma cells. We collate infection data of multiple neuroblastoma cell lines by different ZIKV strains from a body of published literature to inform neuroblastoma susceptibility to ZIKV oncolysis. Integrating publicly available transcriptomics, interaction proteomics, dependency factor and compound datasets, we propose the involvement of multiple host systems during ZIKV infection. Through data mining of published literature, we observed most paediatric neuroblastoma cell lines to be highly susceptible to ZIKV infection. We propose the PRVABC59 ZIKV strain as a leading candidate for neuroblastoma oncolytic virotherapy. ZIKV infection upregulates TNF signalling, lipid metabolism and the UPR, and downregulates cell cycle and DNA replication processes. ZIKV infection is dependent on sterol regulatory element binding protein (SREBP)-regulated lipid metabolism and three protein complexes: V-ATPase, endoplasmic reticulum (ER) Membrane Protein Complex (EMC) and mammalian translocon. We propose ZIKV non-structural protein 4B (NS4B) as a likely mediator of ZIKV interaction with IRE1-mediated UPR, lipid metabolism and mammalian translocon. Our work provides a significant understanding of ZIKV infection in neuroblastoma cells, which will

facilitate the progression of oncolytic ZIKV (oZIKV) therapy through pre-clinical research and clinical trials.

Keywords: Neuroblastoma, oncolytic virotherapy, Zika virus, transcriptomics, proteomics

Key points:

- ZIKV may provide the basis for oncolytic virotherapy against neuroblastoma
- Most paediatric neuroblastoma cell lines are susceptible to ZIKV infection
- We highlight molecular mechanisms that may contribute to the oncolytic response in neuroblastoma

Contribution to the field

The ability to both induce direct oncolysis and provoke an anti-tumoural immune response makes oncolytic virotherapy an attractive candidate to combat aggressive and heterogeneous cancers, such as high-risk neuroblastoma. To progress oncolytic virotherapy to clinical trial it is essential to understand the host mechanisms the virus manipulates to kill cancer cells, alongside any pathology resulting from infection of normal cells. Through data mining and reanalysing publicly available data, we observed that ZIKV efficiently infects and induces oncolysis of paediatric neuroblastoma cells, and we propose a potential TNF pathway-driven immune response. ZIKV's specificity for infection of nervous system cancer cells, while rarely causing nervous system-related pathology in young children, addresses many of its safety concerns. The inclusion of more effective and less toxic novel therapies, such as a potential oZIKV therapy, in multimodal treatment regimens will pave the way for improving paediatric patients' long-term health and overall survival.

2.3 Introduction

Neuroblastoma is the most common extracranial solid cancer in children, accounting for 6–10% of all paediatric cancers and disproportionately causing 12–15% of paediatric cancer-related deaths (10). It is an embryonal tumour originating from transformed cells of neural crest lineage and predominately forms in the adrenal medulla and paraspinal sympathetic ganglia. Whilst the majority of patients are diagnosed by the age of five years, the median age of patients is 18 months. Prognosis is highly heterogenous and can be predicted by several factors, including the presence of metastatic disease, age, chromosomal aberrations and molecular signatures, such as MYCN amplification (48). Patients are categorised according to internationally agreed risk groups, and treatment is stratified accordingly.

Outcome for low- and intermediate-risk neuroblastoma is good, with some patients requiring little or no treatment. However, approximately 50% of patients have high-risk disease for which prognosis is poor, with overall survival (OS) of less than 60% (51). Current high-risk neuroblastoma treatment regimens are aggressive. These include multiple rounds of induction chemotherapy, surgical resection, myeloablative chemotherapy, autologous stem cell transplantation and post-consolidation therapy such as immunotherapy (52). The aggressive nature of this regimen carries significant treatment-related mortality and frequently results in long-term sequelae impacting the quality of life for surviving patients. Consequently, there is a clear and unmet need for safer and less toxic treatment regimens to combat high-risk neuroblastoma.

Oncolytic virotherapy exploits viruses that preferentially infect and destroy cancer cells via two distinct routes of therapeutic action. Following infection, intense viral replication induces oncolysis, releasing virions into the tumour microenvironment (TME) to infect neighbouring tumour cells. Induction of a tumour-specific immune response is a crucial secondary mechanism employed by oncolytic virotherapy that can address highly heterogeneous tumours such as high-risk neuroblastoma and central nervous system (CNS) tumours. There is significant interest in combining immuno-modulating cancer therapies with oncolytic virotherapy to augment the anti-tumoural immune response. Oncolytic virotherapy clinical studies have, in general, reported low toxicity and minimal adverse effects in patients, mainly low-grade constitutional symptoms (301).

ZIKV is a mosquito-borne flavivirus consisting of historical African and epidemic-associated Asian lineages. The latter can access the CNS and may cause microcephaly in the developing fetus through infection of neural stem and progenitor cells, causing cell death and growth reduction (178,180). By contrast, ZIKV rarely causes adverse effects in children and adults, with the majority of cases being asymptomatic (215). In symptomatic children, ZIKV may cause short-term side effects, namely rash, fever and gastrointestinal symptoms, and in rare instances in adults can cause more severe conditions, such as Guillain-Barré syndrome (GBS), meningitis and encephalitis (215,233).

Since 2017, the concept of employing ZIKV as oncolytic virotherapy against brain tumours has gained momentum. ZIKV infection induces oncolysis of infected paediatric brain tumour cells *in vitro* and *in vivo*, and induces an immune response against spontaneous canine brain tumours (249,250,264). An initial study assessing ZIKV infection in multiple neuroblastoma cell lines demonstrated ZIKV's potential as a novel neuroblastoma oncolytic virotherapy (251). Here, we survey over 35 studies that have used neuroblastoma cell lines to model ZIKV infection. These

studies focused on understanding ZIKV pathology and assessing antiviral compounds. Through re-analysis and integration of the transcriptomics, proteomics and dependency factor screens from these studies, we propose multiple molecular mechanisms to be implicated in ZIKV infection of neuroblastoma which help to determine its potential as oncolytic virotherapy.

2.4 Methods

2.4.1 RNA sequencing data source and processing

RNA-Seq data files (.fastq.gz paired-end) were acquired from the European Nucleotide Archive (ENA) (accession: PRJNA630088). Bonenfant et al. generated this data by infecting SH-SY5Y cells in monolayer culture with ZIKV PRVABC59 at multiplicity of infection (MOI) 5 for 1 hour and collected RNA at 24 hours post-infection (hpi) via TRIzol extraction (302). RNA-seq libraries were prepared and sequenced using an Illumina NextSeq500. Our RNA-Seq processing pipeline consisted of FastQC (V0.11.9-0) (RRID:SCR_014583), Trim Galore (V0.6.6-0) (RRID:SCR_011847), HISAT2 (V2.2.0) (RRID:SCR_015530), SAMTOOLS (V1.11) (RRID:SCR_002105) and Subread (V2.0.1) (RRID:SCR_009803) (303–307). Reads were aligned against the *Homo sapiens* GRCh38 genome.

2.4.2 Differential gene expression and pathway analysis

Differential gene expression analysis was performed using DESeq2 (RRID:SCR_015687) to compare the ZIKV-infected SH-SY5Y cells versus the non-infected control cells at 24 hpi (N = 3) (308). DEGs were plotted on bar charts, volcano and scatter plots using GraphPad Prism (9.2.0) (RRID:SCR_002798). DEGs (padj \leq 0.05, fold change > 1.5) were submitted to Database for Annotation, Visualization and Integrated Discovery (DAVID) (RRID:SCR_001881) as official gene symbols for Gene Ontology (GO) (RRID:SCR_002811) (Biological Process Direct), Kyoto Encyclopedia of Genes and Genomes (KEGG) (RRID:SCR_012773) and Reactome (RRID:SCR_003485) pathway analysis (309–315). ZIKV-induced DEGs were mapped onto KEGG pathways using Pathview (RRID:SCR_002732) (316). Significance values of DEG and pathway analysis were corrected for multiple testing using the Benjamini and Hochberg method (padj \leq 0.05).

2.4.3 ZIKV interactome source and analysis

We sourced 130 and five high-confidence interactions of ZIKV NS4B and NS2B/3, respectively, in SK-N-BE2 paediatric neuroblastoma cells from The International Molecular Exchange

Consortium (IMEx) (RRID:SCR_002805) (IM-26452) (317). Scaturro et al. produced this interactome through stable expression of HA-tagged ZIKV proteins in SK-N-BE2 cells, isolation of ZIKV-host protein complexes through HA-affinity purifications, then sample preparation and run for LC-MS/MS (N = 4) (318). Scaturro et al. processed the raw data using MaxQuant with Andromeda search engine (False Discovery Rate (FDR) \leq 0.01), and determined high-confidence interactions by Bayesian statistical modelling, with Log2(Fold Change) \geq 2.5; unadjusted one-sided p \leq 0.05. The current study used the processed results obtained by Scaturro et al. Further data processing and analysis details can be sourced from the original Scaturro et al. publication (318).

The viral-host interactome was submitted to STRING (RRID:SCR_005223) for high confidence (0.7) evidence-based physical subnetwork analysis to identify host-host interactions (319). We integrated and mapped the viral-host and STRING-derived host-host interactions in Cytoscape (3.9.1) (RRID:SCR_003032) to identify possible interaction of ZIKV NS4B with host protein complexes (320). ZIKV NS4B host interaction partners were also submitted to DAVID for GO, KEGG and Reactome enrichment analysis to shed light on the possible host processes and pathways which ZIKV may interact with through NS4B. ZIKV dependency factors were integrated into the Cytoscape map to identify protein interaction of ZIKV dependency factors with ZIKV proteins.

2.4.4 ZIKV dependency factor source and analysis

Extensive data mining revealed there are currently only 22 known ZIKV dependency factors in neuroblastoma cells, identified via a shRNA screen in paediatric SK-N-BE2 neuroblastoma cells (318). In an attempt to supplement this limited pool of ZIKV dependency factors, we sourced known factors from genome-wide CRISPR-Cas9 screens performed in glioma stem cells (GSCs), human induced pluripotent stem cell-derived neural precursor cells (hiPSC-NPCs), HEK293FT and HeLa cells (268,292,321). All ZIKV dependency factors are shown in **Supplementary Table 2.1**. A combination of DAVID Gene Ontology (GO) and pathway analysis, STRING interaction and literature mining approaches were employed to identify relationships between host factors to inform ZIKV dependencies on host protein complexes and cell machinery.

2.5 Results and Discussion

2.5.1 ZIKV displays strong oncolytic properties against neuroblastoma cells

ZIKV infects and significantly reduces the cell viability of a multitude of neuroblastoma cell lines from both primary tumour and metastatic sites (Table 2.1). ZIKV can significantly reduce neuroblastoma cell viability at MOI as low as 0.001 (322). The cell viability of 11/15 neuroblastoma cell lines is significantly reduced to approximately 20% or less following ZIKV infection, and these observations are apparent despite the differences in the cell line, ZIKV strain, viral MOI and the type of assay performed (Table 2.1). SK-N-BE1 and SK-N-BE2 cells are from bone marrow metastasis from the same patient before and after treatment, respectively, and are both highly susceptible to ZIKV. SK-N-AS, T-268 and JFEN are highly resistant (cell viability > 80%) to ZIKV infection. Susceptibility is independent of patient sex, cell line origin, morphology and MYCN status (Table 2.1). The non-sympathetic nervous system and nonpaediatric origin of the T-268 and JFEN cells likely explain their resistance to ZIKV infection, as ZIKV has a tropism for paediatric nervous system cancer cells (249). The resistance of the paediatric SK-N-AS cell line is governed by CD24 expression, which regulates the basal antiviral state of these cells (251,261). Whilst LA-N-6 shows partial resistance to ZIKV infection (Table 2.1), bulk mRNA and protein analysis shows LA-N-6 cells to express CD24 (251). Potential reasoning for this partial resistance is that subpopulations within LA-N-6 may be CD24- or employ a CD24-independent mechanism to infer resistance. From Table 2.1, we conclude ZIKV to be a promising oncolytic virotherapy candidate to employ against paediatric neuroblastoma since in vitro it can infect neuroblastoma cells originating from the primary tumour, metastatic sites, and metastatic sites that are resistant to standard neuroblastoma therapy.

2.5.2 ZIKV strains present with differential therapeutic potential against neuroblastoma cell lines

Independent studies have demonstrated inherent differences in the ability of varying ZIKV strains to infect, replicate, and kill neuroblastoma cells (323,324). Here, we assess published data concerning ZIKV infection of neuroblastoma cells and ranked the viral strains based on their ability to infect them, produce fresh viral progeny and reduce cell viability (**Table 2.2**). Data mining showed the PRVABC59 Asian and Uganda #976 African strains as the top two candidates (**Table 2.2**). The PRVABC59 Asian strain induces significantly more DEGs and splice events of immune and inflammatory response genes in SH-SY5Y cells compared to the African MR766 strain, which has 99.95% sequence identity to Uganda #976 (302). Brain metastases develop in

5–11% of neuroblastoma patients and are correlated with poor prognosis (325). The ability of the Asian lineage to access the brain may enhance the therapeutic potential of ZIKV by targeting these brain metastases. Population-level data from the Asian ZIKV lineage epidemics has highlighted that postnatal Asian lineage infection only results in neurological complications in 0.52% of children, thus indicating the safe nature of employing an Asian strain (232). Consequently, from those tested to date, we propose that the PRVABC59 Asian strain is a leading candidate for development as oncolytic virotherapy against paediatric neuroblastoma.

2.5.3 ZIKV infection of neuroblastoma cells induces changes at the transcriptome level

Differential gene expression analysis identifies 453 and 256 significantly upregulated and downregulated genes, respectively, in paediatric neuroblastoma SH-SY5Y cells infected with our leading ZIKV strain candidate (PRVABC59, MOI 5) (Figure 2.1A). GO, Reactome and KEGG pathway analysis identifies nine significantly upregulated and twelve significantly downregulated terms (Figures 2.1B and 2.1C). Upregulated processes include "TNF signalling pathway", lipid metabolism ("Cholesterol biosynthesis", "Cholesterol biosynthetic process", "Activation of gene expression by SREBF (SREBP)"), ER stress ("Response to endoplasmic reticulum stress", "XBP1(S) activates chaperone genes") and transcription ("BMAL1:CLOCK, NPAS2 activates circadian gene expression", "Positive regulation of transcription from RNA polymerase II promoter"). The downregulated terms are predominantly cell cycle- and DNA replication-related processes, and this downregulation is apparent when the DEGs are mapped onto the "Cell Cycle" KEGG pathway (Figure 2.2B). A potential explanation for this observation is that ZIKV can disrupt the cell cycle by targeting the centrioles in neuroblastoma cells (326).

2.5.4 ZIKV infection upregulates TNF and cytokine gene signatures in neuroblastoma cells

Of the top ten upregulated DEGs in ZIKV-infected SH-SY5Y cells, four (BIRC3, TNFAIP3, ICAM1 and BCL3) are components of the TNF signalling pathway (**Figure 2.1A**). The TNF pathway is particularly noteworthy to consider for oncolytic virotherapy since it may play a role in both oncolysis (direct cell death) and the anti-tumoural immune response. Here, mapping the KEGG "TNF signaling pathway" for ZIKV-infected SH-SY5Y cannot deduce if ZIKV may activate CASP-mediated apoptosis or CASP-independent necroptosis (**Figure 2.2A**). However, ZIKV-infected SH-SY5Y cells show significant upregulation of downstream transcription factors (AP-1, cEBPβ and CREB), leukocyte recruitment and activation (CCL2 and CSF1), intracellular signalling

(BCL3, NFKBIA, TNFAIP3 and TRAF1) and cell adhesion genes (ICAM1 and VCAM1) (**Figure 2.2A**). ZIKV significantly upregulates the expression of multiple AP-1 transcription factors, including members from all four AP-1 subfamilies (ATF, JUN, FOS and MAF) in SH-SY5Y cells (**Figure 2.3A**). AP-1 can regulate the expression of a diverse set of genes in response to nutrients, cytokines, stress or pathogen infection, and is involved in innate and adaptive immunity, differentiation, proliferation, survival and apoptosis (327). AP-1 transcription factors can regulate the immune response of tumours, and significant AP-1 upregulation by ZIKV infection potentially identifies AP-1 as a mechanism through which ZIKV could yield an anti-tumoural immune response against neuroblastoma (328). Supporting the notion of a ZIKV-induced inflammatory response, 32 genes implicated in cytokine signalling are significantly differentially expressed in ZIKV-infected SH-SY5Y cells: 27 upregulated and five downregulated (**Figure 2.3B**).

Interestingly, the pro-inflammatory cytokine CCL2 (MCP-1) is significantly upregulated at the transcriptome level following ZIKV infection, and two independent studies have shown CCL2 to be secreted by ZIKV-infected SH-SY5Y cells (329,330). CCL2 is secreted by ZIKV-infected cultured canine glioblastoma cells when in the presence of monocytes and is detected in serum and CSF samples of canines bearing spontaneous brain tumours following ZIKV infection (264). Additionally, a non-neurotoxic herpes simplex virus (HSV)-based OV engineered to express physiologically relevant levels of CCL2 (M010), significantly reduced Neuro-2a neuroblastoma growth in the flank of immunocompetent mice and recruited CD4+ and CD8+ T cells into the tumour (331). We propose that CCL2 may present as a promising transgene candidate for oZIKV therapy.

2.5.5 ZIKV infection upregulates lipid metabolism gene signatures in neuroblastoma cells

ZIKV infection significantly upregulates lipid metabolism-related terms in SH-SY5Y cells; specifically, "Cholesterol biosynthesis" and "Activation of gene expression by SREBF (SREBP)" (Figure 2.1B). Cholesterol and lipids are essential cellular components, and complex systems regulate their intracellular abundance and localisation. These systems include regulation of cholesterol biosynthesis by the SREBP pathway, intracellular cholesterol trafficking, and cholesterol efflux by the liver X receptor (LXR) pathway. Cholesterol and fatty acids are required for multiple stages of the flavivirus life cycle, including regulating viral entry, remodelling the ER membrane to form viral replication complexes, and viral egress (332). ZIKV infection elevates lipogenesis and remodels the composition of the lipid classes in infected SK-N-SH cells (333). Our data mining of published literature highlighted numerous compounds that modify

intracellular lipid levels were capable of regulating ZIKV infection in paediatric neuroblastoma cells *in vitro* (**Table 2.3**). These include supplementation with pathway regulators (PF-429242, fenofibrate, lovastatin, U18666A and LXR 623) or exogenous lipids (oleic acid, docosahexaenoic acid (DHA) and cholesterol).

Three SREBP pathway inhibitors (PF-429242, fenofibrate and lovastatin) reduce ZIKV infection of SK-N-SH neuroblastoma cells (Table 2.3). The SREBP pathway is a principal regulator of fatty acid and cholesterol biosynthesis regulated by the transcription factors SREBF1 and SREBF2. Whilst SREBF1 and SREBF2 share a small degree of redundancy, they primarily regulate the expression of fatty acid biosynthesis and cholesterol biosynthesis target genes, respectively (334). Both SREBF2 and SREBF2-AS1 are significantly upregulated in ZIKV-infected SH-SY5Y cells, and the most highly upregulated SREBF downstream gene (HMGCS1) is a SREBF2 responsive gene (Figure 2.4A). Pathway analysis identifies significant upregulation of "Cholesterol biosynthesis" (Figure 2.1B) and here we observe significant upregulation of multiple enzymes of the SREBF2 cholesterol biosynthetic pathway (HMG-CoA synthase (HMGCS1), Mevalonate Diphosphate Decarboxylase (MVD), CYP51 (CYP51A1), Mevalonate Kinase (MVK), squalene synthase (FDFT1), Squalene Epoxidase (SQLE), Lanosterol Synthase (LSS), Lathosterol Oxidase (SC5D)) (Figure 2.4A). Data mining highlighted that the SREBP pathway is needed for efficient ZIKV infection, and we propose that the SREBF2 transcriptional pathway may contribute to the upregulation of cholesterol biosynthesis in ZIKV-infected neuroblastoma cells.

Both U18666A and exogenous cholesterol restrict ZIKV infection of neuroblastoma cells (**Table 2.3**). U18666A is an intracellular cholesterol transport inhibitor that causes the accumulation of cholesterol in lysosomes to hinder the endosomal-lysosomal system (335). Exogenous cholesterol also leads to the inactivation of the late endosomal-lysosomal compartments through a build-up of cholesterol (335). Collectively, this indicates a dependence of ZIKV on cholesterol homeostasis in neuroblastoma cells, likely due to its involvement in endosomallysosomal system function.

The LXR pathway agonist (LXR 623) promotes cholesterol efflux (**Table 2.3**). Flaviviruses require cholesterol for the restructuring of host membranes, and LXR 623 treatment impairs ZIKV-induced vesicle production and ER expansion in SK-N-SH cells (161). The LXR pathway and expression of its downstream lipid homeostasis genes are regulated by the transcription factors LXR- α (NR1H3) and LXR- β (NR1H2). LXR- α protein is significantly increased in ZIKV-infected SK-N-SH neuroblastoma cells from 48 hours (161). Although LXR- α mRNA is only moderately upregulated in our study, two major cholesterol efflux factors downstream of the LXR pathway,

ATP-Binding Cassette A1 and G1 (ABCA1 and ABCG1), are significantly upregulated (**Figure 2.4B**). Interestingly, oleic acid is one of the main monounsaturated fatty acids synthesised by the LXR pathway, and exogenous oleic acid treatment enhances ZIKV infection in neuroblastoma cells (**Table 2.3**). FASN and SCD regulate oleic acid synthesis, and here we observe both to be significantly upregulated in ZIKV-infected neuroblastoma cells (**Figure 2.4B**) (336). Thus, we propose that oleic acid synthesis may be involved during ZIKV infection of neuroblastoma cells. Collectively, our data mining identifies a dependence of ZIKV on the LXR pathway and indicates that ZIKV infection may lead to upregulated cholesterol efflux and oleic acid synthesis through this pathway.

To conclude, we identify various components of host cell lipid metabolism to be differentially regulated following ZIKV infection. We propose that infection-induced remodelling of lipid composition may promote a favourable environment for efficient replication.

2.5.6 ZIKV infection upregulates the ER stress response in neuroblastoma cells

ZIKV significantly upregulates ER-stress-related terms in SH-SY5Y cells, principally "Response to endoplasmic reticulum stress" and "XBP1(S) activates chaperone genes" (Figure 2.1B). The IRE1-, PERK- and ATF6-mediated unfolded protein response (UPR) pathways govern the ER-stress response. Activation of IRE1-mediated UPR leads to XBP1 mRNA splicing to produce the active transcription factor XBP1(S). ZIKV infection significantly upregulates 15 genes of the IRE1-mediated "XBP1(S) activates chaperone genes" Reactome pathway in SH-SY5Y cells, including XBP1, the ERAD gene SYVN1 and chaperones (DNAJC3 and DNAJB9) (Figure 2.5A). Multiple IRE1-mediated UPR genes (EDEM1, SYVN1, SSR1, SRPRB, ATP6V0D1 and EXTL3) are ZIKV dependency factors in hiPSC-NPCs (Supplementary Table 2.1). This indicates a dependence of ZIKV on the IRE1 pathway, which is supported by chemical inhibition of IRE1 by 4μ8C impairing ZIKV infection *in vivo* (337).

ZIKV infection significantly upregulates seven genes of the "ATF4 activates genes in response to endoplasmic reticulum stress" Reactome pathway (**Figure 2.5B**), including the ERAD gene HERPUD1 and the transcription factors ATF3, CEBPB and CEBPG. The PERK-mediated UPR regulates the expression of apoptosis, redox, amino acid transport and autophagy genes through eIF2 phosphorylation and the transcription factor ATF4. GADD34 (PPP1R15A), which dephosphorylates eIF2α in a negative feedback loop, is significantly upregulated here by ZIKV infection, and ZIKV infection has been shown to induce eIF2 phosphorylation in SK-N-SH cells (338). GADD34 is likely upregulated during infection to combat ER stress-induced translational repression, as the viral life cycle is heavily dependent on *de novo* protein synthesis. DDIT3

(CHOP) is a pro-apoptotic protein downstream of the PERK-mediated UPR pathway that others have shown to be significantly upregulated in ZIKV-infected SH-SY5Y and SK-N-SH cells (302,338,339). Notably, multiple PERK-mediated UPR genes (ATF4, EIF2AK1, EIF2AK2, EIF2AK3 and EIF2AK4) are ZIKV dependency factors in hiPSC-NPCs (**Supplementary Table 2.1**).

To conclude, our data mining, integration and re-analysis highlights that ZIKV infection upregulates gene signatures indicative of both the IRE1- and PERK-mediated UPR components of the ER stress response in SH-SY5Y cells. These observations are supported by those shown by others, and build on their observations by indicating a dependence of ZIKV on both pathways for efficient infection (338,339). This response may occur to mitigate viral replication-induced ER stress.

2.5.7 ZIKV infection is dependent on the ER Membrane Protein Complex (EMC)

To investigate which host mechanisms ZIKV may be dependent on, we cross-referenced the 22 known proteins that ZIKV requires for efficient infection of neuroblastoma cells with ZIKV dependency factors from four other cell lines (Figure 2.6A, Supplementary Table 2.1). Between 72–94% of the dependency factors identified across the five different cell lines are cell-specific, highlighting how ZIKV likely utilises differing host factors across varying cell types for efficient infection. The sparse overlap of ZIKV dependency factors identifies only one factor common to all five cell types: MMGT1 (EMC5), which is a key component of the ER Membrane Protein Complex (EMC). The EMC is a hetero-oligomer composed of ten subunits, has chaperone properties by assisting multi-transmembrane protein folding, and is implicated in ER stress, flavivirus infection and lipid trafficking (340). Integration of all five ZIKV dependency factor datasets shows ZIKV to have a strong dependence on the EMC independent of cell type; all ten EMC proteins are ZIKV-dependency factors in hiPSC-NPC, eight are in HeLa and three in GSC and HEK293FT cells (Figure 2.6B). Our observations are supported by work by others showing that (i) EMC facilitates the expression of ZIKV transmembrane proteins (NS2B, NS4A and NS4B) and (ii) disrupting the EMC impedes infection by ZIKV and other flaviviruses (341,342). We propose that the EMC stabilises newly synthesised ZIKV proteins through integration into the ER membrane, thus supporting efficient neuroblastoma cell infection. We expect that additional EMC subunits would present as ZIKV dependency factors in neuroblastoma cells if investigated.

2.5.8 ZIKV infection is dependent on the V-ATPase in neuroblastoma cells

Many viruses utilise the endosomal-lysosomal system's V-ATPase-driven acidification to release their nucleocapsid into the cytosol. ATP6V0C, a central component of the V-ATPase, is a

ZIKV-dependency factor in neuroblastoma, hiPSC-NPC and HEK293FT cells (**Figure 2.6A**). The ATP6V0C subunit-specific V-ATPase inhibitor Bafilomycin A1 inhibits ZIKV infection of SH-SY5Y cells (**Table 2.3**) (343). Twelve additional V-ATPase subunits are ZIKV dependency factors across GSC, hiPSC-NPC and HeLa cells (**Figure 2.6C**). Multiple subunits from both the Vo proton translocation and V₁ ATP hydrolytic domains are ZIKV dependency factors, indicating a functional dependence of ZIKV on the entire V-ATPase complex. Supporting this, siRNA silencing of the V-ATPase significantly impairs ZIKV infection of T98G glioblastoma cells, highlighting a dependency of ZIKV on the V-ATPase across different nervous system tumour cells (159). Here, we highlight a dependency of ZIKV on the V-ATPase in neuroblastoma cells and propose that loss of V-ATPase function may impair infection due to the absence of a pH gradient and concomitant endosomal system acidification. This would prevent the fusion of the viral envelope with the endosomal membrane for release of the nucleocapsid, subsequently trapping ZIKV for degradation in the lysosome, as observed in Vero cells (344).

2.5.9 ZIKV NS4B protein-protein interactions may explain its apoptotic capability against neuroblastoma cells

ZIKV NS4B protein is the principal ZIKV protein with an apoptotic effect in SH-SY5Y cells (345). Determining the interactions and mechanisms underpinning this may yield opportunities to develop a paediatric neuroblastoma therapy based on ZIKV NS4B. ZIKV NS4B has 130 known host interaction partners in SK-N-BE2 neuroblastoma cells (318). Re-analysing this interactome, we observe host proteins involved in multiple pathways previously implicated during ZIKV infection of neuroblastoma cells, including mitochondrial-, lipid metabolism- and ER-associated processes (Figure 2.7). ZIKV NS4B interacts with three SREBP pathway downstream proteins (SCD, SC5D and DHCR7). These protein-protein interactions (PPIs) between ZIKV and the SREBP pathway and host lipid metabolism build on our observations of ZIKV upregulating these processes in neuroblastoma cells (Figure 2.7, Table 2.3).

Notably, we observe ZIKV NS4B to interact with a multitude of mitochondrial proteins; electron transport chain proteins (TIMMDC1, MT-CO2, COX15 and OXA1L), mitochondrial translocases that import proteins into the mitochondrial matrix (TOMM22, TIMM23, TIMM50 and TIMM17B) and Solute Carrier Family 25 members for transport of solutes across the mitochondrial membrane (SLC25A1, SLC25A3, SLC25A6, SLC25A11, SLC25A12, SLC25A13 and SLC25A22) (**Figure 2.7**). ZIKV NS4B recruits BAX to the mitochondria, triggers its activation and releases Cytochrome c to induce mitochondrial cell death in SH-SY5Y cells (345). MT-CO2, COX15 and OXA1L are conserved catalytic core, assembly and accessory subunits of the Cytochrome c

oxidase complex that tightly couple Cytochrome c to the inner mitochondrial membrane, respectively (**Figure 2.7**). We propose that interactions between ZIKV NS4B and the Cytochrome c oxidase complex could uncouple and lead to Cytochrome c release into the cytosol and activation of the mitochondrial cell death pathway.

2.5.10 ZIKV NS4B interacts with the Mammalian Translocon in neuroblastoma cells

ZIKV is dependent on multiple proteins of the mammalian translocon for efficient infection, and ZIKV NS4B interacts with multiple subunits of the mammalian translocon (**Figures 2.6A and 2.7**). The mammalian translocon is primarily composed of the Oligosaccharyl Transferase (OST) complex, the Sec61 complex and the translocon-associated protein (TRAP) complex (346). The multimeric OST complex co-translationally N-glycosylates proteins within the ER to assist protein folding, stability and trafficking. The Sec61 complex, a heterotrimer of Sec61 α , Sec61 β and Sec61 γ , co-translationally translocates newly synthesised proteins across the ER and, during ER stress, can regulate IRE1 α activity. TRAP is a heterotetramer of SSR1, SSR2, SSR3 and SSR4 that assists co-translational translocation of proteins into the ER and can prevent aberrant N-linked glycosylation during ER stress.

STT3A, a principal component of the OST complex, interacts with ZIKV NS4B and is a ZIKV dependency factor in neuroblastoma, GSC, hiPSC-NPC and HeLa cells (Figures 2.6A and 2.7). Regarding the additional OST subunits, ZIKV NS4B interacts with DDOST, RPN1, RPN2 and KRTCAP2, and in HeLa and GSC cells OSTC and OST4 are ZIKV dependency factors, respectively (Figures 2.6A and 2.7). Two forms of the OST complex exist: the STT3A and STT3B OST paralogs. KRTCAP2 and OSTC are STT3A-specific OST factors, which permit interaction of STT3A with the translocon, whilst TUSC3 and MAGT1 are STT3B-specific OST factors (346). STT3A and both STT3A-specific OST factors are ZIKV interaction partners and/or dependency factors, but neither STT3B nor the STT3B-specific OST factors are. In addition to the OST factors, multiple N-linked glycosylation-related proteins (DPM1, DERL3, SYVN1, UBE2G2 and UBE2J1) are also ZIKV dependency factors in non-neuroblastoma cells (Supplementary Table 2.1). The OST complex inhibitor NGI-1 blocks ZIKV infection of Huh7 cells, and disrupting ZIKV pre-membrane (prM) and E protein N-glycosylation impairs the release of infectious ZIKV particles from Vero cells (144,347). We identify that STT3A is a bonafide ZIKV dependency factor in multiple cell types, and we propose that efficient neuroblastoma cell infection is likely dependent on the STT3A OST paralog due to viral protein N-glycosylation.

ZIKV NS4B interacts with SEC61A1 and SEC61B of the Sec61 complex in neuroblastoma cells (**Figure 2.7**), and the Sec61α inhibitor Mycolactone impedes ZIKV infection of HeLa cells (348).

ZIKV NS4B interacts with SSR3 of the TRAP complex in neuroblastoma cells, and ZIKV is dependent on at least two of the four TRAP complex subunits for infection of GSC, hiPSC-NPC and HeLa cells (**Figures 2.6A and 2.7**). Additionally, ZIKV is dependent on the (i) signal recognition particle subunit SRPRB, (ii) signal peptidase complex subunit SPCS3, and (iii) translocating chain-associated membrane protein subunit TRAM1; further supporting our observed dependence of ZIKV infection on the mammalian translocon. Notably, the viral protease NS2B/3 also interacts with subunits of the OST complex (STT3A and RPN1), Sec61 complex (SEC61B) and TRAP complex (SSR3) (**Figure 2.7**). These interactions likely facilitate the co-translational cleavage of the viral polypeptide by NS2B/3 into its individual viral proteins.

From our re-analysis of a publicly available ZIKV interactome, we propose ZIKV NS4B and NS2B/3 to interact with the core complexes of the mammalian translocon and hypothesise that ZIKV infection in neuroblastoma cells may be dependent on these interactions. The dependency of ZIKV likely stems from the mammalian translocon facilitating viral polyprotein cotranslational translocation, viral polyprotein cleavage, viral membrane protein insertion or viral protein N-glycosylation. Additionally, ZIKV may utilise its protein interactions with the Sec61 complex, TMEM33 and VAPB to regulate the IRE1- and PERK-mediated UPR ER stress responses, which we observed to be significantly upregulated at the transcriptome level in ZIKV infected-neuroblastoma cells (Figure 2.5).

2.6 Conclusions

Our study highlights the strong therapeutic potential of ZIKV against multiple neuroblastoma cell-lines. Our data mining, integration and re-analysis suggest ZIKV to interact with, and be dependent on, multiple host protein complexes and pathways for its life cycle in paediatric neuroblastoma cells and for inducing oncolysis (Figure 2.8). Although this area of research is still at an early stage, our extensive survey of neuroblastoma ZIKV infection studies clearly demonstrates the potential of oZIKV therapy. There are a few avenues that need to be addressed to progress this area of research, including (i) assessing ZIKV's oncolytic effect against neuroblastoma in xenograft mouse models, (ii) assessing ZIKV's capability to induce an antitumoural immune response against neuroblastoma in immunocompetent *in vivo* models, and (iii) considering the effectiveness and safety of employing different forms of oZIKV therapy against neuroblastoma. Examples of the latter may include live attenuated ZIKV strains or the construction of a virotherapy that collectively expresses ZIKV NS4B and CCL2, which we observe here to hold elements of ZIKV's oncolytic and immune activation potential, respectively.

2.7 Data Availability

European Nucleotide Archive: Asian Zika virus isolate significantly changes the transcriptional profile and alternative RNA splicing events in a neuroblastoma cell line. Accession number PRJNA630088 (https://www.ebi.ac.uk/ena/browser/view/PRJNA630088).

2.8 Acknowledgements

The authors would like to thank the original curators of the datasets used in this study. This work was supported by Neuroblastoma UK (NBUKEwing22, PI: RME), Children's Cancer and Leukaemia Group and Little Princess Trust (2019LPT77, PI: RME), Wessex Medical Research and The Rosetrees Trust (A2927 / M925, PI; RME) and MRC (MR/S01411X/1, PI; RME).

2.9 Competing interests

Keith Okamoto declares a competing interest as an advisor of the biotechnology company Vyro. No other competing interests were disclosed.

2.10 Figures

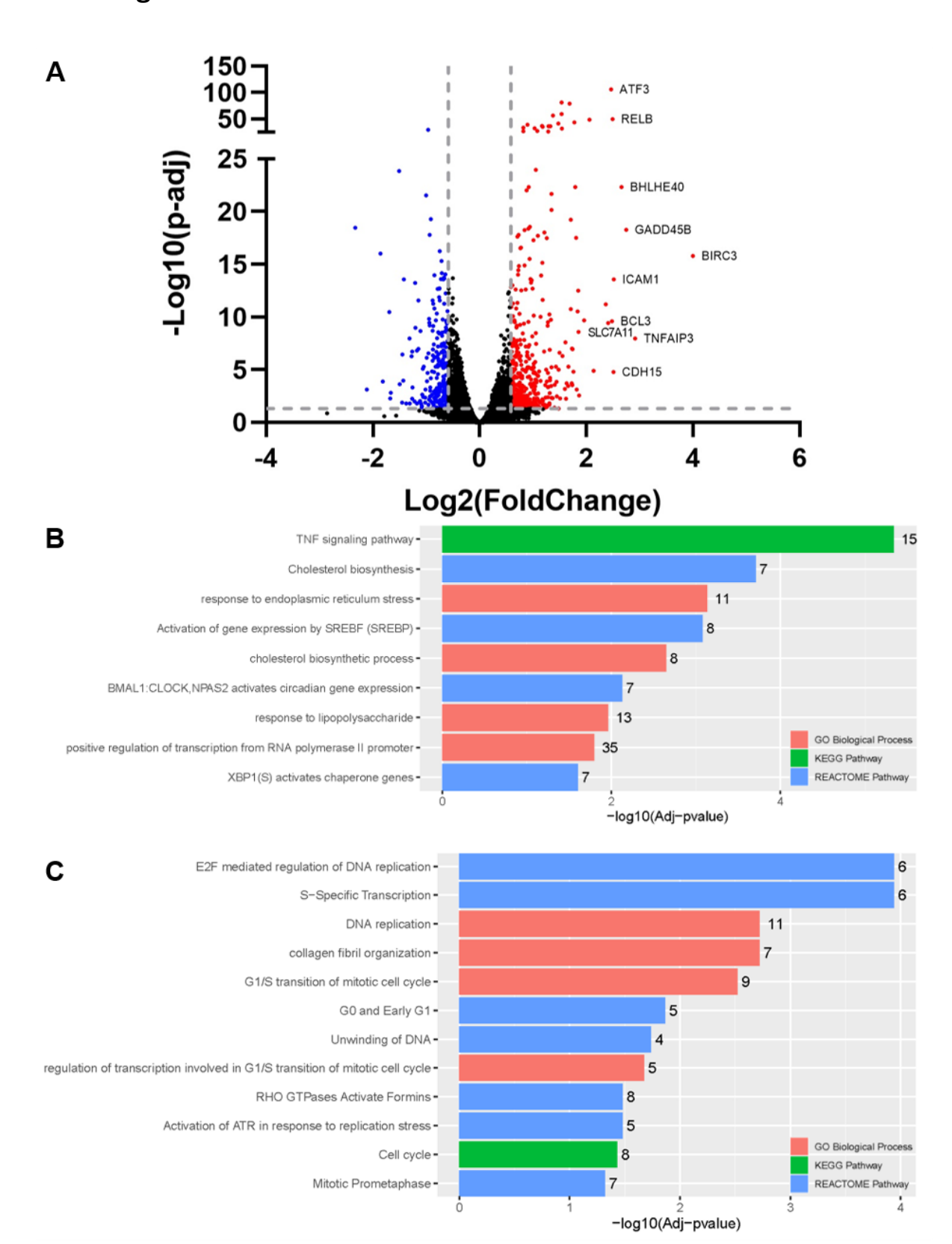
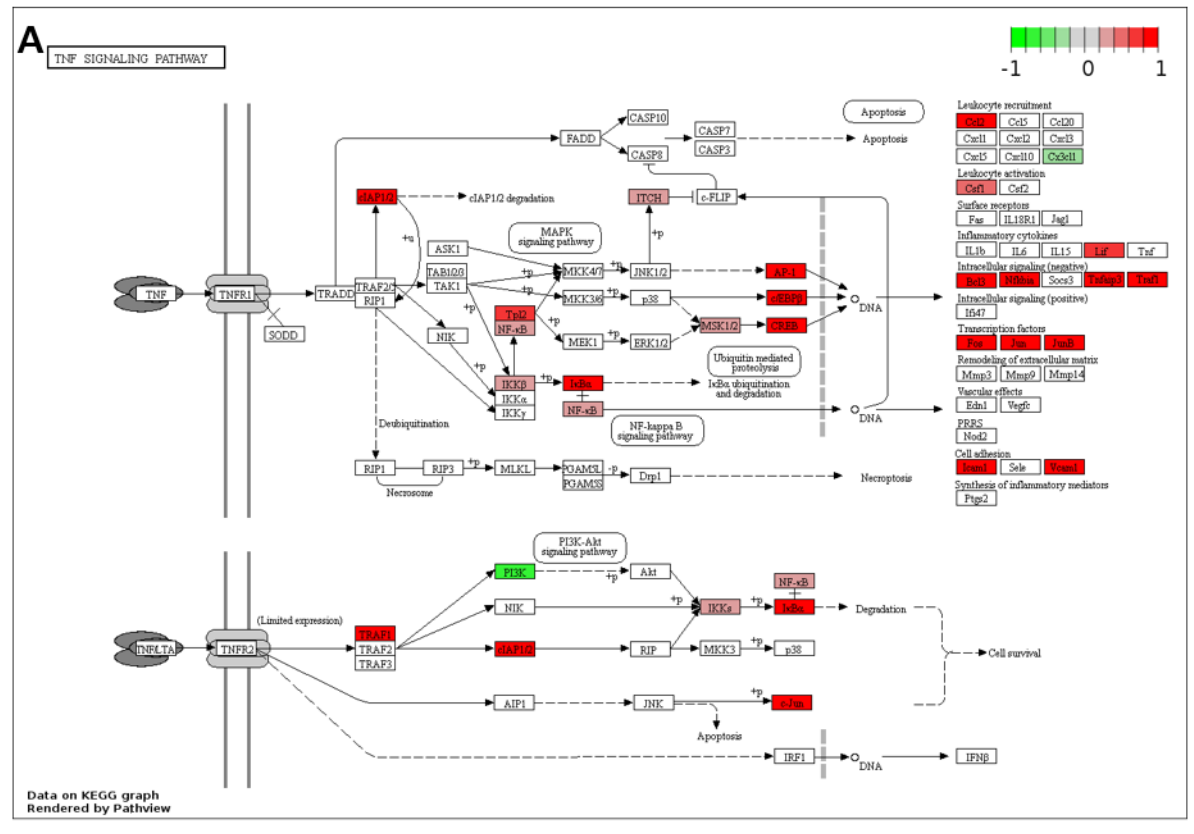


Figure 2. 1. Differential gene expression, GO biological process and pathway analysis of ZIKV infection in SH-SY5Y cells.

(A) Volcano plot of genes differentially expressed in response to ZIKV infection of SH-SY5Y cells, with the top 10 upregulated genes labelled (fold change > 1.5). Significantly (B) upregulated and (C) downregulated GO Biological Processes, KEGG and Reactome pathways in response to ZIKV infection in SH-SY5Y neuroblastoma cells. The number at the end of each bar in the bar chart denotes the number of DEGs identified for the given term. Significance values are corrected for multiple testing using the Benjamini and Hochberg method (padj \leq 0.05). Abbreviations, Gene Ontology (GO), Zika virus (ZIKV), differentially expressed gene (DEG).



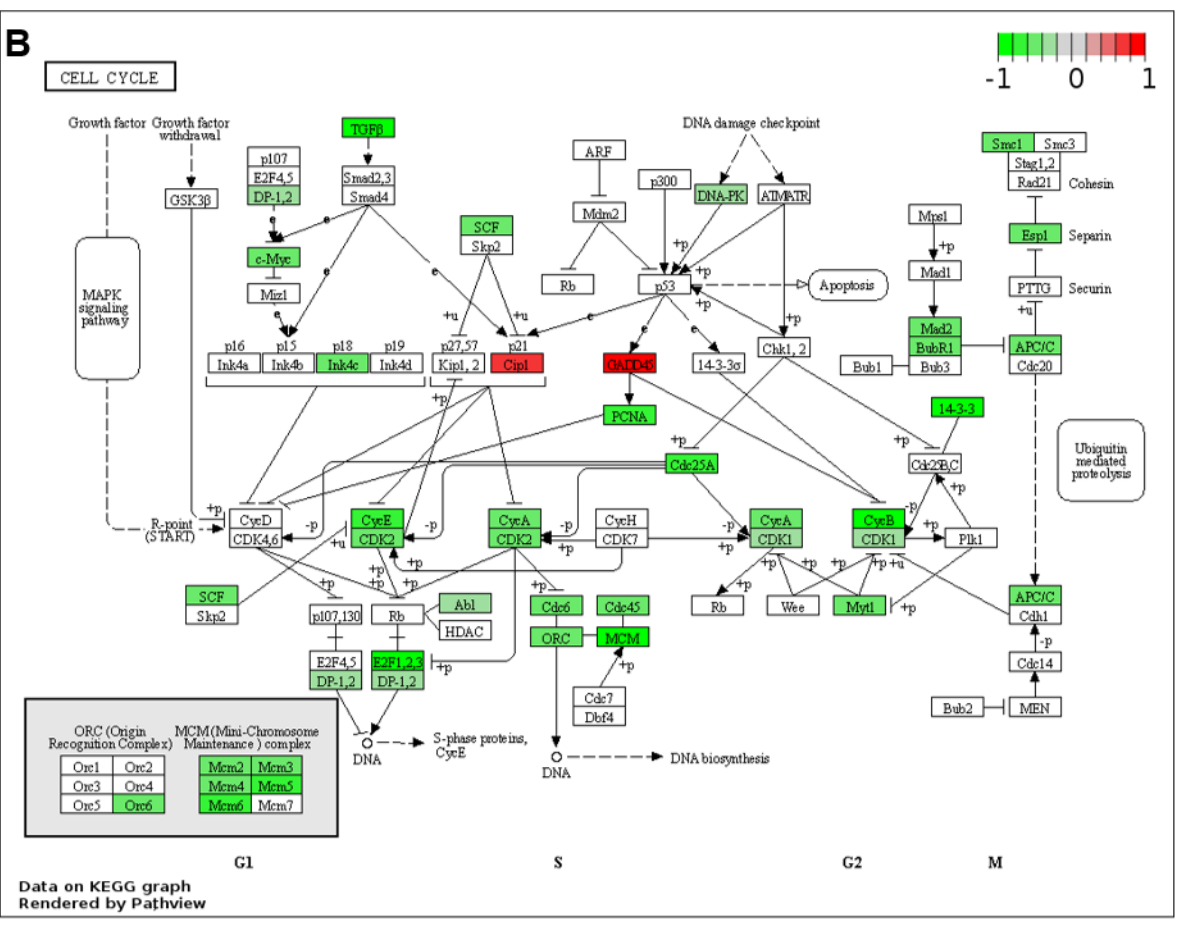
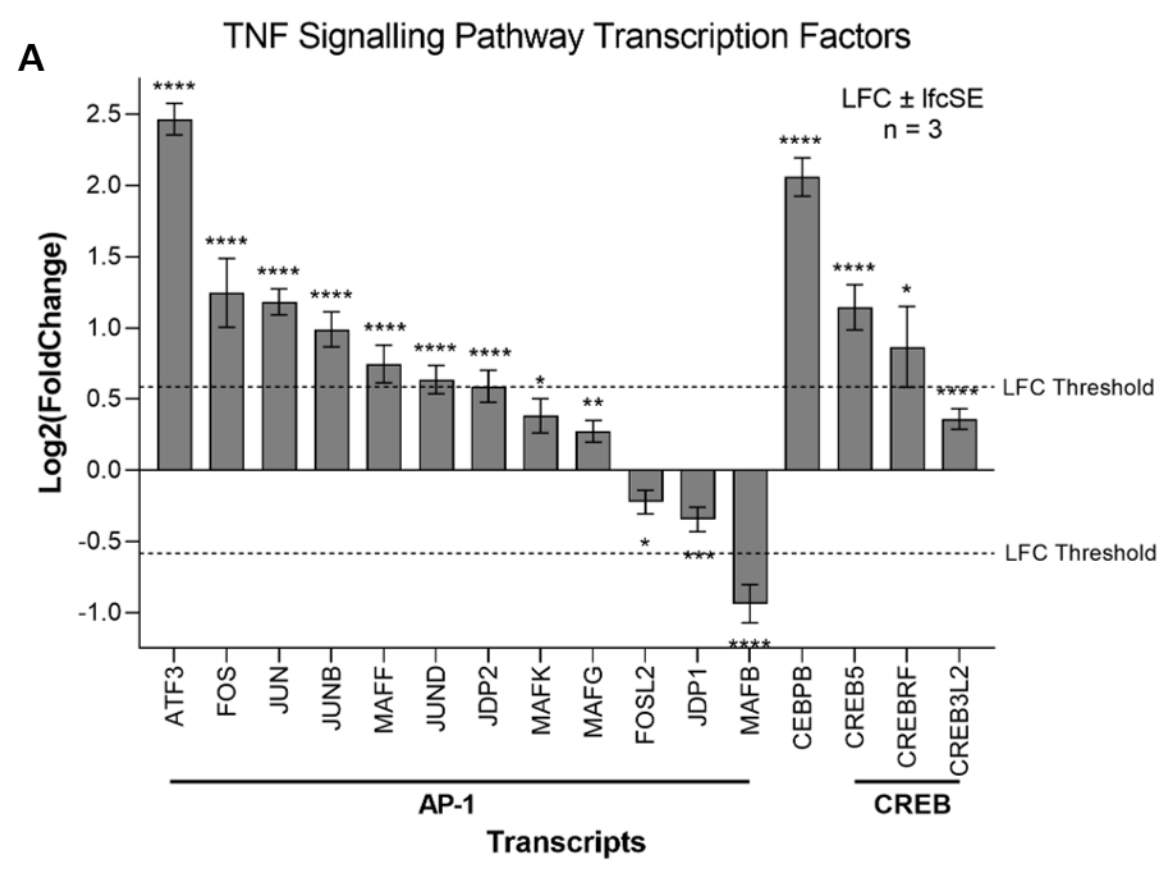


Figure 2. 2. Pathway mapping of ZIKV infection in SH-SY5Y cells.

KEGG pathway maps of the **(A)** up-regulated TNF Signalling Pathway and **(B)** down-regulated Cell Cycle with ZIKV-infected SH-SY5Y DEGs mapped (fold change > 0). Significance values are corrected for multiple testing using the Benjamini and Hochberg method (padj \leq 0.05). Abbreviations, Zika virus (ZIKV), Kyoto Encyclopedia of Genes and Genomes (KEGG), differentially expressed gene (DEG).



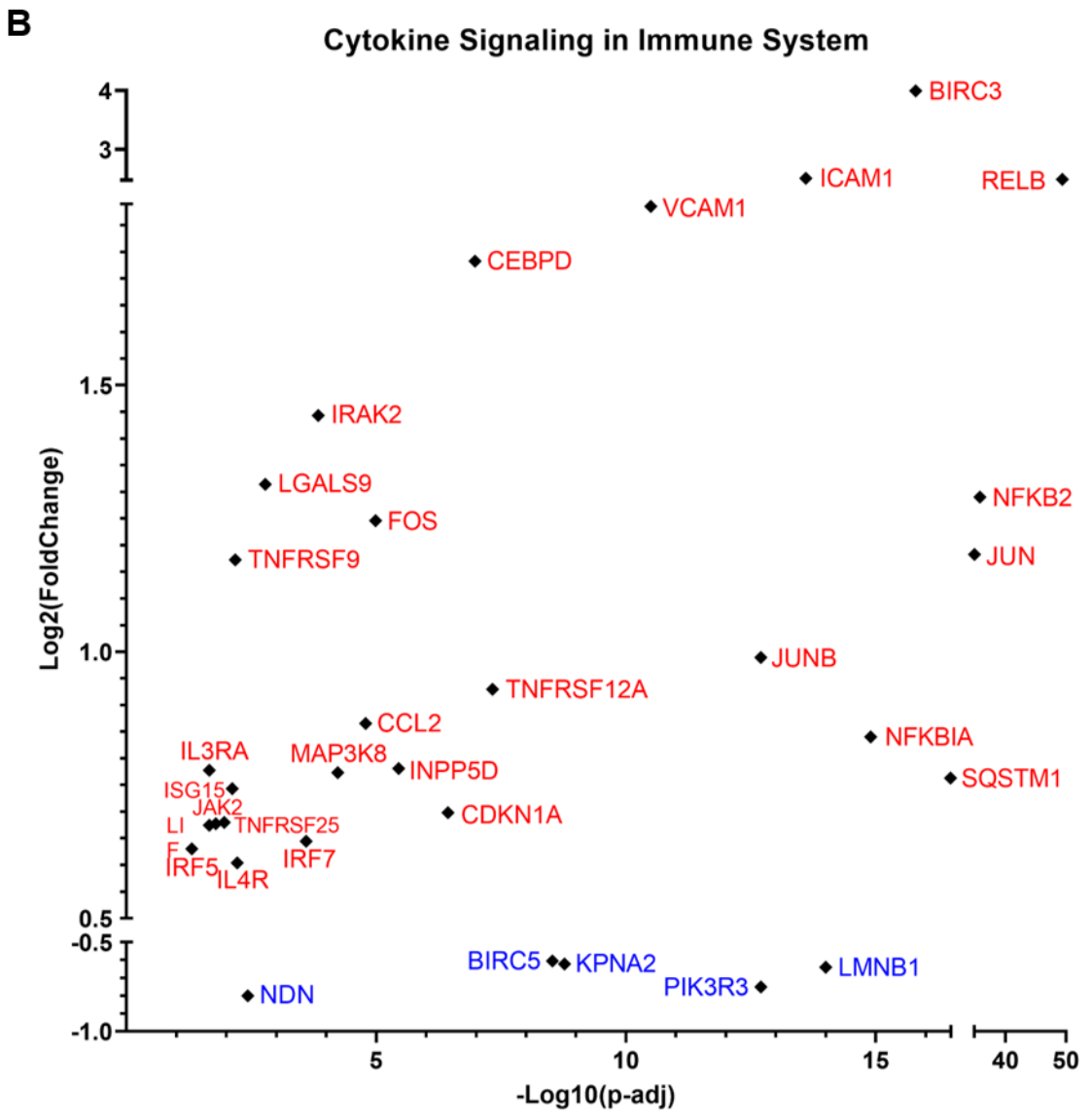
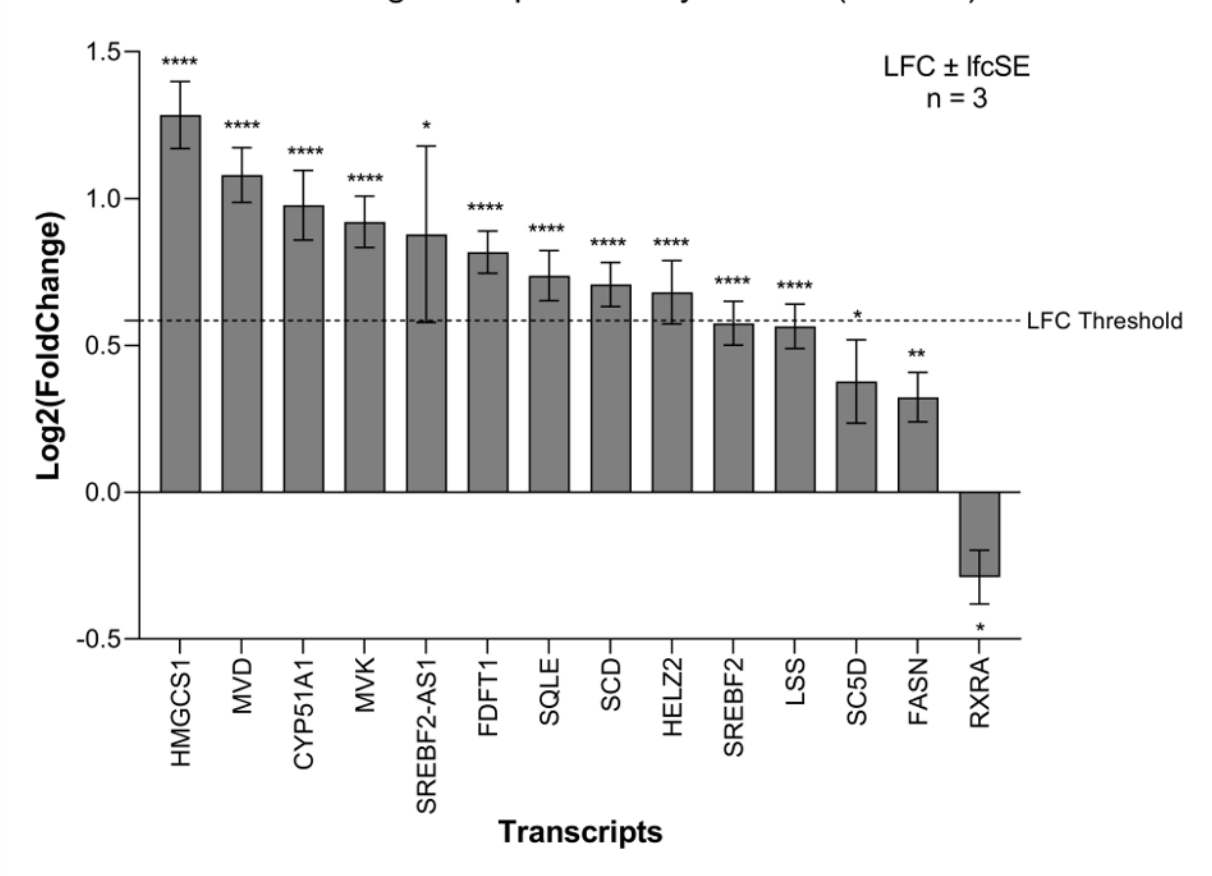


Figure 2. 3. ZIKV infection upregulates TNF and cytokine signalling gene signatures in neuroblastoma cells.

Differential expression of **(A)** TNF transcription factors and **(B)** cytokine signalling in immune system genes in ZIKV-infected SH-SY5Y cells. Significance values are corrected for multiple testing using the Benjamini and Hochberg method (padj \leq 0.05). A threshold line of Log2(1.5 Fold Change) has been applied for the expression values. Log2FoldChange (LFC) \pm standard error of the LFC estimate (lfcSE), N = 3. Asterisk symbol denotes level of significance: *padj \leq 0.05; **padj \leq 0.01; ***padj \leq 0.001; ***padj \leq 0.001. Abbreviations, Zika virus (ZIKV), differentially expressed gene (DEG), activator protein 1 (AP-1), cAMP response element-binding protein (CREB).

A Activation of gene expression by SREBF (SREBP)



B LXR Pathway

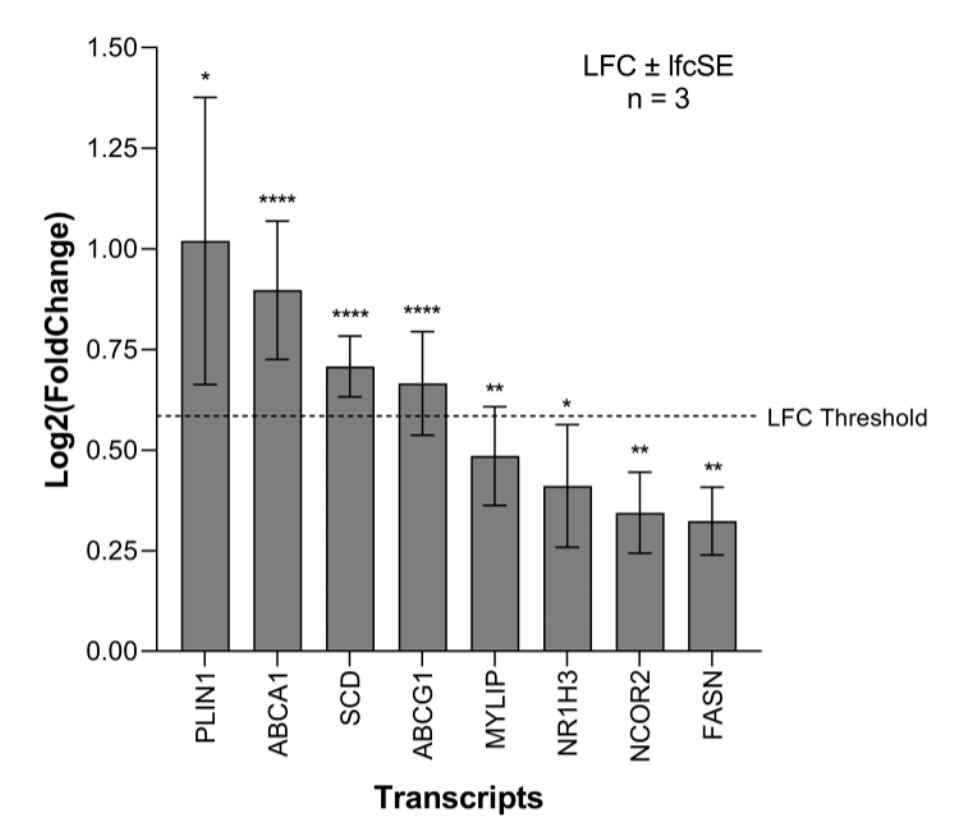
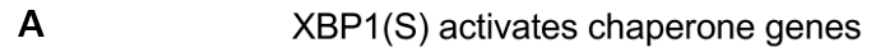
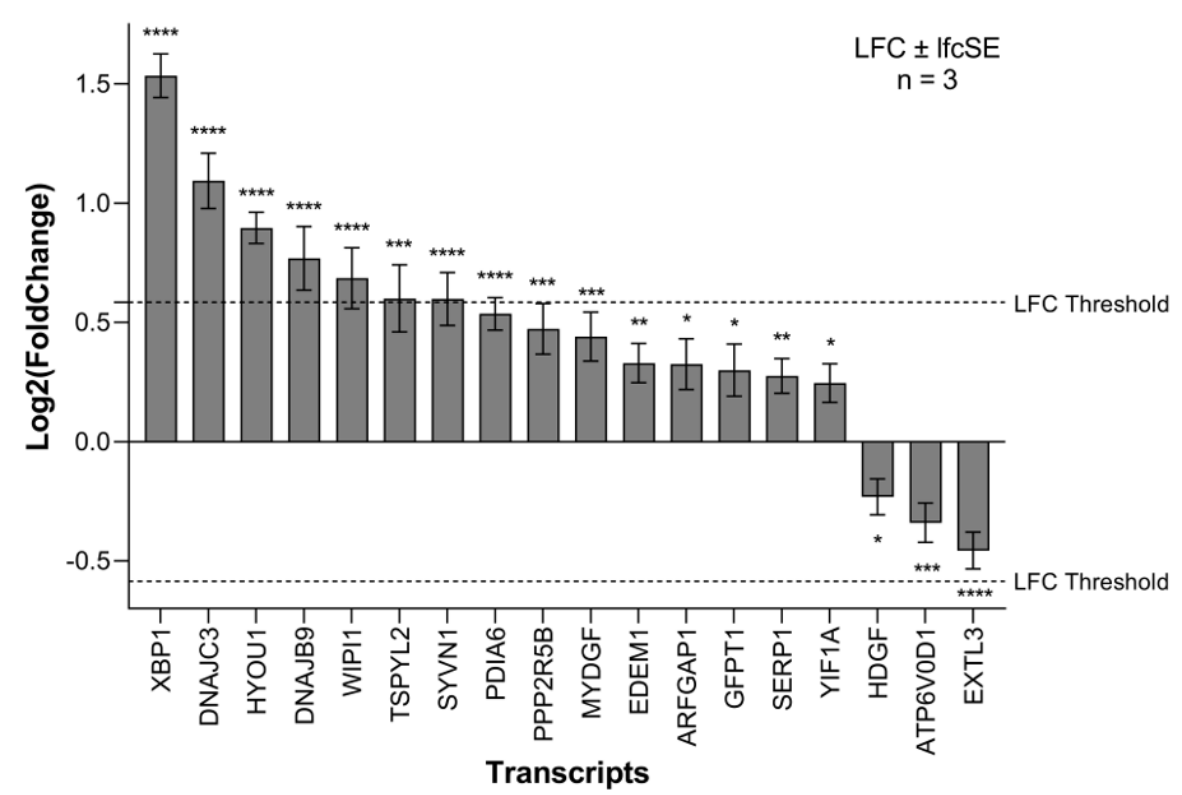


Figure 2. 4. ZIKV infection upregulates lipid metabolism gene signatures in neuroblastoma cells.

Differential expression of **(A)** SREBP pathway and **(B)** LXR pathway genes in ZIKV-infected SH-SY5Y cells. Significance values are corrected for multiple testing using the Benjamini and Hochberg method (padj \leq 0.05). A threshold line of Log2(1.5 Fold Change) has been applied for the expression values. Log2FoldChange (LFC) \pm standard error of the LFC estimate (lfcSE), N = 3. Asterisk symbol denotes level of significance: *padj \leq 0.05; **padj \leq 0.01; ****padj \leq 0.0001. Abbreviations, Zika virus (ZIKV), sterol regulatory element binding protein (SREBP), liver X receptor (LXR).





B ATF4 activates genes in response to ER stress

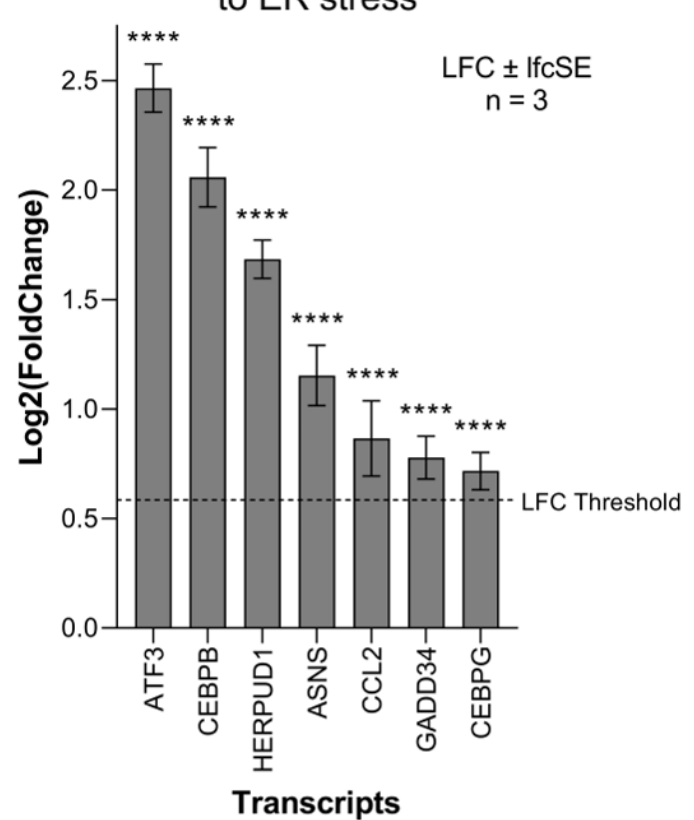


Figure 2. 5. ZIKV infection upregulates UPR gene signatures in neuroblastoma cells.

Differential expression of **(A)** XBP1(S) activates chaperone genes and **(B)** ATF4 activates genes in response to endoplasmic reticulum stress genes in ZIKV-infected SH-SY5Y cells. Significance values are corrected for multiple testing using the Benjamini and Hochberg method (padj \leq 0.05). A threshold line of Log2(1.5 Fold Change) has been applied for the expression values. Log2FoldChange (LFC) \pm standard error of the LFC estimate (IfcSE), N = 3. Asterisk symbol denotes level of significance: *padj \leq 0.05; **padj \leq 0.01; ***padj \leq 0.001; ****padj \leq 0.0001. Abbreviations, Zika virus (ZIKV), Unfolded Protein Response (UPR), endoplasmic reticulum (ER).

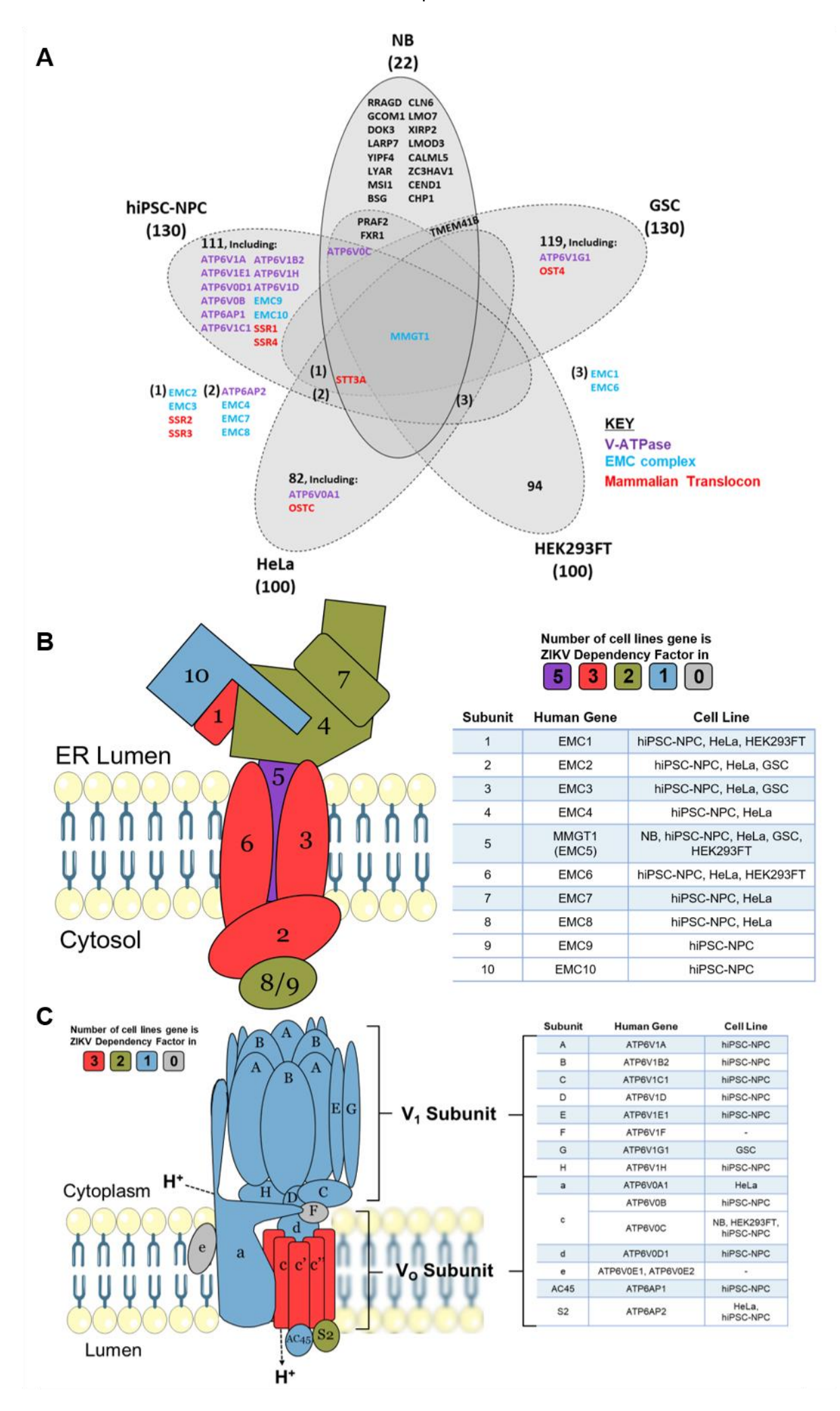


Figure 2. 6. ZIKV dependency factors.

(A) Venn diagram of known ZIKV dependency factors across NB, GSC, hiPSC-NPC (NPC), HEK293FT and HeLa cells. Diagram of the (B) EMC and (C) V-ATPase, based on their crystal structures. For the subunits in B and C, colours denote the number of cell types in which they act as ZIKV dependency factors (cell types stated in the adjacent tables). Abbreviations, Zika virus (ZIKV), neuroblastoma (NB), glioma stem cell (GSC), endoplasmic reticulum membrane protein complex (EMC).

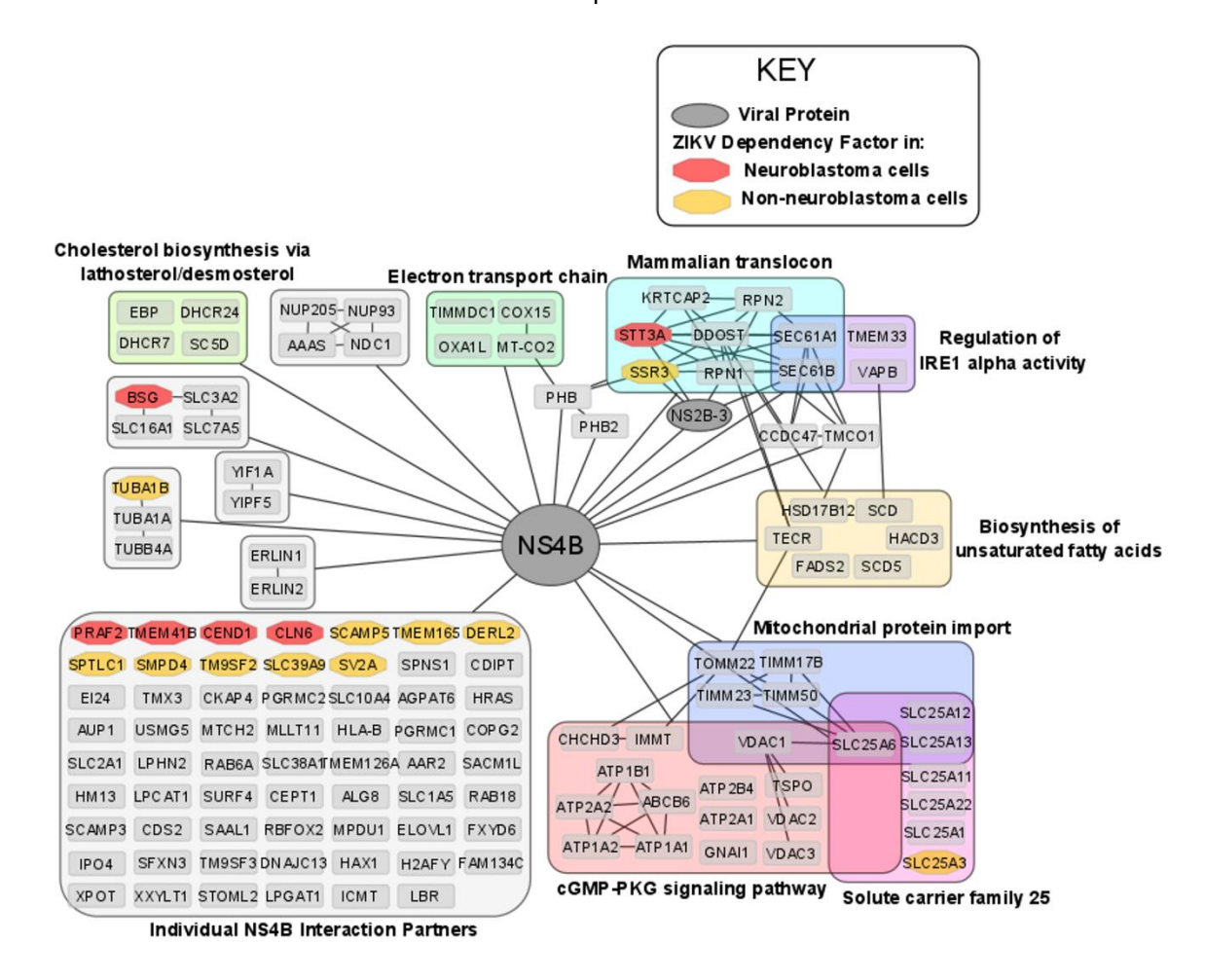


Figure 2. 7. ZIKV NS4B interacts with host proteins and known ZIKV dependency factors in neuroblastoma cells.

Nodes are grouped according to sets of high-confidence interactions between the host proteins and labelled by biological process they are involved in. Cross-referencing the ZIKV interactome with the ZIKV dependency factor datasets identifies the interaction of NS4B with dependency factors in neuroblastoma cells (red) and in GSC, hiPSC-NPC, HeLa and HEK293FT cells (collectively termed non-neuroblastoma cells, orange). To aid visualisation, nodes with no high-confidence interactions other than their interaction with NS4B have been grouped (bottom left). All nodes within Figure 2.7 interact with NS4B; thus, to aid visualisation, all edges between NS4B and nodes within a group have been condensed into a single edge between NS4B and the grouped set of nodes. Abbreviations, Zika virus (ZIKV), non-structural protein 4B (NS4B), glioma stem cell (GSC), human induced pluripotent stem cell (hiPSC), neural precursor cell (NPC).

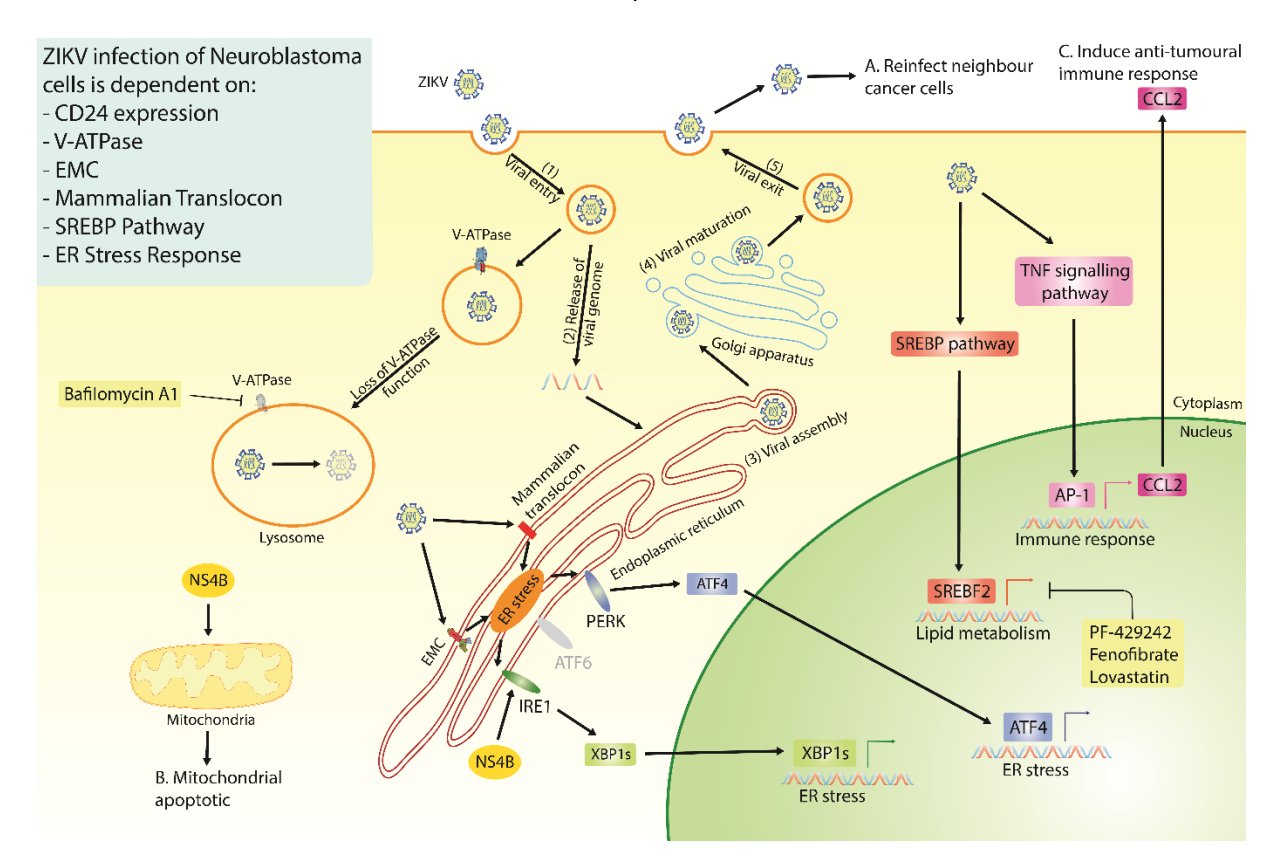


Figure 2. 8. ZIKV life cycle in neuroblastoma cells

A diagram that integrates the observations from the current study with that published in the literature to propose the ZIKV life cycle in neuroblastoma cells (Steps 1-5). A summary of all the dependencies that ZIKV has for infection of neuroblastoma cells is listed (top left). Highlighted are the three attractive properties of an oncolytic virus: (A) the production of new viral particles to infect additional cancer cells, (B) the ability to induce cancer cell death and (C) a mechanism through which ZIKV may induce an anti-tumoural immune response. Abbreviations, Zika virus (ZIKV), endoplasmic reticulum membrane protein complex (EMC), sterol regulatory element binding protein (SREBP), endoplasmic reticulum (ER), non-structural protein 4B (NS4B).

2.11 Tables

Table 2. 1. ZIKV infects and reduces cell viability of paediatric neuroblastoma cell lines.

Cell line	Cell Viability	Viability Reagent/Marker (timeframe in days)	Patient Age/Sex	Cancer type	Cell line origin	Morphology	MYCN status
SH-SY5Y	<20%	Annexin V ² (345), Annexin V/7-AAD ⁵ (349),	4/F	NB	BM metastasis (thorax)	Epithelial	Non-amp
		Eosin-Y ³ (350)					
SK-N-SH	<20%	Reliablue ^{3.5} (324), Giemsa ⁵ (253)	4/F	NB	BM metastasis (thorax)	Epithelial	Non-amp
SK-N-BE2	<20%	Eosin-Y ³ (350)	2/M	NB	BM metastasis	Neuroblast	Amplified
SK-N-DZ	<20%	Eosin-Y ³ (350)	2/F	NB	BM metastasis	Epithelial	Amplified
IMD 20		MTC10 (251) Facin V3 (250)	1 / N 4	ND	Abdominal mass	Neuroblast,	A ma m lifi a al
IMR-32	<20%	MTS ¹⁰ (251), Eosin-Y ³ (350)	1/M	NB	primary tumour	Fibroblast	Amplified
SMS-KAN	<20%	MTS ¹⁰ (251)	3/F	NB	Pelvic primary tumour	Neuroblast	Amplified
SMS-KCNR <20%	Facin V ³ (250)	1 / N 4	NID	BM metastasis	Navvalalaat	A ma m lifi a al	
SMS-KCNK	<20%	Eosin-Y ³ (350)	1/M	NB	(adrenal)	Neuroblast	Amplified
SK-N-FI	<20%	Eosin-Y ³ (350)	11/M	NB	BM metastasis	Epithelial	Non-amp
CHLA-42	<20%	MTS ¹⁰ (251)	1/NA	NB	BM metastasis	Epithelial	Non-amp
SK-N-BE1	~20%	MTS ¹⁰ (251)	2/M	NB	BM metastasis	Neuroblast	Amplified
LA-N-6	~60%	MTS ¹⁰ (251)	5/M	NB	BM metastasis (adrenal)	Neuroblast	Non-amp

Cell line	Cell Viability	Viability Reagent/Marker (timeframe in days)	Patient Age/Sex	Cancer type	Cell line origin	Morphology	MYCN status
SK-N-AS	>80%	MTS ¹⁰ (251)	6/F	NB	BM metastasis (adrenal)	Epithelial	Non-amp
T-268	>80%	Eosin-Y ³ (350)	22/F	Olfactory Metastasis (paraspinal		NA	NA
1-200	~80 %	E08III-1 (330)	22/17	NB	mass)	INA	INA
JFEN	>80%	Eosin-Y ³ (350)	22/M	Olfactory	Metastasis	NA	NA
)ı.EIN	~60 %		22/14	NB	(chest wall)	INA	INA

Cell lines are ranked by the degree to which ZIKV infection reduces their cell viability. Cell viability assay reagent/marker used in the original assay is stated with its accompanying reference. Superscript numbers in the Viability Reagent/Marker column denote the timepoint in days at which the assay was performed. Data was sourced from PubMed using the search terms 'Zika virus' and the name of commonly used neuroblastoma cell lines. Abbreviations, Zika virus (ZIKV), neuroblastoma (NB), bone marrow (BM), non-amplified (Non-amp), MYCN Proto-Oncogene (MYCN), not applicable (NA).

Table 2. 2. Different ZIKV strains demonstrate varying clinical potential against paediatric neuroblastoma cells.

ZIKV Strain	Lineage	Cell Viability	Viability Reagent/Marker (timeframe in days)	Degree of infection	Viral Titre	моі	Data Accordanc e	Infection Conditions
PRVABC59	Asian	<20%	MTS ¹⁰ (251), Eosin-Y ³ (350)	>80%	>10 ⁷ / ml	0.5-10	5	All cell lines in Table 2.1 (251,350,351)
Uganda #976	African	<20%	Reliablue ^{3.5} (324)	>60%	10 ⁶⁻⁷ /ml	0.01-10	4	SH-SY5Y (335), SK-N-SH (323,324)
Brazil PE/243	Asian	20-40%	MTT ⁴ (330), Annexin V/7-AAD ⁵ (349)	>60%	>10 ⁷ /ml	0.5-10	4	SH-SY5Y (330,349,352)
MR766	African	20-40%	Annexin V ² (345), Giemsa ⁵ (253)	>60%	>10 ⁷ /ml	0.01-10	3	SH-SY5Y (339,345,353,354), SK-N-SH (253,323,351,355)
SZ01/2016/ China	Asian	<20%	Annexin V² (345)	NA	>10 ⁷ /ml	1	NA	SH-SY5Y (345)
French Polynesia/2013	Asian	20-40%	Reliablue ^{3.5} (324)	>20%	10 ⁶⁻⁷ /ml	0.01-10	4	SH-SY5Y (335,356), SK-N-SH (323,324)
HS-2015-BA-01	Asian	40-60%	WST-1 ² (357)	NA	>10 ⁷ /ml	0.01-1	4	SH-SY5Y (322,357)

ZIKV Strain	Lineage	Cell Viability	Viability Reagent/Marker (timeframe in days)	Degree of infection	Viral Titre	MOI	Data Accordanc e	Infection Conditions
Paraiba/ 2015	Asian	20-40%	Giemsa⁵ (253)	NA	10 ⁶⁻⁷ /ml	0.1-10	2	SK-N-SH (160,253)
BR/800/16 Brazil 2016	Asian	40-60%	Reliablue ^{3.5} (324)	>20%	10 ⁶⁻⁷ /ml	0.1-1	NA	SK-N-SH (324)
PLCal_ZV	Asian	>80%	WST-1 ² (357)	NA	<10 ⁴ /ml	0.01-1	NA	SH-SY5Y (357)

ZIKV strains are ranked by their ability to infect (Degree of Infection), replicate within (Viral titre) and significantly reduce the cell viability (Cell Viability) of a multitude of neuroblastoma cells. The Data accordance is a qualitative measure that we employed to describe the degree of similarity of the results between publications that performed ZIKV infection assays of neuroblastoma cells using the same ZIKV strain. Data accordance of five denotes that the findings of one publication closely supports the findings from another, and data accordance of one denotes publications reporting vastly contrasting results. When a viral strain is published in only one paper, it is allocated a data accordance of NA. Superscript numbers in the Viability Reagent/Marker column denote the timepoint in days at which the assay was performed. Data was sourced from PubMed using the search terms 'Zika virus' and the name of commonly used neuroblastoma cell lines. Abbreviations, Zika virus (ZIKV), not applicable (NA).

Table 2. 3. ZIKV infection in neuroblastoma cells can be regulated through modifying lipid abundance, composition and localisation.

Compound	Cell line	Mechanism of action	Effect on ZIKV nfection	References
Bafilomycin A1 (V-ATPase inhibitor)	SH-SY5Y	Impairs acidification of endosomal-lysosomal compartments	Restrict	(335)
U18666A	SH-SY5Y	Cholesterol accumulation impairs late endosomes and lysosomes	Restrict	(335)
LXR 623 (LXR pathway agonist)	SK-N-SH	Induces cholesterol efflux	Restrict	(161)
PF-429242 (SREBP pathway inhibitor)	SK-N-SH	Reduces intracellular lipid levels	Restrict	(333)
Fenofibrate (SREBP pathway inhibitor)	SK-N-SH	Reduces intracellular lipid levels	Restrict	(333)
Lovastatin (SREBP pathway inhibitor)	SK-N-SH	Reduces intracellular lipid levels	Restrict	(333)
Oleic Acid	SK-N-SH	Increases lipid droplet abundance	Enhance	(333)
Cholesterol	SK-N-SH	Increases lipid droplet abundance	Restrict	(333)
DHA	SH-SY5Y	Anti-inflammatory and neuroprotective effects against ZIKV infection	Restrict	(330)

List of compounds that regulate lipid homeostasis and can restrict or enhance ZIKV infection in paediatric neuroblastoma cells. Abbreviations, Zika virus (ZIKV), liver X receptor (LXR), sterol regulatory element binding protein (SREBP), docosahexaenoic acid (DHA).

Chapter 3

Chapter 3 Multi-omics analysis reveals key

immunogenic signatures induced by oncolytic Zika

virus infection of paediatric brain tumour cells.

Matt Sherwood^{1,3}, Thiago G. Mitsugi², Carolini Kaid², Brandon Coke¹, Mayana Zatz², Kevin

Maringer^{3*}, Oswaldo K. Okamoto^{2*}, Rob M. Ewing^{1*}

¹School of Biological Sciences, Faculty of Environmental and Life Sciences, University of

Southampton, United Kingdom

²Centro de Estudos do Genoma Humano e Células-Tronco, Departamento de Genética e

Biologia Evolutiva, Instituto de Biociências, Universidade de São Paulo, Cidade Universitária,

São Paulo 05508-090, SP, Brazil

³The Pirbright Institute, Ash Road, Pirbright, Surrey, GU24 0NF, UK

ORCIDs:

Matt Sherwood: 0000-0002-1912-9758

Thiago Giove Mitsugi: 0000-0001-5940-194X

Carolini Kaid: 0000-0002-1852-6997

Brandon Coke: 0000-0002-0847-6885

Mayana Zatz: 0000-0003-3970-8025

Kevin Maringer: 0000-0003-0977-8807

Oswaldo Keith Okamoto: 0000-0002-8528-6225

Rob M. Ewing: 0000-0001-6510-4001

*Article Correspondence to:

rob.ewing@soton.ac.uk; keith.okamoto@usp.br or kevin.maringer@pirbright.ac.uk

Contact Author

Professor Rob M. Ewing

103

B85, Life Sciences Building
University of Southampton
University Road
Highfield
Southampton, Hants.
SO17 1BJ

Tel No: +44(0)2380 59 5503

email: rob.ewing@soton.ac.uk

3.1 Authorship Statement

This chapter is the product of: **Sherwood M**, Mitsugi TG, Kaid C, Coke B, Zatz M, Maringer K, et al. Multi-omics analysis reveals key immunogenic signatures induced by oncolytic Zika virus infection of paediatric brain tumour cells. Sci Rep. 2025 Apr 16;15(1):13090.

Matthew Sherwood, Carolini Kaid, Thiago G. Mitsugi, Rob M. Ewing and Oswaldo K. Okamoto jointly conceptualised and planned the study. Matthew Sherwood, Carolini Kaid and Thiago G. Mitsugi jointly performed the initial ZIKV infection experiments for RNA sequencing (RNA-Seq), and Matthew Sherwood performed all other infection experiments. Matthew Sherwood prepared and sent all samples for RNA-Seq and performed the RNA-Seq processing alongside Brandon Coke. Matthew Sherwood performed all RNA-Seq analysis. Matthew Sherwood also performed the 49-plex multiplex ELISA assay and its analysis, all laboratory validation experiments and all *in silico* modelling. Matthew Sherwood performed the investigation, created Figures 3.1B-3.8, created all tables and wrote the manuscript in its entirety. Carolini Kaid produced Figure 3.1A. Rob M. Ewing, Kevin Maringer and Oswaldo K. Okamoto supervised the research performed in this chapter and reviewed the finalised manuscript alongside Mayana Zatz. Matthew Sherwood, Rob M. Ewing and Oswaldo K. Okamoto acquired funding for the study.

Supplementary material for this chapter can be found in **Appendix B**.

3.2 Abstract

Brain tumours disproportionately affect children and are the largest cause of paediatric cancerrelated death. Despite decades of research, paediatric standard-of-care therapy still predominantly relies on surgery, radiotherapy, and systemic use of cytotoxic chemotherapeutic

agents, all of which can result in debilitating acute and late effects. Novel therapies that engage the immune system, such as OVs, hold great promise and are desperately needed. Zika virus (ZIKV) infects and destroys aggressive cells from paediatric medulloblastoma, atypical teratoid rhabdoid tumour (ATRT) diffuse midline glioma (DMG), ependymoma and neuroblastoma. Despite this, the molecular mechanisms underpinning this therapeutic response are grossly unknown. By profiling the transcriptome across a time course, we comprehensively investigated the response of paediatric medulloblastoma and ATRT brain tumour cells to ZIKV infection at the transcriptome level for the first time. We observed conserved TNF signalling and cytokine signalling-related signatures following ZIKV infection. We demonstrated that the canonical TNFalpha signalling pathway is implicated in oncolysis by reducing the viability of ZIKV-infected brain tumour cells and is a likely contributor to the anti-tumoural immune response through TNF-alpha secretion. Our findings have highlighted TNF-alpha as a potential prognostic marker for oncolytic ZIKV virotherapy. Performing a 49-plex ELISA, we generated the most comprehensive ZIKV-infected cancer cell secretome to date. We demonstrated that ZIKV infection induces a clinically relevant and diverse pro-inflammatory brain tumour cell secretome, thus circumventing the need for transgene modification to boost efficacy. We assessed publicly available scRNA-Seq data to model how the ZIKV-induced secretome may (i) interact with medulloblastoma tumour microenvironment (TME) cells via paracrine signalling and (ii) polarise lymph node immune cells via endocrine signalling. Our modelling has provided significant insight into the cytokine response that orchestrates the diverse anti-tumoural immune response during oncolytic Zika virus (oZIKV) infection of brain tumours. Our findings have significantly contributed to understanding the molecular mechanisms governing oZIKV infection and will help pave the way towards oZIKV therapy.

Keywords:

Paediatric brain tumours, Zika virus, Oncolytic Virotherapy, RNA sequencing, TNF Signalling, Multiplex ELISA, Cytokine

3.3 Introduction

Malignant paediatric central nervous system (CNS) tumours, including medulloblastoma and ATRT, are the most common solid childhood cancer and are the leading cause of mortality in paediatric cancer patients (11). Current therapy regimens are aggressive and frequently result in debilitating long-term sequelae that ultimately impair the quality of life of patients who do not succumb to fatal tumour recurrence. There is a clear and unmet need for less toxic and more

targeted therapies, especially those capable of co-opting the immune system against the tumour. Oncolytic viruses selectively infect and kill cancer cells, thus minimising long-term sequelae by reducing the need for high doses of chemotherapy and radiotherapy. Their efficacy stems from a two-pronged mechanism of action where the virus can directly lyse infected cancer cells (oncolysis) and elicit an anti-tumoural immune response. Many cancers, including medulloblastoma and ATRT, contain cancer stem-like cells (CSCs) that drive poor prognosis factors such as elevated tumour heterogeneity, metastasis and therapeutic resistance (67,68). The ability of OVs to target these aggressive stem-like cells is a unique advantage in overcoming the therapeutic resistance of these highly heterogeneous and malignant cancers. To date, four OVs have been been approved for clinical use, and over 200 OV clinical trials are underway to treat aggressive forms of cancer (358). OV research has gained momentum since 2015, when the first FDA approval was granted for a modified form of herpes simplex virus (HSV) type 1 (T-VEC) to treat recurrent adult melanoma (113). In 2022, a breakthrough in the fight against brain cancer was made when the Japanese Ministry of Health, Labor and Welfare approved the oncolytic herpes virus Delytact (G47 Δ) for the treatment of residual or recurrent adult glioblastoma (115). A dozen clinical trials have assessed OV therapy against paediatric brain tumours, half of which have been completed, and some have reported improved patient survival. Crucially, all report that OVs are primarily accompanied by low-grade adverse events, with only rare instances of grade 3 adverse events (116–120).

Zika virus (Orthoflavivirus zikaense) is a positive-sense single-stranded RNA (+ssRNA) virus in the Orthoflavivirus genus. Maternal ZIKV infection during the first, second and third trimesters of human pregnancy results in vertical transmission in 47%, 28% and 25% of cases, and congenital Zika syndrome (CZS) symptoms in 9%, 3% and 1% of cases, respectively (214). ZIKV infects radial glial cells (RGCs) and neural precursor cells (NPCs), leading to cell death and growth reduction in the fetal brain (177–180). Postnatal ZIKV infection can also result in CNS cell infection, including neural progenitors, mature neurons, and various glial cells (astrocytes, oligodendrocytes and microglia) (359–361). Postnatal ZIKV infection is primarily asymptomatic, with the disease generally being self-limiting and symptoms resolving within two to seven days (215). Both ZIKV-infected children and adults suffer from the same main acute symptoms: headache, fever, rash (exanthema), joint pain (arthralgia), conjunctivitis, and muscle pain (myalgia) (231,232). In rare instances, more severe conditions such as Guillain-Barré syndrome (GBS), meningitis and encephalitis can occur; however, these primarily affect adults rather than children (215,233). Work by ourselves and others has shown that ZIKV can infect and destroy aggressive cells from paediatric (medulloblastoma, ATRT, DMG, ependymoma and neuroblastoma) and adult (glioma and meningioma) nervous system tumours (243,249251,260,265,279,362). We demonstrated that ZIKV effectively targets and destroys human CNS tumour cells and can inhibit metastatic spread without causing neurological damage in xenograft mouse models (249,256). ZIKV-induced tumoural immune cell infiltration has been documented to include lymphoid (CD4+ T, CD8+ T and NK cells) and myeloid (monocytes, macrophages, dendritic cells (DCs) and microglia) cells (266,271,277). This leads to ZIKV-induced tumour clearance and long-term immunity against tumour cells in immunocompetent glioma mice models, which is dependent on CD4+ and CD8+ T cells (266,271,277). In a preclinical study, members of our research team confirmed ZIKV efficacy against spontaneous intracranial canine tumours (264). ZIKV infection reduced tumour volume, induced an antitumoural immune response, improved clinical symptoms, and did not cause any persisting adverse conditions in canines (264).

Large data and omics techniques have revolutionised our understanding of biological systems. As these techniques are yet to be applied to oZIKV infection, the biology governing the response in paediatric brain tumour cells is generally unknown, with WNT signalling being the only known molecular mechanism involved (249). Assessing oZIKV infection of tumour cells alongside clinically relevant CZS patient-derived NPCs is important to tease out any common or differential mechanisms that ZIKV utilises for either tumour cell oncolysis or its fetal neuropathology. Despite this, CZS patient-derived NPCs are yet to be incorporated into oncolytic ZIKV research. The efficacy of most OVs is heavily dictated by the ability to induce immunogenic cell death (ICD) and a concomitant anti-tumoural immune response (363). It is currently unclear how intracellular or extracellular factors, such as signalling pathways or cytokine secretion, may contribute to ZIKV ICD and orchestrate the anti-tumoural immune response.

In the current study, we first performed a transcriptomic temporal survey and observed cell type-specific responses of paediatric brain tumour cells and CZS patient-derived NPCs during early ZIKV infection (12-24 hours post-infection (hpi)). NPCs are highly sensitive to ZIKV infection and undergo vast downregulation of neurodevelopmental processes and essential upstream signalling pathways, likely underpinning the development of CZS in these patients (193). In ZIKV-infected paediatric brain tumour cells, we observe transcriptomic signatures indicative of ICD, TNF pathway and cytokine signalling responses. We show the upregulation of canonical and non-canonical TNF signalling pathways following infection, and we identify TNF-alpha as a potential prognostic marker for brain tumour oZIKV therapy. Investigating cytokine signalling, we generate the most comprehensive ZIKV-infected cancer cell secretome to date and show that ZIKV infection induces a diverse and predominantly pro-inflammatory secretome from

paediatric brain tumour cells. Assessing publicly available scRNA-Seq data, we employ an *in silico* approach to model how the ZIKV secretome may contribute to an anti-tumoural immune response. We achieved this by assessing how our identified ZIKV-induced pro-inflammatory secretome may interact with medulloblastoma TME cells via paracrine signalling or polarise lymph node immune cells via endocrine signalling. In summary, our findings shed light onto the molecular mechanisms underpinning oZIKV infection of paediatric brain tumour cells and contribute to the ultimate goal of developing an oncolytic ZIKV virotherapy for paediatric oncology.

3.4 Methods

3.4.1 Cell and Viral Culture

Paediatric USP7-ATRT (USP7) and USP13-Med (USP13) medulloblastoma cells were cultured as previously described (249,255), as were the paediatric CZS-affected patient-derived NPCs (NPC-763-1 and NPC-788-1) (193). Vero cells were cultured in complete DMEM (Gibco, 41966029) with 10% FBS and 1% Penicillin-Streptomycin (5% CO₂, 37°C) and passaged 1:12 every 72 hours. Stocks of two highly conserved Brazilian epidemic ZIKV strains, BeH819966 (KU365779.1) and Paraiba_01 (KX280026.1), were maintained at Instituto Butantan (USP) and The Pirbright Institute, respectively. To maintain stocks, Vero cells in serum-free DMEM were infected for 90 min. At 96 hpi or when sufficient CPE was detected, virus was collected, clarified, filtered (0.22 µm) and stored as single-use aliquots at -80°C. Virus was titrated in technical duplicate in Vero cells by plaque forming units (PFU) assay, using a 10-fold dilution series in serum-free DMEM. Following 90 min infection, cells were washed with PBS, a solid overlay of UltraPure 1% LMP agarose (Invitrogen, 16520-100) containing 0.83% complete DMEM was added, and plates were incubated for 72 hours. Plaques were fixed with formalin overnight, washed with PBS, and stained with crystal violet for 5 min. All brain tumour cell and NPC infection experiments were performed at a multiplicity of infection (MOI) of 2 for 60 min. Infection experiments for confocal microscopy and RNA-Seq used BeH819966, whilst all remaining infection experiments used Paraiba_01.

3.4.2 Confocal Microscopy

Brain tumour cells were plated on coverslips for 24 hours prior to infection, infected and then fixed with 4% PFA for 40 min. Cells were permeabilised and blocked with PBSAT for 30 min, incubated in primary antibody anti-NS2B (Genetex, GTX133308) for 90 min, and then secondary

antibody (ThermoFisher, A-11007) for 60 min. Cells mounted in VECTASHIELD Medium with DAPI (Vector Laboratories, H-1200-10). Coverslips were washed with PBS three times between incubations. Coverslips were stored until imaged via confocal microscopy with ZEN Software.

3.4.3 RNA Sequencing

At 12, 18 and 24 hpi, cells were collected, washed with PBS and stored as pellets at -80°C (N = 3). High-quality total RNA was purified using the Monarch Total RNA Miniprep Kit (NEB #T2010S) per the manufacturer's protocol. mRNA sequencing was performed by Novogene (UK) Company Limited using the Illumina NovaSeq 6000 system (≥20 million 150 bp paired-end reads per sample). The RNA-Seq data processing pipeline consisted of FastQC (V0.11.9-0), Trim Galore (V0.6.6-0), HISAT2 (V2.2.0), Samtools (V1.11) and Subread (V2.0.1). Reads were aligned against the Homo Sapien GRCh38 and ZIKV BeH819966 genome, and differential gene expression analysis was performed using DESeq2 to identify brain tumour (padj \leq 0.05, Fold Change \geq 0) and NPC (padj ≤ 0.05, Fold Change ≥ 1.5) DEGs. All DEGs are presented as Log2(Fold Change) (LFC) with p-values corrected for multiple testing by the Benjamini and Hochberg method (padj ≤ 0.05). Upregulated and downregulated DEGs were submitted to DAVID to identify upregulated and downregulated Gene Ontology (GO) Biological Processes, KEGG pathways and Reactome pathways, respectively (310). For enrichment analysis, significance values were corrected for multiple testing using the Benjamini and Hochberg method (padj ≤ 0.05). Hierarchical clustering ordered the terms (rows) by similarity across the twelve infection conditions. The top 120 DEGs were determined by ranked absolute Log2(Fold Change) value, and KEGG pathway analysis was performed for these brain tumour DEGs using DAVID.

3.4.4 Recombinant TNF Assays

USP7 and USP13 cells were treated with 100µg/ml recombinant TNF-alpha (Peprotech, 300-01A), TNFSF9 (Peprotech, 310-11), TNFRSF9 (Peprotech, 310-15) or a 0.1% BSA vehicle control. For Incucyte Live Cell Growth Analysis, USP7 and USP13 cells were plated at low confluence in sufficient media and allowed to grow until the first condition of each cell line reached 95% confluency. Confluence was determined by the Confluence Basic Analyser, with the phase map trained using AI specifically off each cell line (label-free) at varying confluency to ensure the accuracy of readings during live cell imaging. Cell culture supernatant was collected at 48 hpi for infection experiments, clarified, stored as single-use aliquots at -80°C, and titrated via PFU in Vero cells. Cell viability was determined using the CellTiter-Glo Assay (Promega, G7572), per the manufacturer's protocol. For all recombinant TNF assays, significance was defined and

corrected for multiple testing by two-way ANOVA with Dunnett's multiple correction (padj ≤ 0.05).

3.4.5 Medulloblastoma Patient Survival Analysis

Medulloblastoma patient gene expression and survival data were sourced from the Gene Expression Omnibus (GEO) using GEO2R with accession GSE85218 (GPL22286) (17). ATRT patient survival analysis could not be performed due to the extreme scarcity of ATRT datasets. Patient survival was censored at five years, and Kaplan-Meier survival analysis was performed for the remaining 375 patients. Logrank P value was determined by univariate Cox regression (p ≤ 0.05), comparing survival between the upper and lower quartiles based on candidate gene expression. Hazard rate (HR) with 95% confidence intervals are reported. Analysis was performed using KMplot (364).

3.4.6 ProcartaPlex Multiplex ELISA Assay

At 12, 24 and 48 hpi, cell culture supernatant was collected from infected USP7 and USP13 cells, centrifuged, and stored as single-use aliquots at -80°C (n = 2, N = 3). ProcartaPlex kits quantified supernatant protein concentration of 34 cytokines (Invitrogen, EPXR340-12167-901) and 15 immune checkpoint proteins (Invitrogen, EPX010-15901-901 and EPX14A-15803-901), as per the manufacturer's protocol. Data was collected using a Bio-Plex 200 and processed on the ThermoFisher ProcartaPlex Analysis App. Optimised standard curves were plotted with a 5 PL Logistic fit. For each condition, outliers were omitted and technical duplicates were averaged. Multiple unpaired t-tests defined significance with Benjamini and Hochberg correction (False Discovery Rate (FDR) \leq 0.05). Principal components analysis (PCA) was performed on the averaged Net MFI values.

3.4.7 Paracrine Signalling Analysis

A scRNA-Seq log-transformed normalised gene counts matrix of 28 untreated primary paediatric human medulloblastoma tumours was sourced from the Tumor Immune Single-cell Hub 2 (TISCH2) (365). Analysis was limited to medulloblastoma due to the absence of ATRT scRNA-Seq datasets. The scRNA-Seq dataset consisted of 37,445 cells: 32,926 Tumour cells, 2,665 monocytes/macrophages, 1,590 CD8+ T cells and 264 neutrophils (GEO accession GSE155446) (366). TISCH2 processed and analysed the dataset using the MAESTRO workflow, and the gene counts matrix reports the average expression per cell type. Gene set enrichment analysis (GSEA) and the expression of specific cytokine receptors of interest were plotted using

the log-transformed normalised gene counts matrix. GSEA was performed by comparing each immune cell type against the tumour cells for immune cell pathway enrichment, and then tumour cells against all immune cells for tumour cell pathway enrichment (367). Analysis was performed with the Reactome database, and significant pathways ($p \le 0.05$ and FDR ≤ 0.25) relating to Interleukin-, Interferon-, TNF- and Chemokine-receptor signalling were plotted.

3.4.8 Endocrine Signalling Analysis

Dominant cytokine drivers of immune cell polarisation were identified from the Immune Dictionary publication (368). scRNA-Seq of mouse lymph node cells following individual recombinant cytokine treatment *in vivo* was sourced using the Immune Dictionary Application (IDA). Within the IDA, DEGs were determined by a two-sided Wilcoxon rank-sum test comparing normalised gene expression values of cytokine treatment versus PBS control (N = 3), with significance corrected for multiple testing (FDR \leq 0.05). The Top 20 upregulated DEGs for each cytokine-immune cell interaction of interest (**Supplementary Tables 3.2-3.5**) were used to deduce the cytokine-induced immune cell polarisation phenotype. DEGs of interest were mapped to their human orthologs using g:Profiler for inclusion in **Figure 3.7** (369).

3.5 Results

3.5.1 ZIKV infection induces cell type-specific transcriptome responses

Following ZIKV infection, we observe distinct sub-cellular staining of ZIKV non-structural (NS) protein 2B from 12 hpi in the aggressive paediatric USP7 ATRT and USP13 medulloblastoma cell lines (Figure 3.1A). Viral titration primarily identifies an increase in the release of mature viral particles between 12 hpi and 24 hpi (Figure 3.1B). Collectively, this indicates 12-24 hpi as a biologically relevant timeframe during early ZIKV infection. To investigate this, we infected USP7 (P7) and USP13 (P13) brain tumour cells and NPC-763-1 (N3) and NPC-788-1 (N7) NPCs for 12, 18, and 24 hours and we performed RNA-Seq. We observed that both in the presence and absence of ZIKV infection, the brain tumour cell transcriptomes highly contrast that of the NPCs (Figure 3.1C, Supplementary Figure 3.1A). In most instances, hierarchical clustering and PCA group the RNA-Seq samples by experimental condition, cell line, and disease state (Figure 3.1C, Supplementary Figure 3.1B). Assessing ZIKV genome expression, we observe approximately 32, 131 and 356 times more viral genome counts in the tumour cells than in the NPCs at 12, 18 and 24 hpi, respectively (Figure 3.1D). This highlights a greater propensity for ZIKV to replicate in brain tumour cells than in NPCs, possibly due to the dysregulation of

antiviral responses during transformation. Despite the low accumulation of ZIKV genomes in the NPCs, thousands of DEGs are observed (**Table 3.1**), supporting the well-known highly sensitive nature of NPCs to ZIKV infection.

Gene Ontology (GO) enrichment analysis identifies a multitude of differentially regulated biological processes in ZIKV-infected brain tumour and neural precursor cells (Figure 3.2A). We observe vast downregulation of developmental biological processes in ZIKV-infected NPCs that are known to contribute to CZS development, including terms related to morphogenesis, CNS development, neuron migration, and differentiation (Figure 3.2A). Multiple developmental signalling pathways which govern and coordinate these biological processes are also differentially regulated in ZIKV-infected NPCs, including WNT, Hippo, MAPK, Notch, TGF-beta, and PI3K-Akt signalling pathways (Figure 3.2B). The largest differential gene, biological process, and pathway responses in brain tumour cells occur at 24 hpi (Table 3.1, Figure 3.2). By 24 hpi, multiple terms implicated in cell interaction and the extracellular matrix are downregulated, whilst "apoptotic process", "protein ubiquitination", "protein processing in endoplasmic reticulum" and "negative regulation of transcription from RNA polymerase II promoter" terms are upregulated in both ZIKV-infected brain tumour cells (Figure 3.2). Multiple cell cycle, DNA replication and DNA repair terms are significantly upregulated specifically in USP13 cells during 12-18 hpi, whereas cell cycle-related terms are significantly downregulated in USP7 at 24 hpi, indicating that ZIKV may differentially regulate brain tumour cell growth.

Comparing the highest-ranked DEGs at 24 hpi, we sought to identify the main conserved molecular mechanisms between the brain tumour cell lines. We observed a 34.2% overlap for brain tumour cell lines, a 42.5% overlap for NPCs, and no overlap between brain tumour cells and NPCs (Figure 3.3A). Plotting the 41 shared brain tumour DEGs (Figure 3.3B) and 51 shared NPC DEGs (Figure 3.3C) highlights a conserved cell-type specific transcriptome response to ZIKV infection as the directionality of all DEGs plotted are the same. KEGG pathway analysis on the highest ranked brain tumour DEGs identified ten significantly enriched terms that are predominantly involved in pathogen-host interaction ("Viral protein interaction with cytokine and cytokine receptor", "Toll-like receptor signalling pathway", "Influenza A" and "Amoebiasis"), immune response ("Cytokine-cytokine receptor interaction", "TNF signalling pathway", "NF-kappa B signalling pathway" and "IL-17 signalling pathway") and cell death ("Apoptosis") (Figure 3.3D). Considering the 41 shared brain tumour DEGs (Figure 3.3B), we sought to gain further insight into these enriched pathways to identify candidates for validation. We identify genes involved in TNF signalling and its downstream activity (TNF, TNFSF9, TNFRSF9, CCL5, MAP3K8, TRIB3, NFKBIE and OTUD1), the unfolded protein response (UPR)

(ERN1, DDIT3, DNAJB9, ATF3 and HERPUD1), cell death (DDIT3, PMAIP1, BBC3, and CHAC1), antiviral responses (IFIT1, IFIT2, RSAD2, IFIH1 and OASL), interleukins (IL1A, IL7R and NFIL3), neuronal processes (RND1, LRRN3 and UNC5B), and lipid homeostasis (STARD4 and CH25H) (Figure 3.3B). Notably, we observe joint upregulation of the UPR-regulated pro-apoptotic transcription factor DDIT3 (CHOP), its downstream pro-apoptotic gene CHAC1 and two BCL2-homologous (BH)-3-only proteins that are effectors of canonical mitochondrial apoptosis (PMAIP1 (NOXA) and BBC3 (PUMA)) (Figure 3.3B). These pro-apoptotic and ER stress signatures indicate ZIKV as a Type II ICD inducer for brain tumour cells, as expected for an ER-tropic virus. TNF and pro-inflammatory cytokine signalling are principal outcomes of ICD, and we observe terms related to these as the top two ZIKV-infected brain tumour cell-enriched KEGG pathways (Figure 3.3D). To conclude, (i) ZIKV infection leads to conserved cell type-specific transcriptomic responses, (ii) NPCs undergo vast downregulation of neurodevelopmental processes following infection, and (iii) ZIKV-infected brain tumour cells portray ICD transcriptomic signatures.

3.5.2 TNF-alpha is a potential prognostic marker for brain tumour oZIKV therapy

Assessing all differentially expressed TNF ligands, receptors, and adaptors, we observe the most highly upregulated DEGs in both ZIKV-infected USP7 and USP13 cells to be key components of the canonical TNF pathway (TNF-alpha) and non-canonical TNF receptor superfamily member 9 pathway (TNFSF9, TNFRSF9 and TRAF1) (Figure 3.4A). Activation of either pathway results in downstream NF-kappa B signalling, which we observe to be significantly enriched in the highest-ranked ZIKV-infected brain tumour DEGs (Figure 3.3D). Data mining publicly available ZIKV-infected glioma and neuroblastoma RNA-Seq datasets, we observe that TNFRSF9 and one of its adaptors (TRAF1) are significantly upregulated in all cases, TNFSF9 is significantly upregulated in three instances, and TNF-alpha is significantly upregulated in all four brain tumour datasets (Figure 3.4B). Thus, these responses appear conserved across different ZIKV-infected nervous system tumour cells. Performing ProcartaPlex ELISA assays, we assessed whether the soluble TNF factors of these pathways (TNF-alpha, TNFSF9 and TNFRSF9) were secreted following infection and observed significantly increased secretion of TNF-alpha (Figure 3.4C) and TNFRSF9 (Figure 3.4D) from both USP7 and USP13 cells at 48 hpi. TNFSF9 was not reliably detected or quantified under any condition (Figure 3.4E). Thus, we show that ZIKV infection of brain tumour cells leads to the upregulated expression and secretion of key members of both canonical and non-canonical TNF signalling pathways.

Next, we sought to functionally assess these soluble proteins for their (i) effect on brain tumour cell growth, (ii) anti- or pro-viral properties, and (iii) effect on brain tumour cell viability following ZIKV infection. We employed Incucyte Live Cell Imaging to analyse USP7 and USP13 cell growth by tracking cell confluence following treatment with recombinant TNF proteins (Figures 3.4F and 3.4G). None of the recombinant TNF proteins were cytotoxic, and TNF-alpha significantly increased both USP7 and USP13 confluence, indicating that soluble TNF-alpha enhances brain tumour cell growth (Figures 3.4F and 3.4G). Next, we assessed the effect of recombinant protein treatment on ZIKV titre (Figure 3.4H) and tumour cell viability (Figure 3.4I). Viral titre was unaffected by all TNF proteins, suggesting that none possess anti- or pro-viral properties (Figure 3.4H). TNF-alpha significantly reduced ZIKV-infected USP7 cell viability, and a modest but nonsignificant reduction was observed in ZIKV-infected USP13 cells (Figure 3.4I). Performing a fiveyear survival analysis on clinical and gene expression data for 375 medulloblastoma patients, we observe high TNF-alpha expression to be significantly correlated with worse survival (Figure 3.4J) and high TNFRSF9 expression to be significantly correlated with improved survival (Figure **3.4K**). Thus, TNF-alpha is a marker of poor prognosis for medulloblastoma patients, possibly by enhancing brain tumour cell growth. Here, we show that TNF-alpha (i) is a brain tumour cell growth factor, (ii) reduces brain tumour cell viability in the presence of ZIKV infection, and (iii) is a marker of poor prognosis for medulloblastoma. Collectively, our results indicate that TNFalpha holds promise as a potential prognostic marker for brain tumour oZIKV therapy.

3.5.3 ZIKV infection stimulates a diverse pro-inflammatory cytokine secretome from brain tumour cell lines

Extending our TNF ELISA assays to a 49-plex ELISA, we sought to validate the cytokine-related transcriptomic signatures enriched in ZIKV-infected brain tumour cells (**Figure 3.3D**). Assessing the temporal secretion of 34 cytokines (including TNF-alpha) and 15 immune checkpoint proteins (including TNFRSF9 and TNFSF9), we generate the most comprehensive ZIKV-infected cancer cell secretome to date (**Supplementary Table 4.1**). PCA clusters the secretome by cell line and highlights the 48-hour ZIKV-infected condition for both cell lines to vary from all other samples (**Figure 3.5A**). In addition to TNF-alpha (**Figure 3.4C**), we observe significantly increased secretion of 18 cytokines, predominately at 48 hpi (**Figure 3.5B**). Seven cytokines are significantly secreted by both infected cells (CXCL1, IL-1 alpha, IL-6, CXCL10 (IP-10), CCL3, CCL4 and CCL5 (RANTES)), six from infected USP7 cells only (CCL11, IL-4, IL-8 (CXCL8), IL-9, IL-21 and SDF-1 alpha) and five from infected USP13 cells only (GM-CSF, IFN alpha, IL-1 beta, IL-1RA and IL-5) (**Figure 3.5B**). Strikingly, of the 15 immune checkpoint proteins, TNFRSF9 was the only significantly secreted protein (**Figure 3.4D**), and PD-L2 was the only other protein detected

across all conditions (**Supplementary Table 3.1**). ZIKV infection did not significantly reduce the secretion of any protein. Integrating the 49-plex ELISA and RNA-Seq data, we observe 27 of the 49-plex proteins to be significantly differently expressed or secreted by USP7 or USP13 following ZIKV infection (**Figure 3.6A**). These diverse proteins encompass chemokine, interleukin, tumor necrosis factor, interferon, colony stimulating factor and programmed cell death proteins. Considering the primary role of each protein during an immune response, we identify that ZIKV infection predominantly promotes a pro-inflammatory rather than anti-inflammatory cytokine profile (**Figure 3.6A**). Additionally, we identify many cytokines which orchestrate adaptive immune responses. Crucially, many of these proteins are current OV transgenes or immunotherapy candidates. To conclude, ZIKV infection induces a diverse pro-inflammatory secretome from brain tumour cells, containing many cytokines which can mediate an OV-stimulated anti-tumoural immune response.

3.5.4 In silico modelling predicts the medulloblastoma tumour immune microenvironment (TIME) is primed to respond to pro-inflammatory ZIKV secretome paracrine signalling

Employing an in silico approach, we sought to model how the ZIKV-induced pro-inflammatory USP13 medulloblastoma secretome may interact with tumour and immune cells of the medulloblastoma TME. Our model predicts the indirect effects of ZIKV infection (i.e. through the ZIKV-induced brain tumour secretome) rather than the direct effects (i.e. direct interaction through ZIKV infection) on these cells. Analysing publicly available medulloblastoma scRNA-Seq, we identify positive enrichment of many cytokine-related Reactome pathways by GSEA (Figures 3.6B and 3.6C) and greater cytokine receptor expression (Figure 3.6D) in monocytes/macrophages, CD8+ T cells and neutrophils than in medulloblastoma tumour cells. All immune cells express receptors for TNF-alpha (TNFRSF1A and TNFRSF1B) and IFN alpha (IFNAR1 and IFNAR2) and are enriched for these pathways, indicating that all these immune cell types are primed to respond to secreted TNF-alpha and IFN alpha in the medulloblastoma TME (Figures 3.6B-D). Monocytes/macrophages and neutrophils express the CCL3 and CCL5 receptor CCR1, while CD8+T cells express the CXCL10 receptor CXCR3 and the CCL4 and CCL5 receptor CCR5. All three immune cell types are enriched for the "Chemokine receptors bind chemokines" Reactome pathway and are, therefore, likely to respond to these secreted chemokines. Additionally, monocytes/macrophages and neutrophils express the main GM-CSF receptor CSF2RA and are enriched in the "Interleukin-3, Interleukin-5 and GM-CSF signalling pathway", indicating potential to respond to secreted GM-CSF. Finally, neutrophils express receptors for IL-1 (IL1R2 and IL1RAP) and IL-6 (IL6R and IL6ST) and are the only cell type

enriched for their related pathways, indicating a possible neutrophil-specific response to secreted interleukins. Collectively, our modelling predicts that secretion of the cytokines which make up the ZIKV-induced pro-inflammatory secretome would remodel the medulloblastoma TIME.

3.5.5 In silico modelling predicts the pro-inflammatory ZIKV secretome to stimulate diverse immune cell polarisations through endocrine signalling

Employing an in silico approach, we next sought to model how our ZIKV-induced proinflammatory secretome may interact with lymph node (i.e. non-tumour-resident) immune cells, and predict if the secretome would induce immune cell polarisations towards an antitumoural state. To achieve this, we interrogated scRNA-Seq data in the Immune Dictionary (a dictionary documenting over 17 immune cell type responses to 86 different cytokines at the single-cell transcriptome level) (368). Six of our 20 differentially secreted proteins (IFN alpha, IL-1 alpha, IL-1 beta, IL-4, TNF-alpha and GM-CSF) are documented in the Immune Dictionary as dominant cytokines which drive polarisation states of the main lymphoid (CD4+ T, CD8+ T and NK cells) and myeloid (monocytes, macrophages, DCs and neutrophils) cell types implicated in anti-tumoural immune responses (368). We sought to elucidate the immune cell phenotypes following cytokine stimulation by assessing individual cytokine-immune cell interactions, the resulting immune cell polarisation states, and the top-upregulated DEGs (Figure 3.7). We observe all six cytokines to be pleiotropic, polarising the eight immune cell types into 26 distinct states (Figure 3.7). IFN alpha, IL-1 alpha, and IL-1 beta polarise every cell type. IFN alpha induces a unique polarisation (suffix -a), and IL-1 alpha and IL-1 beta (collectively referred to as IL-1) induce a conserved polarisation (suffix -c). We observe self-regulation of cytokine signalling transduction by positive feedback receptor upregulation (e.g. IL4R), negative feedback inhibitory receptor upregulation (e.g. IL1R2), and upregulation of cytokine signalling regulators (SOCS1, SOCS3, CISH and DUSP10). Most cytokines sensitise or suppress the immune cells to other cytokine signalling through upregulated expression of cytokines (e.g. CXCL9), receptors (e.g. IFNGR1), or receptor antagonists (e.g. IL1RN).

We observe TNF-alpha to act on myeloid rather than lymphoid lineage cells (**Figure 3.7**). All TNF-alpha and GM-CSF-stimulated myeloid cells upregulate the anti-apoptotic BCL2A1 gene, indicating a BCL2A1-mediated pro-survival mechanism. TNF-alpha induces the expression of IL1RN (IL-1RA) and the pattern recognition receptors CLEC6A and CLEC4E in monocytes, macrophages and cDC2s, possibly suppressing IL-1 responses and priming myeloid cells for innate immune recognition. Upregulation of LY6S indicates CD4+ and CD8+ T cell activation by

IFN alpha and IL-1 (T4-a, T4-c, T8-a and T8-c). Upregulation of the effector memory T cell marker GBP2 indicates that T4-a and T4-c likely become effector memory CD4+ T cells. Upregulation of the principal cytotoxic granzyme GZMB indicates that T8-c are likely cytotoxic CD8+ T cells. T cell survival may be driven in a BCL2-mediated manner following IL-4 stimulation (T4-f and T8-f) and a STAT3/BCL3-mediated manner following IL-1 stimulation (T4-c and T8-c). IFN alpha and IL-1 beta upregulate cytotoxic granzyme GZMB expression in NK-a and NK-c cells, and the cytotoxicity regulator KLRB1 may govern the NK-c cytotoxic state. As IFN gamma (IFNG) signalling promotes cytotoxicity, all observed cytotoxic polarisation will likely be augmented by their upregulation of IFNG (NK-a) or its receptor IFNGR1 (NK-c and T8-c). Notable upregulation of C-C Motif Chemokine Ligands (CCL) known to govern immune cell chemotaxis are observed for all macrophage polarisations, with a conserved CCR2 axis (CCL2, CCL7 and CCL8) for Maca, Mac-c and Mac-e. The Mac-c and Mac-e polarisations present with upregulated M2 macrophage marker (MRC1 (CD206) or CD209) expression, implicating them as M2-like macrophages. Conversely, Mac-a presents with upregulated expression of pro-inflammatory CXCL9 and CXCL10 cytokines, indicative of M1-like macrophages. IL-1 and GM-CSF-induced Mono-c and Mono-e polarisations upregulate M1 macrophage differentiation marker VCAN, suggestive of monocyte to M1-like macrophage differentiation. Both IL-1-induced Mono-c and IL-1 beta-induced Mac-c polarisations have upregulated monocyte/macrophage migration (JAML) and differentiation (MAFB) marker expression. To conclude, in silico modelling of ZIKVinduced secretome endocrine signalling indicates a diverse immune cell response, including (i) effector memory CD4+ T cells (T4-a and T4-c), (ii) cytotoxic CD8+ T cells (T8-c), (iii) cytotoxic natural killer (NK) cells (NK-a and NK-c), (iv) M1-like (Mac-a) and M2-like (Mac-c and Mac-e) macrophages, (v) M1-like macrophage-destined monocytes (Mono-c and Mono-e), and (vi) neutrophils, cDC and other immune cell polarisations of currently unknown phenotype.

3.6 Discussion

In the current study, we conducted the first multi-omics-based investigation of ZIKV infection in paediatric brain tumour cells and demonstrated a stark contrast in their response compared to that of CZS patient-derived NPCs. While brain tumour cells presented with high ZIKV genome count levels and low DEG numbers, NPCs presented with low ZIKV genome count levels and high DEG numbers. Notably, antiviral response processes, such as the "response to interferonbeta" GO biological process, were upregulated in infected NPCs, but not in infected brain tumour cells. Collectively, our results indicate that the stark contrast observed between the different ZIKV-infected cell types is due to NPCs mounting an antiviral response following infection to curb ZIKV replication, whereas productive brain tumour cell infection is established in the absence of an antiviral response. In light of these findings, it is unsurprising that we observed no overlap between the top DEGs across the different cell types, and that this likely reflects a difference in infection status rather than cell-type-specific responses to infection.

ZIKV infection leads to a potent anti-tumoural immune response against mouse glioma, resulting in tumour clearance and long-term immunity against tumour cells (266,271,277). It is currently unknown what ICD mechanisms orchestrate this crucial efficacious response. Here, our RNA-Seq analysis highlighted the involvement of TNF and cytokine signalling as indicators of ICD in ZIKV-infected paediatric brain tumour cells (370). Previous observations by members of our research team support these observations and have shown that (i) this upregulated transcriptomic TNF and cytokine response is also observed in ZIKV-infected neuroblastoma cells, (ii) ZIKV-infected brain organoids co-cultured with USP7 or USP13 cells upregulate expression of TNF and a limited number of related cytokines, and (iii) ZIKV-infected canine glioblastoma cells secrete elevated levels of interleukins (256,264,362).

TNF signalling is a diverse signalling pathway capable of regulating cell proliferation, cell death and immune responses (371). Contrasting studies report TNF-alpha as anti-tumoural (cytotoxic and cytostatic) or pro-tumoural for medulloblastoma, and that both TNF-alpha transgene and TNFR antagonist treatment portray favourable outcomes in xenograft models (372–374). Regarding OVs, two independent groups working on the oncolytic myxoma virus report contrasting results that either TNF-alpha transgene or blockade enhances OV efficacy (375,376). Thus, the clinical utility of TNF-alpha in paediatric brain tumour therapy and OV therapy requires further delineation. Here, we observe recombinant TNF-alpha as pro-tumoural rather than cytotoxic to medulloblastoma and ATRT cells under normal conditions. Additionally, we identify TNF-alpha as a marker of poor prognosis in medulloblastoma, likely in part due to

enhanced tumour growth (371). Interestingly, recombinant TNF-alpha reduces cell viability of ZIKV-infected brain tumour cells, suggesting that in the context of oZIKV therapy, TNF-alpha is anti-tumoural as it enhances brain tumour cell oncolysis. This response is TNFR1-dependent, as TNFR2 activation requires membrane-bound TNF-alpha (377). While we did not observe TNF-alpha as anti- or pro-viral in medulloblastoma or ATRT cells, it is antiviral in ZIKV-infected adult glioblastoma cells (378). Our *in silico* analysis indicates that all medulloblastoma TME immune cells are primed to respond to TNF-alpha paracrine signalling and that TNF-alpha endocrine signalling would polarise myeloid cells to upregulate pro-survival and innate immune recognition genes. Our observed anti-tumoural role of TNF-alpha during ZIKV oncolysis, its reported antiviral property, and our *in silico* prediction of its involvement in anti-tumoural immune responses highlight that oZIKV infection could likely be augmented by adjuvant therapy targeting TNF-alpha. This concept is exemplified by oncolytic HSV-1 inducing TNF-alphamediated glioma cell death, with transient TNF-alpha blockade being able to enhance both viral replication and mouse survival (379).

Pro-inflammatory cytokine secretion is a hallmark signature of ICD, and here, we demonstrate by multiplex ELISA that ZIKV infection induces a diverse pro-inflammatory secretome from paediatric brain tumour cells. This natural induction of a diverse pro-inflammatory secretome is essential to oZIKV therapy efficacy because ZIKV's limited RNA genome size is a barrier to enhancing this response by stable transgene modification. Currently, only a limited number of multiplex ELISA assays have assessed the secretome of ZIKV-infected brain tumour cells (264,265). A 25-plex ELISA, measuring 23 of the 34 cytokines we consider here, showed that ZIKV infection only significantly increased CXCL10 and CCL5 secretion and decreased CCL2 secretion from adult glioblastoma cells (265). The size and diversity of this cytokine response is much smaller than that we show for ZIKV-infected paediatric medulloblastoma and ATRT cells, suggesting that oZIKV infection is more immunogenic for paediatric rather than adult brain tumour cells.

Here, we observe ZIKV infection to elevate secretion of the principal triad of pro-inflammatory cytokines (IL-1, IL-6, and TNF-alpha) by both brain tumour cell lines, in addition to many other cytokines that we report for the first time to be a component of oZIKV infection. Corroborating our findings, three key pro-inflammatory cytokines with known anti-tumoural functions (IL-6, CCL5 and CXCL10) are significantly secreted by ZIKV-infected glioblastoma cells as well as ZIKV-infected USP7 and USP13 cells (264,265). We observe ZIKV to upregulate secretion of numerous drivers of OV-induced anti-tumoural immune responses, including but not limited to IFN alpha, IL-1, IL-6, CCL5, CXCL8, CXCL10, CXCL12, GM-CSF and TNF-alpha; as reviewed in

(380). In addition to detecting the secretion of numerous cytokines that are OV transgenes or immunotherapy target candidates (**Figure 3.6A**), we observe ZIKV-infected USP13 cells to specifically upregulate IFN alpha and GM-CSF secretion, both of which are FDA-approved cytokine therapies (104). IFN alpha is a monotherapy for treating various adult cancers and GM-CSF is an adjuvant to high-risk neuroblastoma anti-GD2 immunotherapy (93,104,105). Here, we report that ZIKV infection induces a clinically diverse pro-inflammatory and anti-tumoural brain tumour secretome primarily composed of cytokines currently employed as OV transgenes, immunotherapy targets or cytokine therapies.

A crucial element of oZIKV efficacy is the ability to heat up the immunosuppressive TIME by paracrine signalling to co-opt tumour-resident immune cell activity and endocrine signalling to orchestrate immune cell infiltration. ZIKV-induced brain tumour immune cell infiltration includes CD4+ T cells, CD8+ T cells, NK cells, monocytes, macrophages, DCs and microglia cells (266,271,277). Modelling these *in silico*, we predict distinct polarisation states of the majority of these infiltrating immune cells in response to oZIKV infection. Both CD8+ T cells and NK cells infiltrate ZIKV-infected mouse glioma, and here, our modelling indicates anti-tumoural cytotoxic CD8+ T and NK cell polarisations in response to ZIKV-induced brain tumour cell secretome endocrine signalling (277). This anti-tumoural phenotype is characterised by upregulated expression of the pro-apoptotic granzyme B, which is a principal component of cytotoxic granules, in addition to key markers of IFN gamma signalling, which orchestrate interferon-mediated anti-tumoural immune responses (381). ZIKV-induced tumour clearance is dependent on cytotoxic CD8+ T cells, and our modelling indicates that this cytotoxic polarisation is in response to IL-1 (277).

Tumour-associated macrophages generally exist in the pro-tumoural and immunosuppressive M2-like state and commonly undergo a phenotypic shift to a pro-inflammatory and antitumoural M1-like state following OV infection (382). M1-like macrophage infiltration has been reported following ZIKV infection of mouse and canine brain tumours *in vivo*, however, the mechanisms that orchestrate this response are unknown (264,277). Of the 13 significantly secreted cytokines from ZIKV-infected USP13 medulloblastoma cells, nine (TNF-alpha, GM-CSF, IL-1 beta, IL-6, CXCL1, CXCL10 and CCL3-5) are known to induce the M1-like phenotype, whilst only CCL5 and high levels of IL-1RA may lead to the M2-like phenotype (383). Here, we observe high TNF-alpha and GM-CSF receptor expression and significant enrichment of their respective pathways in medulloblastoma TAMs. As such, we propose that in response to ZIKV-induced secretion of either TNF-alpha or GM-CSF, these medulloblastoma TAMs would adopt a pro-inflammatory and anti-tumoural phenotype. Utilising the Immune Dictionary, we identify

that macrophages are stimulated by IFN alpha and monocytes are stimulated by both IL-1 and GM-CSF to express M1-like macrophage gene markers. In contrast, IL-1 and IL-4 stimulate M2 gene markers in macrophages, which supports the known immunosuppressive effects of these cytokines on TAMs (384). Therefore, our modelling indicates a predominantly M1-like macrophage phenotype following oZIKV infection with potential for some M2-like macrophage populations.

To conclude, we investigate ICD signatures following oZIKV infection of paediatric brain tumour cells and propose TNF-alpha as a potential prognostic marker for brain tumour oZIKV therapy, with the only other known prognostic marker being CD24 for neuroblastoma oZIKV therapy (262). We observe a clinically relevant pro-inflammatory and anti-tumoural ZIKV-induced brain tumour secretome. Through *in silico* modelling, we indicate that ZIKV secretome paracrine signalling likely targets TME immune cells over non-infected medulloblastoma tumour cells and endocrine signalling to drive diverse immune cell polarisations. We propose that this would collectively lead to a pro-inflammatory and anti-tumoural immune response that would heat up the paediatric brain TME and be fundamental to the efficacy of oZIKV therapy. The research we perform here contributes to understanding the molecular mechanisms governing oZIKV infection and the cytokine response which orchestrates the anti-tumoural immune response. This work contributes to the growing body of research indicating the clinical utility of ZIKV as an oncolytic virotherapy for nervous system tumours and will help pave the way towards its application in clinical trials.

3.7 Data Availability

The RNA-Seq data generated in the present study have been deposited to the NCBI GEO with the GEO accession GSE277900. The publicly available RNA-Seq datasets of ZIKV-infected tumour cells were sourced from GEO2R with the GEO accessions GSE114907 (4121 GSC, MOI 1, 48 hpi, N = 3), GSE102924 (387, 3565 and 4121 GSC, MOI 5, 48 hpi, N = 3) and GSE149775 (SH-SY5Y, MOI 5, 24 hpi, N = 3) (243,265,302).

3.8 Acknowledgements

The authors acknowledge financial support from UKRI (MR/S01411X/1) (to RME and OKO), Wessex Medical Research Trust (to RME), Rosetrees Trust (to RME), The Little Princess Trust (to RME), FAPESP-CEPID (Proc. No. 2013/08028-1) (to OKO), and CNPq (Proc. No. 302736/2022-0) (to OKO) for this project. KM receives salary and research support from BBSRC grants

Chapter 3

BBS/E/PI/230001A and BBS/E/PI/23NB0003. The authors would like to thank the Elma Tchilian research group at The Pirbright Institute for sharing their Bio-Plex 200 calibration and validation kits, and Ehsan Rostami in particular for his support in setting up the 49-plex ProcartaPlex ELISA assay.

3.9 Figures

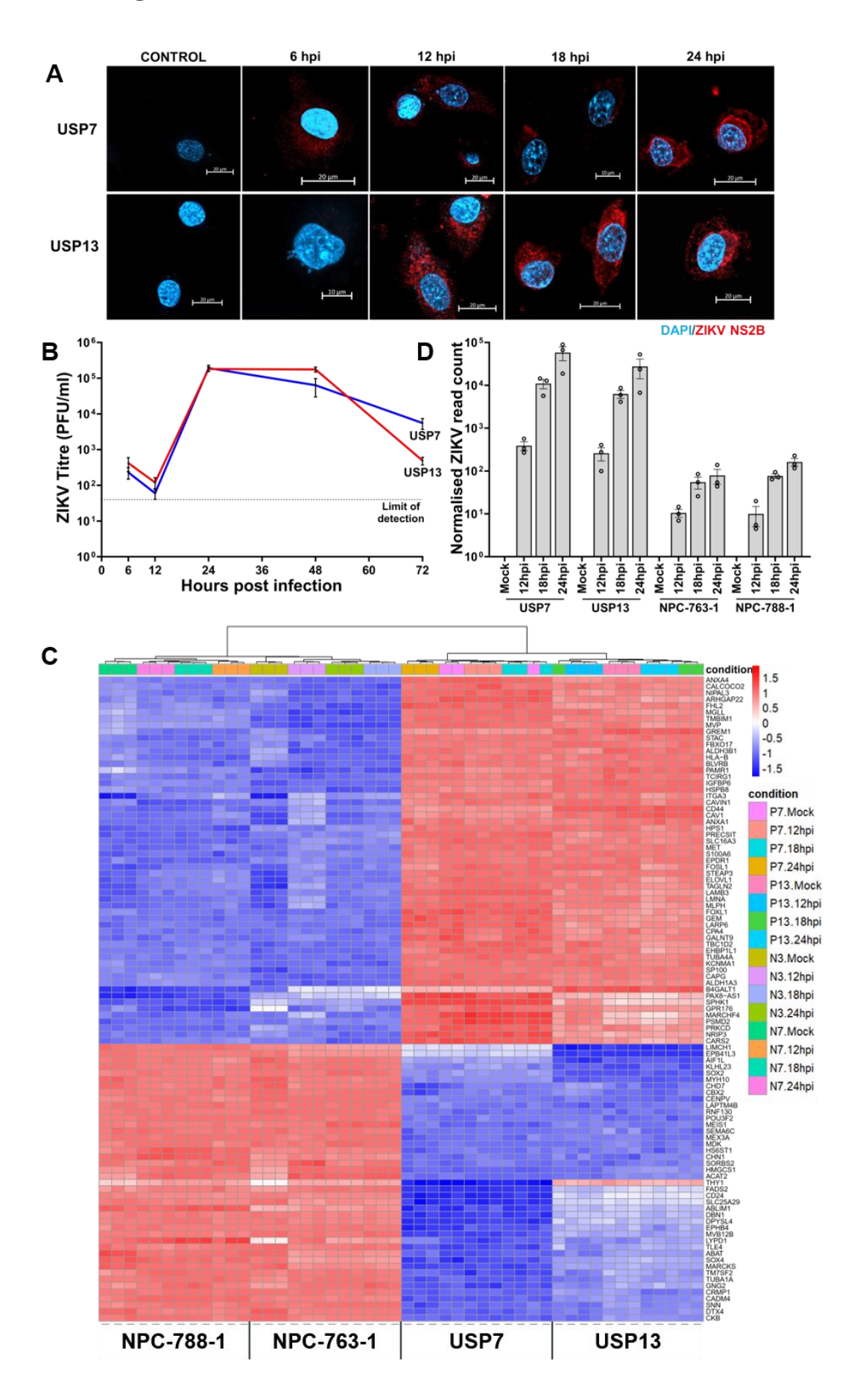
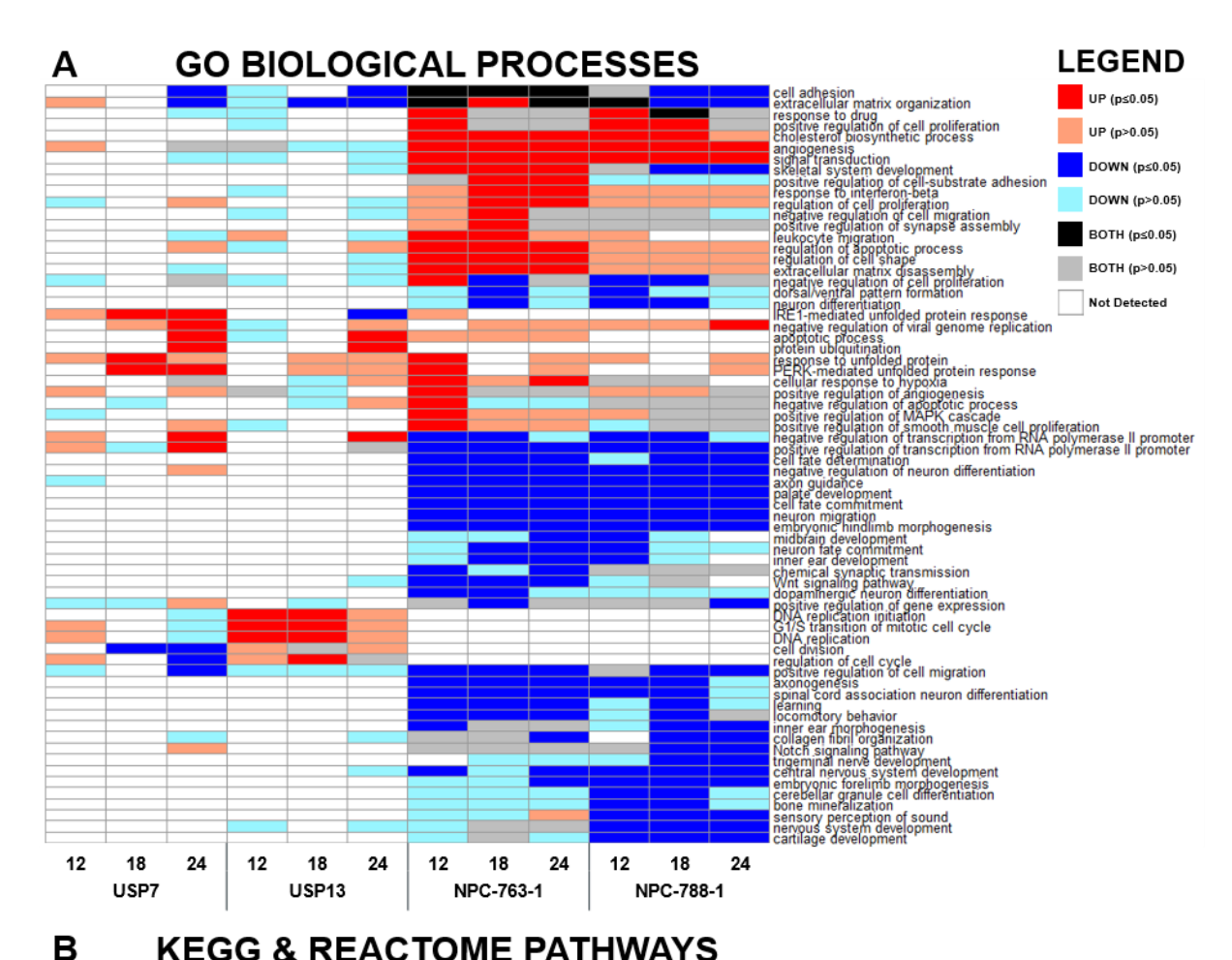


Figure 3. 1. ZIKV infection dynamics in brain tumour and neural precursor cells.

(A) Confocal microscopy of ZIKV-infected USP7 and USP13 brain tumour cells across the first 24 hours of infection, staining for ZIKV replication (ZIKV NS2B, red) and the nucleus (DAPI, blue). (B) ZIKV titre in USP7 and USP13 cells across 72 hours of infection (Mean \pm SEM, N = 4). (C) Heatmap of the Top 100 differential genes across all 48 RNA-Seq samples. Hierarchical clustering arranged the heatmap by condition (columns) and genes (rows); the dendrogram for the latter was omitted to aid visualisation. (D) RNA-Seq ZIKV genome count across the different infection conditions in USP7, USP13, NPC-763-1, and NPC-788-1 cells (Mean \pm SEM, N = 3). Abbreviations, Zika virus (ZIKV), non-structural (NS), USP7 (P7), USP13 (P13), NPC-763-1 (N3), NPC-788-1 (N7), hours post-infection (hpi), adjusted p-value (padj).





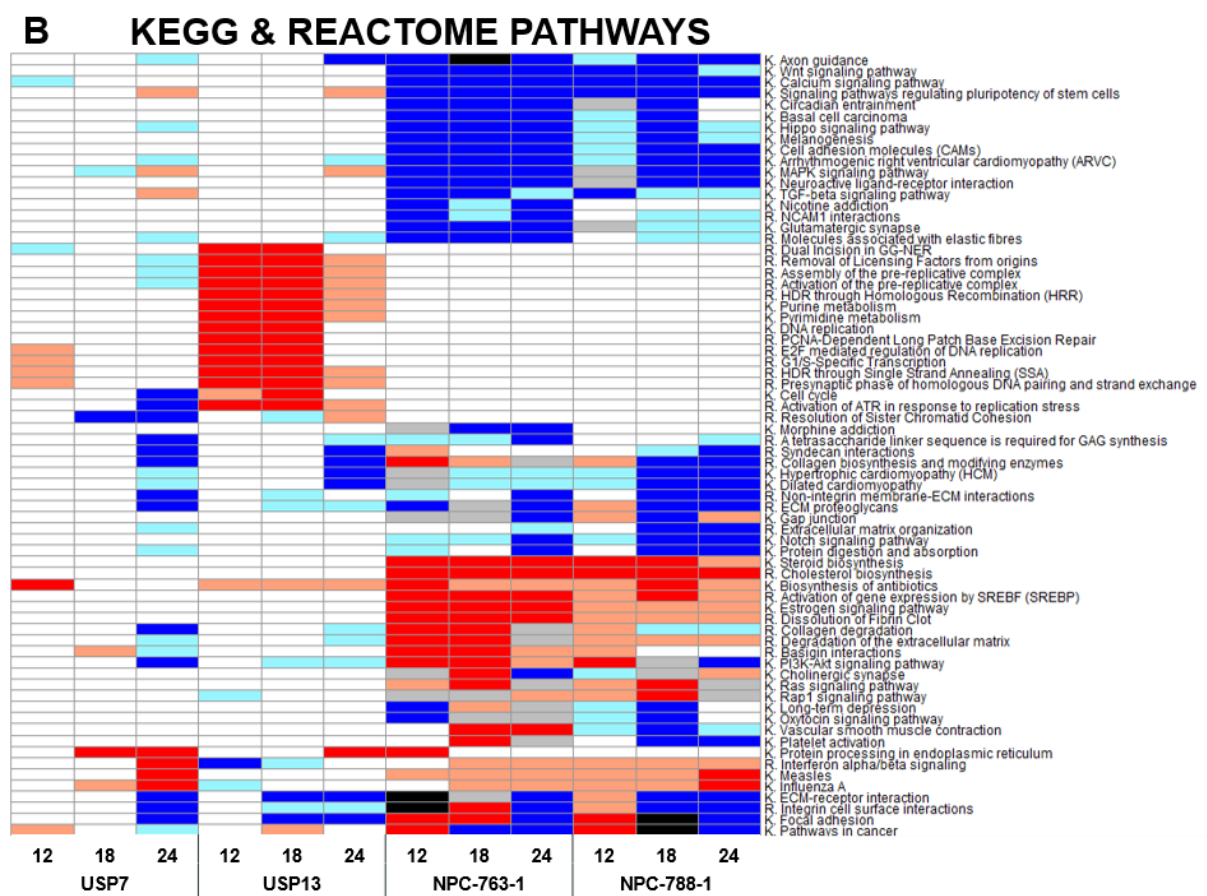


Figure 3. 2. Differential biological processes and pathways following ZIKV infection.

Heatmaps to show the **(A)** Gene Ontology (GO) Biological Processes and **(B)** KEGG and Reactome Pathways that are differentially regulated following 12, 18 and 24 hours of ZIKV infection in brain tumour and neural precursor cells. KEGG and Reactome pathways terms are labelled with the prefix of K. or R., respectively. All terms which were significant ($p \le 0.05$) in at least one condition were plotted, and non-significant (p > 0.05) enrichment for these terms across the other conditions was included. If a given term was enriched in both the upregulated and downregulated DEG lists, it was labelled BOTH. Significance values were corrected for multiple testing using the Benjamini and Hochberg method (padj ≤ 0.05). Abbreviations, Zika virus (ZIKV), USP7 (P7), USP13 (P13), NPC-763-1 (N3), NPC-788-1 (N7), Gene Ontology (GO), KEGG (K.), Reactome (R.), hours post-infection (hpi), adjusted p-value (padj).

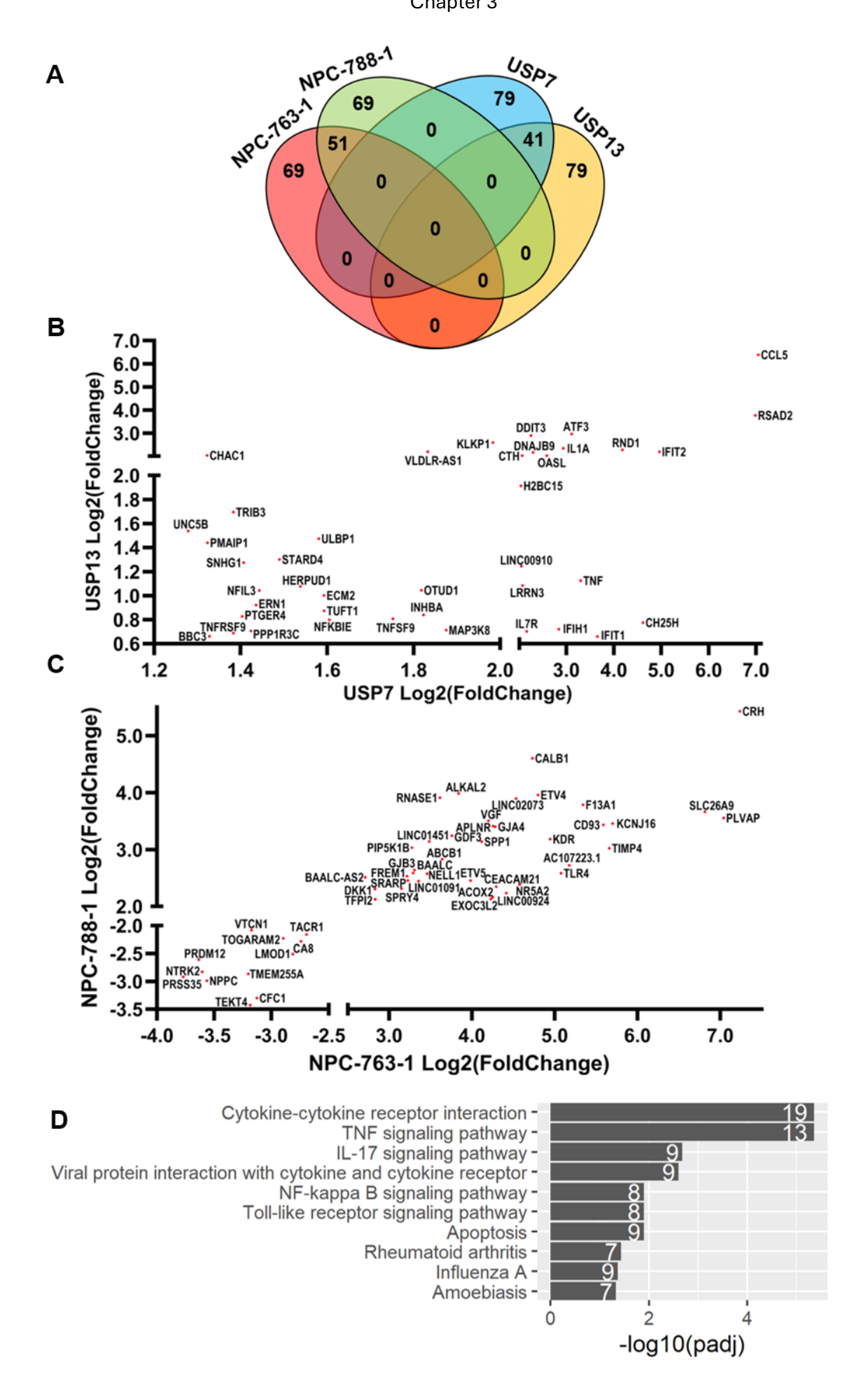


Figure 3. 3. Cell type-specific responses in the highest ranked DEGs following ZIKV infection.

(A) Venn diagram of the highest ranked DEGs in each cell line at 24 hpi. Scatter plots of RNA-Seq Log2(Fold Change) for (B) the 41 overlapping brain tumour DEGs and (C) the 51 overlapping NPC DEGs at 24 hpi. (D) Barplot of KEGG pathways significantly enriched in the highest ranked brain tumour DEGs at 24 hpi. The white numbers at the end of each bar denote the number of DEGs identified for the given term. Significance values were corrected for multiple testing using the Benjamini and Hochberg method (padj \leq 0.05). Abbreviations, adjusted p-value (padj).

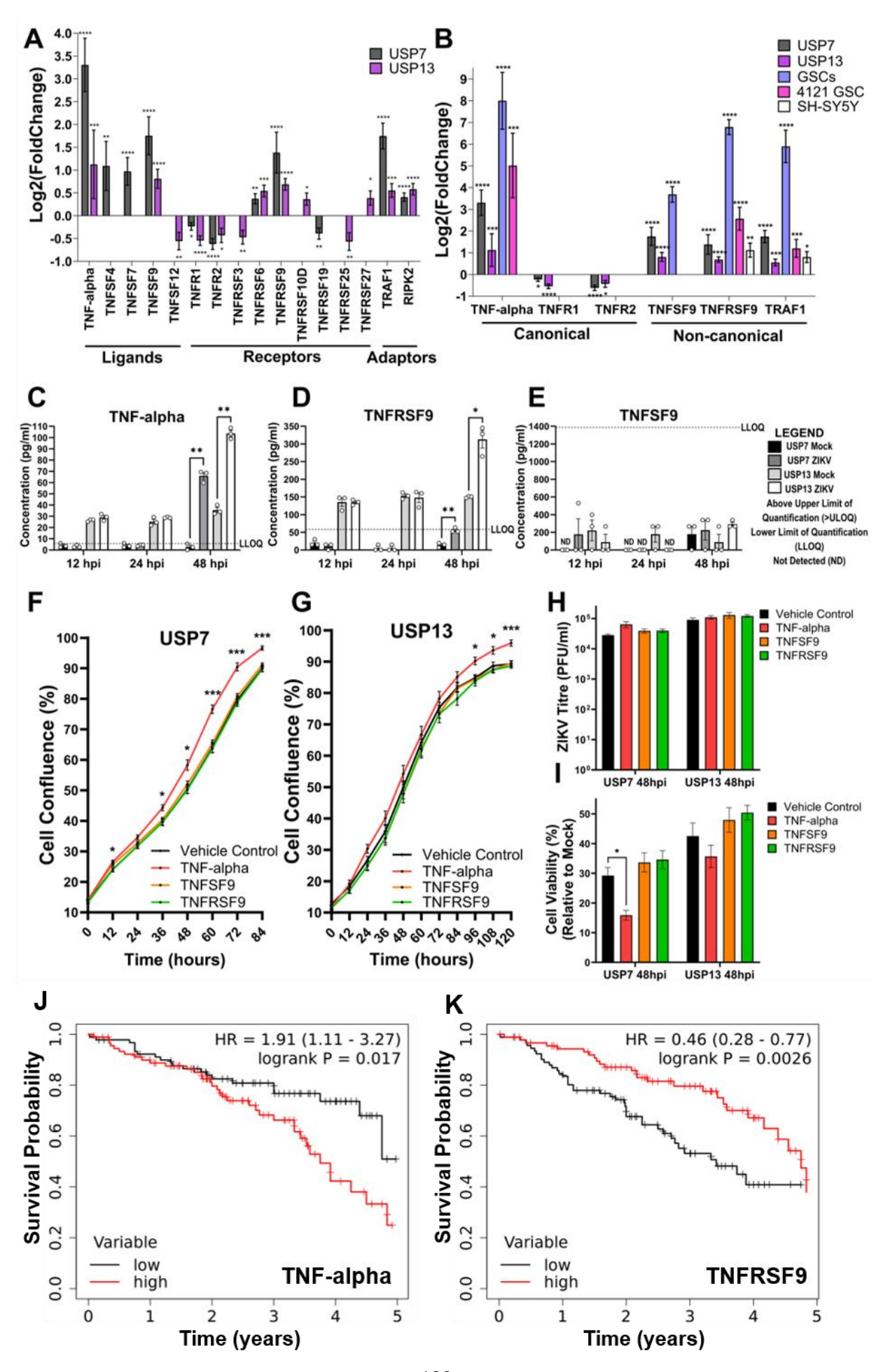


Figure 3. 4. TNF signalling pathways during ZIKV infection of brain tumour cells.

(A) Differentially expressed TNF pathway ligands, receptors, and receptor adaptors in ZIKVinfected USP7 and USP13 brain tumour cells at 24 hpi (LFC ± lfcSE, N = 3). (B) Differential expression of principal genes of the canonical TNF-alpha and non-canonical TNFSF9/TNFRSF9 signalling pathways in nervous system tumour cells following ZIKV infection. ZIKV-infected RNA-Seq datasets include that generated in the current study for USP7 and USP13, and three sourced from GEO2R for GSCs, 4121 GSCs and SH-SY5Y neuroblastoma cells (LFC ± lfcSE, N = 3). Protein concentration of secreted **(C)** TNF-alpha, **(D)** TNFRSF9 and **(E)** TNFSF9 from USP7 and USP13 cells following 12, 24 and 48 hours of ZIKV infection (Mean \pm SEM, N = 3). (F) USP7 and (G) USP13 cell confluence following recombinant TNF protein treatment (Mean ± SEM, n = 8). (H) ZIKV titre following recombinant TNF protein treatment and ZIKV infection of USP7 and USP13 cells (Mean \pm SEM, N = 3, n = 3). (I) USP7 and USP13 cell viability following recombinant TNF protein treatment and ZIKV infection (Mean \pm SEM, N = 3, n = 3). Kaplan Meier plots to assess the correlation between medulloblastoma patient survival and the upper vs lower quartiles of (J) TNF-alpha and (K) TNFRSF9 gene expression. Logrank P and hazard rate (HR) with 95% confidence intervals are reported. Significance values were corrected for multiple testing using the Benjamini and Hochberg method for **A-B** (padj \leq 0.05) and **C-E** (FDR \leq 0.05) and Dunnett's method for F-I (padj ≤ 0.05). Asterisk symbol denotes level of significance: *padj \leq 0.05; **padj ≤ 0.01; ***padj ≤ 0.001; ****padj ≤ 0.0001. Abbreviations, Zika virus (ZIKV), Glioma Stem Cell (GSC), Log2(Fold Change) (LFC), standard error of the LFC estimate (lfcSE), Above Limit of Quantification (>ULOQ), Lower Limit of Quantification (LLOQ), Not Detected (ND), hours post-infection (hpi), adjusted p-value (padj).

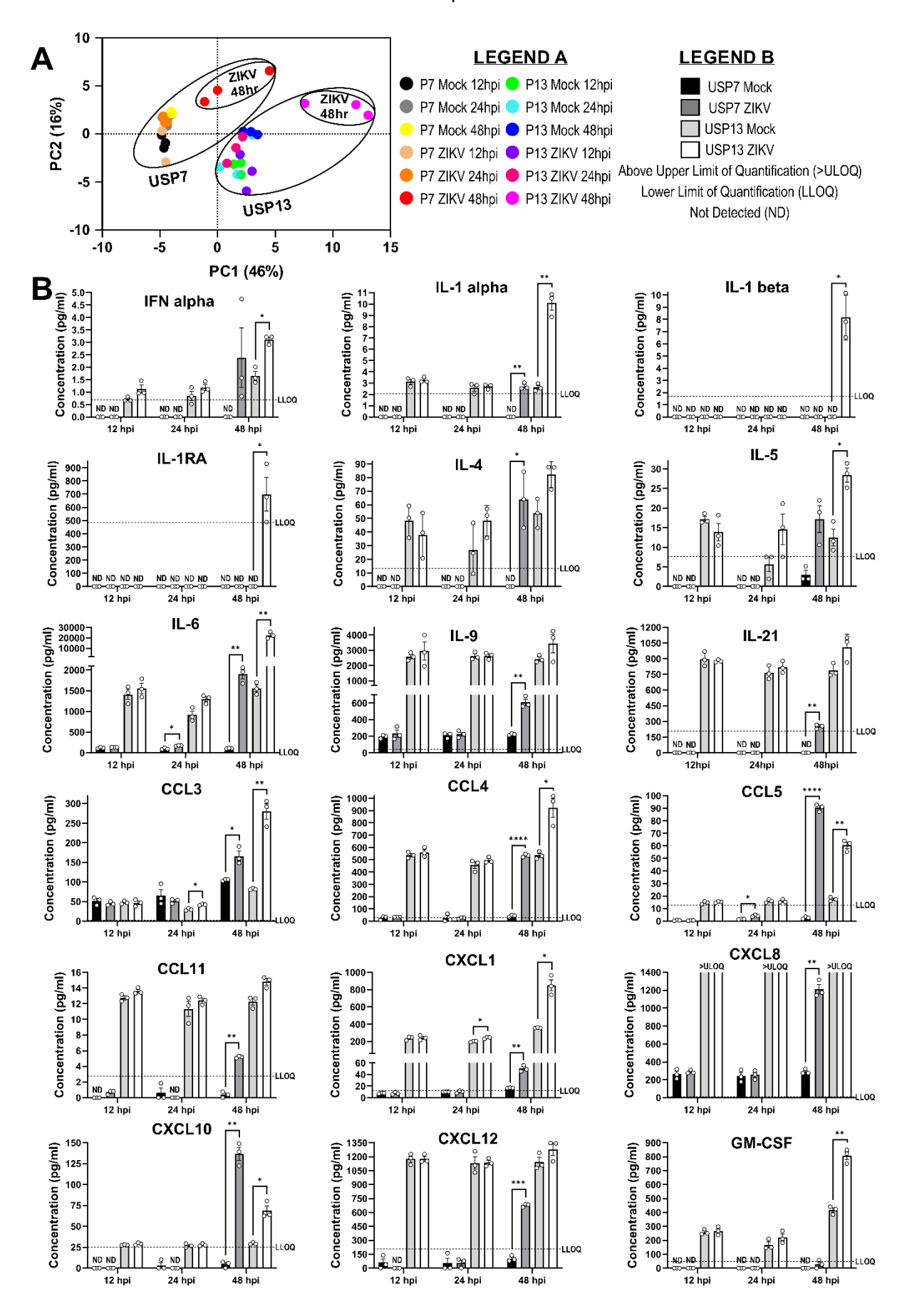
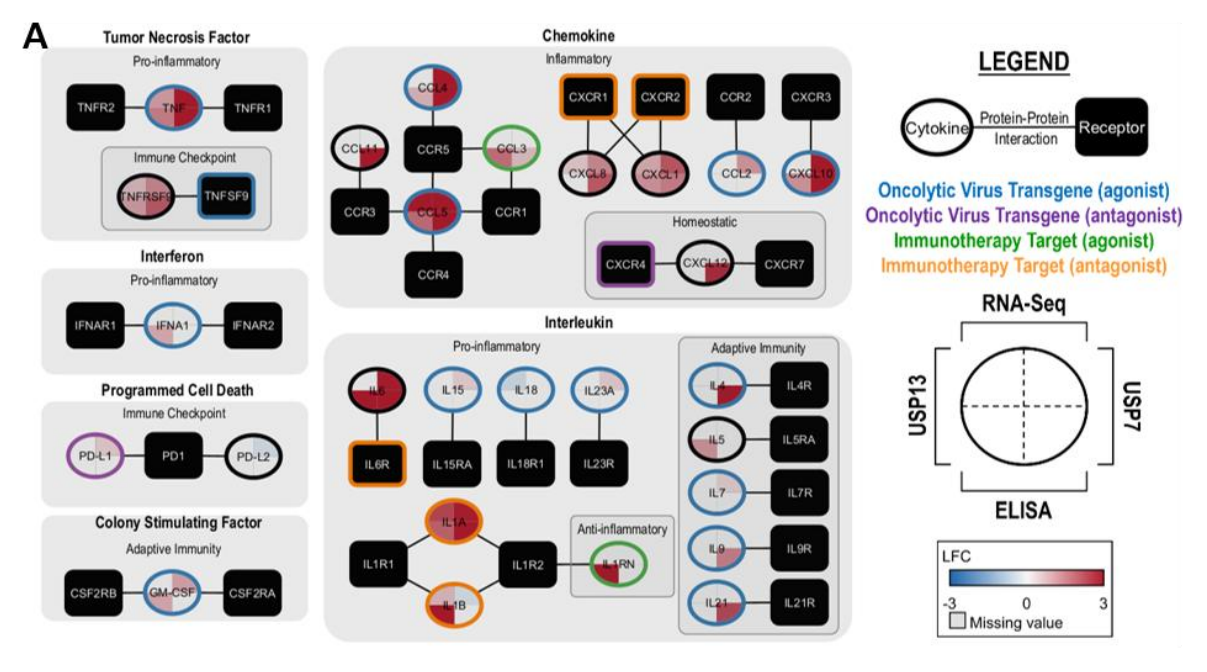
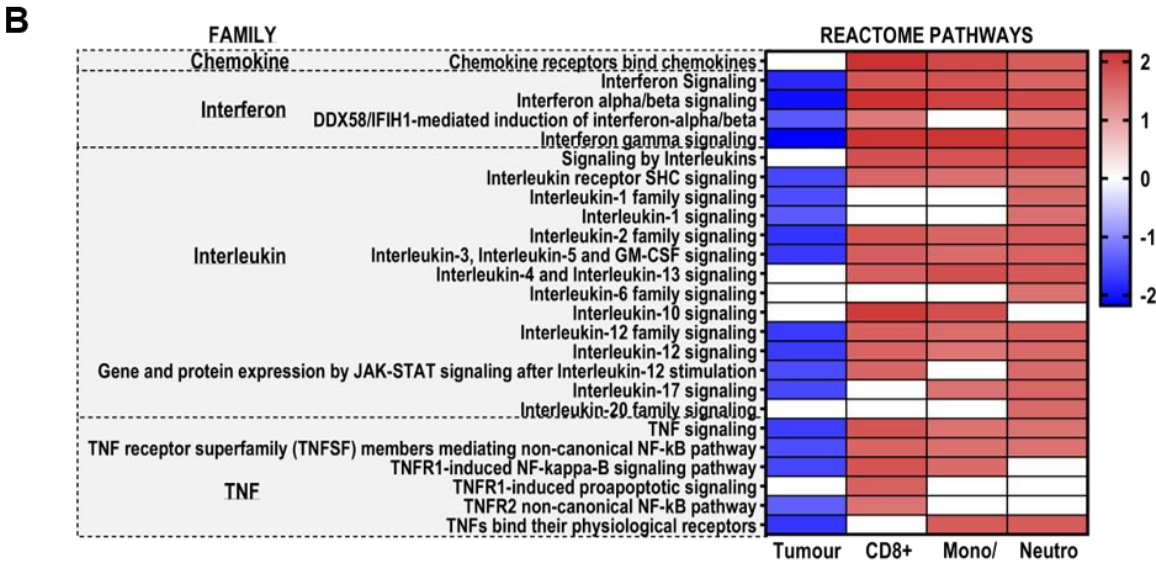


Figure 3. 5. ZIKV-infected brain tumour cell secretome.

(A) PCA plot of the 49-plex ELISA averaged Net MFI values (N=3). (B) Differential secretion of cytokines from USP7 and USP13 cells following 12, 24 and 48 hours of ZIKV infection (Mean \pm SEM, N=3). Significance values were corrected for multiple testing using the Benjamini and Hochberg method (FDR \le 0.05). Asterisk symbol denotes level of significance: *padj \le 0.05; **padj \le 0.01; ***padj \le 0.001; ***padj \le 0.0001. Abbreviations, Zika virus (ZIKV), USP7 (P7), USP13 (P13), Above Limit of Quantification (>ULOQ), Lower Limit of Quantification (LLOQ), Not Detected (ND), hours post-infection (hpi), Principal Component (PC).





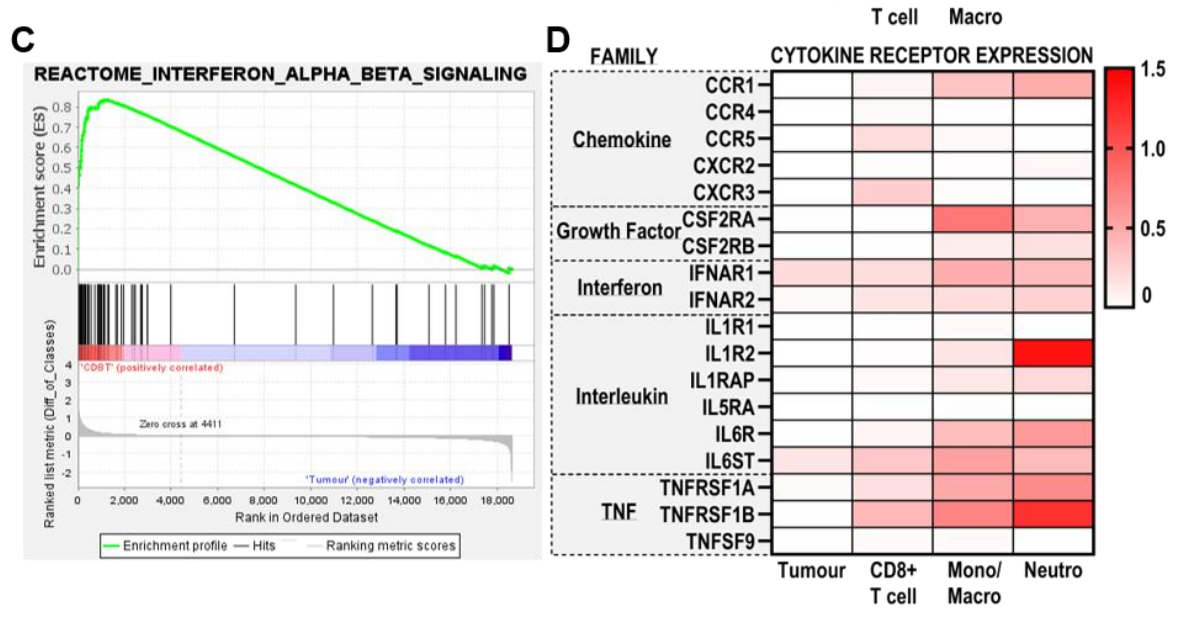


Figure 3. 6. The pro-inflammatory ZIKV secretome and its predicted medulloblastoma TME paracrine signalling.

(A) An integrated map of the 27 significantly expressed or secreted cytokines in at least one brain tumour cell line following ZIKV infection. Cytokines and their cognate receptors are clustered by their family class and sub-clustered by their primary role in the immune response. Edges denote cytokine-cytokine receptor interactions. Node shape denotes if the protein is a cytokine (oval) or receptor (rectangle). Piechart quadrants denote the maximum LFC value observed for the given cell line (USP7 or USP13) in the given assay (RNA-Seq or ELISA). Border colour denotes if the cytokine-receptor signalling is a current target of oncolytic virotherapy or immunotherapy and highlights which of the two proteins is the transgene or immunotherapy target. Heatmaps showing the (B) GSEA normalised enrichment score (NES) of significantly enriched cytokine-related Reactome pathways ($p \le 0.05$, FDR ≤ 0.25) and **(D)** cytokine receptor expression (log-transformed normalised gene count) in the four major cell types annotated in the medulloblastoma scRNA-Seq dataset. Rows for **(B)** and **(D)** are arranged by cytokine family. (C) Representative positively enriched cytokine-related GSEA enrichment plot (Interferon alpha/beta signalling) in immune cells (CD8+ T cells). Abbreviations, Zika virus (ZIKV), Log2(Fold Change) (LFC), Tumour microenvironment (TME), CD8+ T cells (CD8T), Monocyte/Macrophage (Mono/Macro), Neutrophil (Neutro), Gene Set Enrichment Analysis (GSEA), Normalised Enrichment Score (NES).

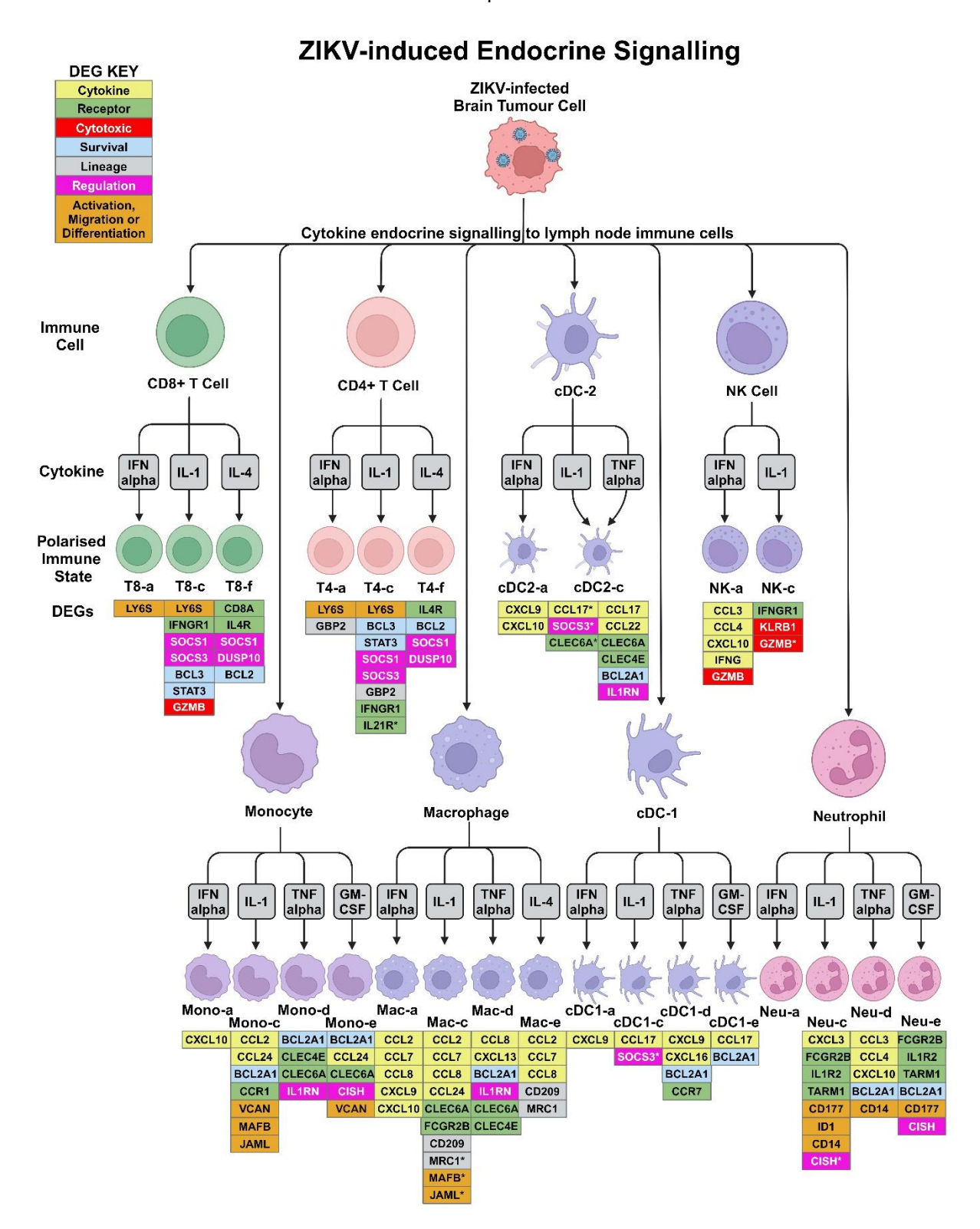


Figure 3. 7. Modelling of ZIKV-induced secretome endocrine signalling to lymph node immune cells.

Diagram detailing polarisation states of lymph node immune cells following cytokine stimulation, as reported by the Immune Dictionary (368). Only ZIKV-induced brain tumour cell-secreted cytokines that are dominant drivers of immune cell polarisation were assessed, as determined by the Immune Dictionary. Polarisation states, their nomenclature and the top 20 upregulated cytokine-induced DEGs (FDR ≤ 0.05) were sourced from the Immune Dictionary. Phenotypic DEG markers that indicate immune cell activity or phenotype following cytokine stimulation are listed below the respective polarised state, with colours denoting if the DEG is a cytokine (yellow), receptor (green), cytotoxicity-related gene (red), survival-related gene (blue), cell lineage marker (grey), cytokine signalling regulator (pink), or a gene indicating general immune cell activity (activation, migration or differentiation) (orange). IL-1 alpha and IL-1 beta induce the same polarisation state and are thus collectively represented as IL-1. * denotes a DEG induced by either IL-1 alpha or IL-1 beta, but not both. Abbreviations, Zika virus (ZIKV), differentially expressed gene (DEG), conventional Dendritic Cell (cDC), Natural Killer (NK), CD8+ T cell (T8), CD4+ T cell (T4), Monocyte (Mono), Macrophage (Macro), Neutrophil (Neu). Figure created in BioRender. BioRender.com/u63c617.

3.10 Tables

Table 3. 1. Differentially expressed genes (DEGs) observed following ZIKV infection in all four cell lines.

		Differentially Expressed Genes			
	USP7	USP13	NPC-763-1	NPC-788-1	
12 hpi	446	2012	3826	1726	
18 hpi	86	325	3066	2049	
24 hpi	2349	3017	2644	1732	

Significance was corrected for multiple testing by the Benjamini and Hochberg method for brain tumour DEGs (padj \leq 0.05, Fold Change \geq 0) and NPC DEGs (padj \leq 0.05, Fold Change \geq 1.5). Abbreviations, differentially expressed genes (DEG), hours post-infection (hpi).

Chapter 4 Identification of natural Zika virus peptides presented on the surface of paediatric brain tumour cells by HLA class I

Matt Sherwood¹, Ben Nicholas¹, Alistair Bailey^{1,2}, Thiago G. Mitsugi³, Carolini Kaid³, Oswaldo K. Okamoto³, Paul Skipp^{1*}, Rob M. Ewing^{1*}

¹Centre for Proteomic Research, Biological Sciences and Institute for Life Sciences, Building 85, University of Southampton, UK

²Centre for Cancer Immunology and Institute for Life Sciences, Faculty of Medicine, University of Southampton, UK

³ Centro de Estudos do Genoma Humano e Células-Tronco, Departamento de Genética e Biologia Evolutiva, Instituto de Biociências, Universidade de São Paulo, Cidade Universitária, São Paulo 05508-090, SP, Brazil

*Equal contributions

ORCIDs:

Matt Sherwood: 0000-0002-1912-9758

Ben Nicholas: 0000-0003-1467-9643 Alistair Bailey: 0000-0003-0023-8679

Thiago Giove Mitsugi: 0000-0001-5940-194X

Carolini Kaid: 0000-0002-1852-6997

Oswaldo Keith Okamoto: 0000-0002-8528-6225

Rob M. Ewing: 0000-0001-6510-4001 Paul Skipp: 0000-0002-2995-2959

Correspondence:

Professor Rob Ewing

B85, Life Sciences Building

University of Southampton

University Road

Highfield

Southampton, Hants.

SO17 1BJ

Tel No: +44(0)2380 59 5503

email: rob.ewing@soton.ac.uk

4.1 Authorship Statement

This chapter is the product of: **Sherwood M**, Nicholas B, Bailey A, Mitsugi TG, Kaid C, Okamoto OK, et al. Identification of natural Zika virus peptides presented on the surface of paediatric brain tumour cells by HLA class I | PLOS One. 2025 Nov 6.

Matthew Sherwood, Carolini Kaid, Thiago G. Mitsugi, Rob M. Ewing, Paul Skipp and Oswaldo K. Okamoto jointly conceptualised and planned the study. Matthew Sherwood, Carolini Kaid and Thiago G. Mitsugi jointly performed ZIKV infection experiments. Matthew Sherwood prepared and sent all samples for RNA Sequencing (RNA-Seq), and Alistair Bailey analysed the RNA-Seq dataset. Matthew Sherwood prepared global proteome samples for Mass Spectrometry, and Ben Nicholas prepared immunopeptidome samples. Ben Nicholas and Alistair Bailey performed Mass Spectrometry proteomics. Matthew Sherwood performed the analysis relating to Figures 4.1 and 4.4, Table 4.5, and Supplementary Table 4.1, whilst Alistair Bailey performed the analysis pertaining to Figures 4.2 and 4.3, and Tables 4.1-4.4. Matthew Sherwood and Alistair Bailey jointly wrote the results and methods sections, and the remaining sections of the manuscript were written solely by Matthew Sherwood. Rob M. Ewing, Paul Skipp and Oswaldo K. Okamoto supervised the research performed in this chapter and reviewed the finalised manuscript. Matthew Sherwood, Rob M. Ewing, Paul Skipp and Oswaldo K. Okamoto acquired funding for the study.

Supplementary material for this chapter can be found in **Appendix C**.

4.2 Abstract

Despite decades of research, survival from brain cancer has scarcely improved and is drastically lower than that of other cancers. Novel therapies, such as immunotherapy, hold great promise for treating brain tumours and are desperately needed. Zika virus (ZIKV) infects and kills aggressive cancer cells with stem-like properties (CSCs) from both paediatric and adult brain tumours. Whilst T cell recruitment into ZIKV-infected brain tumours is becoming well documented, the specific mechanisms through which they are activated are poorly understood.

We address this by employing a combined LC-MS/MS global proteome and immunopeptidome approach to describe, for the first time, human leukocyte antigen (HLA) presentation of ZIKV peptides on the surface of infected brain tumour cells. We first show that antigen processing and presentation by HLA class I (HLA-I) is the top enriched immune response pathway in the global proteome of aggressive paediatric USP7 brain tumour cells following ZIKV infection. We identify USP7 cells as a desirable immunopeptidome model as they express the globally most common HLA-A allotype (A*02:01). We predict the majority of our 19 identified ZIKV peptides to strongly bind and be presented by HLA-A*02:01. We observe that immunopeptide presentation corresponds with cellular ZIKV protein abundance, with nearly half of the peptides arising from the most abundant viral protein; non-structural protein 3 (NS3). We show the ZIKV NS3 helicase domain to be a particularly rich source of peptides. Finally, we verify that the 19 ZIKV peptides identified here are not predicted to mimic peptides of the human proteome. The ZIKV peptides we identify here are novel targets for immunotherapy, and our findings provide potential insight into the efficacious cytotoxic T cell response that oncolytic ZIKV virotherapy can induce against brain tumours.

Keywords:

Zika virus, oncolytic virotherapy, HLA-I, immunopeptidome, antigen presentation

4.3 Author Summary

Oncolytic viruses can attack cancer through two mechanisms: 1) infecting and killing the cancer cell and 2) activating the immune system against the tumour. ZIKV employs both mechanisms to kill cancer cells and render the tumour recognisable by the immune system. Here, we employ a powerful proteomic technique to identify fragments of viral proteins (peptides) presented by cell surface receptors on brain cancer cells infected with ZIKV. In the human body, immune system cells such as T cells recognise and become activated in response to these viral peptides, subsequently attacking the infected patient tumour. We identify 19 ZIKV peptides, three of which have been shown previously to elicit T cell responses, four identified elsewhere, and twelve are novel. Our work helps delineate a component of how ZIKV acts as an immunotherapy, this being the T cell-specific immune response that the virus raises to promote clearance of brain tumours. The significance of our study is that we further understanding of oncolytic Zika virus (oZIKV) infection by identifying tumour-presented ZIKV peptides for the first time, and this may contribute to the development of a novel brain tumour immunotherapy.

4.4 Introduction

Central nervous system (CNS) tumours account for approximately one-fifth of all childhood cancer cases and are disproportionately the largest cause of cancer-related mortality in children (1,33). These tumours exhibit high lethality, and the aggressive nature of standard-of-care therapy often leaves survivors with severe sequelae that significantly affect their quality of life. CNS tumours often present with a suppressive tumour immune microenvironment (TIME) through a combination of intrinsic (reduced antigen presentation, immune checkpoint blockade and immunosuppressive cytokine secretion) and extrinsic (immunosuppressive immune cell recruitment) factors (82). There is significant interest in developing immunotherapeutic strategies to circumvent this suppression by activating the patient's immune system against their tumour (385).

Oncolytic virotherapy, a specific class of immunotherapy, exploits viruses that preferentially infect and destroy tumour cells with minimal pathology against non-cancerous cells and tissue. The second pillar of oncolytic virotherapy is the mounting of anti-tumoural immune responses following immunogenic cell death (ICD) of cancer cells. Tumour antigens, viral antigens, cytokines, damage-associated molecular patterns (DAMPs) and viral pathogen-associated molecular patterns (PAMPs) are released into the tumour microenvironment (TME) during OVinduced ICD, and this leads to inflammation (108). Initially, these factors recruit and stimulate innate immune cells such as monocytes, macrophages, dendritic cells (DCs), neutrophils, and natural killer (NK) cells. Antigen-presenting cells (APCs) such as macrophages and DCs bridge innate and adaptive immunity by processing and presenting tumour and viral antigens on their cell surface. Adaptive immune system cells such as T cells migrate along chemokine and molecular gradients to locate, infiltrate and drive an adaptive immune response against the infected tumour. Thus, the efficacy of OV therapy arises from various components, including oncolysis, the innate immune response and the adaptive immune response. This gives viruses a unique advantage in targeting highly heterogeneous and immunosuppressive cancers, such as CNS tumours.

Oncolytic virotherapy clinical studies have generally reported low toxicity and minimal adverse effects in patients, and there are over 200 clinical trials underway to treat aggressive forms of cancer using OVs (109,110,358). Recently, the oncolytic herpes virus G47 Δ was approved in Japan for glioblastoma treatment, the first oncolytic virotherapy against any nervous system tumour in the clinic (115). As OVs can remodel the immunosuppressive TIME, there is significant interest in employing them as adjuvants to other immunotherapies, including monoclonal

antibodies, CAR-T cells, cancer vaccines, checkpoint inhibitors and small molecule inhibitors (386,387).

ZIKV is neuropathogenic and causes congenital Zika syndrome (CZS) 5-14% of babies born to women who contract ZIKV during pregnancy and pass the virus to the fetus via vertical transmission (215). ZIKV infects and diminishes the pool of fetal neural stem and progenitor cells through induction of differentiation or cell death, subsequently leading to the underdevelopment of the fetal brain (177–180). In contrast, postnatal ZIKV infection in children is mild, and only 1:5 people are symptomatic. ZIKV infection is generally self-limiting as symptoms resolve within a week or less, and the majority of symptomatic children present primarily with flu-like symptoms (215,233). This mild infection in children and ZIKV's neurotropism highlights the virus as a promising candidate against paediatric CNS tumours.

Since 2017, members of our research team and others have demonstrated that ZIKV infects and induces oncolysis of paediatric brain tumour cells *in vitro* and *in vivo* and mounts an immune response against spontaneous brain tumours in canines (243,249,256). ZIKV infection stimulates the infiltration of multiple immune cell types into CNS tumours, including CD8+ and CD4+ T cells, which contribute to ZIKV-induced tumour clearance (266,271,277). This branch of the adaptive immune response is brought about by viral peptide presentation by the HLA class I and II on the cell surface to T cell receptors (TCRs) on CD8+ and CD4+ T cells, respectively. HLA-presented peptide recognition and binding leads to TCR signalling, and co-stimulatory and co-inhibitory molecules govern the outcome of this signalling with regards to T cell function and fate (388). Whilst the recruitment of T cells into ZIKV-infected CNS tumours is becoming well documented, their cognate HLA-presented ZIKV peptides remain unknown.

Previously, we demonstrated the aggressive paediatric atypical teratoid rhabdoid tumour (ATRT) cell line, USP7, to have CSC properties and to be highly susceptible to ZIKV infection and oncolysis (249). In the present study, we show ZIKV infection to enrich major histocompatibility complex (MHC) class I antigen processing and presentation at the proteome level in these paediatric brain tumour cells. To investigate this response further, we perform HLA typing to show that USP7 cells express all three classical HLA-I alleles, including the globally most common HLA-A allotype (A*02:01). Performing immunopeptidome profiling, we identify a specific list of 19 ZIKV peptides from infected USP7 cells, predicted to be processed and presented by HLA-I molecules. The mass spectrometry proteomics and analysis used here are similar to our recent influenza work (389). To our knowledge, we document ZIKV epitopes presented by human CNS tumour cells for the first time. We provide new ZIKV epitopes as novel

targets for immunotherapy, and their identification should lead to future work that facilitates understanding of how the immune response can be coupled with the ZIKV oncolytic response.

4.5 Methods

4.5.1 Cell Culture and ZIKV infection

Paediatric USP7 cells were cultured as previously described (249,255). Brazilian ZIKV KU365771 stocks were established by the Instituto Butantan (USP, Brazil) in Vero cells and titrated by plaque-forming units (PFU) assay. For all infection experiments, USP7 cells were infected with ZIKV for 60 minutes prior to replacement with complete media. Twenty-four hours post-infection (hpi) cells were collected, washed with PBS and stored as pellets at -80°C. The infection experiments were performed in triplicate for the global proteome and once for the immunopeptidome. All controls were non-infected Mock samples.

4.5.2 Transcriptomics

4.5.2.1 HLA typing

High-quality total RNA was purified using the Monarch Total RNA Miniprep Kit (NEB #T2010S) as per the kit protocol from wildtype USP7 cells and sent to Novogene (UK) Company Limited for mRNA sequencing using the Illumina NovaSeq 6000 system (≥20 million 150 bp paired-end reads per sample). HLA typing was then performed using HISAT2 v2.2.0 with HISAT-genotype v1.3.0 in the default settings (305).

4.5.2.2 Adult glioma RNA sequencing data mining

RNA-Seq raw abundances of ZIKV-mCherry positive and ZIKV-mCherry negative primary cells isolated from eight glioblastoma (GBM) patients (IDs 42, 43, 45, 46, 50, 51, 54 and 57) at 72 hpi were downloaded from the Gene Expression Omnibus (GEO) (GSE178621) (230). The data was normalised using DESeq2, and gene set enrichment analysis (GSEA) was performed comparing the ZIKV-mCherry positive versus negative samples, as per the ZIKV-infected USP7 global proteome analysis (308,390).

4.5.3 Proteomics

4.5.3.1 Global proteome sample preparation

50µg protein from Mock and 24-hour infected USP7 cells (multiplicity of infection (MOI) 2) was mixed with 600µL methanol and 150µL chloroform for protein extraction. 450µL water was added to the sample, briefly vortexed and centrifuged at 14,000g for 5 min at room temperature (RT). The upper aqueous was removed and replaced with 450µL of methanol, and the sample was then briefly vortexed and centrifuged again to pellet the proteins. The protein pellet was airdried briefly before resuspension in 100µL 6M urea/50 mM Tris-HCl pH 8.0. The protein was reduced by 5 mM dithiothreitol for 30 min at 37°C and alkylated by 15 mM iodoacetamide for 30 min at RT in the dark. Protein was digested with 2µg trypsin/LysC mix (Promega) for 4h at 37°C. 750µL 50mM Tris-HCl pH 8.0 was added, and the sample was incubated overnight at 37°C. The addition of 4μ L TFA terminated the digestion. The resultant peptide mixture was purified using HLB prime reverse phase μ -elution plates (Waters) by elution in 50 μ L 70% acetonitrile according to the manufacturers' instructions, and then lyophilised.

4.5.3.2 LC-MS/MS analysis of global proteome

Tryptic peptides were reconstituted in 0.1% formic acid and applied to an Orbitrap Fusion Tribrid Mass Spectrometer with a nano-electrospray ion source. Peptides were eluted with a linear gradient of 3-8% buffer B (Acetonitrile and 0.1% formic acid) at a flow rate of 300nL/min over 5 minutes and then from 8-30% over a further 192 minutes. Full scans were acquired in the Orbitrap analyser using the Top Speed data dependent mode, preforming a MS scan every 3 second cycle, followed by higher energy collision-induced dissociation (HCD) MS/MS scans. MS spectra were acquired at resolution of 120,000 at 300-1,500m/z, RF lens 60% and an automatic gain control (AGC) ion target value of 4.0e5 for a maximum of 100ms and an exclusion duration of 40s. MS/MS data were collected in the Ion trap using a fixed collision energy of 32% with a first mass of 110 and AGC ion target of 5.0e3 for a maximum of 100ms.

4.5.3.3 Data analysis for global proteome

Raw global proteome mass spec files were analysed using Peaks Studio 10.0 build 20190129 with spectra searched against the same database as used for immunopeptidomics. The False Discovery Rate (FDR) was estimated with decoy-fusion database searches and were filtered to 1% FDR. Relative protein quantification was performed using Peaks quantification module and normalized between samples using a histone ruler (391). Downstream analysis and visualizations were mainly performed in R using associated packages (392–395). GSEA analysis

was performed on Log2(LFQ intensities) of Mock and 24-hour infected USP7 cells (N = 3) using a gene set database of Reactome innate and adaptive immune system pathways, a nominal p-value of 0.05 adjusted for multiple hypotheses testing (FDR \leq 0.25) (367). The top 50 and bottom 50 GSEA-ranked proteins were plotted on a heatmap using GraphPad PRISM (10.0.3), with the ZIKV polyprotein manually ranked and incorporated.

4.5.4 Immunopeptidome analysis

4.5.4.1 Purification of HLA immunopeptides

Protein-A sepharose beads (Repligen, Waltham, Mass. USA) were covalently conjugated to 10 mg/mL W6/32 (pan-anti-HLA-I) or 5mg/mL HB145 (pan-anti-HLA-II) monoclonal antibodies (SAL Scientific, Hampshire, UK) using DMP as previously described (396). Frozen pellets of 1x108 Mock and ZIKV-infected USP7 cells (MOI 1) were re-suspended in 5mL of lysis buffer (0.02M Tris, 0.5% (w/v) IGEPAL, 0.25% (w/v) sodium deoxycholate, 0.15mM NaCl, 1mM EDTA, 0.2mM iodoacetamide supplemented with EDTA-free protease inhibitor mix), and rotated on ice for 30 min to solubilise. Homogenates were clarified for 10 min at 2,000g, 4°C and then for a further 60 min at 13,500g, 4°C. 2mg of anti-HLA-I conjugated beads were added to the clarified supernatants and incubated with constant agitation for 2h at 4°C. The captured HLA- I/β_2 microglobulin/immunopeptide complex on the beads was washed sequentially with 10 column volumes of low (isotonic, 0.15M NaCl) and high (hypertonic, 0.4M NaCl) TBS washes prior to elution in 10% acetic acid and dried under vacuum. Column eluates were diluted with 0.5 volumes of 0.1% TFA and then applied to HLB-prime reverse phase columns (Waters, 30mg sorbent/column). The columns were rinsed with 10 column volumes of 0.1% TFA and then the peptides were eluted with 12 sequential step-wise increases in acetonitrile from 2.5-30%. Alternate eluates were pooled and dried using a centrifugal evaporator and re-suspended in 0.1% formic acid.

4.5.4.2 LC-MS/MS analysis of HLA immunopeptides

HLA peptides were separated by an Ultimate 3000 RSLC nano system (Thermo Scientific) using a PepMap C18 EASY-Spray LC column, 2μm particle size, 75μm x 50cm column (Thermo Scientific) in buffer A (0.1% formic acid) and coupled on-line to an Orbitrap Fusion Tribrid Mass Spectrometer (Thermo Fisher Scientific, UK) with a nano-electrospray ion source. Peptides were eluted with a linear gradient of 3%-30% buffer B (Acetonitrile and 0.1% formic acid) at a flow rate of 300nL/min over 110 minutes. Full scans were acquired in the Orbitrap analyser using the Top Speed data dependent mode, performing a MS scan every 3 second cycle, followed by higher

energy collision-induced dissociation (HCD) MS/MS scans. MS spectra were acquired at resolution of 120,000 at 300 m/z, RF lens 60% and an AGC ion target value of 4.0e5 for a maximum of 100ms. MS/MS resolution was 30,000 at 100m/z. Higher-energy collisional dissociation (HCD) fragmentation was induced at an energy setting of 28 for peptides with a charge state of 2-4, while singly charged peptides were fragmented at an energy setting of 32 at lower priority. Fragments were analysed in the Orbitrap at 30,000 resolution. Fragmented m/z values were dynamically excluded for 30 seconds.

4.5.4.3 Data analysis for immunopeptidome

Raw spectrum files were analysed using Peaks Studio 10.0 build 20190129, with the data processed to generate reduced charge state and deisotoped precursor and associated product ion peak lists which were searched against a Uniprot database (20,350 entries, 2020-04) appended with the full sequences for ZIKV strain (Brazil KU365779.1; 2015): 10 entries. A contaminants list (245 entries) in unspecific digest mode was applied (397). Parent mass error tolerance was set a 5ppm and fragment mass error tolerance at 0.03 Da. Variable modifications were set for N-term Acetylation (42.01 Da), Methionine oxidation (15.99 Da) and carboxyamidomethylation (57.02 Da) of cysteine. A maximum of three variable modifications per peptide were set. The FDR was estimated with decoy-fusion database searches and were filtered to 1% FDR. The search results were further refined using the MS-Rescue package (398). Downstream analysis and visualizations were performed in R using associated packages (392-395). Peptide binding motifs were identified using unsupervised clustering methods MixMHCp2.1 and MoDec, for class I and class II HLA peptides, respectively (399,400). Peptide binding affinities predicted using NetMHC 4.0 and NetMHCIIpan 4.0 for class I and class II HLA peptides, respectively (401–403). The IEDB T cell class I Immunogenicity (1.0) tool predicted ZIKV peptide: HLA-I complex immunogenicity, with selected settings of Peptide Length(s) 9-11mer, MHC Allele(s) HLA-A*02:01 and HLA-B*44:02, and Allele Specific anchor positions (404). The IEDB PEPMatch (0.9) tool performed ZIKV peptide sequence matching against the human proteome, with the result specifying the best match per peptide and a maximum mismatch of three (405). Global population coverage of HLA allotypes was sourced using the IEDB Population Coverage epitope analysis tool (406).

4.6 Results

4.6.1 ZIKV infection enriches HLA Class I presentation pathways in brain tumour cell lines

We first investigated if ZIKV infection moderates innate or adaptive immune responses within the aggressive paediatric brain tumour cell line USP7. Performing global proteome analysis of 24-hour ZIKV-infected USP7 cells and plotting the top and bottom 50 ranked proteins highlighted the ZIKV polyprotein as the second most highly ranked protein (Figure 4.1A). Performing Gene Set Enrichment Analysis (GSEA) with an innate and adaptive immune response specific Reactome database, we observe the adaptive immune system "Class I MHC mediated antigen processing & presentation" term to be the most highly enriched pathway following ZIKV infection (p = 0.016, FDR = 0.243) (**Figures 4.1B and 4.1C**). Supporting this, 20% of the 30 most highly ranked proteins from the ZIKV-infected USP7 samples (HUWE1, LTN1, PSMB5, PSMD1, RNF213 and SEC61G) are involved in antigen processing and presentation by MHC Class I (Supplementary Table 4.1). To determine if this response is also observed for ZIKV-infected adult brain tumour cells, we repeated our GSEA analysis on a publicly available RNA-Seq dataset from eight glioblastoma patients comparing ZIKV-mCherry-positive versus -negative primary cell populations (Figure 4.1D). "Class I MHC mediated antigen processing & presentation" (p < 0.0001, FDR = 0.051) and "TCR Signalling" (p < 0.0001, FDR = 0.025) were the most highly enriched immune response terms in the ZIKV-mCherry positive glioblastoma cells (Figure 4.1D). To conclude, ZIKV infection enriches signatures indicative of antigen processing and presentation by MHC Class I in paediatric and adult brain tumour cells at the proteome and transcriptome levels, respectively. We sought to investigate this pathway further.

4.6.2 USP7 brain tumour cells predominantly present HLA-A*02:01 peptides

Prior to investigating whether infection led to ZIKV-derived HLA immunopeptide presentation by USP7 cells, we first sought to understand what HLA allotypes USP7 cells express and what peptides these HLA molecules present. HLA typing of USP7 cell bulk RNA-Seq identifies that they express all three classical HLA-I alleles (**Table 4.1**). This analysis indicates that USP7 cells are homozygous for all three classical HLA-I alleles, but this may be a byproduct of HLA heterozygosity loss during transformation. USP7 cells express the globally most common HLA-A allotype (HLA-A*02:01), which is expressed by nearly 40% of the human population (**Table 4.1**). Additionally, USP7 also expresses HLA-B*44:02 and HLA-C*05:01, which are expressed by 7.61% and 7.85% of the human population, respectively (**Table 4.1**). We demonstrate USP7

cells as a desirable immunopeptidome model due to their high HLA-A population coverage (407). Performing immunopeptidomics, we assessed the class I and II HLA immunopeptidomes of Mock and ZIKV-infected USP7 cells (Table 4.2). Supporting our observations at the global proteome level, we predominantly observe peptides with lengths consistent with the nine amino acid (aa) preference for presentation by HLA-I rather than the longer peptides presented by HLAclass II (HLA-II) (Figure 4.2A). As expected for non-professional antigen-presenting cells, only modest numbers of HLA-II immunopeptides were recovered (Table 4.2). ZIKV infection did not affect the length distribution of the peptides presented (Figure 4.2A). Unbiased cluster analysis of all the distinct observed 9-mer peptides from ZIKV-infected USP7 cells identified 74%, 14%, and 12% of the 9-mer peptides to be presented by HLA-A*02:01, HLA-B*44:02 and HLA-C*05:01, respectively (Figure 4.2B). These are consistent with the USP7 HLA-I allotypes identified by HLA typing (Table 4.1). Peptide length distributions from ZIKV-infected USP7 cells show a dominance of 9-mer peptides, with differing minor populations of 8, 10 or 11-mer peptides, across the three classical HLA-I molecules (Figure 4.2C). To conclude, USP7 cells predominantly present 9-mer peptides by the three classical HLA-I molecules, with nearly three-quarters predicted to be presented by the globally most common HLA-A allotype HLA-A*02:01.

4.6.3 USP7 brain tumour cells present ZIKV HLA-I immunopeptides, and presentation corresponds with protein abundance in the HLA-I pathway

Next, we investigated whether infection led to ZIKV-derived HLA immunopeptide presentation and identified 19 HLA-I peptides derived from six of the ten ZIKV proteins (**Table 4.3**). Consistent with the low HLA-II expression by non-professional antigen-presenting cells, no HLA-II-presented ZIKV peptides were observed. To examine which HLA-I allotypes the observed ZIKV peptides were likely presented by, and to place these observations in the context of the host cell 9,10 and 11-mer peptides, we predicted ZIKV peptide binding affinities using NetMHC (**Figure 4.3A, Table 4.4**). HLA-A*02:01, HLA-B*44:02 and HLA-C*05:01 were predicted to bind and present twelve, six and one ZIKV peptides, respectively (**Table 4.4**). For HLA-A*02:01, all peptides are strong binders, and at least one of the 9, 10 and 11-mers are within the top three predicted binding peptides (**Figure 4.3A**). For HLA-B*44:02, the ZIKV NS5 9-mer is the top predicted binding peptide, all four ZIKV 10-mers are within the top seven predicted binding peptides, and the ZIKV NS3 11-mer is a low-affinity binder (**Figure 4.3A**). For HLA-C*05:01, the ZIKV NS3 9-mer is a low-affinity binder and was not plotted (**Table 4.4**). This data indicates that 17 identified ZIKV peptides are high-affinity binding peptides commonly found within the top predicted binding peptides for each HLA allotype. Interestingly, we observe most ZIKV

immunopeptides to be derived from the ZIKV NS3 followed by the NS5 RNA-dependent RNA polymerase (**Table 4.3**). To investigate the potential reason for this, we plotted the protein abundances of the ten ZIKV proteins and observed NS3 as the most abundant ZIKV protein, followed by NS5 (**Figure 4.3B**). A clear trend can be observed when protein abundances are considered alongside the ZIKV peptide number (**Figures 4.3B, Table 4.3**). ZIKV NS3 and NS5 are the most abundant proteins and yield the most immunopeptides, indicating that HLA-I presentation corresponds to protein abundance within its peptide processing pathway. This is further supported by the absence of immunopeptides derived from ZIKV Envelope and Membrane proteins, as HLA-I peptides are predominately derived from intracellular cytosolic proteins (408). To conclude, HLA-A*02:01 and HLA-B*44:02 high-affinity ZIKV peptide presentation is predicted to occur on the surface of USP7 cells, and peptide presentation may correspond with protein abundance in the HLA-I pathway.

4.6.4 ZIKV NS3 helicase is a rich source of immunopeptides

Mapping the 19 ZIKV peptides presented by HLA-I on USP7 cells onto the ZIKV polyprotein identifies two peptide-rich regions in the NS3 helicase domain and one in NS5 (Figure 4.4). For NS3, RMLLDNIYL, YLQDGLIASL, and LQDGLIASL overlap and reside within the continuous 17aa sequence RMLLDNIYLQDGLIASL, whilst AEMEEALRGL and EEALRGLPVRY overlap and reside within the continuous 14aa sequence AEMEEALRGLPVRY. For NS5, QEWKPSTGW and EEVPFCSHHF are non-overlapping and reside within the 22aa sequence QEWKPSTGWDNWEEVPFCSHHF. Performing in silico immunogenicity modelling of the 18 identified HLA-A*02:01 and HLA-B*44:02 presented ZIKV peptides predicts 13 as immunogenic and five as non-immunogenic (Table 4.4). Interestingly, all eight ZIKV NS3 helicase peptides are predicted to be immunogenic, and out of all 19 ZIKV peptides, the top three predicted immunogenic peptides are all ZIKV NS3 helicase peptides (VLPEIVREA, AEMEEALRGL and TEVEVPERAW) (Table 4.4). Performing peptide sequence matching, we compare our 19 ZIKV peptides to all theoretical peptides of the human proteome to assess whether they are predicted to mimic endogenous human peptides. We identify 16 ZIKV peptides to have some degree of homology with human peptides (Table 4.5). Notably, every comparison has a mismatch of at least two, and no more than seven matched amino acids are in continuous order. As eight is the minimum peptide length for binding to the HLA-I groove, none of the identified ZIKV peptides are predicted to mimic endogenous human peptides, thus supporting the predicted immunogenicity of these viral peptides. To conclude, ZIKV NS3 helicase is predicted to be a rich source of immunogenic peptides, and the identified viral peptides do not mimic predicted peptides of the human proteome.

4.7 Discussion

Downregulating HLA-I presentation is a method which cancer cells frequently utilise to help produce an immunosuppressive TIME (409). Here, we investigate and show that ZIKV infection enriches the HLA-I pathway in both paediatric and adult brain tumour cells. Since brain tumour cells are non-professional antigen-presenting cells, enrichment of HLA-I instead of HLA-II was expected. Supporting our observation of HLA-I pathway enrichment in brain tumour cells, HLA-A and HLA-B protein expression is significantly upregulated in ZIKV-infected U251 glioblastoma cells, where they act as a viral dependency factor and a regulator of cell viability in response to ZIKV infection, respectively (410). We propose that the enrichment of the HLA-I pathway following ZIKV infection of brain tumour cells may contribute to remodelling the TIME to make these commonly immunosuppressed tumours immunogenic.

Here, we identify 19 HLA-I ZIKV peptides presented on the surface of USP7 brain tumour cells. Our work indicates the relevance of the HLA-I pathway and protein abundance to ZIKV peptide presentation and suggests a relationship as the most highly expressed viral proteins (NS3 and NS5) present with the greatest number of presented peptides. The paediatric brain tumour cell line USP7 has highly advantageous traits for use in our study because it possesses stem-like characteristics, is highly susceptible to ZIKV infection, and expresses the HLA-A allotype HLA-A*02:01. HLA-A*02:01 is the most common HLA-A allotype globally (39.08%); however, although it ranks among the top three HLA-A allotypes in a cohort of 23 ATRT patients, its coverage is lower than in the global population (14%) (249,411). Additionally, HLA-B*44:02 and HLA-C*05:01 coverage is lower across these 23 ATRT patients than in the global population. Whilst the small sample size is a limitation of the published HLA coverage in ATRT, it is critical to note that the USP7 ZIKV immunopeptidome results presented here likely only relate to a subset of ATRT patients.

Of the 19 peptides observed here, twelve peptides are novel and seven have been previously observed elsewhere. Six of our HLA-A*02:01 peptides (RMLLDNIYL, YLQDGLIASL, ALWDVPAPKEV, YLIPGLQAA, SLINGVVRL and TMMETLERL) are presented on ZIKV-infected immortalised Priess B cells that are homozygous for HLA-A*02:01 (412). This supports our observations and indicates these six peptides as bona fide HLA-A*02:01 presented ZIKV epitopes. The peptides YLQDGLIASL, SLINGVVRL and AEMEEALRGL are recorded on the Immune Epitope Database (IEDB) under epitope IDs 2243385, 1311496 and 182464, respectively. NS3 YLQDGLIASL, NS4B YLIPGLQAA and NS5 SLINGVVRL stimulate memory T cell recall response in 57%, 14% and 57% of peripheral blood mononuclear cells (PBMCs) from

human patients previously infected with ZIKV (412,413). Additionally, SLINGVVRL was one of the top dominant ZIKV epitopes in an immunocompetent HLA-A2 transgenic mouse model, capable of stimulating CD8+ T cells to produce IFN gamma and TNF-alpha (414). These observations validate our LC-MS/MS model as a viable approach to identify immunogenic HLA-I presented ZIKV epitopes. An inherent limitation of our work with non-professional antigen-presenting cells, is that our model was not optimal for considering HLA-II-presented ZIKV peptides. There is great interest in performing this work as the infiltration and induction of CD4+ T cells contribute to oZIKV therapy efficacy (271,277). This would require feeding of infected cells to professional antigen-presenting cells, such as DCs, from which immunopeptidomes could then be captured as per (389).

It is important to understand if our ZIKV peptides have autoimmune implications by mimicking human peptides or if they may cross-react to stimulate memory T cells from previously encountered viral epitopes. Here, we predict none of our ZIKV peptides to mimic human peptides, thus minimising the risk of autoreactive T cell activity and autoimmunity (415). The HLA-I peptides ZIKV NS3 AEMEEALRGL and NS5 SLINGVVRL are homologous to a dengue virus (DENV) epitope and can stimulate memory cytotoxic T cells in Japanese encephalitis virus (JEV)-vaccinated HLA-A2 transgenic mice, respectively (414). It is currently unknown if and how host humoral and cellular immunity to previous viral infection or immunisation may enhance or hinder oZIKV efficacy. It is interesting to speculate that brain tumour cell HLA-I presentation of a ZIKV epitope may enhance OV efficacy by co-opting a patient's memory cytotoxic T cell immunity from a previous viral encounter against the tumour, but this requires investigation.

There are a multitude of complex interactions between an infected tumour and the immune system. Whilst both CD8+ and CD4+ T cells assist in glioblastoma tumour clearance, myeloid cells protect glioblastoma tumour cells from ZIKV infection through the secretion of type 1 interferons (230). NK cells can present with dichotomous function in response to OVs due to their contrasting antitumor and antiviral functions (416). Thus, it cannot be assumed that all ZIKV-stimulated immune cells will promote the therapeutic properties of ZIKV, and we must elucidate the roles and interplay between these cell types. Knowledge of the mechanisms of immune activation will factor into how ZIKV can be employed as an adjuvant for current immunotherapies. Thus far, ZIKV has proved an effective adjuvant to both immune checkpoint blockade (PD-1 and PD-L1) and vaccine-based immunotherapy to combat glioma and improve survival in mouse models (266,271,277). Our identification of novel HLA-I presented ZIKV epitopes contributes to the growing knowledge of how ZIKV can be employed as an

immunotherapy and may assist in the development of novel epitope-specific immunotherapies against brain tumours.

Whilst our primary focus was to investigate the immunotherapeutic potential of oZIKV therapy, our research here is wider reaching, and has potential implications for (i) understanding fetal neural precursor cell (NPC) depletion following ZIKV infection and (ii) ZIKV epitope vaccination. CZS is primarily brought about by the depletion of fetal NPCs. ZIKV infection upregulates HLA-I processing and presentation in human NPCs at the transcriptome level and in microcephalic mouse brains at the transcriptome and proteome levels (417,418). HLA-I presenting cells costain with infiltrating murine immune cells, resulting in neuronal cell death and microcephaly (418). Thus, cytotoxic CD8+T cell clearance may contribute to NPC depletion. To date, the immunopeptidome of ZIKV-infected NPCs is unknown, primarily due to the technical challenge of culturing NPCs to the high quantities required for immunopeptidomics. USP7 cells are of embryonal origin, closely resemble NPCs at the global gene expression level, and are immortalised so can be cultured to such quantities (249). As such, USP7 cells are an potential model to investigate the immunopeptidome of ZIKV-infected fetal NPCs. Interestingly, HLA-C is one of only 25 genes significantly upregulated in NPCs from CZS-affected patients compared to their unaffected dizygotic twin; possibly indicating HLA-I involvement in CZS development following congenital ZIKV infection (193). In the context of the developing fetus, the HLA-I peptides that we identify here may contribute to cytotoxic CD8+ T cell-mediated depletion of fetal NPC and subsequent CZS, and this deeply warrants investigation.

ZIKV exists as a single serotype and all strains could prove susceptible to a single vaccine (419). Despite this, a vaccine is yet to be approved so ZIKV still poses a pregnancy risk and potential for re-emergence. Here, we identify ZIKV NS3 as a rich source of immunopeptides, producing over half of our observed epitopes. ZIKV NS3 peptides can promote NK cells and PBMC immune cell activity (412,420,421). Additionally, ZIKV NS3 is the main antigenic T cell target, plays important roles during anti-ZIKV immunity, and a ZIKV NS3-based vaccine can stimulate the production of polyfunctional CD8+ T cells (422). Multiple *in silico* studies employ computational approaches to propose novel ZIKV epitope vaccines, one of which predicted the NS3 helicase sequence WLEARMLLDNIYLQDGLIASLYR as the richest ZIKV polyprotein epitope source (423–426). Our top identified region (RMLLDNIYLQDGLIASL) resides within this proposed vaccine. Additionally, we show all three ZIKV peptides within this region to be presented by the globally most common HLA-A*02:01 allotype, alongside identifying five more HLA-I peptides within the NS3 helicase domain. Thus, we confirm the ZIKV NS3 helicase as a rich epitope source and a promising vaccine candidate.

To summarise, immunopeptidomics is a potent and powerful tool to investigate viral peptide presentation to further our understanding of the immune responses orchestrated following ZIKV infection. Our results have possible future implications for the development of oZIKV therapy, epitope-specific immunotherapies or ZIKV epitope vaccines.

4.8 Data Availability

The mass spectrometry proteomics data have been deposited to the ProteomeXchange Consortium via the PRIDE partner repository with the dataset identifier PXD037627 and 10.6019/PXD037627. The RNA sequencing data have been deposited to the NCBI GEO with the GEO accession GSE277900.

4.9 Acknowledgments

The authors acknowledge financial support from UKRI (MR/S01411X/1) (to RME and OKO), Wessex Medical Research Trust (to RME), Rosetrees Trust (to RME), The Little Princess Trust (to RME), FAPESP-CEPID (Proc. No. 2013/08028-1) (to OKO), and CNPq (Proc. No. 302736/2022-0) (to OKO) for this project.

4.10 Figures

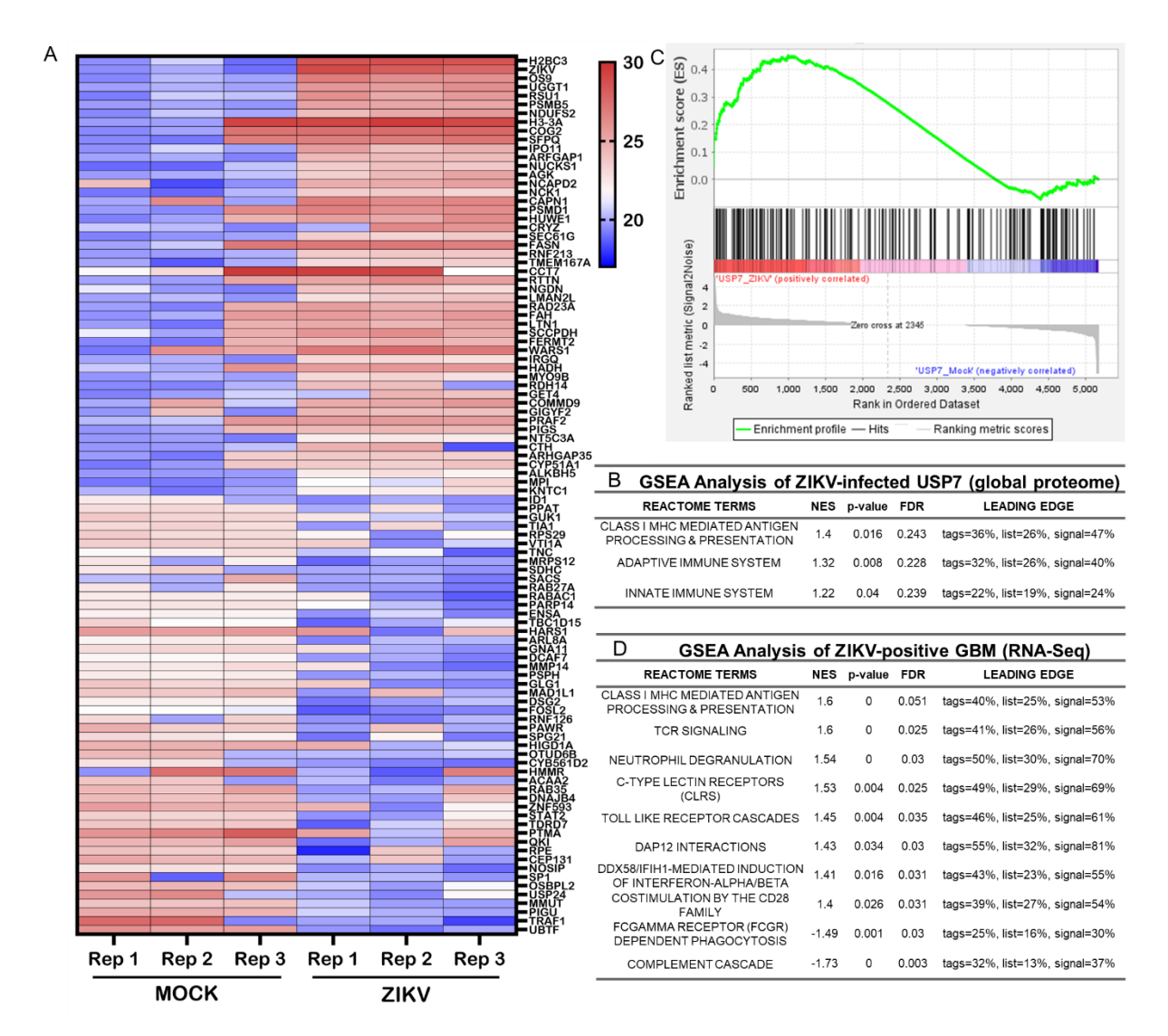


Figure 4. 1. ZIKV infection enriches the HLA Class I pathway in brain tumour cells.

(A) Heatmap plotting Log2(LFQ intensity) values of the top and bottom 50 ranked proteins in the ZIKV-infected USP7 cell global proteome. GSEA analysis to assess for enrichment of innate and adaptive immune system Reactome pathways in (B) the ZIKV-infected USP7 cell global proteome (N = 3) and (D) the ZIKV-mCherry positive primary glioblastoma (GBM) cell transcriptome (N = 8). (C) The enrichment plot of the GSEA "Class I MHC mediated antigen processing & presentation" enrichment analysis for ZIKV-infected USP7 cells. Normalised enrichment score (NES) denotes the degree to which the enrichment increased (+) or decreased (-) ($p \le 0.05$, $FDR \le 0.25$). Abbreviations, Zika virus (ZIKV), human leukocyte antigen (HLA), major histocompatibility complex (MHC), Gene Set Enrichment Analysis (GSEA), enrichment score (ES), normalised enrichment score (NES), false discovery rate (FDR), label free quantitation (LFQ), glioblastoma (GBM).

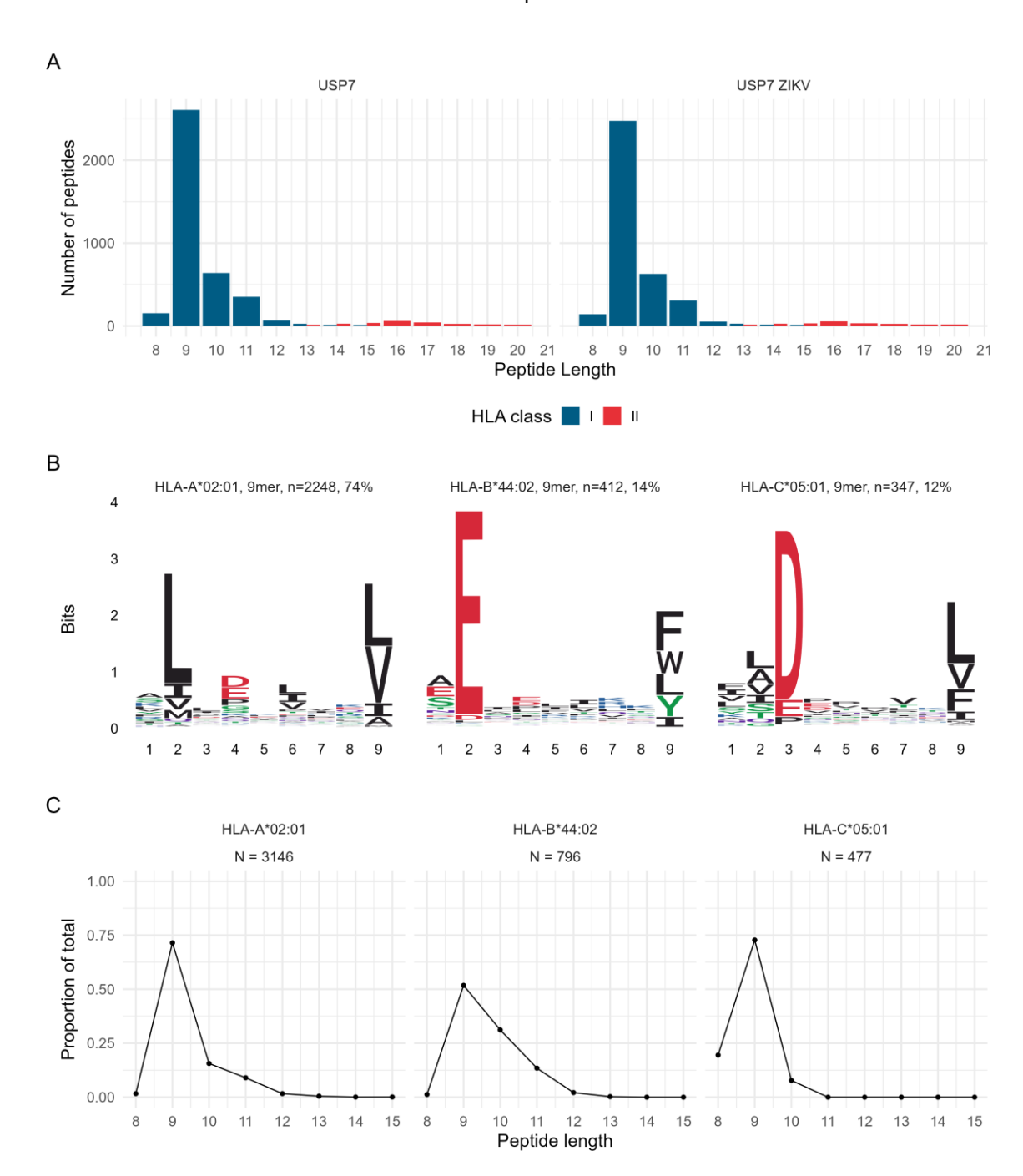


Figure 4. 2. The immunopeptidomes of USP7 brain tumour cells.

(A) Length distribution of HLA-I and II immunopeptides presented by Mock or ZIKV-infected USP7 cells. HLA-I peptides in blue and HLA-II peptides in red. (B) Class I HLA allotype 9-mer binding motifs derived from ZIKV-infected USP7 immunopeptides by unsupervised clustering using MixMHCp. (C) Length distributions of peptides from ZIKV-infected USP7 cells according to clustered HLA-I allotype. Abbreviations, Zika virus (ZIKV), human leukocyte antigen (HLA).

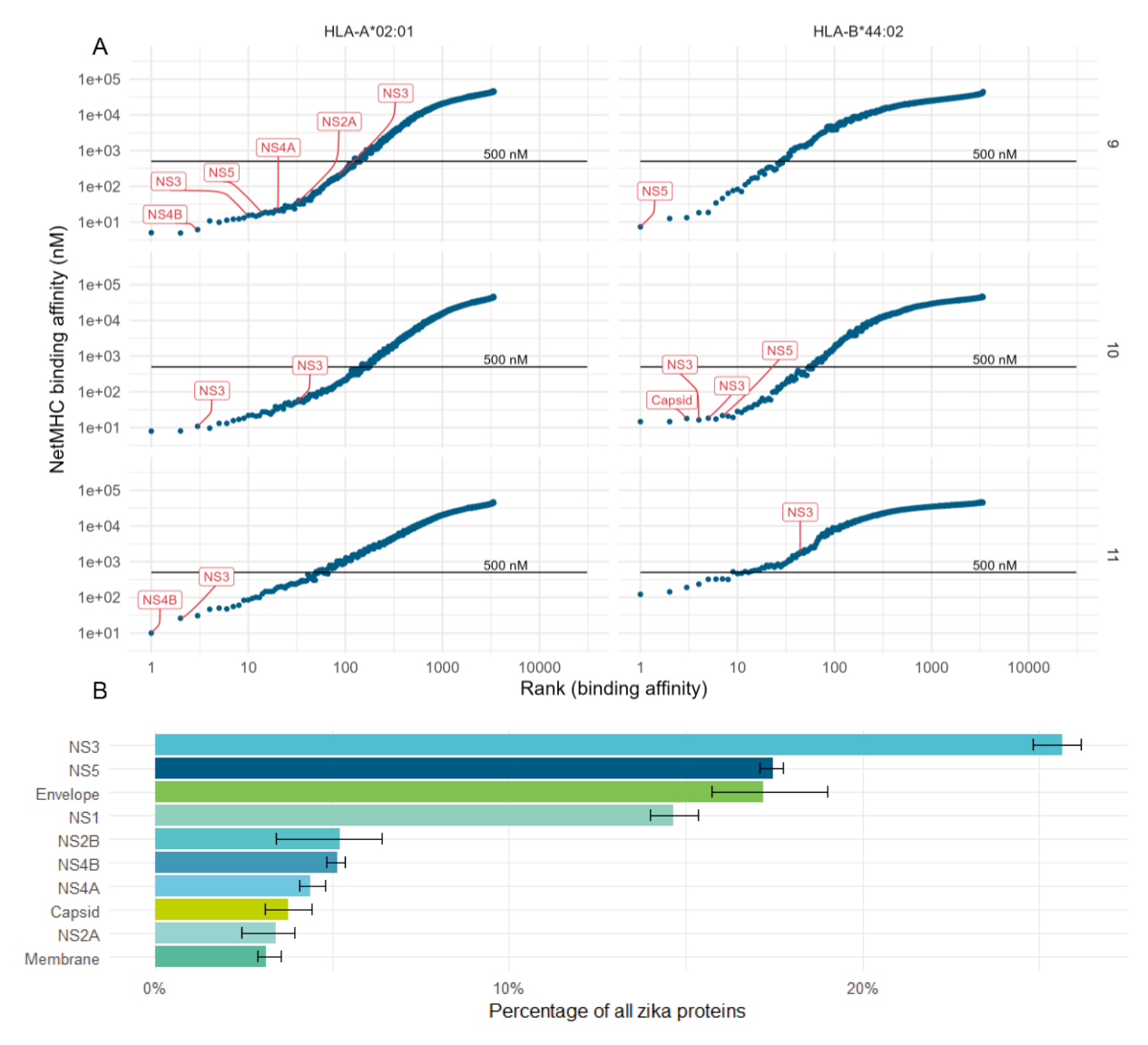


Figure 4. 3. ZIKV immunopeptides binding affinity and viral protein abundance.

(A) NetMHC binding predictions of all possible 9,10 and 11-mer ZIKV peptides (rows) to the USP7 HLA-I allotypes (columns). HLA binding affinity (y-axis) is plotted against the peptides rank (x-axis). Observed peptides and their source protein are indicated in red, with the black line indicating the 500 nM threshold below which a peptide is considered a strong binder. (B) Barplot of the proportion of ZIKV proteins observed in the global proteome of ZIKV-infected USP7 cells. Abbreviations, Zika virus (ZIKV), human leukocyte antigen (HLA), major histocompatibility complex (MHC), non-structural protein (NS).

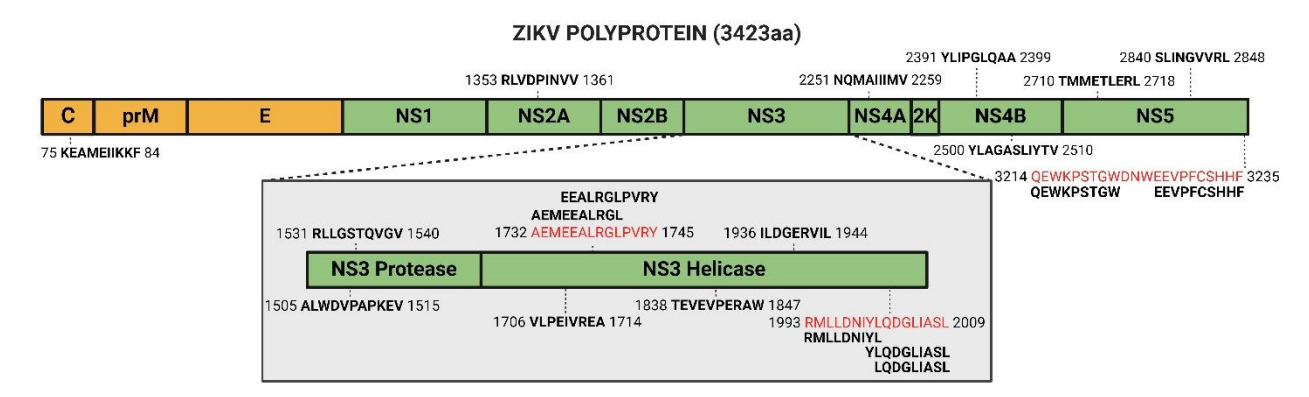


Figure 4. 4. ZIKV polyprotein with mapped immunopeptides.

The 19 identified ZIKV peptides are in bold, with the flanking numbers denoting the site in the polyprotein of the first and last amino acid. Peptide-rich sequences are indicated in red, with their correspliponding peptides aligned above or below. ZIKV polyprotein not to scale. Figure created in BioRender. BioRender.com/r34k740BioRender.com. Abbreviations, Zika virus (ZIKV), amino acid (aa), capsid (C), pre-membrane (prM), envelope (E), non-structural protein (NS).

4.11 Tables

Table 4. 1. USP7 cell HLA allotypes and their expression across the human population

Locus	HLA allotype	Population Coverage	ATRT Coverage
HLA-A	A*02:01	39.08%	14%
HLA-B	B*44:02	7.61%	6%
HLA-C	C*05:01	7.85%	4%
HLA-DRB1	DRB1*15:01	18.41%	20%

HLA allotypes determined from RNA sequencing of USP7 cells. ATRT Coverage sourced from Marcu et al. (411). Abbreviations, Zika virus (ZIKV), human leukocyte antigen (HLA), atypical teratoid rhabdoid tumour (ATRT).

Table 4. 2. Number of USP7 cell-presented ZIKV immunopeptides

Condition	HLA class	Number of peptides
USP7 Mock	I	3,866
COI / HOCK	II	240
USP7 ZIKV	I	3,658
USF / ZIKV	II	222

Abbreviations, Zika virus (ZIKV).

Table 4. 3. Number of USP7 cell-presented ZIKV immunopeptides per protein

Protein	Number of immunopeptides		
NS3	10		
NS5	4		
NS4B	2		
Capsid	1		
NS2A	1		
NS4A	1		

Abbreviations, Zika virus (ZIKV), non-structural (NS).

Table 4. 4. USP7 cell-presented ZIKV immunopeptides and their predicted properties

ZIKV Peptide	Protein	Length	*Binding affinity	**Immunogenicity	Predicted HLA
KEAMEIIKKF	Capsid	10	17.9nM	-0.006	HLA-B*44:02
RLVDPINVV	NS2A	9	32.5nM	0.169	HLA-A*02:01
ALWDVPAPKEV	NS3	11	26nM	0.210	HLA-A*02:01
YLQDGLIASL	NS3	10	10.8nM	0.165	HLA-A*02:01
RMLLDNIYL	NS3	9	15.3nM	0.111	HLA-A*02:01
VLPEIVREA	NS3	9	296.3nM	0.368	HLA-A*02:01
LQDGLIASL	NS3	9	201nM	0.092	HLA-A*02:01
RLLGSTQVGV	NS3	10	53.3nM	-0.167	HLA-A*02:01
AEMEEALRGL	NS3	10	16.3nM	0.270	HLA-B*44:02
TEVEVPERAW	NS3	10	18.3nM	0.268	HLA-B*44:02
EEALRGLPVRY	NS3	11	1796nM	0.081	HLA-B*44:02
ILDGERVIL	NS3	9	6064.7nM	NA	HLA-C*05:01
NQMAIIIMV	NS4A	9	21.2nM	0.247	HLA-A*02:01
YLIPGLQAA	NS4B	9	6.1nM	-0.020	HLA-A*02:01
YLAGASLIYTV	NS4B	11	10nM	0.061	HLA-A*02:01
TMMETLERL	NS5	9	10.1nM	0.186	HLA-A*02:01
SLINGVVRL	NS5	9	17.5nM	0.174	HLA-A*02:01
EEVPFCSHHF	NS5	10	21.6nM	-0.078	HLA-B*44:02
QEWKPSTGW	NS5	9	7.3nM	-0.331	HLA-B*44:02

^{*} Predicted by NetMHC 4.0, a binding affinity < 500 nM is usually considered the threshold for a strong binder. ** Positive values denote predicted immunogenic peptides, and negative values denote non-immunogenic peptides. Abbreviations, Zika virus (ZIKV), non-structural protein (NS), human leukocyte antigen (HLA).

Table 4. 5. ZIKV: human peptide homology

ZIKV Peptide	Human Sequence	Protein ID	Gene Name	Mismatch Positions
ILDGERVIL	ELDGERVAL	P52429.1	DGKE	[1, 8]
LQDGLIASL	LQDGLCHSL	O15021.4	MAST4	[6, 7]
RLVDPINVV	ILVDPIQVV	O75907.2	DGAT1	[1, 7]
TMMETLERL	TMMETLSRY	P21217.1	FUT3	[7, 9]
VLPEIVREA	VLPELLREA	Q92504.2	SLC39A7	[5, 6]
YLIPGLQAA	YLVPGLVAA	Q9H4B8.2	DPEP3	[3, 7]
YLQDGLIASL	YLQHGLIASA	Q5VXJ0.2	LIPK	[4, 10]
AEMEEALRGL	AEEREALGGL	O15550.2	KDM6A	[3, 4, 8]
EEALRGLPVRY	EEALRGLYGRV	P50053.2	КНК	[8, 9, 11]
KEAMEIIKKF	KEMKESIKKF	O43615.2	TIMM44	[3, 4, 6]
NQMAIIIMV	NLMAFLIMV	Q9UBY5.1	LPAR3	[2, 5, 6]
QEWKPSTGW	QEHKPSTQN	A0A1B0GUV7.1	TEX48	[3, 8, 9]
RLLGSTQVGV	QLLLSTVVGV	P01019.3	AGT	[1, 4, 7]
RMLLDNIYL	DDLLDNITL	O43524.1	FOXO3	[1, 2, 8]
SLINGVVRL	SLINFRVLL	O60287.4	URB1	[5, 6, 8]
TEVEVPERAW	TEAEVLERAN	P49189.3	ALDH9A1	[3, 6, 10]
ALWDVPAPKEV	-	-	-	-
EEVPFCSHHF	-	-	-	-
YLAGASLIYTV	-	-	-	-

Abbreviations, Zika virus (ZIKV), identifier (ID).

Chapter 5 General discussion and future directions

5.1 Overview

Despite the growing body of research investigating the development of congenital Zika syndrome (CZS) or oncolytic Zika virus (oZIKV) therapy for paediatric nervous system tumours, few large data and omics investigations have attempted to examine the molecular mechanisms involved. In my thesis, I presented the use of multiple large data and omics techniques to elucidate the cellular response of human nervous system cells to ZIKV infection. The overarching aim of generating and analysing these datasets was to identify the individual host genes, proteins, and pathways implicated during ZIKV infection in the varying cell types. My work primarily focused on the infection of cancerous nervous system cells, but I also investigated infection of CZS-affected patient-derived neural precursor cells (NPCs). The datasets I have generated and presented are bulk RNA sequencing (RNA-Seq), global proteomics, immunopeptidomics, and multiplex ELISA. Integrating these datasets with publicly available resources and datasets allowed me to validate these approaches and yield deeper molecular and functional insights. The main publicly available datasets and resources that I incorporated into my research and presented as a part of my thesis are genome-wide DNA methylation, bulk RNA-Seq, scRNA-Seq, interaction proteomics, genome-wide CRISPR-Cas9 screens, patient survival data, and the Immune Dictionary. Targeted in vitro exploration of some of my findings has led to a deeper understanding of the interaction between ZIKV and host systems during infection. In brief, I first investigated the molecular mechanisms involved in oZIKV infection of paediatric neuroblastoma (Chapter 2), medulloblastoma and atypical teratoid rhabdoid tumour (ATRT) (Chapter 3) cells. Finally, I presented work that investigated the immunological responses of brain tumour cell lines to infection. Employing in silico modelling and bioinformatic tools, I predicted how these responses may orchestrate an immune response against the patient's tumour (Chapters 3 and 4).

5.2 Chapter 2 Discussion

5.2.1 Summary of results

In **Chapter 2**, I employed extensive data mining, re-analysis, and integration to investigate ZIKV as a possible candidate for neuroblastoma oncolytic virotherapy. Data mining of ZIKV infection assays demonstrated potent ZIKV infection and reduced viability of multiple neuroblastoma cell

lines. I identified the PRVABC59 strain as a leading candidate for neuroblastoma oZIKV therapy. At the transcriptome level, ZIKV infection upregulated TNF signalling, cytokine signalling, lipid metabolism (SREBP and LXR pathways), ER stress (IRE1- and PERK-mediated UPR), and downregulated cell cycle and DNA replication terms. My work indicated that ZIKV infection of neuroblastoma was dependent on lipid homeostasis mediated by SREBP, LXR and cholesterol abundance, and the host protein complexes ER Membrane Protein Complex (EMC), V-ATPase and mammalian translocon. I investigated the ZIKV NS4B interactome in neuroblastoma cells and observed interactions with electron transport chain proteins, giving molecular insight into NS4B-induced mitochondrial cell death. Additionally, ZIKV NS4B interacted with components of the IRE1-mediated UPR, SREBP-regulated lipid metabolism and the mammalian translocon. Finally, I incorporated my results with additional observations from the literature to map the ZIKV life cycle in cancer cells.

5.2.2 Strengths and relevance of findings

A primary strength and relevance of my work was that I performed the first comprehensive systemic re-analysis and review of ZIKV infection of neuroblastoma cells. My re-analysis of all the published literature and publicly available data from an oncological perspective has shed significant light and insight into numerous host processes and pathways that ZIKV interacts with and is dependent on for neuroblastoma cell infection. Integration and re-analysis across multiple large datasets yielded new findings that were not observed by the original creators of the datasets. A particular strength of my work in this chapter was that following the identification of ZIKV PRVABC59 as a leading neuroblastoma OV candidate, I investigated the response of the highly susceptible and well-studied SH-SY5Y neuroblastoma cell line to this exact strain. Due to the broad utilisation of SH-SY5Y in research, I cross-referenced my observations to functional experiments specifically in SH-SY5Y or its close derivative SK-N-SH to help validate my work. Due to the breadth of my work, the ZIKV life cycle in neuroblastoma cells was mapped for the first time. This map will be an instrumental reference tool to aid future neuroblastoma oZIKV research in further delineating the neuroblastoma ZIKV life cycle. At the time of submission for pre-print, two publications assessing oZIKV against neuroblastoma existed, and only one more has been published since (251,261,262). Thus, my research and observations are relevant and particularly pertinent because, even to date, there is very little molecular understanding of oZIKV infection for neuroblastoma in the literature.

Interestingly, whilst I identified the Asian PRVABC59 strain as a leading oZIKV candidate, Mazar et al. recently demonstrated that intratumoural African ZIKV administration is efficacious for treating human neuroblastoma in xenograft mouse models (262). The benefit of an Asian ZIKV strain for neuroblastoma treatment is that it can be delivered systemically, and theoretically, it should be capable of targeting neuroblastoma brain metastases due to its neurotropism. Conversely, intratumoural African ZIKV administration may serve neuroblastoma patients better as it is less pathogenic and transmissible. Thus, whilst my work identifies an Asian strain and Mazar et al. focus on an African strain, collectively our work highlights the need for future neuroblastoma oZIKV research to incorporate both lineages to investigate their differing therapeutic potential.

5.2.3 Limitations

An inherent and universal limitation of *in silico* studies is the lack of laboratory-based validation. Several approaches were taken to help mitigate this limitation. Firstly, for observations from the RNA-Seq data, internal validation of pathway activity was drawn from assessing the expression of multiple downstream genes. Secondly, for observations drawn from datasets, such as the ZIKV-infected SH-SY5Y RNA-Seq dataset, cross-referencing to functional experiments primarily in SH-SY5Y or SK-N-SH cells was performed. Lastly, any novel observations that could not be cross-referenced to published functional experiments were omitted from the study due to their weak validity in the absence of supporting functional experiments. Despite this, the lack of functional validation remained a key limitation of my work. The research I performed here led to the establishment of an adjacent PhD project to help validate and build on my *in silico* study, as continuing this work was out of the scope of my PhD project.

An additional limitation was that any inaccuracy in data presentation and reporting by authors of the original publications inherently predisposed my observations to inaccuracy. Key examples are the results drawn from **Tables 2.1 and 2.2** for the infection and oncolytic capabilities of different ZIKV strains against different neuroblastoma cell lines, as they were assessed under various conditions by different research groups.

The RNA-Seq, NS4B interactome, and CRISPR-Cas9 datasets were all from metastatic neuroblastoma, and the publications I incorporated into my re-analysis predominately used neuroblastoma cell lines derived from metastases. Whilst metastasis is common in neuroblastoma, metastatic disease does not fully represent the primary disease, so it is important to note that the current study's results represent that of metastatic rather than primary disease.

A potentially perceived limitation of the study could be how I structured the manuscript, with the **Results and Discussion** written as one. The manuscript was written in this format as extensive referencing was performed throughout this section to (i) introduce the different areas being investigated and (ii) reference the numerous functional experiments which were unsuitable for incorporation into the study's Figures or Tables. Additionally, this format was chosen to simplify the reader experience, as the results have ten subsections.

5.2.4 Future work

In **Chapter 2**, ZIKV-infected SH-SY5Y cells showed a strong TNF and cytokine signalling response at the transcriptome level. Experimental investigation and validation of the TNF signalling pathway in ZIKV-infected neuroblastoma cells should be carried out as performed (**Chapter 3**) and proposed later (**Section 5.3.4**) for medulloblastoma and ATRT cells. Performing a ProcartaPlex multiplex ELISA assay would generate a comprehensive dataset to investigate and validate the profile of secreted cytokines and immune checkpoint proteins from ZIKV-infected neuroblastoma cells. Comparison against the ZIKV-infected medulloblastoma and ATRT cell secretomes I presented in **Chapter 3** would identify any conserved and differential cytokine responses across these different paediatric nervous system tumour cells. Elucidating the cytokine profiles may identify opportunities to augment oZIKV therapy with adjuvant cytokine therapy, as done in a Phase I trial for paediatric high-grade glioma (HGG) patients receiving GM-CSF treatment before Pelareorep OV therapy (120).

Oncolytic ZIKV infection can directly perturb cancer cells by inducing differentiation, perturbing proliferation, reducing cancer cell migration or inducing oncolysis. Besides neuroblastoma oncolysis by live ZIKV or NS4B, it is unknown how live ZIKV or its individual proteins may contribute to these other efficacious effects. To investigate this, neuroblastoma cells must first be transiently transfected or stably transduced with ZIKV gene-expressing lentiviral plasmids to examine the individual ZIKV proteins. Enrichment via a drug selection marker (e.g. ampicillin) or a fluorescent tag (e.g. GFP) for fluorescence-activated cell sorting (FACS) would enrich the population of ZIKV protein-expressing cells. The differentiation status of neuroblastoma cells in response to live ZIKV or its individual proteins can be determined by assessing (i) morphological differentiation by a neurite outgrowth assay and (ii) expression of neuronal differentiation markers such as NeuN (RBFOX3) or NSE (ENO2) by RT-qPCR, western blotting or fluorescence microscopy. Additional functional assays to assess live ZIKV or its individual proteins in neuroblastoma cells include: (i) Incucyte live cell analysis to assess 2D cell proliferation (as performed in Chapter 3), (ii) tumorsphere formation assay to assess 3D neuroblastoma

spheroid growth, and (iii) spheroid cell invasion assay to assess neuroblastoma tumorsphere invasion into the surrounding 3D environment. ZIKV NS5, not NS4B, is the principal oncolytic protein in adult glioma (274). Performing these experiments in tandem with medulloblastoma and ATRT cells would identify the conserved or differential roles of live ZIKV and its proteins across different paediatric tumours.

In **Chapter 2**, I characterised the transcriptomic response of neuroblastoma cells to ZIKV infection, but their response at other omics layers is virtually unknown. The generation of such datasets is deeply warranted to investigate these responses. A whole-genome CRISPR-Cas9 screen would be particularly insightful by comprehensively identifying ZIKV dependency factors in neuroblastoma cells. This would identify the dependency of ZIKV on novel host complexes and is expected to support my findings by highlighting ZIKV dependency on additional EMC, V-ATPase, and Mammalian Translocon components. Including medulloblastoma and ATRT cells in these screens would yield more profound insight into the ZIKV life cycle in nervous system tumour cells.

5.3 Chapter 3 Discussion

5.3.1 Summary of results

In Chapter 3, I employed transcriptomics to analyse ZIKV infection of USP7 ATRT and USP13 medulloblastoma cells. I identified signatures indicative of immunogenic cell death (ICD), principally ER stress-mediated pro-apoptotic gene expression, TNF pathway, and cytokine signalling. Cross-referencing with publicly available RNA-Seq datasets highlighted that upregulation of canonical and non-canonical TNF signalling pathways were conserved responses across different ZIKV-infected nervous system tumour cells. I demonstrated that recombinant TNF-alpha was pro-tumoural by increasing brain tumour cell growth under normal conditions in vitro. Supporting this, I showed high TNF-alpha expression to be significantly correlated with worse medulloblastoma survival, highlighting it as a marker of poor prognosis for medulloblastoma. Interestingly, when considered in the context of oZIKV infection, recombinant TNF-alpha was anti-tumoural by reducing the cell viability of ZIKV-infected brain tumour cells. Performing a 49-plex ELISA, I showed that ZIKV infection induced a diverse and predominantly pro-inflammatory secretome from medulloblastoma and ATRT brain tumour cells. I assessed publicly available scRNA-Seq data and modelled in silico how the ZIKVinduced brain tumour secretome may orchestrate anti-tumoural immune responses. I achieved this by predicting how the secretome may interact with medulloblastoma TIME cells via

paracrine signalling or polarise lymph node immune cells via endocrine signalling. I observed that the paracrine signalling likely targeted tumour-resident immune cells over non-infected medulloblastoma tumour cells, and endocrine signalling to polarise a diverse and predominantly anti-tumoural immune response.

TNF-alpha presented as a key component of oZIKV infection of paediaitric brain tumour cells., I showed that it was pro-tumoural for brain tumour cells, and its expression was correlated with reduced medulloblastoma survival. However, it also enhanced brain tumour cell oncolysis. My *in silico* modelling predicts all medulloblastoma TME resident immune cells to be primed to respond to TNF-alpha, and TNF-alpha endocrine signalling to polarise myeloid linage cells to express gene signatures indicative or pro-survival and innate immune recognition. Therefore, based on my research, therapeutic targeting of tumoural TNF-alpha signalling may be a viable approach to enhance oncolysis and modulate the anti-tumoural immune response.

5.3.2 Strengths and relevance of findings

A primary strength and relevance of my work was that I performed the first omics study of any kind to investigate oZIKV infection in paediatric brain tumour cells. I followed this up by producing the most comprehensive ZIKV-infected cancer cell secretome to date. Performing the transcriptomic and multiplex ELISA assays across multiple time points has provided extensive details on the temporal responses following ZIKV infection. Additionally, performing these experiments in multiple cell lines allowed the identification of cell type-specific and cell line-specific responses, increasing the validity of the research. I used highly aggressive paediatric cell lines from both tumour types, characterised by their aberrant expression of neural stem cell (NSC) markers and elevated proliferation, invasion, drug resistance and tumorigenicity *in vivo*. Relatively few paediatric brain tumour cell lines have been established that have aggressive stem-like properties. Therefore, using USP7 and USP13 cell lines, which have cancer stem-like cell (CSC) characteristics, was a strength of my research as they are desirable 2D culture *in vitro* models for testing the efficacy of novel therapeutics designed to target aggressive cancer stem-like cells (CSCs).

A particularly relevant finding in **Chapter 3** was that I demonstrated that ZIKV can naturally induce a diverse secretome from infected brain tumour cell lines. My work supports ZIKV as a good candidate for OV development by identifying 15 new cytokines to be components of oZIKV infection: IFN alpha, IL-1 alpha, IL-1 beta, IL-1RA, IL-4, IL-5, IL-8 (CXCL8), IL-9, IL-21, CXCL1, CCL3, CCL4, CCL11, GM-CSF and SDF-1 alpha. These findings build on the current literature, as only limited details of the ZIKV-induced secretome are known for other brain tumour cell types,

including ZIKV-infected human adult glioblastoma cells (CXCL10 and CCL5 (RANTES)) and ZIKV-infected canine glioblastoma cells (IL-2, IL-6, IL-7, IP-10 (CXCL10), and IL-15) (264,265).

Additionally, only IL-8, CCL2 and KC-like are detected at greater levels in CSF and serum from canines with naturally occurring brain tumours following administration of ZIKV (264).

The vast complexity of the human immune system and its diverse interactions with viral infections and cancer make it incredibly experimentally challenging to assess how different ICD factors may orchestrate anti-tumoural immunity. This has started to be investigated for adult glioma, but not for childhood nervous system tumours (264,266,271,277). To address this gap and to circumvent the experimental challenges of investigating anti-tumoural immunity, I exploited the ability of single-cell-resolution transcriptomic technology to detect specific cell types and states within heterogeneous populations to model ZIKV-induced brain tumour cell secretome paracrine and endocrine signalling in silico. Significant relevance and impact of my modelling came from utilising the recently assembled Immune Dictionary to identify immune cell polarisation states. This valuable resource extensively documented the polarisation states of specific immune cell types in response to interaction with individual cytokines in vivo for the first time (368). Integrating this powerful resource with my ZIKV-induced brain tumour secretome provided unique insight into both the immune cell composition and phenotypes that likely arise from ZIKV-induced brain tumour cell secretome endocrine signalling. My predictions of the immune cell composition in response to oZIKV infection support findings from immunological studies investigating ZIKV infection in adult glioma (264,266,271,277). Infiltration of both innate (NK cells, monocytes, macrophages, DCs and microglia) and adaptive (CD4+ and CD8+ T cells) immune cells occurs in ZIKV-infected glioma (266,271,277). My modelling of immune cell phenotypes in response to the ZIKV-induced secretome builds on this literature by predicting that (i) CD8+ T and NK cells will be cytotoxic, (ii) macrophages will predominantly be in a M1-like state, and (iii) effector memory CD4+ T cells will be produced.

5.3.3 Limitations

Although my multiplex ELISA and recombinant TNF assays validated the RNA-Seq results, a limitation to my research here was having to use two different ZIKV strains (despite their highly similar RNA sequence identity of 99.74%). This limitation was a byproduct of producing the RNA-Seq samples with my USP collaborators and not having access to the same strain when performing the validation experiments at TPI. I attempted to minimise this limitation by maintaining ZIKV stocks at TPI the same way as at USP (Section 3.4.1). To manage the complexity and cost of the large RNA-Seq dataset that I produced, the research team and I

decided at the time the experiments were conducted to collect Mock-infected samples only at 24 hours post-infection (hpi). This weakened the validity of the results observed at 12 and 18 hpi as they were not made relative to time-matched Mock samples. To mitigate this limitation, I primarily focused my investigation and validation of pathways and processes on those observed at 24 hpi. Despite a clear oncolytic response of both USP7 and USP13 cells to ZIKV infection, only a modest response was observed at the DEG level, with few DEGs reaching a notable fold change level. This restricted the application of a fold change threshold to the brain tumour DEGs, thus affecting the initial identification of biologically interesting and relevant processes and pathways (Figure 3.2). To circumvent this, I took a conservative approach and assessed only the pathways enriched in the most highly ranked DEGs from the ZIKV-infected brain tumour cells. Applying this approach revealed the ZIKV-induced ICD signatures, which I then validated and investigated further.

Despite observing 20 proteins to be significantly secreted by ZIKV-infected tumour cells, I only modelled endocrine signalling for six. This was a limitation as the remaining 70% of the secretome could not be assessed due to the proteins either being absent from the Immune Dictionary or not being identified as a dominant cytokine driver of immune cell polarisation. I solely relied on *in silico* modelling to predict the immune response that the ZIKV-induced secretome may generate. As such, the clinical relevance of my research was limited by a lack of validation *in vitro* and *in vivo*.

5.3.4 Future work

The PFU and cell viability assays (**Section 3.4.4**) should be repeated in the presence of specific antibodies that have an opposing effect to that of the recombinant TNF proteins. This would extend findings from the individual TNF protein level to its respective TNF subpathway level. Using clinical antibodies, such as the TNF-alpha neutralising antibody Infliximab or the TNFRSF9 agonist Utomilumab, may highlight potential multimodal therapy options and would increase the clinical relevance of the results obtained. As sTNFSF9 and sTNFRSF9 inhibit their respective membrane receptors, antibodies which are receptor agonists (e.g. Utomilumab) should be used for pathway activation. To address the potential antibody off-target effects, the functional assays should be repeated following siRNA knockdown of the given TNF gene or its cognate receptor. Following this, the impact of TNF signalling modulation on oZIKV therapy *in vivo* should be assessed using 7-week-old Balb/C nude mice bearing right lateral ventricle USP7 or USP13 tumours, as previously described (249). TNF pathway regulation *in vivo* should occur via antibody, siRNA KO or recombinant TNF protein treatment, depending on the results obtained

for the proposed work above. Tumour establishment after tumour cell injection, tumour growth and metastasis can all be monitored by bioluminescence imaging through tumour cell firefly luciferase expression.

Infection studies should be conducted *in vivo* to validate my *in silico* modelling of the immune cell response to the ZIKV-induced brain tumour secretome. Orthotopic xenograft models are highly applicable for paediatric oncology due to the rarity of access to human paediatric brain tumour samples. However, as they are immunodeficient, they do not permit investigation into the anti-tumoural immune response. Administering oZIKV to immunocompetent mice bearing paediatric tumours, followed by tumour harvesting and scRNA-Seq, would allow the infiltrating immune cells and their polarisation states to be studied. Using a fluorescently labelled ZIKV strain would allow for FACS enrichment of ZIKV+ and ZIKV- tumour cell populations prior to scRNA-Seq. This may shed insight into the refractory mechanisms of some tumour cell populations to ZIKV infection and indicate potential multimodal therapy options to address these refractory cells.

In **Chapter 2**, I demonstrated that ZIKV-infected neuroblastoma cells also showed upregulation of TNF and cytokine signalling at the transcriptome level. All experiments proposed above for brain tumour cells should also incorporate neuroblastoma cells to help delineate ICD responses in this paediatric tumour.

5.4 Chapter 4 Discussion

5.4.1 Summary of results

In **Chapter 4**, I generated and analysed proteomic datasets to investigate the human leukocyte antigen (HLA) class I pathway and its presentation of ZIKV peptides on the surface of brain tumour cells. I first analysed global gene and protein expression datasets and identified that ZIKV infection significantly enriched human leukocyte antigen class I (HLA-I) antigen processing and presentation in adult and paediatric brain tumour cells, respectively. Investigating this further, we HLA typed the aggressive paediatric brain tumour cell line USP7. We demonstrated them to express the globally most common HLA-A allotype (A*02:01). USP7 cells predominantly presented endogenous 9-mer peptides by the three classical HLA-I molecules, with nearly three-quarters presented by HLA-A*02:01. We identified 19 ZIKV peptides, predominantly presented by HLA-A*02:01 and HLA-B*44:02 on the surface of USP7 cells. Twelve of these peptides are novel, and seven have been previously identified experimentally. We identified a

correlative trend between ZIKV peptide presentation and viral protein abundance and proposed that peptide presentation corresponded with protein abundance in the HLA-I pathway. I identified ZIKV NS3 helicase as a rich source of peptides predicted to be immunogenic and showed that the identified viral peptides did not mimic predicted peptides of the human proteome.

5.4.2 Strengths and relevance of findings

In **Chapter 4**, I performed the first study of its kind to investigate and discover brain tumour cell-presented ZIKV peptides. These identified ZIKV epitopes provide insight into oZIKV therapy and may serve as potential targets for immunotherapy. The multi-omics nature of the study design was a particular strength, as analysis across different omics layers has yielded a more complete and robust understanding of HLA-I presentation of both endogenous and ZIKV peptides by USP7 cells. A key example of this is where we utilised the superior sequencing depth of RNA-Seq to HLA type the USP7 cells, and this proved to be in perfect agreement with the reverse HLA typing performed from the sequence of the identified peptides, thus strengthening the validity of our observations. Additionally, combining a robust immunopeptidome isolation technique with high bioinformatic accuracy has allowed a small-scale study to generate results that align well and further build on the currently accepted literature (412–414,423).

Over 35 thousand HLA alleles have been recorded within the human population (427). Thus, identifying cell lines which express HLA alleles that are representative of a maximal proportion of the human population is challenging. We showed that USP7 cells expressed the three classical HLA-I alleles HLA-A*02:01, HLA-B*44:02 and HLA-C*05:01, which are expressed by 39.08%, 7.61% and 7.85% of the human population, respectively. With the wide population coverage of HLA-A*02:01, we identified USP7 as a desirable model cell line for immunopeptidomics. Furthermore, as the majority of the identified endogenous and ZIKV HLA-I presented peptides were predicted as high affinity HLA-A*02:01 binders, the peptides we identified are highly relevant to this research area and nearly 40% of the human population. The strength and relevance of this cell line was further corroborated by its resemblance to fetal NPCs, thus presenting it as a potential model for investigating T cell-mediated depletion of fetal NPCs.

A benefit of mass spectrometry immunopeptidomics is that it employs de novo sequencing, which allowed me to identify novel peptides, including twelve ZIKV peptides. One of my 19 identified ZIKV peptides (NS3 AEMEEALRGL) is a homolog of a previously identified dengue virus peptide (428). Homology such as this between viruses raise potential concerns with regard to

both the efficacy of oZIKV therapy and patient safety. Pre-existing virus-specific humoral immunity can affect OV anti-tumoural immune responses, and it is currently unknown what effect this pre-existing immunity may have on oZIKV therapy (429). Due to the epidemic nature of ZIKV infection and the cross-reactive nature of humoral immunity for specific flaviviruses, such as dengue virus (DENV), cancer patients may present suboptimal responses due to the neutralisation of oZIKV by pre-existing humoral immunity. Conversely, other aspects of this pre-existing immunity, such as memory T cells, may yield enhanced therapeutic efficacy when orientated against the infected tumour. This concept is supported by a report where one of the 19 ZIKV peptides I identified in my research (NS5 SLINGVVRL) stimulated memory cytotoxic T cells in mice with prior Japanese encephalitis virus (JEV) vaccination (414). As such, patient screening to determine their naïve status for flavivirus infection or immunisation would help inform their treatment and help control for adverse effects, such as antibody-dependent enhancement of infection (245,430). These risks could be mitigated partly by intratumoural delivery of a replication-incompetent oZIKV.

5.4.3 Limitations

Due to experimental limitations such as inadequate access to ZIKV and the 108 cells required for immunopeptidomics, my small-scale study was limited by the immunopeptidome sample size. This limited the clinical relevance, and the work thus only acts as a starting point for understanding the interaction between infected tumour cells and immune cells. A highly robust immunopeptidome pipeline has mitigated this limitation to a certain degree. This was evident by the identified ZIKV peptide sequences accurately matching the exact HLA allotypes expressed by USP7 cells, and the results being strongly supported by multiple published in silico predictions of ZIKV peptides and an immunopeptidome from ZIKV-infected B cells (412). Whilst we identified USP7 as a good model for assessing the HLA-I immunopeptidome, they're nonprofessional antigen-presenting cells. As such, we could not investigate human leukocyte antigen class II (HLA-II)-presented ZIKV peptides in detail. Additionally, monolayer culture is an inferior model to 3D in vitro, ex vivo, or in vivo systems, including those previously employed by co-authors of this study to investigate influenza virus infection (389). Due to certain project restrictions during the first half of my research, such as not having live ZIKV at UoS and the subsequent need for a research exchange trip to USP to generate the samples, applying the immunopeptidomics platform to anything other than monolayer cells was unattainable at the time the study was conducted.

A limitation of my research in **Chapter 5** was that I did not validate the immunogenicity of the viral peptides in the laboratory, as this was outside the practical scope and expertise for this project due to some of the restrictions detailed previously. I attempted to circumvent this by employing a robust and experimentally validated *in silico* immunogenicity prediction method (404). This approach predicted the immunogenicity of the peptide-HLA complex by assessing favourable aa features such as large or aromatic aa side chains and the location of each aa within the peptide, primarily at the non-anchoring positions 4-6 (404). Supporting my *in silico* prediction, three of our identified ZIKV peptides have been validated to be immunogenic ZIKV peptides, two of which were validated in two independent studies (412–414).

5.4.4 Future work

ZIKV infection assays followed by staining for cell surface HLA complexes and flow cytometry would validate if infection upregulates the HLA-I antigen processing and presentation pathway in USP7 cells, as observed by gene set enrichment analysis (GSEA) enrichment of the global proteome dataset. Staining with the anti-NS2B antibody (Section 3.4.2) would first permit gating on the infected cells before assessing the HLA changes within this population. Following this, the HLA binding and immunogenicity predictions would be validated in vitro. To achieve this, the peptides would be synthesised, and enzyme-linked immunospot assay (ELISpot) would assess their ability to stimulate cytotoxic T cell responses through HLA-I presentation directly by antigen-presenting cells (APCs) to patient peripheral blood mononuclear cells (PBMCs) (431). IFN gamma secretion is the primary correlate used to assess cytotoxic T cell activation by ELISpot. Polyfunctional T cell activation can be evaluated through FluoroSpot by assessing the secretion of additional molecules such as TNF-alpha, perforin and granzyme B. Following this validation, work should build on the ZIKV immunopeptidome assays to allow the comparison of HLA-I ZIKV peptide presented by ATRT cells to that of medulloblastoma cells (e.g. USP13) and neuroblastoma cells (e.g. SH-SY5Y). This would allow the identification of bona fide tumour cellpresented ZIKV peptides.

Oncolytic ZIKV efficacy relies on CD4+ T cells as well as cytotoxic CD8+ T cells (271,277). As such, the HLA-II ZIKV peptides should also be determined for paediatric nervous system tumours to help inform CD4+ T cell responses. This would be achieved by cancer cell and dendritic cell (DC) co-culture infection assays or by feeding the ZIKV-infected cancer cells to DCs. The DCs would process and present both ZIKV and tumour peptides by HLA-II, which could then be identified by immunopeptidomics (**Section 4.5.4**) and validated as I describe above for HLA-I ZIKV peptides above (389). The clinical relevancy of this work would be significantly

enhanced if patient samples could be obtained to assess *ex vivo* ZIKV infection of tumour samples by immunopeptidomics, followed by validation of the peptide candidates' immunogenicity using patient-matched PBMCs. Tumour antigen-loaded or -expressing OVs can have elevated anti-tumoural immune responses (432,433). Thus, determining the paediatric nervous system tumour antigens alongside the ZIKV peptides may enhance oZIKV therapy opportunities by identifying avenues to produce an oZIKV cancer vaccine.

5.5 Collective summary and insight

An original contribution of my research was that I conducted a systematic investigation of four different cell types that have never before had their responses to oncolytic ZIKV infection assessed at the molecular level via omics techniques. My work significantly builds on the limited research into oZIKV infection in paediatric tumours (medulloblastoma, diffuse midline glioma (DMG), ATRT and neuroblastoma), and also complements work performed in adult tumours (glioma, ependymoma and meningioma) (249–251,262,264). Defining the molecular signatures of oZIKV infection across different paediatric nervous system tumour cells has served as a crucial stage in ascertaining the range of paediatric tumours that might be receptive to oZIKV therapy. My collective research efforts to investigate oZIKV infection of both central and peripheral nervous system tumour cell lines for the first time identified conserved responses between these different cell types, principally TNF and cytokine signalling. Oncolytic ZIKV infection has been shown to induce pro-inflammatory responses in glioma stem cells (GSC), including TNF, NF-κB, and cytokine signalling (243,265,271). Thus, placing my research in the context of current literature reveals that this pro-inflammatory response is conserved across both paediatric and adult nervous system tumour cell lines.

Cross **Chapters 2-4**, I identified a variety of components which collectively contribute to the immunogenic nature of oZIKV infection in paediatric nervous system tumour cells and would likely orchestrate the remodelling of the TIME. Firstly, I identified upregulation in ER stress responses in ZIKV-infected neuroblastoma, medulloblastoma, and ATRT cells at the transcriptome level. This indicated ZIKV as a Type II inducer of paediatric nervous system tumour cell immunogenic cell death (ICD) (434). Observing upregulation of cytokine signalling across all three ZIKV-infected cell types, I validated and further investigated this immunogenic response by multiplex ELISA for ZIKV-infected brain tumour cells. I identified secreted proteins from diverse families: chemokines, interleukins, tumour necrosis factors, interferons, colony-stimulating factors and programmed cell death proteins. This cytokine response was much greater than that observed for non-paediatric brain tumour cells, indicating a more

immunogenic response of paediatric brain tumour cells to oZIKV infection (264,265). Modelling the paracrine signalling from this secretome, I predicted the primary responders of the medulloblastoma TME to be tumour-resident immune cells rather than medulloblastoma tumour cells. Modelling the endocrine signalling, I predicted diverse immune cell polarisations, including memory CD4+ T cells, cytotoxic CD8+ T and natural killer (NK) cells, M1 and M2 macrophages, and more. Following recruitment and tumour infiltration, T cell activity is initiated by T cell receptor (TCR) binding to HLA-presented peptides, and co-stimulatory and co-inhibitory molecules regulate this. My research identified that ZIKV-infected brain tumour cells presented an array of ZIKV peptides by HLA-I molecules, the majority of which are predicted to be immunogenic to activate TCR signalling.

The immunogenic nature of oZIKV infection, as indicated from my research findings detailed in the previous paragraph, highlights oZIKV as a potential adjuvant for immunotherapy. To date, this has only been investigated for glioma, where oZIKV improved mouse survival by remodelling the TIME to sensitise glioma to immune checkpoint blockade (PD-1 and PD-L1) and tumour vaccination (266,271,277). Two possible multimodal treatment regimens for neuroblastoma that warrant investigation include oZIKV therapy as an adjuvant to retinoic acid differentiation therapy or anti-GD2 immunotherapy. Whilst the efficiency of oZIKV infection for adult glioma is stemness dependent, this is not the case for neuroblastoma, and retinoic acid differentiation has been shown to elevate neuroblastoma susceptibility to ZIKV infection in vitro (251,261,262,353). This highlights retinoic acid differentiation as a potential pre-treatment for oZIKV therapy in neuroblastoma patients. In Chapter 4, I identified that ZIKV significantly upregulates the secretion of GM-CSF from medulloblastoma cells. GM-CSF cytokine therapy is an adjuvant that enhances anti-GD2 immunotherapy against high-risk neuroblastoma (93,105). Therefore, if GM-CSF is also secreted by ZIKV-infected neuroblastoma cells, synergistic effects between anti-GD2 immunotherapy and this endogenously secreted GM-CSF may make GM-CSF cytokine therapy obsolete. One of the mechanisms of action of anti-GD2 immunotherapy is the induction of antibody-dependent cellular cytotoxicity (ADCC), where coating of neuroblastoma cells directs immune cells such as NK cells and macrophages against the tumour (92,93). In Chapter 3, my in silico modelling predicted that ZIKV-induced cytokine secretion from brain tumour cell lines would induce a diverse immune cell response, including polarisation of macrophages towards an M1-like phenotype and cytotoxic NK cell activation. Observations in mouse and canine brain tumours in vivo support my predictions, where oZIKV infection was shown to induce NK cell and M1-like macrophage infiltration (264,266,271,277). If this immune cell infiltration is also observed for oZIKV-infected neuroblastoma, then oZIKV may prove capable of augmenting anti-GD2-induced ADCC. This may occur by oZIKV stimulating

infiltration of the immune cells which are required to detect anti-GD2 coated tumour cells (i.e. cytotoxic NK cells and M1-like macrophages), therefore, promoting ADCC. A strong caveat is that these recommended regimens are currently just concepts and, as such, require thorough investigation and validation.

In addition to being a promising adjuvant to immunotherapy, oZIKV shows potential for use in conjunction with standard-of-care therapies, such as chemotherapy. To date, this has only been demonstrated for adult glioma, where oZIKV infection sensitised drug-resistant glioma cells to the chemotherapy Temozolomide in vitro (243). Cisplatin is a standard-of-care chemotherapy for both medulloblastoma and high-risk neuroblastoma (435,436). In Chapter 3, I identified that ZIKV infection significantly upregulates DNA damage and repair processes in USP13 medulloblastoma cells at the transcriptome level. These ZIKV-induced DNA mechanisms may synergise with Cisplatin-induced DNA damage (i.e. intra- and interstrand crosslinking of purine bases) to increase DNA damage burden and subsequent tumour cell apoptosis (437,438). Notably, Cisplatin can induce ICD and engage the TIME by (i) polarising macrophages towards an M1-like phenotype, (ii) increasing cytotoxic CD8+ T cell infiltration, and (iii) polarising immune suppressive myeloid-derived suppressor cells (MDSCs) into immune stimulatory dendritic cells (DCs) (438). My in silico modelling in Chapter 3 predicted that oZIKV infection would remodel the TIME composition in a similar manner, which is supported by current literature for glioma (266,271,277). Hence, oZIKV may synergise with Cisplatin in heating the tumour microenvironment. An example of this synergism is that the polarisation of MDSCs into DCs by Cisplatin would likely support the establishment of an oZIKV-induced anti-tumoural immune response, as the Cisplatin-induced immune stimulatory DCs could process and present oZIKV antigens to T cells to prime an adaptive immune response (438). Finally, oZIKV and Cisplatin may also synergise via oZIKV infection disrupting the blood-brain barrier (BBB), resulting in increased Cisplatin levels in the brain and penetration into brain tumours such as medulloblastoma (439,440). This final proposed mechanism is a prime example of how combining oZIKV with a standard-of-care therapy can enhance the efficacy of the standard-ofcare therapy, thereby resulting in lower and safer levels of the therapy being required.

Interestingly, whilst I identified ZIKV infection to induce a diverse cytokine profile response, I did not detect upregulated secretion of known immune checkpoint proteins by ZIKV-infected brain tumour cells. The only exception to this was TNFRSF9. Membrane TNFRSF9 (mTNFRSF9) is a costimulatory receptor with only one known ligand, TNFSF9. Cancer cells secrete soluble TNFRSF9 (sTNFRSF9), which competitively inhibits T cell mTNFRSF9 from binding to mTNFSF9 (441). This impairs the co-stimulation of TCRs following binding to HLA-presented peptides and

consequently promotes an immunosuppressive TME (442). TNFRSF9 being significantly secreted by ZIKV-infected medulloblastoma and ATRT cells *in vitro* suggests that it may oppose the establishment of an anti-tumoural immune response. I identified TNFRSF9 expression to be significantly correlated with improved medulloblastoma patient survival, and TNFSF9 reverse signalling into tumour cells is known to be pro-tumoral (443). Interestingly, TNFRSF9 is one of the only genes which was significantly upregulated across all the different nervous system tumour cell (medulloblastoma, ATRT, neuroblastoma, and adult glioma) RNA-Seq datasets, and it was not differentially expressed in ZIKV-infected CZS-affected patient-derived NPCs. This indicated a conserved tumour-specific response to ZIKV infection, but it was unclear what role non-canonical TNFRSF9 signalling may play in oZIKV infection. This signalling deeply warrants investigation as it may present a way to enhance oZIKV therapy against all these nervous system tumours. To conclude, my work collectively gives insight into a variety of immunogenic signatures of ZIKV-infected cells; whilst the majority likely promote an anti-tumoural immune response, a select few may hinder its establishment.

While my assessment of oZIKV infection in various paediatric nervous system tumour cell types has been valuable in identifying conserved responses across different tumours, it has come at the cost of assessing tumour subgroup responses, as I only examined one cell line per tumour type. Consequently, a limitation of my research is that I have not investigated whether cell lines from different subgroups exhibit conserved or differential responses to oZIKV infection.

Conducting this research is crucial because an oZIKV therapy will likely only be considered for subgroups/treatment groups with a poor prognosis (i.e. high-risk neuroblastoma), as opposed to those with a better prognosis (i.e. very low- and low-risk neuroblastoma). An additional limitation of my research is that I have used cell lines rather than more clinically relevant models, such as patient-derived cells. Immortalised cancer cell lines frequently lack heterogeneity, and they develop mutations throughout continual passaging that reduce their ability to faithfully model the complex biology of a patient's tumour (444). Moving forward, a more translational and clinical focus should be taken through the incorporation of patient-derived cells and additional *in vivo* models into oZIKV research.

5.6 Critical analysis of omics techniques

A key contribution I have made is the creation of multiple resources to facilitate continued progress in oZIKV research. Mapping the life cycle of oZIKV infection in a cancer cell for the first time has created a blueprint for understanding the molecular mechanisms involved in cancer cell oncolysis. This map serves as a template for further improvement by other neuroblastoma

researchers or for modelling oZIKV infection of different cancer cells. The multiple omics datasets I have generated during my PhD will aid the wider community in investigating both neuropathogenic and oncolytic ZIKV infection beyond what I have performed in this thesis. A principal way this may be achieved is through the integration of my ZIKV-infected paediatric brain tumour datasets with those from adult glioma to comprehensively investigate the conserved and differential responses of these brain malignancies to oZIKV infection (230,265,268).

The molecular mechanisms involved in oncolytic ZIKV infection are relatively unknown for paediatric cancer cells (249,256,262). To address this research gap I performed bulk RNA-Seq and mass spectrometry proteomics. Both are cost-effective and time-efficient techniques that have well-established analysis pipelines and are well-suited for discovery due to their high coverage and unbiased nature. However, both approaches produce datasets that do not allow resolution of the different cell phenotypes or their responses to stimuli, as they present an average of the entire cell population. This limited the significance of my research due to the inability to resolve productively infected cell signatures from those of cells refractory to ZIKV infection. Although not used in my research due to prohibitive costs, single-cell RNA-Seq and proteomics address these limitations of bulk omics techniques. Whilst scRNA-Seq is well established, its coverage is lower than bulk RNA-Seq due to the limited starting material to be sequenced, and the coverage of single-cell proteomic techniques is low, with only 300-400 proteins currently being able to be quantified from a single cell (445,446).

Whilst RNA-Seq has significantly greater coverage than proteomics, biological processes are primarily driven at the protein level through regulation of protein expression, modification, interaction and degradation. As such, employing bulk RNA-Seq as the primary omics technique to assess molecular mechanisms is a limitation of my work because there is only a 0.6 correlation between the transcriptome and proteome in human cells and tissues (447). Consequently, some of the results from my functional enrichment analysis that I have not functionally validated in this thesis may not translate through to pathway activity at the protein level. Additionally, the RNA-Seq sample processing step of poly(A) enrichment hinders the ability to confidently quantify and analyse the replication of viral genomes that lack a poly(A) tail, as is the case for ZIKV.

In **Chapter 4**, I employed label-free bottom-up mass spectrometry proteomics to assess ZIKV infection of USP7 cells. A label-free approach was chosen to maximise coverage by being able to use an Orbitrap Fusion Tribrid Mass Spectrometer at the Centre for Proteomic Research.

Additionally, a label-free experimental design was chosen as it is more cost-effective and time-

efficient than labelling methods (i.e. tandem mass tag (TMT), stable isotope labelling by amino acids in cell culture (SILAC), or isobaric tags for relative and absolute quantitation (iTRAQ)) (448). Despite these advantages, label-free methods are less quantitative and precise as they only permit relative quantification of protein expression rather than absolute quantification. Thus, akin to RNA-Seq, I could only quantify protein expression by comparing it to that of another protein (i.e. a different ZIKV protein) or the same protein in a different condition (i.e. mock versus infected). I employed bottom-up proteomics as it is a high-throughput method that is highly sensitive and is currently the gold standard for discovery proteomic research. A limitation is its reliance on protein tryptic digestion to produce peptides with certain sizes and mass-to-charge ratios for detection by a mass spectrometer, which leads to a strong bias towards only detecting peptides with these properties (449). Consequently, these datasets possess a significant amount of missing data, as many small and lowly expressed proteins do not produce sufficient unique peptides for accurate detection (450). New proteomics approaches, such as Olink's proximity extension assay (PEA) technology, address many of these limitations of bottom-up mass spectrometry proteomics. PEA directly detects and quantifies intact proteins by coupling antibody recognition of the protein target to oligonucleotide hybridisation, polymerisation, and next-generation sequencing (451). This technology is currently limited to the quantification of up to 5,400 proteins, so it is not optimal for discovery research (452). However, its sensitivity is far superior to that of traditional mass spectrometry proteomics, thus allowing better detection of small and lowly expressed proteins.

In **Chapter 4**, I performed mass spectrometry immunopeptidomics, as it is currently the only high-throughput discovery approach to identify and investigate HLA presentation on human cells (453). The discovery of novel immunopeptides through de novo sequencing is a key strength of this technique, and I utilised this to identify twelve novel ZIKV peptides. Additionally, a comprehensive suite of peptide analysis tools has been developed by the Immune Epitope Database (IEDB) to provide significant insight into peptide biology and function (428). Utilising these well-established analysis tools, I identified immunogenic peptides of interest for future functional validation. A main limitation of immunopeptidomics is that the peptides I have identified are solely dependent on the HLA alleles expressed by USP7 cells. This limits the generalisability of my results as there are over 35 thousand human HLA alleles (427). Additionally, immunopeptidomics requires significant amounts of starting material (108 cells), which is a barrier to those who use models which cannot generate this large amount of material (i.e. neuroscientists culturing neurons).

5.7 Recommended future directions of the oZIKV research field

The oZIKV research field has grown significantly since Zhu et al. and Kaid et al. first demonstrated oZIKV infection of adult and paediatric brain tumours, respectively, with over 50 publications and a limited number of patents (243,249). Recently, Nemours Children's Health secured a \$7,000,000 grant from the Pass It On To Kids Foundation. This is the most significant development in the oZIKV research field to date as it aims to progress oZIKV therapy towards a Phase I clinical trial for the treatment of neuroblastoma and ovarian cancer. The production of clinical-grade ZIKV is a fundamental step towards its application in clinical trials and has been achieved for some ZIKV strains. ZIKV strains SJRP/2016-184 and Nicaragua/2016 were produced to be cGMP compliant and used in a recent Phase I clinical trial (NCT05123222) (245). ZIKV BeH819966, which I primarily used in my research, has been produced to be cGMP compliant by the Clean Cells laboratory (France) during the production of a ZIKV master bank. The progression of oZIKV therapy into and through clinical trials is, however, dependent on numerous other factors. In this section, I will discuss and make recommendations for the following: (i) continued pre-clinical research to further elucidate the therapeutic potential of oZIKV, (ii) pre-clinical research into the anti-tumoural immune response, (iii) establishment of administration routes, (iv) establishment of dosing protocols, and (v) criteria for patient inclusion or exclusion.

(i) To date, pre-clinical research into oZIKV infection has demonstrated therapeutic potential against a variety of nervous system tumours, including glioma, medulloblastoma, DMG, ATRT, neuroblastoma, ependymoma, and meningioma (249–251,262,264). The future application of oZIKV therapy will likely differ across these different tumour types. However, there is a current lack of understanding regarding the similarities and differences in the responses of these varying tumour types to oZIKV infection. As such, oZIKV research moving forward must incorporate a wider array of these tumour cell types into the same study to allow these similarities and differences to be investigated. One of the landmark studies in this research field briefly achieved this broad scope by investigating ZIKV infection of glioma, DMG, medulloblastoma, ependymoma and meningioma before conducting in-depth research into glioma (250). Additionally, research should prioritise using models that represent molecular subgroups within each tumour type that correlate with the worst treatment and survival outcomes. Key examples of these are non-WNT/SHH medulloblastoma (Group 3 and 4) and high-risk neuroblastoma.

- (ii) The oZIKV anti-tumoural immune response is partly known for adult glioma, but completely unknown for childhood nervous system tumours (264,266,271,277). The main hurdles to investigating the oZIKV anti-tumoural immune response in paediatric oncology are (i) the rarity of patient samples for *ex vivo* infection and (ii) the establishment of appropriate *in vivo* paediatric cancer models. Whilst the former is challenging to address, intense research into the latter should, in time, establish appropriate ZIKV-susceptible immunocompetent mouse models of medulloblastoma, ATRT and neuroblastoma. Potential medulloblastoma and neuroblastoma mouse models exist, such as those employed to study oncolytic measles and herpes simplex viral infections; however, their susceptibility to oZIKV infection should first be established (331,454,455). This is critical work as the anti-tumoural immune response commonly presents as the primary mechanism through which an OV therapy is efficacious. Additionally, the immunogenic nature of oZIKV therapy is important to delineate because whilst a certain degree of immunogenicity will promote an anti-tumoural immune response, a highly immunogenic OV may hamper efficacy by yielding a dominant antiviral immune response (432).
- (iii) ZIKV administration routes and dosing approaches should initially be based on preclinical oZIKV data, administration routes employed for other OVs, results from controlled human infection model (CHIM) studies, and the tumour type to be treated. Surgical resection of operable tumours allows for a single dose of oZIKV to be administered to the resected cavity. Multiple peri-tumoural doses for brain tumour patients are ill-advised as this induces brain damage and reduces survival in paediatric brain tumour-bearing xenograft mouse models (256). Systemic ZIKV administration, however, is viable and safe in these models (256). Additionally, multiple intrathecal doses of ZIKV were beneficial to canines bearing naturally occurring brain tumours and did not damage central nervous system (CNS) tissues (264). Treatment strategies for non-CNS tumours which are more accessible, such as neuroblastoma, will likely differ from that of CNS tumours. Future work must prioritise primary tumour cells and samples, as they are significantly underrepresented in current neuroblastoma oZIKV research. In summary, systemic Asian ZIKV administration is the favoured CNS tumour treatment due to their inaccessibility, its neurotropism, and its ability to treat metastasis. However, both Asian and African ZIKV lineages have unique advantages for neuroblastoma treatment.
- (iv) In a recent Phase I clinical trial of the first ZIKV CHIM, a single subcutaneous dose of 1x10² PFU of cGMP-compliant ZIKV proved efficient for productive infection in healthy adult human females with minimal side effects (NCT05123222) (245). The next stages of this trial have commenced, focusing on the infection of healthy human males. This trial considered a dose escalation of up to 1x10⁴ PFU to be considered safe, and this trial will likely inform the initial

systemic administration and dosing approaches for human cancer patients. However, it is important to note that a significantly greater dose of 1x10⁶ PFU proved safe and efficacious for intrathecal administration to canines with naturally occurring brain tumours (264). A greater dose of 1x10⁷ PFU was followed by cerebral leukoencephalopathy in one canine, possibly indicating a maximum tolerated dose between 1x10⁶ and 1x10⁷ PFU for canines. This ZIKV-induced canine cerebral leukoencephalopathy was treated and managed by the administration of corticosteroid anti-inflammatory drugs (264). As human cancer patients can present with compromised immune systems, there may be significant inter-patient variability in the optimal oZIKV dose required. As ZIKV can induce a strong cytokine response, we must identify anti-inflammatory drugs that can effectively manage any acute adverse effects of ZIKV infection in response to overdosing or excessive viral replication.

(v) The patient eligibility criteria for oZIKV therapy that I can recommend pertain to patient age. Radiotherapy is commonly omitted from treatment regimens for paediatric medulloblastoma and ATRT patients under three years old due to their underdeveloped nature and their high propensity to develop late effects (28,29,44). ZIKV infection during early infancy results in neurodevelopmental and behavioural complications in 15% of cases (237). As such, future oZIKV therapy should likely be withheld during these earlier years of life to allow for the crucial and dynamic neurodevelopmental stages to occur unperturbed. However, this is likely to be context dependent. For example, the risk of a replication-incompetent African oZIKV therapy affecting neurodevelopment in a young neuroblastoma patient whose primary tumour has not metastasised is low if intratumoural administration is used.

5.8 Concluding remarks

My research has significantly contributed to the ZIKV research field. Taking primarily an *in silico* and computational-based approach, I have conducted the first systematic study to define the molecular mechanisms involved in the infection of multiple paediatric nervous system tumour cells and clinically relevant NPCs. I have created multiple large data and omics datasets (bulk transcriptome, global proteome, immunopeptidome, and secretome), which are pertinent as they arise from cell types currently grossly underrepresented in this research field. My integration of these datasets with publicly available datasets and resources (bulk transcriptome, single cell transcriptome, interaction proteome, genome-wide CRISPR-Cas9 screens, patient survival data, and Immune Dictionary) has led to novel findings and shed significant insight into both neuropathogenic and oncolytic ZIKV infection. Principal findings and original contributions of my research to the field include (i) mapping the neuroblastoma cell

ZIKV life cycle, (ii) implicating the TNF signalling pathway across multiple nervous system tumour cell types and in brain tumour cell oncolysis, (iii) identifying a diverse and clinically relevant pro-inflammatory ZIKV-induced brain tumour cell secretome, (iv) modelling paracrine and endocrine signalling responses to the ZIKV-induced secretome, and (v) identifying brain tumour HLA-I presented ZIKV epitopes that are primarily derived from the immunogenic epitope rich ZIKV NS3 helicase. The research I have performed during my PhD candidature collectively supports the clinical utility of oZIKV therapy for treating nervous system tumours and contributes to the growing body of scientific knowledge that will ultimately pave the way towards clinical trials.

5.9 Achievements and additional research contributions

During my PhD, I have written three manuscripts as the primary author: one published in F1000 Research (**Chapter 2**) (362), one published in Scientific Reports (**Chapter 3**) (456), and one published in PLOS One (**Chapter 4**) (457). In addition, I am the second author of a manuscript published in FEBS Letters (not included in this thesis) (458). I significantly contributed to the research of this manuscript by generating both global and interaction proteome mass spectrometry datasets of USP7, USP13, and DAOY brain tumour cells stably expressing either L1TD1-GFP or GFP, and I extensively edited the manuscript written by Thiago Mitsugi. Early research during my PhD (**Chapter 2**) led to the establishment of an adjacent PhD project, which I helped design and have directly contributed to in the form of an interaction proteome mass spectrometry dataset and a limited number of functional *in vitro* assays.

Since starting my PhD, I have helped establish or nurture three collaborations for the Ewing Lab: an inter-faculty collaboration with Juliet Gray (Centre for Cancer Immunology, UoS), a national collaboration with Kevin Maringer (TPI), and an international collaboration with Keith Okamoto (The Human Genome and Stem Cell Research Center, USP). My significant contribution towards building these collaborations was recognised through being awarded the Doctoral College Directors Award solely for this work. I have been successful in securing the Global Partnerships Award as the sole applicant (£5,000) and have significantly contributed to two other successful research grant applications (totalling approximately £40,000).

Appendix A Chapter 2 supplementary material

Supplementary Table 2. 1. ZIKV infection is dependent on multiple host factors.

	-		_		_		_	
SK-N-BE2	G	sc	hiPSO	C-NPC	HEK2	93FT	Не	La
ATP6V0C	AKR1B10	MORF4L1	ANKAR	FBXL21	ALDH1L2	NR6A1	ABI2	МАРКАРК3
BSG	AKT1	MROH2B	AP2B1	FBXO45	AQP5	ORC4	AGAP1	MEN1
CALML5	ANKRD54	MRPS14	ARMCX3	FTH1P18	ARTN	P2RX7	ARF3	MMGT1
CEND1	ANXA2R	MSANTD3	ASCC3	HECTD4	ATP5F1	PADI1	ARHGEF6	MPI
CHP1	ARHGEF10L	MTRNR2L2	ATF4	HS6ST1	ATP6V0C	PBRM1	ATP6AP2	NEK2
CLN6	ARHGEF40	MYO18A	ATP6AP1	HSPA5	AURKAIP1	PDILT	ATP6V0A1	NIPAL2
DOK3	ATG3	NIF3L1	ATP6AP2	IFT27	BAK1	PDZK1	AXL	NIT1
FXR1	ATP6V1G1	NKX1-1	ATP6V0B	ISG15	ВМР8В	PHIP	BET1	NPC2
GCOM1	BAALC	NMS	ATP6V0C	JAG2	C2orf16	PMPCA	BPY2	OR4K13
LARP7	C10orf35	NRSN1	ATP6V0D1	KIAA0040	CALCOCO2	POLR3C	BPY2B	OSTC
LMO7	C11orf52	NUDT19	ATP6V1A	KRTAP19-8	CERS1	PPARGC1B	C1ORF227	PER3
LMOD3	C14orf119	NUGGC	ATP6V1B2	MIDN	CLECL1	PPP2R3C	CCDC171	PLA2G16
LYAR	C16orf70	ODF3L1	ATP6V1C1	MMGT1	CNKSR1	PRAF2	СРО	PPP2R5A
MMGT1	C19orf57	OR10AG1	ATP6V1D	MSMO1	COMMD7	PRPS2	CT47A4	PRAC1
MSI1	C1orf116	OR10T2	ATP6V1E1	NBPF9	COPB2	PSMC3	CTTNBP2NL	RAB5C
PRAF2	C21orf91	OR5AS1	ATP6V1H	NDST1	COPS2	PSMD4	CXORF22	RABEP1
	1		J		1		I	

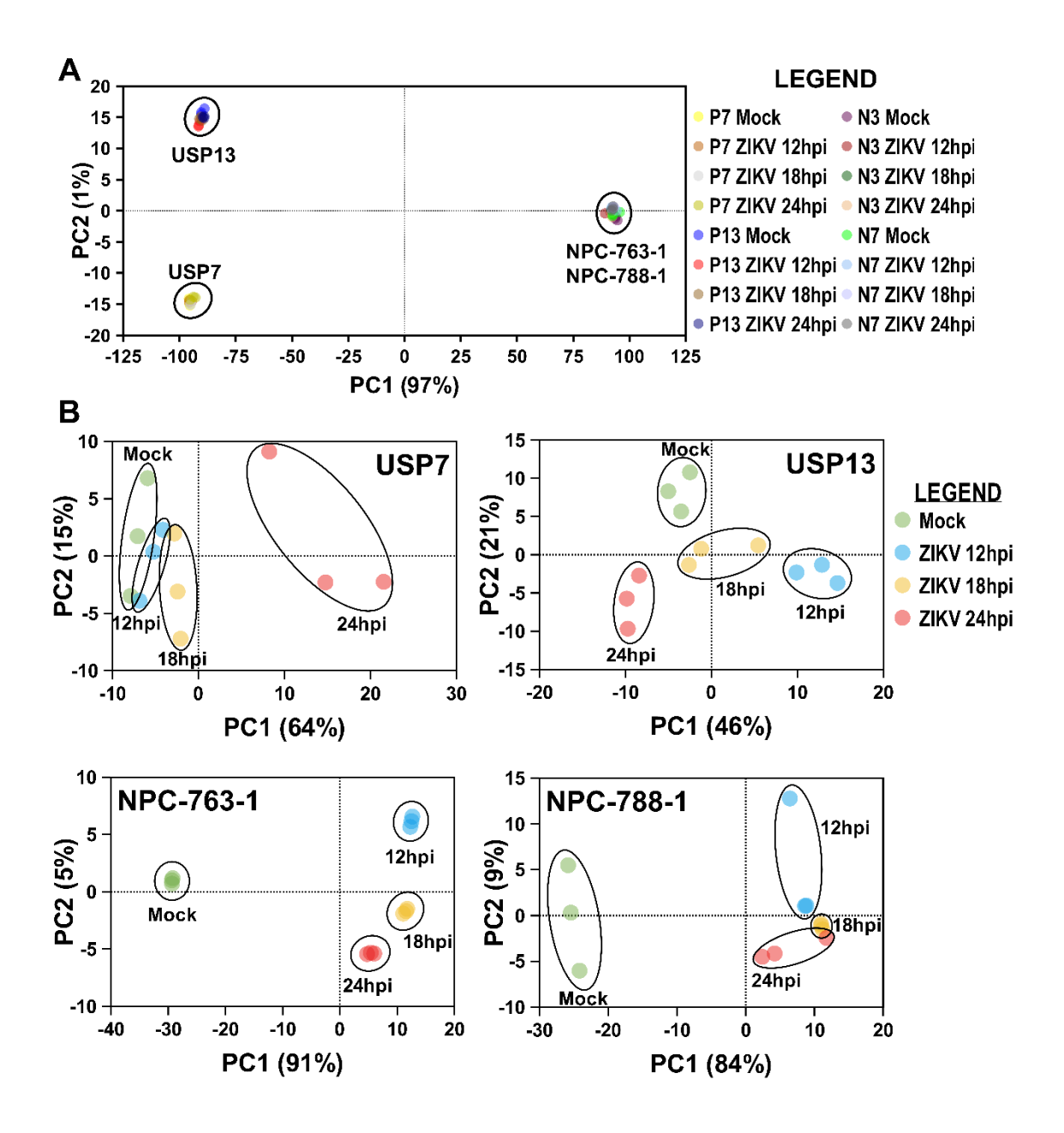
SK-N-BE2	G	SC	hiPSO	C-NPC	HEK2	93FT	Не	eLa
RRAGD	CENPH	OST4	ATP8B4	NGB	CTSF	PTPRT	DACT2	RABGEF1
STT3A	CFAP47	OXGR1	B3GALT6	NPVF	DNAJC24	RNF115	DCTPP1	RAI14
TMEM41B	CHD9	PARP9	B4GALT7	NUDT18	DNM2	RPL23	DPM1	RFX4
XIRP2	CLDN20	PLAC8L1	C14orf169	OS9	EDC4	RPL37A	E4F1	RTKN
YIPF4	CLSTN2	PLEKHM3	C3orf58	PAPSS1	EFCAB4B	RPP21	ECM2	SAA2
ZC3HAV1	CPVL	PPAN	CA4	PHPT1	EHHADH	RPS15A	EMC1	SH3GLB2
	CSDC2	PRB2	CD302	PLAC4	ELOVL7	RSL24D1	EMC2	SIPA1L3
	CSMD3	PRRT3	CKMT2	PRAC2	EMC1	SCGB1D1	EMC3	SLC9A3
	CYB561A3	PRY2	CLK2	PTPN2	EMC6	SCYL1	EMC4	SLCO4C1
	CYP26B1	QRICH1	COG1	RNASEK	EPHB3	SDAD1	EMC6	SND1
	DCDC5	RAB42	COG2	RYBP	ESM 1	SLC25A3	EMC7	SPATA31C
	DCP1B	RASSF3	COG3	SCARB1	FAM178A	SMPD4	EMC8	SPTBN2
	DCUN1D3	RHOU	COG4	SEL1L	FAM200B	SNRPB	EXT1	SSR2
	DERL2	RIMKLA	COG5	SLC22A20	FBXO4	SPATA16	EXTL3	SSR3
	DNAH7	RNF152	COG6	SLC28A3	FUNDC1	SPCS3	FAM179B	STARD10
	DNAJB8	SBK3	COG7	SLC35B2	FXR1	STOM	FAM43B	STMN4
	ELK3	SCAMP5	COG8	SLC39A9	GHRHR	SV2C	GAD1	STT3A
	EMC2	SIAH3	CSAG3	SOCS3	GK5	TBX2	GLP2R	TAF7L
	EMC3	SNX30	CTAG2	SPATA31C1	GNB2L1	TGFB3	GRIN3A	TGFBRAP
	EPHA10	SRGAP2B	DCAF7	SPATA8	HEATR1	THAP2	HDLBP	THUMPD2

SK-N-BE2	G	sc	hiPSO	C-NPC	HEK2	293FT	He	La
	FAM78A	SSR2	DDX3X	SPON1	IMPDH2	TMEM108	HEBP2	TMEM2
	FGFBP2	SSR3	DERL1	SPTLC1	IPO9	TMTC3	HHIP	TRAM1
	GABBR2	STK33	DERL2	SRPRB	IQGAP3	TRIM35	НІВСН	TRIM16
	GATA5	STRN3	DERL3	SSR1	LSM2	TRNT1	MIR-4429	TSNAX
	GCNT7	STT3A	DNAJB3	SSR2	LSM5	TROVE2	MIR-451A	TSPY2
	GJD2	SULT1C4	DNAJC10	SSR3	MATK	TSR2	MIR-451B	TSPY4
	GLTPD2	SV2A	EDDM3A	SSR4	MED6	TUBA1B	MIR-944	VCX2
	GNS	TET3	EDDM3B	STAT1	MIA	UBQLN1	HSF5	VPS45
	GPR33	THUMPD2	EDEM1	STAT2	MMGT1	WDR77	IFRD2	WDR7
	GPX6	TLR9	EDEM2	STAT3	MTA2	YWHAH	IQCB1	ZFYVE20
	GTF2F1	TMC7	EDEM3	STT3A	NKX2-8	ZNF584	ISG15	ZNF540
	IL17F	TMEM150B	EHMT2	SUDS3	NOL8	ZNF705D	KIAA1147	ZNF567
	IL27	TMEM176A	EIF2AK1	SYVN1	NPFF	ZNF845	KRTAP20-2	ZNF71
	IRGQ	TMEM41B	EIF2AK2	TM2D3	NR1H3	ZSWIM4	LRRC29	ZNF844
	ITGB5	TMPRSS11F	EIF2AK3	TM9SF2				
	KATNAL1	TNFAIP8L2	EIF2AK4	TMEM165				
	KIAA1522	TOR4A	EMC1	TMEM199				
	LACC1	TPT1	EMC10	TP53				
	LDLRAD1	TRAM1	EMC2	TXNRD3				
	LHX9	UBE2G2	EMC3	UBE2G2				

SK-N-BE2	G	sc	hiPSO	C-NPC	HEK293FT	HeLa
	LOXL2	UBE2J1	EMC4	UBE2J2		
	LRRC61	URAD	EMC6	UGDH		
	LY6K	USP43	EMC7	UHRF1		
	LYPD8	VIPAS39	EMC8	USP17L7		
	LYRM2	WFDC12	EMC9	UXS1		
	MAGEL2	WIPF3	ERLEC1	VMA21		
	MGAM	XYLT2	EXT1	WDR7		
	MMGT1	YDJC	EXT2	ZBED5		
	MORC2	ZNF805	EXTL3	ZNF761		

Lists of known ZIKV dependency factors across SK-N-BE2 (NB), GSC, hiPSC-NPC (NPC), HEK293FT and HeLa cells. Abbreviations, Zika virus (ZIKV), glioma stem cell (GSC), human induced pluripotent stem cell (hiPSC), neural precursor cell (NPC), neuroblastoma (NB).

Appendix B Chapter 3 supplementary material



Supplementary Figure 3. 1. PCA of ZIKV-infected RNA-Seq samples.

PCA plots of **(A)** all RNA-Seq samples together and **(B)** individual cell lines. Abbreviations, Zika virus (ZIKV), USP7 (P7), USP13 (P13), NPC-763-1 (N3), NPC-788-1 (N7), hours post-infection (hpi), Principal Component (PC).

Supplementary Table 3. 1. 49-plex ELISA of ZIKV-infected brain tumour cells.

-	ι	JSP7 Moc	k		USP7 ZIK\	<i>I</i>	U	SP13 Mod	k	ι	ISP13 ZIK	V
Protein	12 hpi	24 hpi	48 hpi	12 hpi	24 hpi	48 hpi	12 hpi	24 hpi	48 hpi	12 hpi	24 hpi	48 hpi
BTLA	Х			Х	Х		Х	Х		Х		
CD27	Х			Х			Х	Х	Х			
CD28	Х			Х	Х		Х	Х		Х	Х	
CD80	Х			Х			Х	Х		Х		
CD137 (TNFRSF9)	Х	Х	Χ	Х	Х	Х	Х	Х	Х	Х	Х	Х
CD152 (CTLA4)												
GITR	Х			Х			Х	Х		Х	Х	
HVEM	Х	Х		Х			Х	Х		Х	Х	
IDO	Х	Х		Х			Х			Х	Х	
LAG-3	Х	Х		Х			Х	Х		Х	Х	
PD-1	Х	Х		Х	Х		Х	Х		Х	Х	
PD-L1												
PD-L2	Х	Х	Х	Х	Х	Х	Х	Х	Х	Х	Х	Х
TIM-3								Х		Х		
Eotaxin (CCL11)		Х	Х	Х		Х	Х	Х	Х	Х	Х	Х
GM-CSF						Х	Х	Х	Х	Х	Х	Х
GRO alpha (CXCL1)	Х	Х	Х	Х	Х	Х	Х	Х	Х	Х	Х	Х
IFN alpha						Х	Х	Х	Х	Х	Х	Х
IFN gamma							Х	Х	Х	Х	Х	Х
IL-1 alpha						Х	Х	Х	Х	Х	Х	Х
IL-1 beta												Х

	ι	JSP7 Moc	k		USP7 ZIK\	1	u	SP13 Mod	k	ι	JSP13 ZIK	V
Protein	12 hpi	24 hpi	48 hpi	12 hpi	24 hpi	48 hpi	12 hpi	24 hpi	48 hpi	12 hpi	24 hpi	48 hpi
IL-1RA												Х
IL-2												Х
IL-4						Х	Х	Х	Х	Х	Х	Х
IL-5			Х			Х	Х	Х	Х	Х	Х	Х
IL-6	Х	Х	Х	Х	Х	Х	Х	Х	Х	Х	Х	Х
IL-7		Х	Х		Х	Х	Х	Х	Х	Х	Х	Х
IL-8 (CXCL8)	Х	Х	Х	Х	Х	Х	Х	Х	Х	Х	Х	Х
IL-9	Х	Х	Х	Х	Х	Х	Х	Х	Х	Х	Х	Х
IL-15							Х	Х	Х	Х	Х	Х
IL-18						Х	Х	Х	Х	Х	Х	Х
IL-21						Х	Х	Х	Х	Х	Х	Х
IL-22							Х	Х	Х	Х		Х
IL-23							Х	Х	Х	Х	Х	Х
IL-27								Х	Х			Х
IL-31							Х	Х	Х	Х	Х	Х
IP-10 (CXCL10)		Х	Х			Х	Х	Х	Х	Х	Х	Х
MCP-1 (CCL2)	Х	Х	Х	Х	Х	Х	Х	Х	Х	Х	Х	Х
MIP-1 alpha (CCL3)	Х	Х	Х	Х	Х	Х	Х	Х	Х	Х	Х	Х
MIP-1 beta (CCL4)	Х	Х	Х	Х	Х	Х	Х	Х	Х	Х	Х	Х
RANTES (CCL5)	Х	Х	Х	Х	Х	Х	Х	Х	Х	Х	Х	Х
SDF-1 alpha (CXCL12)	Х	Х	Х		х	Х	х	Х	Х	Х	х	Х

	l	USP7 Mock			USP7 ZIK\	/	USP13 Mock			USP13 ZIKV		
Protein	12 hpi	24 hpi	48 hpi	12 hpi	24 hpi	48 hpi	12 hpi	24 hpi	48 hpi	12 hpi	24 hpi	48 hpi
TNF alpha	Х	Х	Х	Х	Х	Х	Х	Х	Х	Х	Х	Х
TNF beta							Х	Х	Х	Х	Х	Х
IL-10												
IL-12p70												
IL-13												
IL-17A (CTLA-8)												
TNFSF9			Х	Х		Х	Х	Х	Х	Х	Х	Х

X denotes if the given protein was detected in the given condition. Abbreviations, Zika virus (ZIKV), hours post-infection (hpi).

Supplementary Table 3. 2. T cell polarisation states following cytokine-immune cell interaction and top-upregulated DEGs.

Cell type		CD4+	T Cell			CD8+	T Cell	
Polarisation State	T4-a	Т4-с	T4-c	T4-f	Т8-а	Т8-с	Т8-с	T8-f
Cytokine	IFN alpha	IL-1 alpha	IL-1 beta	IL-4	IFN alpha	IL-1 alpha	IL-1 beta	IL-4
Top DEG	Isg15	Ly6a	Ly6a	H2-DMa	lsg15	lgfbp4	lgfbp4	H2-DMa
2nd DEG	ifit3	lgfbp4	lgfbp4	Bcl2	Bst2	Ly6a	Ly6a	Plac8
3rd DEG	Bst2	Socs3	Socs3	Il4ra	ifit3	Socs3	Socs3	Bcl2
4th DEG	lsg20	Ndrg3	Ndrg3	Socs1	lsg20	Gadd45g	Apobec3	Il4ra
5th DEG	Slfn5	lfngr1	Arid5b	Cnp	Slfn5	lfngr1	lfngr1	Ppa1
6th DEG	ifitm3	Arid5b	lfngr1	Foxn3	ifit1	Apobec3	Gzmb	Phgdh
7th DEG	ifit1	Bcl3	Apobec3	Eno1	Ifi27l2a	Socs1	Gadd45g	Socs1
8th DEG	Ifi27l2a	Socs1	Bcl3	Glipr2	Plac8	Plac8	Socs1	Dusp10
9th DEG	Ly6a	Apobec3	Socs1	Trat1	Ly6a	Fam241a	Bcl3	Cd8a
10th DEG	Phf11b	Stat3	Mxd1	Dusp10	Phf11b	Arid5b	Arid5b	Ncl
11th DEG	Rsad2	Arid5a	Stat3	Phgdh	Zbp1	Arid5a	Stat3	Eif5a
12th DEG	Samhd1	Mxd1	Ly6e	Eif2s2	Samhd1	Bcl3	Plac8	Eif2s2
13th DEG	Zbp1	Ly6e	Ssh2	lgfbp4	Usp18	Gzmb	Ssh2	Eno1
14th DEG	Usp18	Cdkn2d	Sbno2	Jund	Ppa1	Stat3	Gzma	Nop56
15th DEG	ligp1	Gbp2	Tcf7	Lyst	Rnf213	Ppa1	Tcf7	Mbd2
16th DEG	Gbp2	Zbp1	Rapgef6	Nop56	Irf7	Zbp1	Arid5a	Pa2g4

Cell type		CD4+	T Cell		CD8+ T Cell						
Polarisation State	T4-a	Т4-с	T4-c	T4-f	Т8-а	Т8-с	Т8-с	T8-f			
Cytokine	IFN alpha	IL-1 alpha	IL-1 beta	IL-4	IFN alpha	IL-1 alpha	IL-1 beta	IL-4			
17th DEG	Irf7	Nfkbia	Il21r	Mbd2	lfi209	Gpr18	Satb1	Cycs			
18th DEG	Rnf213	Myl12b	Gbp2	Gm47283	Rsad2	Sbno2	Ndrg3	Nme1			
19th DEG	Ifi203	Gadd45g	Gadd45g	Ррр3сс	ifitm3	Satb1	Rapgef6	C1qbp			
20th DEG	ifit3b	Cd53	Arid5a	Ppa1	Ifi203	Cdkn2d	Fam241a	Ppp1r14b			

The top 20 upregulated mouse DEGs were sourced from the Immune Dictionary for each cytokine-immune cell interaction. Abbreviations, Zika virus (ZIKV), differentially expressed gene (DEG), CD4+ T Cell (T4), CD8+ T Cell (T8).

Supplementary Table 3. 3. Dendritic Cell polarisation states following cytokine-immune cell interaction and top-upregulated DEGs.

Cell type			cDC1				cDC2	
Polarisation State	cDC1-a	cDC1-c	cDC1-c	cDC1-d	cDC1-e	cDC2-a	cDC2-c	cDC2-c
Cytokine	IFN alpha	IL-1 alpha	IL-1 beta	TNF-alpha	GM-CSF	IFN alpha	IL-1 beta	TNF-alpha
Top DEG	lsg15	Ccl17	Serpina3g	Apol7c	Ccl17	Cxcl9	Ccl17	Fabp5
2nd DEG	Cxcl9	Wfdc17	Ccl17	Cxcl9	Itgae	lsg15	Fabp5	Ccl17
3rd DEG	Irf7	Serpina3g	Wfdc17	Basp1	Pfkp	Irf7	AA467197	Ccl22
4th DEG	ifitm3	ifitm2	Mkrn1	Marcksl1	Bcl2a1a	Cxcl10	Ms4a6d	AA467197
5th DEG	Slfn5	Mt1	Ifi205	Bcl2a1b	Bcl2a1d	ifit3	Ccnd2	Il4i1
6th DEG	lsg20	Ifi205	Kmo	Traf1	Cd207	Ifi204	ld2	Marcksl1
7th DEG	Serpina3g	Mkrn1	lgfbp4	ifitm2	Prkcd	lsg20	Ptpn1	Slc7a11
8th DEG	lfi204	Cytip	ifitm2	Serpina3g	Cdkn1a	Pnp	Cytip	Tspan3
9th DEG	Zbp1	Ptpn1	Cdk2ap2	Nabp1	Snx3	Phf11b	Xbp1	Cdkn1a
10th DEG	Pnp	Rap2a	Mt1	Nfkbia	Kmo	Rsad2	H2afx	Tnfaip2
11th DEG	Sct	Socs3	Pfkp	Cdkn1a	Bcl2a1b	Slfn5	Socs3	Nrp2
12th DEG	Phf11b	Fh1	Ptpn1	Cxcl16	Gnb4	ifitm3	Ube2s	ll1rn
13th DEG	Ifi205	Xbp1	Gnb4	Ccr7	Irf5	Bst2	Mt1	Clec4n
14th DEG	Ms4a4c	Slfn2	Irf5	Bcl2a1d	Denr	Mndal	Top2a	Cd63
15th DEG	Mndal	Tnfrsf13b	Ccnd3	Ccnd2	Lims1	ifit1	lgfbp4	Clec4e
16th DEG	Tspo	Fth1	Picalm	Dusp2	Ppp1r14b	Ms4a4c	Tuba1b	Bhlhe40

Cell type			cDC1				cDC2	
Polarisation State	cDC1-a	cDC1-c	cDC1-c	cDC1-d	cDC1-e	cDC2-a	cDC2-c	cDC2-c
Cytokine	IFN alpha	IL-1 alpha	IL-1 beta	TNF-alpha	GM-CSF	IFN alpha	IL-1 beta	TNF-alpha
17th DEG	Slfn2	Fabp5	Slfn2	Ncoa7	Lgals3	Zbp1	Srp9	ld2
18th DEG	lfi47	Wnk1	Tle3	Mkrn1	Naaa	Oasl2	Clec4n	Bcl2a1d
19th DEG	Usp18	Cdkn1a	Xbp1	Dnase1l3	Cst3	lfi47	Dok2	Malt1
20th DEG	Samhd1	Pfkp	Fkbp5	Serpinb9	Ifi205	Gbp2	Birc5	Fscn1

The top 20 upregulated mouse DEGs were sourced from the Immune Dictionary for each cytokine-immune cell interaction. Abbreviations, Zika virus (ZIKV), differentially expressed gene (DEG), conventional dendritic cell type 1 (cDC1), conventional dendritic cell type 2 (cDC2).

Supplementary Table 3. 4. Macrophage and Neutrophil polarisation states following cytokine-immune cell interaction and top-upregulated DEGs.

Cell type			Macrophage				Neut	rophil	
Polarisation State	Мас-а	Мас-с	Мас-с	Mac-d	Мас-е	Neu-c	Neu-c	Neu-d	Neu-e
Cytokine	IFN alpha	IL-1 alpha	IL-1 beta	TNF-alpha	IL-4	IL-1 alpha	IL-1 beta	TNF-alpha	GM-CSF
Top DEG	Cxcl10	Ccl9	Ccl9	Saa3	Ccl7	Cxcl3	Cxcl3	Sod2	Ffar2
2nd DEG	Ccl12	Ccl12	Ccl12	Ccl9	Ccl2	Gm5483	Wfdc17	Lcn2	Gm5483
3rd DEG	lsg15	Ccl7	Ccl7	Cxcl13	Ccl12	Fcgr2b	Gm5483	Cxcl10	Fcgr2b
4th DEG	Cxcl9	Ccl6	Wfdc17	Marcksl1	Chchd10	Wfdc17	ifitm6	Chil1	Cish
5th DEG	Rsad2	Ccl2	Sdc4	Sod2	Glrx	Xbp1	Lcn2	Cd14	Xbp1
6th DEG	Serpina3g	Wfdc17	Ccl6	Wfdc17	Serpina3g	Cish	Thbs1	Prdx5	Cd177
7th DEG	Irf7	Sdc4	Cd209e	Ccl12	Hmox1	Rnasel	Rnasel	Bcl2a1a	Tarm1
8th DEG	ifit2	Mt1	Mt1	Mt1	Nabp1	Cd14	Cd177	Wfdc21	Pnp
9th DEG	Pnp	Dab2	Ccl2	Bcl2a1b	Dab2	Il1r2	Il1r2	Cybb	ll1r2
10th DEG	Cmpk2	Serpina3g	Dab2	Sdc4	Cd209e	Plaur	Xbp1	AA467197	Car4
11th DEG	ifit3	Ptpn1	Ccl24	Il1rn	Mrc1	ifitm6	Spp1	Marcksl1	Basp1
12th DEG	Ccl7	Cd209e	Clec4n	Clec4e	Sdc4	Ffar2	ld1	lcam1	Bcl2a1a
13th DEG	ligp1	Fabp5	Mt2	Ehd1	Snx2	Cd177	Cd14	Ccl3	Upp1
14th DEG	lfi204	Ccl17	Serpina3g	Clic4	Ap2m1	Thbs1	ler3	Ccl4	Bcl2a1d
15th DEG	Ccl2	Ccl24	Ptpn1	Fscn1	Srm	Ccl4	Plaur	Ehd1	Hbegf
16th DEG	Ifi205	Xbp1	Mrc1	Mt2	Retnla	Lcn2	Tarm1	Bcl2a1b	Naaa

Cell type			Macrophage)	Neutrophil				
Polarisation State	Мас-а	Мас-с	Мас-с	Mac-d	Мас-е	Neu-c	Neu-c	Neu-d	Neu-e
Cytokine	IFN alpha	IL-1 alpha	IL-1 beta	TNF-alpha	IL-4	IL-1 alpha	IL-1 beta	TNF-alpha	GM-CSF
17th DEG	AW112010	Mafb	Fcgr2b	Atp6v1b2	Ncl	Tarm1	Wfdc21	Fpr2	Cd24a
18th DEG	lfih1	Clec4n	Fabp5	Procr	Cebpd	ler3	Fcgr2b	N4bp1	Gm14005
19th DEG	lfi47	Jaml	Xbp1	Clec4n	Srsf9	Tes	Basp1	Dusp16	Rab44
20th DEG	ifit1	Fcgr2b	Lgmn	Il4i1	Cd209d	ld1	Ccl6	Ikbke	Glipr2

The top 20 upregulated mouse DEGs were sourced from the Immune Dictionary for each cytokine-immune cell interaction. Abbreviations, Zika virus (ZIKV), differentially expressed gene (DEG), Macrophage (Mac), Neutrophil (Neu).

Appendix B

Supplementary Table 3. 5. Monocyte and NK Cell polarisation states following cytokine-immune cell interaction and top-upregulated DEGs.

					ĺ			
Cell type			Monocyte	NK Cell				
Polarisation State	Mono-a	Mono-c	Mono-c	Mono-d	Mono-e	NK-a	NK-c	NK-c
Cytokine	IFN alpha	IL-1 alpha	IL-1 beta	TNF-alpha	GM-CSF	IFN alpha	IL-1 alpha	IL-1 beta
Top DEG	Cxcl10	Ccl24	Fabp5	Saa3	Fabp5	Gzmb	lfngr1	lfngr1
2nd DEG	lsg15	Fabp5	Sdc4	Sod2	Naaa	lsg15	Bcl2l11	Crem
3rd DEG	Rsad2	Sdc4	Ccl24	Bcl2a1b	Clec4n	Bst2	Vps37b	Sh2d2a
4th DEG	Phf11b	Dab2	Saa3	Marcksl1	Vcan	Cxcl10	Crem	Serpinb6b
5th DEG	lsg20	Thbs1	Dab2	Slpi	Pilra	Ccl4	Odc1	Gzmc
6th DEG	ifit1	Bcl2a1b	Thbs1	Bcl2a1d	Cish	Ifi204	Hvcn1	Vps37b
7th DEG	ifit3	Srgn	Dmkn	Clec4e	Dok2	ifitm3	Sh2d2a	Klrb1b
8th DEG	Fcgr1	Ccl2	Srgn	Ehd1	Bcl2a1b	Zbp1	Fam107b	Bcl2l11
9th DEG	Pnp	Ccr1	Vcan	Fth1	Bcl2a1d	Ccl3	Serpinb6b	Txnip
10th DEG	Irf7	Ms4a6d	Ms4a6d	Sdc4	Sdc4	Xcl1	Litaf	Hvcn1
11th DEG	Gbp2	Mafb	Ccr1	Fpr2	Chil3	Phf11b	Klrb1b	Stat3
12th DEG	lfi209	Jaml	Jaml	Bcl2a1a	Batf3	ifit3	Dgat1	Gzmb
13th DEG	ifit2	C5ar1	Mafb	Il1rn	H2-DMa	lsg20	Plac8	Tsc22d3
14th DEG	Phf11d	Lgmn	Clec4n	AA467197	Dab2	Usp18	Serpina3g	Epb41
15th DEG	Usp18	Vcan	Adam8	Mmp14	Ppp1r14b	Gadd45g	Irf8	Serinc3
16th DEG	lfi47	Dmkn	Lcn2	Plek	Cd24a	Ppa1	Txnip	Gimap3

Cell type			Monocyte	NK Cell				
Polarisation State	Mono-a	Mono-c	Mono-c	Mono-d	Mono-e	NK-a	NK-c	NK-c
Cytokine	IFN alpha	IL-1 alpha	IL-1 beta	TNF-alpha	GM-CSF	IFN alpha	IL-1 alpha	IL-1 beta
17th DEG	Oasl1	Tfec	Spp1	Gpr84	Reep3	Rnf213	Serpinb9	Fryl
18th DEG	Ube2l6	Adam8	Ccl2	Ptges	Bcl2a1a	Ifng	Dennd4a	Irf8
19th DEG	Fgl2	Ccl7	Bcl2a1b	Tnip1	Ccl24	Trim30a	Celf2	Celf2
20th DEG	Cd69	F10	Msr1	Clec4n	Dmkn	ifit1	Tsc22d3	Irak2

The top 20 upregulated mouse DEGs were sourced from the Immune Dictionary for each cytokine-immune cell interaction. Abbreviations, Zika virus (ZIKV), differentially expressed gene (DEG), Monocyte (Mono), Natural Killer (NK).

Appendix C Chapter 4 supplementary material

Supplementary Table 4. 1. Top-ranked proteins from ZIKV-infected USP7 global proteome.

Rank	Name	Mock 1	Mock 2	Mock 3	ZIKV 1	ZIKV 2	ZIKV 3
Тор	H2BC3	19.500	20.680	18.891	28.563	28.782	28.612
2nd	ZIKV	19.465	19.993	18.946	28.993	28.196	27.798
3rd	OS9	19.358	20.251	19.847	26.916	26.167	26.074
4th	UGGT1	19.821	20.119	19.865	25.787	25.555	26.158
5th	RSU1	19.190	20.604	20.404	26.093	25.045	25.702
6th	PSMB5	19.739	19.964	19.629	25.360	25.176	25.125
7th	NDUFS2	19.392	20.496	19.946	24.312	25.008	25.637
8th	H3-3A	19.743	19.794	29.236	29.157	29.569	29.006
9th	COG2	19.386	19.892	27.307	27.454	27.590	27.759
10th	SFPQ	19.389	19.117	26.850	26.817	26.930	27.246
11th	IPO11	19.510	20.774	19.854	25.548	24.080	24.766
12th	ARFGAP1	19.855	20.045	19.279	24.378	24.280	24.317
13th	NUCKS1	18.858	18.806	20.456	23.537	24.095	23.710
14th	AGK	19.724	20.013	20.439	23.495	24.407	25.262
15th	NCAPD2	24.168	18.314	19.517	24.858	25.015	25.465
16th	NCK1	19.058	18.830	20.228	23.560	23.663	23.254
17th	CAPN1	19.961	26.356	19.829	26.919	26.342	26.541
18th	PSMD1	19.726	19.415	26.381	26.761	26.059	26.208
19th	HUWE1	19.243	19.865	24.612	25.497	25.041	26.283
20th	CRYZ	20.568	20.315	19.294	20.148	26.409	25.854
21st	SEC61G	19.271	19.585	19.832	23.542	23.285	23.732
22nd	FASN	19.871	20.564	27.074	27.060	27.101	26.780
23rd	RNF213	19.733	19.749	20.123	23.675	23.780	23.812
24th	TMEM167A	19.928	18.585	20.063	22.996	23.312	23.453
25th	CCT7	21.756	23.086	29.669	29.455	28.905	30.232
26th	RTTN	19.864	19.768	25.245	25.210	26.267	25.462
27th	NGDN	21.094	19.622	19.192	23.998	23.826	22.955
28th	LMAN2L	19.855	20.313	19.603	22.803	23.550	24.005
29th	RAD23A	19.793	19.254	24.848	25.531	24.800	24.867
30th	FAH	19.541	20.058	25.565	25.603	25.173	25.742

The top 30 GSEA-ranked proteins with Log2(LFQ intensities) reported for each replicate of Mock and 24-hour ZIKV-infected USP7 global proteome. Abbreviations, Zika virus (ZIKV).

- Wu Y, Deng Y, Wei B, Xiang D, Hu J, Zhao P, et al. Global, regional, and national childhood cancer burden, 1990–2019: An analysis based on the Global Burden of Disease Study 2019. J Adv Res. 2022 June 11;40:233–47.
- Atun R, Bhakta N, Denburg A, Frazier AL, Friedrich P, Gupta S, et al. Sustainable care for children with cancer: a *Lancet Oncology* Commission. The Lancet Oncology. 2020 Apr 1;21(4):e185–224.
- World Health Organization. Assessing national capacity for the prevention and control of noncommunicable diseases: report of the 2019 global survey [Internet]. World Health Organization; 2020 [cited 2023 May 23]. ix, 101 p. Available from: https://apps.who.int/iris/handle/10665/331452
- Huang J, Chan SC, Ngai CH, Lok V, Zhang L, Lucero-Prisno III DE, et al. Global incidence, mortality and temporal trends of cancer in children: A joinpoint regression analysis.
 Cancer Medicine. 2023;12(2):1903–11.
- 5. Bhakta N, Force LM, Allemani C, Atun R, Bray F, Coleman MP, et al. Childhood cancer burden: a review of global estimates. The Lancet Oncology. 2019 Jan 1;20(1):e42–53.
- Gröbner SN, Worst BC, Weischenfeldt J, Buchhalter I, Kleinheinz K, Rudneva VA, et al. The landscape of genomic alterations across childhood cancers. Nature. 2018 Mar;555(7696):321–7.
- 7. Coorens THH, Behjati S. Tracing and Targeting the Origins of Childhood Cancer. Annual Review of Cancer Biology. 2022 Apr 11;6(Volume 6, 2022):35–47.
- 8. Ricci AM, Emeny RT, Bagley PJ, Blunt HB, Butow ME, Morgan A, et al. Causes of Childhood Cancer: A Review of the Recent Literature: Part I—Childhood Factors. Cancers (Basel). 2024 Mar 27;16(7):1297.
- 9. Pfister SM, Reyes-Múgica M, Chan JKC, Hasle H, Lazar AJ, Rossi S, et al. A Summary of the Inaugural WHO Classification of Pediatric Tumors: Transitioning from the Optical into the Molecular Era. Cancer Discov. 2022 Feb 2;12(2):331–55.

- Johnsen JI, Dyberg C, Wickström M. Neuroblastoma—A Neural Crest Derived Embryonal Malignancy. Frontiers in Molecular Neuroscience. 2019;12:9.
- 11. Pollack IF, Agnihotri S, Broniscer A. Childhood brain tumors: current management, biological insights, and future directions. J Neurosurg Pediatr. 2019 Mar 1;23(3):261–73.
- 12. Shih RY, Koeller KK. Embryonal Tumors of the Central Nervous System: From the Radiologic Pathology Archives. Radiographics. 2018 Apr;38(2):525–41.
- 13. d'Amati A, Bargiacchi L, Rossi S, Carai A, Bertero L, Barresi V, et al. Pediatric CNS tumors and 2021 WHO classification: what do oncologists need from pathologists? Front Mol Neurosci [Internet]. 2024 Mar 13 [cited 2024 June 27];17. Available from: https://www.frontiersin.org/journals/molecular-neuroscience/articles/10.3389/fnmol.2024.1268038/full
- 14. Funakoshi Y, Sugihara Y, Uneda A, Nakashima T, Suzuki H. Recent advances in the molecular understanding of medulloblastoma. Cancer Sci. 2022 Dec 25;114(3):741–9.
- Jessa S, Blanchet-Cohen A, Krug B, Vladoiu M, Coutelier M, Faury D, et al. Stalled developmental programs at the root of pediatric brain tumors. Nat Genet. 2019 Dec;51(12):1702–13.
- Gibson P, Tong Y, Robinson G, Thompson MC, Currle DS, Eden C, et al. Subtypes of medulloblastoma have distinct developmental origins. Nature. 2010 Dec 23;468(7327):1095–9.
- 17. Cavalli FMG, Remke M, Rampasek L, Peacock J, Shih DJH, Luu B, et al. Intertumoral Heterogeneity within Medulloblastoma Subgroups. Cancer Cell. 2017 June 12;31(6):737-754.e6.
- Northcott PA, Buchhalter I, Morrissy AS, Hovestadt V, Weischenfeldt J, Ehrenberger T, et al. The whole-genome landscape of medulloblastoma subtypes. Nature. 2017 July;547(7663):311–7.
- Suzuki H, Kumar SA, Shuai S, Diaz-Navarro A, Gutierrez-Fernandez A, De Antonellis P, et al. Recurrent noncoding U1 snRNA mutations drive cryptic splicing in SHH medulloblastoma. Nature. 2019 Oct;574(7780):707–11.

- Waszak SM, Robinson GW, Gudenas BL, Smith KS, Forget A, Kojic M, et al. Germline Elongator mutations in Sonic Hedgehog medulloblastoma. Nature. 2020 Apr;580(7803):396–401.
- Hendrikse LD, Haldipur P, Saulnier O, Millman J, Sjoboen AH, Erickson AW, et al. Failure of human rhombic lip differentiation underlies medulloblastoma formation. Nature. 2022 Sept;609(7929):1021–8.
- 22. Smith KS, Bihannic L, Gudenas BL, Haldipur P, Tao R, Gao Q, et al. Unified rhombic lip origins of group 3 and group 4 medulloblastoma. Nature. 2022 Sept;609(7929):1012–20.
- 23. Sheng H, Li H, Zeng H, Zhang B, Lu Y, Liu X, et al. Heterogeneity and tumoral origin of medulloblastoma in the single-cell era. Oncogene. 2024 Mar;43(12):839–50.
- 24. Louis DN, Perry A, Wesseling P, Brat DJ, Cree IA, Figarella-Branger D, et al. The 2021 WHO Classification of Tumors of the Central Nervous System: a summary. Neuro Oncol. 2021 June 29;23(8):1231–51.
- 25. Ntenti C, Lallas K, Papazisis G. Clinical, Histological, and Molecular Prognostic Factors in Childhood Medulloblastoma: Where Do We Stand? Diagnostics. 2023 Jan;13(11):1915.
- 26. Bailey S, André N, Gandola L, Massimino M, Wheatley K, Gates S, et al. Clinical Trials in High-Risk Medulloblastoma: Evolution of the SIOP-Europe HR-MB Trial. Cancers. 2022 Jan;14(2):374.
- 27. Gajjar A, Robinson GW, Smith KS, Lin T, Merchant TE, Chintagumpala M, et al. Outcomes by Clinical and Molecular Features in Children With Medulloblastoma Treated With Risk-Adapted Therapy: Results of an International Phase III Trial (SJMB03). JCO. 2021 Mar;39(7):822–35.
- 28. Thomas A, Noël G. Medulloblastoma: optimizing care with a multidisciplinary approach. J Multidiscip Healthc. 2019;12:335–47.
- 29. Timmermann B, Alapetite C, Dieckmann K, Kortmann RD, Lassen-Ramshad Y, Maduro JH, et al. ESTRO-SIOPE guideline: Clinical management of radiotherapy in atypical teratoid/rhabdoid tumors (AT/RTs). Radiotherapy and Oncology [Internet]. 2024 July 1 [cited 2024 July 3];196. Available from: https://www.thegreenjournal.com/article/S0167-8140(24)00149-X/fulltext

- 30. Dho YS, Kim SK, Cheon JE, Park SH, Wang KC, Lee JY, et al. Investigation of the location of atypical teratoid/rhabdoid tumor. Childs Nerv Syst. 2015 Aug;31(8):1305–11.
- Reddy AT. Atypical Teratoid/Rhabdoid Tumors of the Central Nervous System. J Neurooncol. 2005 Dec 1;75(3):309–13.
- 32. Frühwald MC, Hasselblatt M, Nemes K, Bens S, Steinbügl M, Johann PD, et al. Age and DNA methylation subgroup as potential independent risk factors for treatment stratification in children with atypical teratoid/rhabdoid tumors. Neuro Oncol. 2020 July 7;22(7):1006–17.
- 33. Ostrom QT, Price M, Neff C, Cioffi G, Waite KA, Kruchko C, et al. CBTRUS Statistical Report: Primary Brain and Other Central Nervous System Tumors Diagnosed in the United States in 2015–2019. Neuro-Oncology. 2022 Oct 5;24(Supplement_5):v1–95.
- 34. Versteege I, Sévenet N, Lange J, Rousseau-Merck MF, Ambros P, Handgretinger R, et al. Truncating mutations of hSNF5/INI1 in aggressive paediatric cancer. Nature. 1998

 July;394(6689):203–6.
- 35. Johann PD, Hovestadt V, Thomas C, Jeibmann A, Heß K, Bens S, et al. Cribriform neuroepithelial tumor: molecular characterization of a SMARCB1-deficient non-rhabdoid tumor with favorable long-term outcome. Brain Pathol. 2016 Aug 11;27(4):411–8.
- 36. Federico A, Thomas C, Miskiewicz K, Woltering N, Zin F, Nemes K, et al. ATRT–SHH comprises three molecular subgroups with characteristic clinical and histopathological features and prognostic significance. Acta Neuropathol. 2022;143(6):697–711.
- 37. Lobón-Iglesias MJ, Andrianteranagna M, Han ZY, Chauvin C, Masliah-Planchon J,
 Manriquez V, et al. Imaging and multi-omics datasets converge to define different neural
 progenitor origins for ATRT-SHH subgroups. Nat Commun. 2023 Oct 20;14(1):6669.
- 38. Ho B, Johann PD, Grabovska Y, De Dieu Andrianteranagna MJ, Yao F, Frühwald M, et al. Molecular subgrouping of atypical teratoid/rhabdoid tumors—a reinvestigation and current consensus. Neuro Oncol. 2020 May;22(5):613–24.
- 39. Torchia J, Golbourn B, Feng S, Ho KC, Sin-Chan P, Vasiljevic A, et al. Integrated (epi)-Genomic Analyses Identify Subgroup-Specific Therapeutic Targets in CNS Rhabdoid Tumors. Cancer Cell. 2016 Dec 12;30(6):891–908.

- 40. Johann PD, Erkek S, Zapatka M, Kerl K, Buchhalter I, Hovestadt V, et al. Atypical Teratoid/Rhabdoid Tumors Are Comprised of Three Epigenetic Subgroups with Distinct Enhancer Landscapes. Cancer Cell. 2016 Mar 14;29(3):379–93.
- 41. Upadhyaya SA, Robinson GW, Onar-Thomas A, Orr BA, Johann P, Wu G, et al. Relevance of Molecular Groups in Children with Newly Diagnosed Atypical Teratoid Rhabdoid Tumor: Results from Prospective St. Jude Multi-Institutional Trials. Clin Cancer Res. 2021 May 15;27(10):2879–89.
- 42. Bartelheim K, Nemes K, Seeringer A, Kerl K, Buechner J, Boos J, et al. Improved 6-year overall survival in AT/RT results of the registry study Rhabdoid 2007. Cancer Med. 2016 Aug;5(8):1765–75.
- 43. Seeringer A, Reinhard H, Hasselblatt M, Schneppenheim R, Siebert R, Bartelheim K, et al. Synchronous congenital malignant rhabdoid tumor of the orbit and atypical teratoid/rhabdoid tumor--feasibility and efficacy of multimodal therapy in a long-term survivor. Cancer Genet. 2014 Sept;207(9):429–33.
- 44. Aridgides PD, Mahajan A, Eaton B, Wang D, Timmerman B, Früwald MC, et al. Focal versus craniospinal radiation for disseminated atypical teratoid/rhabdoid tumor following favorable response to systemic therapy. Pediatr Blood Cancer. 2023 July;70(7):e30351.
- 45. Gastberger K, Fincke VE, Mucha M, Siebert R, Hasselblatt M, Frühwald MC. Current Molecular and Clinical Landscape of ATRT The Link to Future Therapies. Cancer Manag Res. 2023 Dec 7;15:1369–93.
- 46. Park JR, Eggert A, Caron H. Neuroblastoma: Biology, Prognosis, and Treatment. Pediatric Clinics of North America. 2008 Feb 1;55(1):97–120.
- 47. Mishra A, Beniwal M, Nandeesh BN, Srinivas D, Somanna S. Primary Pediatric Intracranial Neuroblastoma: A Report of Two Cases. J Pediatr Neurosci. 2018;13(3):366–70.
- 48. Campos Cogo S, Gradowski Farias da Costa do Nascimento T, de Almeida Brehm Pinhatti F, de França Junior N, Santos Rodrigues B, Cavalli LR, et al. An overview of neuroblastoma cell lineage phenotypes and in vitro models. Exp Biol Med (Maywood). 2020 Dec;245(18):1637–47.

- 49. Cohn SL, Pearson ADJ, London WB, Monclair T, Ambros PF, Brodeur GM, et al. The International Neuroblastoma Risk Group (INRG) Classification System: An INRG Task Force Report. J Clin Oncol. 2009 Jan 10;27(2):289–97.
- 50. Ramos Elbal E, Galera Miñarro AM, Llinares Riestra ME, Bermúdez Cortés M, Fuster Soler JL. Neuroblastoma: validation of the INRG classification system in a small series. Clin Transl Oncol. 2019 Dec;21(12):1776–80.
- 51. Irwin MS, Naranjo A, Zhang FF, Cohn SL, London WB, Gastier-Foster JM, et al. Revised Neuroblastoma Risk Classification System: A Report From the Children's Oncology Group. Journal of Clinical Oncology [Internet]. 2021 July 28 [cited 2021 Dec 13]; Available from: https://ascopubs.org/doi/pdf/10.1200/JCO.21.00278
- 52. Chung C, Boterberg T, Lucas J, Panoff J, Valteau-Couanet D, Hero B, et al. Neuroblastoma. Pediatric Blood & Cancer. 2021;68(S2):e28473.
- 53. Bhatia S, Tonorezos ES, Landier W. Clinical Care for People Who Survive Childhood Cancer: A Review. JAMA. 2023 Sept 26;330(12):1175–86.
- 54. Hinnen C, von Haeseler E, Tijssens F, Mols F. Adverse childhood events and mental health problems in cancer survivors: a systematic review. Support Care Cancer. 2024 Jan 4;32(1):80.
- 55. Nipp RD, Kirchhoff AC, Fair D, Rabin J, Hyland KA, Kuhlthau K, et al. Financial Burden in Survivors of Childhood Cancer: A Report From the Childhood Cancer Survivor Study. J Clin Oncol. 2017 Oct 20;35(30):3474–81.
- 56. Országhová Z, Mego M, Chovanec M. Long-Term Cognitive Dysfunction in Cancer Survivors. Front Mol Biosci. 2021;8:770413.
- 57. Ness KK, Hudson MM, Ginsberg JP, Nagarajan R, Kaste SC, Marina N, et al. Physical performance limitations in the Childhood Cancer Survivor Study cohort. J Clin Oncol. 2009 May 10;27(14):2382–9.
- 58. Godono A, Felicetti F, Conti A, Clari M, Dionisi-Vici M, Gatti F, et al. Employment among Childhood Cancer Survivors: A Systematic Review and Meta-Analysis. Cancers (Basel). 2022 Sept 22;14(19):4586.

- 59. Khan T, Stewart M, Blackman S, Rousseau R, Donoghue M, Cohen K, et al. Accelerating Pediatric Cancer Drug Development: Challenges and Opportunities for Pediatric Master Protocols. Ther Innov Regul Sci. 2019 Mar;53(2):270–8.
- 60. Mody RJ, Wu YM, Lonigro RJ, Cao X, Roychowdhury S, Vats P, et al. Integrative Clinical Sequencing in the Management of Refractory or Relapsed Cancer in Youth. JAMA. 2015 Sept 1;314(9):913–25.
- 61. Zhang L, He X, Liu X, Zhang F, Huang LF, Potter AS, et al. Single-Cell Transcriptomics in Medulloblastoma Reveals Tumor-Initiating Progenitors and Oncogenic Cascades during Tumorigenesis and Relapse. Cancer Cell. 2019 Sept 16;36(3):302-318.e7.
- 62. Terada Y, Jo N, Arakawa Y, Sakakura M, Yamada Y, Ukai T, et al. Human Pluripotent Stem Cell-Derived Tumor Model Uncovers the Embryonic Stem Cell Signature as a Key Driver in Atypical Teratoid/Rhabdoid Tumor. Cell Rep. 2019 Mar 5;26(10):2608-2621.e6.
- 63. Vega FM, Colmenero-Repiso A, Gómez-Muñoz MA, Rodríguez-Prieto I, Aguilar-Morante D, Ramírez G, et al. CD44-high neural crest stem-like cells are associated with tumour aggressiveness and poor survival in neuroblastoma tumours. EBioMedicine. 2019 Nov;49:82–95.
- 64. Chu X, Tian W, Ning J, Xiao G, Zhou Y, Wang Z, et al. Cancer stem cells: advances in knowledge and implications for cancer therapy. Signal Transduct Target Ther. 2024 July 5;9(1):170.
- 65. Poliwoda S, Noor N, Downs E, Schaaf A, Cantwell A, Ganti L, et al. Stem cells: a comprehensive review of origins and emerging clinical roles in medical practice. Orthop Rev (Pavia). 14(3):37498.
- 66. Bonnet D, Dick JE. Human acute myeloid leukemia is organized as a hierarchy that originates from a primitive hematopoietic cell. Nat Med. 1997 July;3(7):730–7.
- 67. Galli R, Binda E, Orfanelli U, Cipelletti B, Gritti A, De Vitis S, et al. Isolation and characterization of tumorigenic, stem-like neural precursors from human glioblastoma.

 Cancer Res. 2004 Oct 1;64(19):7011–21.
- 68. Liu G, Yuan X, Zeng Z, Tunici P, Ng H, Abdulkadir IR, et al. Analysis of gene expression and chemoresistance of CD133+ cancer stem cells in glioblastoma. Mol Cancer. 2006 Dec 2;5:67.

- 69. Zhou HM, Zhang JG, Zhang X, Li Q. Targeting cancer stem cells for reversing therapy resistance: mechanism, signaling, and prospective agents. Sig Transduct Target Ther. 2021 Feb 15;6(1):1–17.
- 70. Pardridge WM. The blood-brain barrier: bottleneck in brain drug development. NeuroRx. 2005 Jan;2(1):3–14.
- 71. Pardridge WM. Drug transport across the blood-brain barrier. J Cereb Blood Flow Metab. 2012 Nov;32(11):1959–72.
- 72. Castellani G, Croese T, Peralta Ramos JM, Schwartz M. Transforming the understanding of brain immunity. Science. 2023 Apr 7;380(6640):eabo7649.
- 73. Marshall JS, Warrington R, Watson W, Kim HL. An introduction to immunology and immunopathology. Allergy, Asthma & Clinical Immunology. 2018 Sept 12;14(2):49.
- 74. Wang R, Lan C, Benlagha K, Camara NOS, Miller H, Kubo M, et al. The interaction of innate immune and adaptive immune system. MedComm. 2024;5(10):e714.
- 75. Netea MG, Schlitzer A, Placek K, Joosten LAB, Schultze JL. Innate and Adaptive Immune Memory: an Evolutionary Continuum in the Host's Response to Pathogens. Cell Host & Microbe. 2019 Jan 9;25(1):13–26.
- 76. Pradeu T, Thomma BPHJ, Girardin SE, Lemaitre B. The conceptual foundations of innate immunity: Taking stock 30 years later. Immunity. 2024 Apr 9;57(4):613–31.
- 77. Chi H, Pepper M, Thomas PG. Principles and therapeutic applications of adaptive immunity. Cell. 2024 Apr 25;187(9):2052–78.
- 78. Cyster JG, Allen CDC. B Cell Responses: Cell Interaction Dynamics and Decisions. Cell. 2019 Apr 18;177(3):524–40.
- 79. Sun L, Su Y, Jiao A, Wang X, Zhang B. T cells in health and disease. Sig Transduct Target Ther. 2023 June 19;8(1):235.
- 80. Wu B, Zhang B, Li B, Wu H, Jiang M. Cold and hot tumors: from molecular mechanisms to targeted therapy. Sig Transduct Target Ther. 2024 Oct 18;9(1):274.

- 81. Binnewies M, Roberts EW, Kersten K, Chan V, Fearon DF, Merad M, et al. Understanding the tumor immune microenvironment (TIME) for effective therapy. Nat Med. 2018

 May;24(5):541–50.
- 82. Sun J, Zamyatnin AA, Yuan X, Xiao Y, Li H. Editorial: Cancer cell-intrinsic and -extrinsic factors affecting tumor immune evasion. Front Immunol [Internet]. 2023 July 31 [cited 2024 July 29];14. Available from: https://www.frontiersin.org/journals/immunology/articles/10.3389/fimmu.2023.1261820/f ull
- 83. Wang MM, Coupland SE, Aittokallio T, Figueiredo CR. Resistance to immune checkpoint therapies by tumour-induced T-cell desertification and exclusion: key mechanisms, prognostication and new therapeutic opportunities. Br J Cancer. 2023 Oct;129(8):1212–24.
- 84. Grabovska Y, Mackay A, O'Hare P, Crosier S, Finetti M, Schwalbe EC, et al. Pediatric pancentral nervous system tumor analysis of immune-cell infiltration identifies correlates of antitumor immunity. Nat Commun. 2020 Aug 28;11(1):4324.
- 85. Mina M, Boldrini R, Citti A, Romania P, D'Alicandro V, De Ioris M, et al. Tumor-infiltrating T lymphocytes improve clinical outcome of therapy-resistant neuroblastoma.

 Oncoimmunology. 2015 Sept;4(9):e1019981.
- 86. Verhoeven BM, Mei S, Olsen TK, Gustafsson K, Valind A, Lindström A, et al. The immune cell atlas of human neuroblastoma. Cell Rep Med. 2022 June 9;3(6):100657.
- 87. Wienke J, Dierselhuis MP, Tytgat GAM, Künkele A, Nierkens S, Molenaar JJ. The immune landscape of neuroblastoma: Challenges and opportunities for novel therapeutic strategies in pediatric oncology. European Journal of Cancer. 2021 Feb 1;144:123–50.
- 88. Coley WB. The treatment of malignant tumors by repeated inoculations of erysipelas. With a report of ten original cases. 1893. Clin Orthop Relat Res. 1991 Jan; (262):3–11.
- 89. Sadeghi Rad H, Monkman J, Warkiani ME, Ladwa R, O'Byrne K, Rezaei N, et al.

 Understanding the tumor microenvironment for effective immunotherapy. Med Res Rev.

 2021 May;41(3):1474–98.
- 90. Drugs Approved for Childhood Cancers NCI [Internet]. 2016 [cited 2024 July 26]. Available from: https://www.cancer.gov/about-cancer/treatment/drugs/childhood-cancer-fda-approved-drugs

- 91. Nassiri F, Patil V, Yefet LS, Singh O, Liu J, Dang RMA, et al. Oncolytic DNX-2401 virotherapy plus pembrolizumab in recurrent glioblastoma: a phase 1/2 trial. Nat Med. 2023 June;29(6):1370–8.
- 92. Wieczorek A, Zaniewska-Tekieli A, Ehlert K, Pawinska-Wasikowska K, Balwierz W, Lode H. Dinutuximab beta combined with chemotherapy in patients with relapsed or refractory neuroblastoma. Front Oncol. 2023 Feb 3;13:1082771.
- 93. Mora J, Castañeda A, Gorostegui M, Varo A, Perez-Jaume S, Simao M, et al. Naxitamab Combined with Granulocyte-Macrophage Colony-Stimulating Factor as Consolidation for High-Risk Neuroblastoma Patients in First Complete Remission under Compassionate Use—Updated Outcome Report. Cancers (Basel). 2023 Apr 28;15(9):2535.
- 94. Gómez Román VR, Murray JC, Weiner LM. Chapter 1 Antibody-Dependent Cellular Cytotoxicity (ADCC). In: Ackerman ME, Nimmerjahn F, editors. Antibody Fc [Internet]. Boston: Academic Press; 2014 [cited 2025 May 27]. p. 1–27. Available from: https://www.sciencedirect.com/science/article/pii/B9780123948021000017
- 95. Lee W, Lee SM, Jung ST. Unlocking the Power of Complement-Dependent Cytotoxicity: Engineering Strategies for the Development of Potent Therapeutic Antibodies for Cancer Treatments. BioDrugs. 2023 Sept;37(5):637–48.
- 96. Kantoff PW, Higano CS, Shore ND, Berger ER, Small EJ, Penson DF, et al. Sipuleucel-T immunotherapy for castration-resistant prostate cancer. N Engl J Med. 2010 July 29;363(5):411–22.
- 97. Kamat AM, Bellmunt J, Galsky MD, Konety BR, Lamm DL, Langham D, et al. Society for Immunotherapy of Cancer consensus statement on immunotherapy for the treatment of bladder carcinoma. J Immunother Cancer. 2017 Dec 1;5(1):68.
- 98. Schirrmacher V. Cancer Vaccines and Oncolytic Viruses Exert Profoundly Lower Side Effects in Cancer Patients than Other Systemic Therapies: A Comparative Analysis. Biomedicines. 2020 Mar 16;8(3):61.
- 99. Ardon H, De Vleeschouwer S, Van Calenbergh F, Claes L, Kramm CM, Rutkowski S, et al. Adjuvant dendritic cell-based tumour vaccination for children with malignant brain tumours. Pediatr Blood Cancer. 2010 Apr;54(4):519–25.

- 100. Bui TA, Mei H, Sang R, Ortega DG, Deng W. Advancements and challenges in developing in vivo CAR T cell therapies for cancer treatment. eBioMedicine. 2024 Aug 1;106:105266.
- 101. Awasthi R, Maier HJ, Zhang J, Lim S. Kymriah® (tisagenlecleucel) An overview of the clinical development journey of the first approved CAR-T therapy. Hum Vaccin Immunother. 2023;19(1):2210046.
- 102. Straathof K, Flutter B, Wallace R, Jain N, Loka T, Depani S, et al. Antitumor activity without on-target off-tumor toxicity of GD2-chimeric antigen receptor T cells in patients with neuroblastoma. Sci Transl Med. 2020 Nov 25;12(571):eabd6169.
- 103. Heczey A, Louis CU, Savoldo B, Dakhova O, Durett A, Grilley B, et al. CART Cells
 Administered in Combination with Lymphodepletion and PD-1 Inhibition to Patients with
 Neuroblastoma. Mol Ther. 2017 Sept 6;25(9):2214–24.
- 104. Berraondo P, Sanmamed MF, Ochoa MC, Etxeberria I, Aznar MA, Pérez-Gracia JL, et al. Cytokines in clinical cancer immunotherapy. Br J Cancer. 2019 Jan;120(1):6–15.
- 105. Mora J, Modak S, Kinsey J, Ragsdale CE, Lazarus HM. GM-CSF, G-CSF or no cytokine therapy with anti-GD2 immunotherapy for high-risk neuroblastoma. International Journal of Cancer. 2024;154(8):1340–64.
- 106. Xie N, Shen G, Gao W, Huang Z, Huang C, Fu L. Neoantigens: promising targets for cancer therapy. Sig Transduct Target Ther. 2023 Jan 6;8(1):1–38.
- 107. Nguyên TLA, Abdelbary H, Arguello M, Breitbach C, Leveille S, Diallo JS, et al. Chemical targeting of the innate antiviral response by histone deacetylase inhibitors renders refractory cancers sensitive to viral oncolysis. Proc Natl Acad Sci U S A. 2008 Sept 30;105(39):14981–6.
- 108. Mardi A, Shirokova AV, Mohammed RN, Keshavarz A, Zekiy AO, Thangavelu L, et al. Biological causes of immunogenic cancer cell death (ICD) and anti-tumor therapy; Combination of Oncolytic virus-based immunotherapy and CAR T-cell therapy for ICD induction. Cancer Cell Int. 2022 Apr 29;22:168.
- 109. Russell SJ, Peng KW, Bell JC. Oncolytic virotherapy. Nature Biotechnology. 2012 July;30(7):658–70.

- 110. Cook M, Chauhan A. Clinical Application of Oncolytic Viruses: A Systematic Review. Int J Mol Sci. 2020 Oct 12;21(20).
- 111. Alberts P, Tilgase A, Rasa A, Bandere K, Venskus D. The advent of oncolytic virotherapy in oncology: The Rigvir® story. European Journal of Pharmacology. 2018 Oct 15;837:117–26.
- 112. Garber K. China Approves World's First Oncolytic Virus Therapy For Cancer Treatment.

 JNCI: Journal of the National Cancer Institute. 2006 Mar 1;98(5):298–300.
- 113. Andtbacka RHI, Kaufman HL, Collichio F, Amatruda T, Senzer N, Chesney J, et al. Talimogene Laherparepvec Improves Durable Response Rate in Patients With Advanced Melanoma. J Clin Oncol. 2015 Sept 1;33(25):2780–8.
- 114. Frampton JE. Teserpaturev/G47Δ: First Approval. BioDrugs. 2022 Sept 1;36(5):667–72.
- 115. Todo T, Ito H, Ino Y, Ohtsu H, Ota Y, Shibahara J, et al. Intratumoral oncolytic herpes virus G47Δ for residual or recurrent glioblastoma: a phase 2 trial. Nat Med. 2022 Aug;28(8):1630–9.
- 116. Gállego Pérez-Larraya J, Garcia-Moure M, Labiano S, Patiño-García A, Dobbs J, Gonzalez-Huarriz M, et al. Oncolytic DNX-2401 Virus for Pediatric Diffuse Intrinsic Pontine Glioma. N Engl J Med. 2022 June 30;386(26):2471–81.
- 117. Friedman GK, Johnston JM, Bag AK, Bernstock JD, Li R, Aban I, et al. Oncolytic HSV-1 G207 Immunovirotherapy for Pediatric High-Grade Gliomas. N Engl J Med. 2021 Apr 29;384(17):1613–22.
- 118. Freeman AI, Zakay-Rones Z, Gomori JM, Linetsky E, Rasooly L, Greenbaum E, et al. Phase I/II trial of intravenous NDV-HUJ oncolytic virus in recurrent glioblastoma multiforme. Mol Ther. 2006 Jan;13(1):221–8.
- 119. Thompson EM, Landi D, Brown MC, Friedman HS, McLendon R, Herndon JE, et al.

 Recombinant polio-rhinovirus immunotherapy for recurrent paediatric high-grade glioma:
 a phase 1b trial. Lancet Child Adolesc Health. 2023 July;7(7):471–8.
- 120. Schuelke MR, Gundelach JH, Coffey M, West E, Scott K, Johnson DR, et al. Phase I trial of sargramostim/pelareorep therapy in pediatric patients with recurrent or refractory high-grade brain tumors. Neurooncol Adv. 2022 June 17;4(1):vdac085.

- 121. Burke MJ, Ahern C, Weigel BJ, Poirier JT, Rudin CM, Chen Y, et al. Phase I Trial of Seneca Valley Virus (NTX-010) in Children with Relapsed / Refractory Solid Tumors: A Report of the Children's Oncology Group. Pediatr Blood Cancer. 2015 May;62(5):743–50.
- 122. Cripe TP, Ngo MC, Geller JI, Louis CU, Currier MA, Racadio JM, et al. Phase 1 Study of Intratumoral Pexa-Vec (JX-594), an Oncolytic and Immunotherapeutic Vaccinia Virus, in Pediatric Cancer Patients. Mol Ther. 2015 Mar;23(3):602–8.
- 123. Soroush A, Shahhosseini R, Ghavamikia N, Hjazi A, Roudaki S, KhalatbariLimaki M, et al. Improvement of current immunotherapies with engineered oncolytic viruses that target cancer stem cells. Cell Biochemistry and Function. 2024;42(4):e4055.
- 124. Chaurasiya S, Chen NG, Warner SG. Oncolytic Virotherapy versus Cancer Stem Cells: A Review of Approaches and Mechanisms. Cancers (Basel). 2018 Apr 19;10(4):124.
- 125. Friedman GK, Moore BP, Nan L, Kelly VM, Etminan T, Langford CP, et al. Pediatric medulloblastoma xenografts including molecular subgroup 3 and CD133+ and CD15+ cells are sensitive to killing by oncolytic herpes simplex viruses. Neuro Oncol. 2016 Feb;18(2):227–35.
- 126. Martinez-Velez N, Marigil M, García-Moure M, Gonzalez-Huarriz M, Aristu JJ, Ramos-García LI, et al. Delta-24-RGD combined with radiotherapy exerts a potent antitumor effect in diffuse intrinsic pontine glioma and pediatric high grade glioma models. Acta Neuropathol Commun. 2019 Apr 29;7:64.
- 127. Jiang H, Gomez-Manzano C, Aoki H, Alonso MM., Kondo S, McCormick F, et al. Examination of the Therapeutic Potential of Delta-24-RGD in Brain Tumor Stem Cells: Role of Autophagic Cell Death. JNCI: Journal of the National Cancer Institute. 2007 Sept 19;99(18):1410–4.
- 128. Ruano D, López-Martín JA, Moreno L, Lassaletta Á, Bautista F, Andión M, et al. First-in-Human, First-in-Child Trial of Autologous MSCs Carrying the Oncolytic Virus Icovir-5 in Patients with Advanced Tumors. Molecular Therapy. 2020 Apr 8;28(4):1033–42.
- 129. Zitvogel L, Galluzzi L, Kepp O, Smyth MJ, Kroemer G. Type I interferons in anticancer immunity. Nat Rev Immunol. 2015 July;15(7):405–14.
- 130. Lemos de Matos A, Franco LS, McFadden G. Oncolytic Viruses and the Immune System: The Dynamic Duo. Mol Ther Methods Clin Dev. 2020 Jan 15;17:349–58.

- 131. Gujar S, Pol JG, Kim Y, Lee PW, Kroemer G. Antitumor Benefits of Antiviral Immunity: An Underappreciated Aspect of Oncolytic Virotherapies. Trends in Immunology. 2018 Mar 1;39(3):209–21.
- 132. Bernstock JD, Vicario N, Rong L, Valdes PA, Choi BD, Chen JA, et al. A novel in situ multiplex immunofluorescence panel for the assessment of tumor immunopathology and response to virotherapy in pediatric glioblastoma reveals a role for checkpoint protein inhibition. Oncoimmunology. 2019 Oct 21;8(12):e1678921.
- 133. Belcaid Z, Berrevoets C, Choi J, van Beelen E, Stavrakaki E, Pierson T, et al. Low-dose oncolytic adenovirus therapy overcomes tumor-induced immune suppression and sensitizes intracranial gliomas to anti-PD-1 therapy. Neuro-Oncology Advances. 2020 Jan 1;2(1):vdaa011.
- 134. Postler TS, Beer M, Blitvich BJ, Bukh J, de Lamballerie X, Drexler JF, et al. Renaming of the genus Flavivirus to Orthoflavivirus and extension of binomial species names within the family Flaviviridae. Arch Virol. 2023 Aug 10;168(9):224.
- 135. van Leur SW, Heunis T, Munnur D, Sanyal S. Pathogenesis and virulence of flavivirus infections. Virulence. 2021 Dec 31;12(1):2814–38.
- 136. Kostyuchenko VA, Lim EXY, Zhang S, Fibriansah G, Ng TS, Ooi JSG, et al. Structure of the thermally stable Zika virus. Nature. 2016 May;533(7603):425–8.
- 137. Hou W, Cruz-Cosme R, Armstrong N, Obwolo LA, Wen F, Hu W, et al. Molecular cloning and characterization of the genes encoding the proteins of Zika virus. Gene. 2017 Sept;628:117–28.
- 138. Nazneen F, Thompson EA, Blackwell C, Bai JS, Huang F, Bai F. An effective live-attenuated Zika vaccine candidate with a modified 5' untranslated region. npj Vaccines. 2023 Apr 1;8(1):1–12.
- 139. Pallarés HM, Costa Navarro GS, Villordo SM, Merwaiss F, de Borba L, Gonzalez Lopez Ledesma MM, et al. Zika Virus Subgenomic Flavivirus RNA Generation Requires Cooperativity between Duplicated RNA Structures That Are Essential for Productive Infection in Human Cells. J Virol. 2020 Aug 31;94(18):e00343-20.
- 140. Lee I, Bos S, Li G, Wang S, Gadea G, Desprès P, et al. Probing Molecular Insights into Zika Virus Host Interactions. Viruses. 2018;10(5).

- 141. Link N, Harnish JM, Hull B, Gibson S, Dietze M, Mgbike UE, et al. A Zika virus protein expression screen in Drosophila to investigate targeted host pathways during development. Dis Model Mech. 2024 Feb 28;17(2):dmm050297.
- 142. Li T, Zhao Q, Yang X, Chen C, Yang K, Wu C, et al. Structural insight into the Zika virus capsid encapsulating the viral genome. Cell Res. 2018 Apr;28(4):497–9.
- 143. Tan TY, Fibriansah G, Kostyuchenko VA, Ng TS, Lim XX, Zhang S, et al. Capsid protein structure in Zika virus reveals the flavivirus assembly process. Nat Commun. 2020 Feb 14;11(1):895.
- 144. Gwon YD, Zusinaite E, Merits A, Överby AK, Evander M. N-glycosylation in the Pre-Membrane Protein Is Essential for the Zika Virus Life Cycle. Viruses. 2020 Aug 23;12(9):E925.
- 145. Dai L, Song J, Lu X, Deng YQ, Musyoki AM, Cheng H, et al. Structures of the Zika Virus Envelope Protein and Its Complex with a Flavivirus Broadly Protective Antibody. Cell Host Microbe. 2016 May 11;19(5):696–704.
- 146. Puerta-Guardo H, Biering SB, de Sousa FTG, Shu J, Glasner DR, Li J, et al. Flavivirus NS1 Triggers Tissue-Specific Disassembly of Intercellular Junctions Leading to Barrier Dysfunction and Vascular Leak in a GSK-3β-Dependent Manner. Pathogens. 2022 May 24;11(6):615.
- 147. Ci Y, Liu ZY, Zhang NN, Niu Y, Yang Y, Xu C, et al. Zika NS1-induced ER remodeling is essential for viral replication. J Cell Biol. 2020 Feb 3;219(2):e201903062.
- 148. Zhang X, Xie X, Xia H, Zou J, Huang L, Popov VL, et al. Zika Virus NS2A-Mediated Virion Assembly. mBio. 2019 Oct 29;10(5):e02375-19.
- 149. Zhang X, Xie X, Zou J, Xia H, Shan C, Chen X, et al. Genetic and biochemical characterizations of Zika virus NS2A protein. Emerg Microbes Infect. 2019;8(1):585–602.
- 150. Phoo WW, Li Y, Zhang Z, Lee MY, Loh YR, Tan YB, et al. Structure of the NS2B-NS3 protease from Zika virus after self-cleavage. Nat Commun. 2016 Nov 15;7(1):13410.
- 151. Xing H, Xu S, Jia F, Yang Y, Xu C, Qin C, et al. Zika NS2B is a crucial factor recruiting NS3 to the ER and activating its protease activity. Virus Research. 2020 Jan 2;275:197793.

- 152. Xu S, Ci Y, Wang L, Yang Y, Zhang L, Xu C, et al. Zika virus NS3 is a canonical RNA helicase stimulated by NS5 RNA polymerase. Nucleic Acids Res. 2019 Sept 19;47(16):8693–707.
- 153. Surya W, Honey SS, Torres J. Flavivirus Zika NS4A protein forms large oligomers in liposomes and in mild detergent. Sci Rep. 2024 May 31;14(1):12533.
- 154. Bhardwaj T, Kumar P, Giri R. Investigating the conformational dynamics of Zika virus NS4B protein. Virology. 2022 Oct 1;575:20–35.
- 155. Zhao B, Yi G, Du F, Chuang YC, Vaughan RC, Sankaran B, et al. Structure and function of the Zika virus full-length NS5 protein. Nat Commun. 2017 Mar 27;8(1):14762.
- 156. Musso D, Nilles EJ, Cao-Lormeau VM. Rapid spread of emerging Zika virus in the Pacific area. Clin Microbiol Infect. 2014 Oct;20(10):0595-596.
- 157. Gregory CJ, Oduyebo T, Brault AC, Brooks JT, Chung KW, Hills S, et al. Modes of Transmission of Zika Virus. J Infect Dis. 2017 Dec 15;216(Suppl 10):S875–83.
- 158. Beaver JT, Lelutiu N, Habib R, Skountzou I. Evolution of Two Major Zika Virus Lineages:
 Implications for Pathology, Immune Response, and Vaccine Development. Front Immunol
 [Internet]. 2018 July 18 [cited 2024 Aug 16];9. Available from:
 https://www.frontiersin.org/journals/immunology/articles/10.3389/fimmu.2018.01640/full
- 159. Li M, Zhang D, Li C, Zheng Z, Fu M, Ni F, et al. Characterization of Zika Virus Endocytic Pathways in Human Glioblastoma Cells. Front Microbiol [Internet]. 2020 Mar 6 [cited 2020 June 4];11. Available from: https://www.ncbi.nlm.nih.gov/pmc/articles/PMC7069030/
- 160. Offerdahl DK, Dorward DW, Hansen BT, Bloom ME. Cytoarchitecture of Zika virus infection in human neuroblastoma and Aedes albopictus cell lines. Virology. 2017 Jan;501:54–62.
- 161. Mlera L, Offerdahl DK, Dorward DW, Carmody A, Chiramel AI, Best SM, et al. The liver X receptor agonist LXR 623 restricts flavivirus replication. Emerg Microbes Infect. 2021 June 24;1–33.
- 162. Sirohi D, Kuhn RJ. Zika Virus Structure, Maturation, and Receptors. J Infect Dis. 2017 Dec 16;216(suppl_10):S935–44.
- 163. Dick GWA, Kitchen SF, Haddow AJ. Zika Virus (I). Isolations and serological specificity. Transactions of The Royal Society of Tropical Medicine and Hygiene. 1952 Sept 1;46(5):509–20.

- 164. Duffy MR, Chen TH, Hancock WT, Powers AM, Kool JL, Lanciotti RS, et al. Zika virus outbreak on Yap Island, Federated States of Micronesia. N Engl J Med. 2009 June 11;360(24):2536–43.
- 165. Haddow AD, Schuh AJ, Yasuda CY, Kasper MR, Heang V, Huy R, et al. Genetic Characterization of Zika Virus Strains: Geographic Expansion of the Asian Lineage. PLOS Neglected Tropical Diseases. 2012 Feb 28;6(2):e1477.
- 166. Marinho F, Araújo VEM de, Porto DL, Ferreira HL, Coelho MRS, Lecca RCR, et al. Microcephaly in Brazil: prevalence and characterization of cases from the Information System on Live Births (Sinasc), 2000-2015. Epidemiol Serv Saude. 2016;25(4):701–12.
- 167. Styczynski AR, Malta JMAS, Krow-Lucal ER, Percio J, Nóbrega ME, Vargas A, et al. Increased rates of Guillain-Barré syndrome associated with Zika virus outbreak in the Salvador metropolitan area, Brazil. PLOS Neglected Tropical Diseases. 2017 Aug 30;11(8):e0005869.
- 168. Krauer F, Riesen M, Reveiz L, Oladapo OT, Martínez-Vega R, Porgo TV, et al. Zika Virus Infection as a Cause of Congenital Brain Abnormalities and Guillain–Barré Syndrome: Systematic Review. PLoS Med. 2017 Jan 3;14(1):e1002203.
- 169. Smith DR, Sprague TR, Hollidge BS, Valdez SM, Padilla SL, Bellanca SA, et al. African and Asian Zika Virus Isolates Display Phenotypic Differences Both In Vitro and In Vivo. Am J Trop Med Hyg. 2018 Feb;98(2):432–44.
- 170. He MJ, Wang HJ, Yan XL, Lou YN, Song GY, Li RT, et al. Key Residue in the Precursor Region of M Protein Contributes to the Neurovirulence and Neuroinvasiveness of the African Lineage of Zika Virus. J Virol. 2023;97(3):e01801-22.
- 171. Shan C, Xia H, Haller SL, Azar SR, Liu Y, Liu J, et al. A Zika virus envelope mutation preceding the 2015 epidemic enhances virulence and fitness for transmission. Proc Natl Acad Sci U S A. 2020 Aug 18;117(33):20190–7.
- 172. Yuan L, Huang XY, Liu ZY, Zhang F, Zhu XL, Yu JY, et al. A single mutation in the prM protein of Zika virus contributes to fetal microcephaly. Science. 2017 Nov 17;358(6365):933–6.
- 173. Yokoyama S, Starmer WT. Possible Roles of New Mutations Shared by Asian and American Zika Viruses. Molecular Biology and Evolution. 2017 Mar 1;34(3):525–34.

- 174. Dinnon Iii KH, Gallichotte EN, Fritch EJ, Menachery VD, Baric RS. Shortening of Zika virus CD-loop reduces neurovirulence while preserving antigenicity. Pimenta P, editor. PLoS Negl Trop Dis. 2019 Mar 7;13(3):e0007212.
- 175. Cheng ML, Yang YX, Liu ZY, Wen D, Yang P, Huang XY, et al. Pathogenicity and Structural Basis of Zika Variants with Glycan Loop Deletions in the Envelope Protein. Journal of Virology. 2022 Nov 15;96(23):e00879-22.
- 176. Liu Y, Liu J, Du S, Shan C, Nie K, Zhang R, et al. Evolutionary enhancement of Zika virus infectivity in Aedes aegypti mosquitoes. Nature. 2017 May;545(7655):482–6.
- 177. Retallack H, Di Lullo E, Arias C, Knopp KA, Laurie MT, Sandoval-Espinosa C, et al. Zika virus cell tropism in the developing human brain and inhibition by azithromycin. Proc Natl Acad Sci USA. 2016 Dec 13;113(50):14408–13.
- 178. Li C, Xu D, Ye Q, Hong S, Jiang Y, Liu X, et al. Zika Virus Disrupts Neural Progenitor

 Development and Leads to Microcephaly in Mice. Cell Stem Cell. 2016 July 7;19(1):120–6.
- 179. Souza BS, Sampaio GL, Pereira CS, Campos GS, Sardi SI, Freitas LA, et al. Zika virus infection induces mitosis abnormalities and apoptotic cell death of human neural progenitor cells. Sci Rep. 2016 Dec 23;6:39775.
- 180. Tang H, Hammack C, Ogden SC, Wen Z, Qian X, Li Y, et al. Zika Virus Infects Human Cortical Neural Precursors and Attenuates Their Growth. Cell Stem Cell. 2016 May 5;18(5):587–90.
- 181. Miranda-Negrón Y, García-Arrarás JE. Radial glia and radial glia-like cells: Their role in neurogenesis and regeneration. Front Neurosci. 2022 Nov 16;16:1006037.
- 182. Onorati M, Li Z, Liu F, Sousa AMM, Nakagawa N, Li M, et al. Zika Virus Disrupts Phospho-TBK1 Localization and Mitosis in Human Neuroepithelial Stem Cells and Radial Glia. Cell Rep. 2016 Sept 6;16(10):2576–92.
- 183. Shelton SM, Soucy AR, Kurzion R, Zeldich E, Connor JH, Haydar TF. Forebrain Neural Precursor Cells Are Differentially Vulnerable to Zika Virus Infection. eNeuro [Internet]. 2021 Oct [cited 2024 Aug 9];8(5). Available from: https://www.ncbi.nlm.nih.gov/pmc/articles/PMC8431824/

- 184. Wu KY, Zuo GL, Li XF, Ye Q, Deng YQ, Huang XY, et al. Vertical transmission of Zika virus targeting the radial glial cells affects cortex development of offspring mice. Cell Res. 2016 June;26(6):645–54.
- 185. Yoon KJ, Song G, Qian X, Pan J, Xu D, Rho HS, et al. Zika virus-encoded NS2A disrupts mammalian cortical neurogenesis by degrading adherens junction proteins. Cell Stem Cell. 2017 Sept 7;21(3):349-358.e6.
- 186. Martínez-Cerdeño V, Noctor SC. Neural Progenitor Cell Terminology. Front Neuroanat. 2018 Dec 6;12:104.
- 187. Hanners NW, Eitson JL, Usui N, Richardson RB, Wexler EM, Konopka G, et al. Western Zika Virus in Human Fetal Neural Progenitors Persists Long Term with Partial Cytopathic and Limited Immunogenic Effects. Cell Reports. 2016 June 14;15(11):2315–22.
- 188. Van der Hoek KH, Eyre NS, Shue B, Khantisitthiporn O, Glab-Ampi K, Carr JM, et al. Viperin is an important host restriction factor in control of Zika virus infection. Sci Rep. 2017 June 30;7:4475.
- 189. Chavali PL, Stojic L, Meredith LW, Joseph N, Nahorski MS, Sanford TJ, et al.

 Neurodevelopmental protein Musashi-1 interacts with the Zika genome and promotes viral replication. Science. 2017 July 7;357(6346):83–8.
- 190. Ferraris P, Cochet M, Hamel R, Gladwyn-Ng I, Alfano C, Diop F, et al. Zika virus differentially infects human neural progenitor cells according to their state of differentiation and dysregulates neurogenesis through the Notch pathway. Emerg Microbes Infect. 2019 July 8;8(1):1003–16.
- 191. Komarasamy TV, Adnan NAA, James W, Balasubramaniam VRMT. Zika Virus Neuropathogenesis: The Different Brain Cells, Host Factors and Mechanisms Involved. Frontiers in Immunology [Internet]. 2022 [cited 2023 May 3];13. Available from: https://www.frontiersin.org/articles/10.3389/fimmu.2022.773191
- 192. Metzler AD, Tang H. Zika Virus Neuropathogenesis—Research and Understanding. Pathogens. 2024 July;13(7):555.
- 193. Caires-Júnior LC, Goulart E, Melo US, Araujo BHS, Alvizi L, Soares-Schanoski A, et al.

 Discordant congenital Zika syndrome twins show differential in vitro viral susceptibility of neural progenitor cells. Nature Communications. 2018;9(1):475.

- 194. Thulasi Raman SN, Latreille E, Gao J, Zhang W, Wu J, Russell MS, et al. Dysregulation of Ephrin receptor and PPAR signaling pathways in neural progenitor cells infected by Zika virus. Emerg Microbes Infect. 2020 Dec;9(1):2046–60.
- 195. Bhagat R, Rajpara P, Kaur G, Gupta K, Seth P. Zika virus E protein dysregulate mir-204/WNT2 signalling in human fetal neural stem cells. Brain Research Bulletin. 2021 Nov 1;176:93–102.
- 196. Dang J, Tiwari SK, Lichinchi G, Qin Y, Patil VS, Eroshkin AM, et al. Zika Virus Depletes

 Neural Progenitors in Human Cerebral Organoids through Activation of the Innate Immune

 Receptor TLR3. Cell Stem Cell. 2016 Aug 4;19(2):258–65.
- 197. Bhagat R, Kaur G, Seth P. Molecular mechanisms of zika virus pathogenesis: An update. Indian J Med Res. 2021 Sept;154(3):433–45.
- 198. Vasile F, Dossi E, Rouach N. Human astrocytes: structure and functions in the healthy brain. Brain Struct Funct. 2017;222(5):2017–29.
- 199. Meertens L, Labeau A, Dejarnac O, Cipriani S, Sinigaglia L, Bonnet-Madin L, et al. Axl Mediates ZIKA Virus Entry in Human Glial Cells and Modulates Innate Immune Responses. Cell Rep. 2017 Jan 10;18(2):324–33.
- 200. Shao Q, Herrlinger S, Yang SL, Lai F, Moore JM, Brindley MA, et al. Zika virus infection disrupts neurovascular development and results in postnatal microcephaly with brain damage. Development. 2016 Nov 15;143(22):4127–36.
- 201. van den Pol AN, Mao G, Yang Y, Ornaghi S, Davis JN. Zika Virus Targeting in the Developing Brain. J Neurosci. 2017 Feb 22;37(8):2161–75.
- 202. Limonta D, Jovel J, Kumar A, Airo AM, Hou S, Saito L, et al. Human Fetal Astrocytes Infected with Zika Virus Exhibit Delayed Apoptosis and Resistance to Interferon: Implications for Persistence. Viruses. 2018 Nov 17;10(11):646.
- 203. Stefanik M, Formanova P, Bily T, Vancova M, Eyer L, Palus M, et al. Characterisation of Zika virus infection in primary human astrocytes. BMC Neuroscience. 2018 Feb 20;19(1):5.
- 204. Chen J, Yang Y feng, Yang Y, Zou P, Chen J, He Y, et al. AXL promotes Zika virus infection in astrocytes by antagonizing type I interferon signalling. Nat Microbiol. 2018 Mar;3(3):302–9.

- 205. Schultz V, Barrie JA, Donald CL, Crawford CL, Mullin M, Anderson TJ, et al.
 Oligodendrocytes are susceptible to Zika virus infection in a mouse model of perinatal exposure: Implications for CNS complications. Glia. 2021 Aug;69(8):2023–36.
- 206. Cumberworth SL, Barrie JA, Cunningham ME, de Figueiredo DPG, Schultz V, Wilder-Smith AJ, et al. Zika virus tropism and interactions in myelinating neural cell cultures: CNS cells and myelin are preferentially affected. Acta Neuropathol Commun. 2017 June 23;5(1):50.
- 207. Tisoncik-Go J, Stokes C, Whitmore LS, Newhouse DJ, Voss K, Gustin A, et al. Disruption of myelin structure and oligodendrocyte maturation in a macaque model of congenital Zika infection. Nat Commun. 2024 June 18;15(1):5173.
- 208. Gurung S, Reuter N, Preno A, Dubaut J, Nadeau H, Hyatt K, et al. Zika virus infection at midgestation results in fetal cerebral cortical injury and fetal death in the olive baboon. PLoS Pathog. 2019 Jan;15(1):e1007507.
- 209. Adams Waldorf KM, Stencel-Baerenwald JE, Kapur RP, Studholme C, Boldenow E, Vornhagen J, et al. Fetal brain lesions after subcutaneous inoculation of Zika virus in a pregnant nonhuman primate. Nat Med. 2016 Nov;22(11):1256–9.
- 210. Xu P, Shan C, Dunn TJ, Xie X, Xia H, Gao J, et al. Role of microglia in the dissemination of Zika virus from mother to fetal brain. PLoS Negl Trop Dis. 2020 July 6;14(7):e0008413.
- 211. Muffat J, Li Y, Omer A, Durbin A, Bosch I, Bakiasi G, et al. Human induced pluripotent stem cell-derived glial cells and neural progenitors display divergent responses to Zika and dengue infections. Proc Natl Acad Sci U S A. 2018 July 3;115(27):7117–22.
- 212. Lum FM, Low DKS, Fan Y, Tan JJL, Lee B, Chan JKY, et al. Zika Virus Infects Human Fetal Brain Microglia and Induces Inflammation. Clinical Infectious Diseases. 2017 Apr 1;64(7):914–20.
- 213. Wang J, Liu J, Zhou R, Ding X, Zhang Q, Zhang C, et al. Zika virus infected primary microglia impairs NPCs proliferation and differentiation. Biochemical and Biophysical Research Communications. 2018 Mar 4;497(2):619–25.
- 214. Ades AE, Soriano-Arandes A, Alarcon A, Bonfante F, Thorne C, Peckham CS, et al. Vertical transmission of Zika virus and its outcomes: a Bayesian synthesis of prospective studies.

 The Lancet Infectious Diseases. 2021 Apr 1;21(4):537–45.

- 215. Musso D, Ko Al, Baud D. Zika Virus Infection After the Pandemic. Longo DL, editor. N Engl J Med. 2019 Oct 10;381(15):1444–57.
- 216. Moore CA, Staples JE, Dobyns WB, Pessoa A, Ventura CV, Fonseca EB da, et al. Characterizing the Pattern of Anomalies in Congenital Zika Syndrome for Pediatric Clinicians. JAMA Pediatr. 2017 Mar 1;171(3):288–95.
- 217. Freitas DA, Souza-Santos R, Carvalho LMA, Barros WB, Neves LM, Brasil P, et al.

 Congenital Zika syndrome: A systematic review. PLoS One. 2020;15(12):e0242367.
- 218. Aragao MFVV, Holanda AC, Brainer-Lima AM, Petribu NCL, Castillo M, van der Linden V, et al. Nonmicrocephalic Infants with Congenital Zika Syndrome Suspected Only after Neuroimaging Evaluation Compared with Those with Microcephaly at Birth and Postnatally: How Large Is the Zika Virus "Iceberg"? AJNR Am J Neuroradiol. 2017 July;38(7):1427–34.
- 219. Rice ME, Galang RR, Roth NM, Ellington SR, Moore CA, Valencia-Prado M, et al. Vital Signs: Zika-Associated Birth Defects and Neurodevelopmental Abnormalities Possibly Associated with Congenital Zika Virus Infection U.S. Territories and Freely Associated States, 2018. MMWR Morb Mortal Wkly Rep. 2018 Aug 10;67(31):858–67.
- 220. Nielsen-Saines K, Brasil P, Kerin T, Vasconcelos Z, Gabaglia CR, Damasceno L, et al.

 Delayed childhood neurodevelopment and neurosensory alterations in the second year of life in a prospective cohort of ZIKV-exposed children. Nat Med. 2019 Aug;25(8):1213–7.
- 221. Mulkey SB, Arroyave-Wessel M, Peyton C, Bulas DI, Fourzali Y, Jiang J, et al.

 Neurodevelopmental Abnormalities in Children With In Utero Zika Virus Exposure Without

 Congenital Zika Syndrome. JAMA Pediatr. 2020 Mar;174(3):269–76.
- 222. Mulkey SB, Corn E, Williams ME, Ansusinha E, Podolsky RH, Arroyave-Wessel M, et al.

 Neurodevelopmental Outcomes of Preschoolers with Antenatal Zika Virus Exposure Born in the United States. Pathogens. 2024 July;13(7):542.
- 223. Waechter R, Burgen KS, Punch B, Evans R, Blackmon K, Noël T, et al. Improving neurodevelopment in Zika-exposed children: A randomized controlled trial. PLoS Negl Trop Dis. 2022 Mar;16(3):e0010263.

- 224. de O. da Silva LR, Oliveira P, Sardi S, Soares G, Bandeira AC, Costa R dos S, et al. Zika Virus Congenital Syndrome and MTOR gene variants: insights from a family of dizygotic twins. Heliyon. 2021 Apr 1;7(4):e06878.
- 225. Sobhani NC, Avvad-Portari E, Nascimento ACM, Machado HN, Lobato DSS, Pereira JP, et al. Discordant Zika Virus Findings in Twin Pregnancies Complicated by Antenatal Zika Virus Exposure: A Prospective Cohort. J Infect Dis. 2020 June 1;221(11):1838–45.
- 226. Amaral MS, Goulart E, Caires-Júnior LC, Morales-Vicente DA, Soares-Schanoski A, Gomes RP, et al. Differential gene expression elicited by ZIKV infection in trophoblasts from congenital Zika syndrome discordant twins. PLOS Neglected Tropical Diseases. 2020 Aug 3;14(8):e0008424.
- 227. Romanyuk N, Sintakova K, Arzhanov I, Horak M, Gandhi C, Jhanwar-Uniyal M, et al. mTOR pathway inhibition alters proliferation as well as differentiation of neural stem cells. Front Cell Neurosci [Internet]. 2024 May 15 [cited 2024 Aug 15];18. Available from: https://www.frontiersin.org/journals/cellular-neuroscience/articles/10.3389/fncel.2024.1298182/full
- 228. Liang Q, Luo Z, Zeng J, Chen W, Foo SS, Lee SA, et al. Zika Virus NS4A and NS4B Proteins

 Deregulate Akt-mTOR Signaling in Human Fetal Neural Stem Cells to Inhibit Neurogenesis
 and Induce Autophagy. Cell Stem Cell. 2016;19(5):663–71.
- 229. Lima GP, Rozenbaum D, Pimentel C, Frota ACC, Vivacqua D, Machado ES, et al. Factors associated with the development of Congenital Zika Syndrome: a case-control study. BMC Infect Dis. 2019 Mar 22;19:277.
- 230. Bulstrode H, Girdler GC, Gracia T, Aivazidis A, Moutsopoulos I, Young AMH, et al. Myeloid cell interferon secretion restricts Zika flavivirus infection of developing and malignant human neural progenitor cells. Neuron. 2022 Sept 26;S0896-6273(22)00807-8.
- 231. Halani S, Tombindo PE, O'Reilly R, Miranda RN, Erdman LK, Whitehead C, et al. Clinical manifestations and health outcomes associated with Zika virus infections in adults: A systematic review. PLoS Negl Trop Dis. 2021 July 12;15(7):e0009516.
- 232. Ramond A, Lobkowicz L, Clemente NS, Vaughan A, Turchi MD, Wilder-Smith A, et al. Postnatal symptomatic Zika virus infections in children and adolescents: A systematic review. PLoS Negl Trop Dis. 2020 Oct 2;14(10):e0008612.

- 233. Adachi K, Nielsen-Saines K. Zika Clinical Updates: Implications for Pediatrics. Curr Opin Pediatr. 2018 Feb;30(1):105–16.
- 234. Villar J, Fernandes M, Purwar M, Staines-Urias E, Di Nicola P, Cheikh Ismail L, et al.

 Neurodevelopmental milestones and associated behaviours are similar among healthy children across diverse geographical locations. Nat Commun. 2019 Jan 30;10(1):511.
- 235. Kim J, Erice C, Rohlwink UK, Tucker EW. Infections in the Developing Brain: The Role of the Neuro-Immune Axis. Front Neurol. 2022 Feb 17;13:805786.
- 236. Lannuzel A, Fergé JL, Lobjois Q, Signate A, Rozé B, Tressières B, et al. Long-term outcome in neuroZika: When biological diagnosis matters. Neurology. 2019 May 21;92(21):e2406–20.
- 237. Pacheco O, Newton SM, Daza M, Cates JE, Reales JAM, Burkel VK, et al.

 Neurodevelopmental findings in children 20–30 months of age with postnatal Zika infection at 1–12 months of age, Colombia, September-November 2017. Paediatr Perinat Epidemiol. 2021 Jan;35(1):92–7.
- 238. Aida T, Feng G. The dawn of non-human primate models for neurodevelopmental disorders. Curr Opin Genet Dev. 2020 Dec;65:160–8.
- 239. Mavigner M, Raper J, Kovacs-Balint Z, Gumber S, O'Neal JT, Bhaumik SK, et al. Postnatal Zika virus infection is associated with persistent abnormalities in brain structure, function, and behavior in infant macaques. Sci Transl Med. 2018 Apr 4;10(435):eaao6975.
- 240. Raper J, Kovacs-Balint Z, Mavigner M, Gumber S, Burke MW, Habib J, et al. Long-term alterations in brain and behavior after postnatal Zika virus infection in infant macaques. Nat Commun. 2020 May 21;11(1):2534.
- 241. Sacramento CQ, de Melo GR, de Freitas CS, Rocha N, Hoelz LVB, Miranda M, et al. The clinically approved antiviral drug sofosbuvir inhibits Zika virus replication. Sci Rep. 2017 Jan 18;7:40920.
- 242. Medina A, Rusnak R, Richardson R, Zimmerman MG, Suthar M, Schoof N, et al. Treatment with sofosbuvir attenuates the adverse neurodevelopmental consequences of Zika virus infection in infant rhesus macaques. J Neuroimmunol. 2023 Aug 15;381:578148.

- 243. Zhu Z, Gorman MJ, McKenzie LD, Chai JN, Hubert CG, Prager BC, et al. Zika virus has oncolytic activity against glioblastoma stem cells. J Exp Med. 2017 Oct 2;214(10):2843–57.
- 244. Yang L, Gu X, Yu J, Ge S, Fan X. Oncolytic Virotherapy: From Bench to Bedside. Front Cell Dev Biol. 2021 Nov 26;9:790150.
- 245. Kapulu M, Manda-Taylor L, Balasingam S, Means G, Ayiro Malungu M, Bejon P, et al. Fourth Controlled Human Infection Model (CHIM) meeting CHIMs in endemic countries, May 22–23, 2023. Biologicals. 2024 Feb 1;85:101747.
- 246. Moraes-Pinto MI de, Suano-Souza F, Aranda CS. Immune system: development and acquisition of immunological competence. J Pediatr (Rio J). 2020 Nov 9;97(Suppl 1):S59–66.
- 247. Kollmann TR, Kampmann B, Mazmanian SK, Marchant A, Levy O. Protecting the Newborn and Young Infant from Infectious Diseases: Lessons from Immune Ontogeny. Immunity. 2017 Mar 21;46(3):350–63.
- 248. Guilcher GM, Rivard L, Huang JT, Wright NA, Anderson L, Eissa H, et al. Immune Function in Childhood Cancer Survivors: A Children's Oncology Group Review. Lancet Child Adolesc Health. 2021 Apr;5(4):284–94.
- 249. Kaid C, Goulart E, Caires-Junior LC, Araujo BHS, Soares-Schanoski A, Bueno HMS, et al. Zika Virus Selectively Kills Aggressive Human Embryonal CNS Tumor Cells In Vitro and In Vivo. Cancer Res. 2018 June 15;78(12):3363–74.
- 250. Zhu Z, Mesci P, Bernatchez JA, Gimple RC, Wang X, Schafer ST, et al. Zika Virus Targets Glioblastoma Stem Cells through a SOX2-Integrin ανβ5 Axis. Cell Stem Cell. 2020 Feb;26(2):187-204.e10.
- 251. Mazar J, Li Y, Rosado A, Phelan P, Kedarinath K, Parks GD, et al. Zika virus as an oncolytic treatment of human neuroblastoma cells requires CD24. PLoS ONE. 2018;13(7):e0200358.
- 252. Delafiori J, Lima E de O, Dabaja MZ, Dias-Audibert FL, de Oliveira DN, Melo CFOR, et al. Molecular signatures associated with prostate cancer cell line (PC-3) exposure to inactivated Zika virus. Sci Rep. 2019 Oct 25;9(1):15351.

- 253. Mlera L, Bloom ME. Differential Zika Virus Infection of Testicular Cell Lines. Viruses [Internet]. 2019 Jan 9 [cited 2020 Apr 30];11(1). Available from: https://www.ncbi.nlm.nih.gov/pmc/articles/PMC6356326/
- 254. Novaes GM, Lima C, Longo C, Machado PH, Silva TP, Olberg GG de O, et al. Genetically modified ZIKA virus as a microRNA-sensitive oncolytic virus against central nervous system tumors. Molecular Therapy. 2024 Feb 7;32(2):440–56.
- 255. Silva PB, Rodini CO, Kaid C, Nakahata AM, Pereira MC, Matushita H, et al. Establishment of a novel human medulloblastoma cell line characterized by highly aggressive stem-like cells. Cytotechnology. 2016 Aug;68(4):1545–60.
- 256. Ferreira RO, Granha I, Ferreira RS, Bueno H de S, Okamoto OK, Kaid C, et al. Effect of Serial Systemic and Intratumoral Injections of Oncolytic ZIKVBR in Mice Bearing Embryonal CNS Tumors. Viruses. 2021 Oct 19;13(10):2103.
- 257. Jovanovich N, Habib A, Head J, Hameed F, Agnihotri S, Zinn PO. Pediatric diffuse midline glioma: Understanding the mechanisms and assessing the next generation of personalized therapeutics. Neuro-Oncology Advances. 2023 Jan 1;5(1):vdad040.
- 258. Tosi U, Souweidane M. Diffuse Midline Gliomas: Challenges and New Strategies in a Changing Clinical Landscape. Cancers (Basel). 2024 Jan 2;16(1):219.
- 259. Perez-Roca E, Negreiros T, Casavilca-Zambrano S, Ojeda-Medina L, Díaz-Coronado R. Prognostic factors of pediatric ependymomas at a National Cancer Reference Center in Peru. Front Oncol. 2024 Jan 17;13:1331790.
- 260. Kaid C, Sherwood M, Mitsugi T, Zatz M. Chapter 30 Zika virus as an oncolytic therapy against brain tumors. In: Martin CR, Martin CJH, Preedy VR, Rajendram R, editors. Zika Virus Biology, Transmission, and Pathology [Internet]. Academic Press; 2021 [cited 2021 Nov 9]. p. 327–38. Available from: https://www.sciencedirect.com/science/article/pii/B9780128202685000304
- 261. Kedarinath K, Fox CR, Crowgey E, Mazar J, Phelan P, Westmoreland TJ, et al. CD24 Expression Dampens the Basal Antiviral State in Human Neuroblastoma Cells and Enhances Permissivity to Zika Virus Infection. Viruses. 2022 Aug 6;14(8):1735.
- 262. Mazar J, Brooks JK, Peloquin M, Rosario R, Sutton E, Longo M, et al. The Oncolytic Activity of Zika Viral Therapy in Human Neuroblastoma In Vivo Models Confers a Major Survival

- Advantage in a CD24-dependent Manner. Cancer Research Communications. 2024 Jan 9;4(1):65–80.
- 263. Antonelli M, Poliani PL. Adult type diffuse gliomas in the new 2021 WHO Classification. Pathologica. 2022 Dec;114(6):397.
- 264. Kaid C, Madi RA dos S, Astray R, Goulart E, Caires-Junior LC, Mitsugi TG, et al. Safety, Tumor Reduction, and Clinical Impact of Zika Virus Injection in Dogs with Advanced-Stage Brain Tumors. Molecular Therapy. 2020 May;28(5):1276–86.
- 265. Chen Q, Wu J, Ye Q, Ma F, Zhu Q, Wu Y, et al. Treatment of Human Glioblastoma with a Live Attenuated Zika Virus Vaccine Candidate. mBio. 2018 Sept 18;9(5):10.1128/mbio.01683-18.
- 266. Crane AT, Chrostek MR, Krishna VD, Shiao M, Toman NG, Pearce CM, et al. Zika virus-based immunotherapy enhances long-term survival of rodents with brain tumors through upregulation of memory T-cells. PLoS One [Internet]. 2020 Oct 1 [cited 2020 Dec 14];15(10). Available from: https://www.ncbi.nlm.nih.gov/pmc/articles/PMC7529292/
- 267. Garcia G, Chakravarty N, Paiola S, Urena E, Gyani P, Tse C, et al. Differential Susceptibility of Ex Vivo Primary Glioblastoma Tumors to Oncolytic Effect of Modified Zika Virus. Cells. 2023 Sept 29;12(19):2384.
- 268. Wang S, Zhang Q, Tiwari SK, Lichinchi G, Yau EH, Hui H, et al. Integrin ανβ5 Internalizes
 Zika Virus during Neural Stem Cells Infection and Provides a Promising Target for Antiviral
 Therapy. Cell Reports. 2020 Jan;30(4):969-983.e4.
- 269. Zwernik SD, Adams BH, Raymond DA, Warner CM, Kassam AB, Rovin RA, et al. AXL receptor is required for Zika virus strain MR-766 infection in human glioblastoma cell lines.

 Mol Ther Oncolytics. 2021 Nov 11;23:447–57.
- 270. Srivastava M, Zhang Y, Chen J, Sirohi D, Miller A, Zhang Y, et al. Chemical proteomics tracks virus entry and uncovers NCAM1 as Zika virus receptor. Nat Commun. 2020 Aug 4;11(1):3896.
- 271. Chen L, Zhou C, Chen Q, Shang J, Liu Z, Guo Y, et al. Oncolytic Zika virus promotes intratumoral T cell infiltration and improves immunotherapy efficacy in glioblastoma. Mol Ther Oncolytics. 2022 Mar 17;24:522–34.

- 272. Iannolo G, Sciuto MR, Cuscino N, Pallini R, Douradinha B, Vitiani LR, et al. Zika virus infection induces MiR34c expression in glioblastoma stem cells: new perspectives for brain tumor treatments. Cell Death Dis. 2019 Apr;10(4):263.
- 273. Kao YT, Wang HI, Shie CT, Lin CF, Lai MMC, Yu CY. Zika virus cleaves GSDMD to disseminate prognosticable and controllable oncolysis in a human glioblastoma cell model. Mol Ther Oncolytics. 2023 Mar 16;28:104–17.
- 274. Li H, Hu Y, Huang J, Feng Y, Zhang Z, Zhong K, et al. Zika virus NS5 protein inhibits cell growth and invasion of glioma. Biochemical and Biophysical Research Communications. 2019 Aug;516(2):515–20.
- 275. Garcez PP, Guasti A, Ventura N, Higa LM, Andreiuolo F, de Freitas GPA, et al. Case report: Regression of Glioblastoma after flavivirus infection. Frontiers in Medicine [Internet]. 2023 [cited 2023 June 16];10. Available from: https://www.frontiersin.org/articles/10.3389/fmed.2023.1192070
- 276. Tauziède-Espariat A, Pfister SM, Mawrin C, Sahm F. Pediatric meningiomas: A literature review and diagnostic update. Neuro-Oncology Advances. 2023 May 1;5(Supplement_1):i105–11.
- 277. Nair S, Mazzoccoli L, Jash A, Govero J, Bais SS, Hu T, et al. Zika virus oncolytic activity requires CD8+ T cells and is boosted by immune checkpoint blockade. JCI Insight. 2021 Jan 11;6(1):e144619, 144619.
- 278. Baker C, Shi PY. Construction of Stable Reporter Flaviviruses and Their Applications. Viruses. 2020 Sept 25;12(10):1082.
- 279. Trus I, Berube N, Jiang P, Rak J, Gerdts V, Karniychuk U. Zika Virus with Increased CpG Dinucleotide Frequencies Shows Oncolytic Activity in Glioblastoma Stem Cells. Viruses. 2020 May;12(5):579.
- 280. Victorio CBL, Novera W, Ganasarajah A, Ong J, Thomas M, Wu J, et al. Repurposing of Zika virus live-attenuated vaccine (ZIKV-LAV) strains as oncolytic viruses targeting human glioblastoma multiforme cells. Journal of Translational Medicine. 2024 Feb 2;22(1):126.
- 281. Shan C, Muruato AE, Nunes BTD, Luo H, Xie X, Medeiros DBA, et al. A live-attenuated Zika virus vaccine candidate induces sterilizing immunity in mouse models. Nature Medicine. 2017 Apr;23(6):763–7.

- 282. Kretschmer M, Kadlubowska P, Hoffmann D, Schwalbe B, Auerswald H, Schreiber M.

 Zikavirus prME Envelope Pseudotyped Human Immunodeficiency Virus Type-1 as a Novel

 Tool for Glioblastoma-Directed Virotherapy. Cancers (Basel). 2020 Apr 18;12(4).
- 283. Pöhlking C, Beier S, Formanski JP, Friese M, Schreiber M, Schwalbe B. Isolation of Cells from Glioblastoma Multiforme Grade 4 Tumors for Infection with Zika Virus prME and ME Pseudotyped HIV-1. Int J Mol Sci. 2023 Feb 24;24(5):4467.
- 284. Grunwald V, Ngo HD, Formanski JP, Jonas JS, Pöhlking C, Schwalbe B, et al. Development of Zika Virus E Variants for Pseudotyping Retroviral Vectors Targeting Glioblastoma Cells. Int J Mol Sci. 2023 Sept 23;24(19):14487.
- 285. Xiao J, Liang J, Fan J, Hou P, Li X, Zhang H, et al. CDK4/6 Inhibition Enhances Oncolytic Virus Efficacy by Potentiating Tumor-Selective Cell Killing and T-cell Activation in Refractory Glioblastoma. Cancer Research. 2022 Sept 16;82(18):3359–74.
- 286. Sen A, Prager BC, Zhong C, Park D, Zhu Z, Gimple RC, et al. Leveraging Allele-Specific Expression for Therapeutic Response Gene Discovery in Glioblastoma. Cancer Res. 2022 Feb 1;82(3):377–90.
- 287. Mason CE, Porter SG, Smith TM. Characterizing multi-omic data in systems biology. Adv Exp Med Biol. 2014;799:15–38.
- 288. Jean Beltran PM, Federspiel JD, Sheng X, Cristea IM. Proteomics and integrative omic approaches for understanding host-pathogen interactions and infectious diseases.

 Molecular Systems Biology. 2017;13(3):922.
- 289. Santiago-Rodriguez TM, Hollister EB. Multi 'omic data integration: A review of concepts, considerations, and approaches. Semin Perinatol. 2021 Oct;45(6):151456.
- 290. Janssens S, Schotsaert M, Karnik R, Balasubramaniam V, Dejosez M, Meissner A, et al. Zika Virus Alters DNA Methylation of Neural Genes in an Organoid Model of the Developing Human Brain. mSystems. 2018 Feb;3(1):e00219-17.
- 291. Jiang X, Dong X, Li SH, Zhou YP, Rayner S, Xia HM, et al. Proteomic Analysis of Zika Virus Infected Primary Human Fetal Neural Progenitors Suggests a Role for Doublecortin in the Pathological Consequences of Infection in the Cortex. Front Microbiol [Internet]. 2018 June 5 [cited 2024 Aug 27];9. Available from: https://www.frontiersin.org/journals/microbiology/articles/10.3389/fmicb.2018.01067/full

- 292. Li Y, Muffat J, Javed AO, Keys HR, Lungjangwa T, Bosch I, et al. Genome-wide CRISPR screen for Zika virus resistance in human neural cells. PNAS. 2019 May 7;116(19):9527–32.
- 293. Gratton R, Tricarico PM, Agrelli A, Colaço da Silva HV, Coêlho Bernardo L, Crovella S, et al. In Vitro Zika Virus Infection of Human Neural Progenitor Cells: Meta-Analysis of RNA-Seq Assays. Microorganisms. 2020 Feb 17;8(2):270.
- 294. Anderson D, Neri JICF, Souza CRM, Valverde JG, De Araújo JMG, Nascimento MDSB, et al. Zika Virus Changes Methylation of Genes Involved in Immune Response and Neural Development in Brazilian Babies Born With Congenital Microcephaly. J Infect Dis. 2021 Feb 13;223(3):435–40.
- 295. Nunes E da C, de Filippis AMB, Pereira T do ES, Faria NR da C, Salgado Á, Santos CS, et al.

 Untargeted Metabolomics Insights into Newborns with Congenital Zika Infection.

 Pathogens. 2021 Apr 13;10(4):468.
- 296. Arakawa K, Tomita M. Merging multiple omics datasets in silico: statistical analyses and data interpretation. Methods Mol Biol. 2013;985:459–70.
- 297. Agholme L, Lindström T, Kågedal K, Marcusson J, Hallbeck M. An in vitro model for neuroscience: differentiation of SH-SY5Y cells into cells with morphological and biochemical characteristics of mature neurons. J Alzheimers Dis. 2010;20(4):1069–82.
- 298. D'Aloia A, Pastori V, Blasa S, Campioni G, Peri F, Sacco E, et al. A new advanced cellular model of functional cholinergic-like neurons developed by reprogramming the human SH-SY5Y neuroblastoma cell line. Cell Death Discov. 2024 Jan 12;10(1):1–16.
- 299. Northcott PA, Buchhalter I, Morrissy AS, Hovestadt V, Weischenfeldt J, Ehrenberger T, et al. The whole-genome landscape of medulloblastoma subtypes. Nature. 2017;547(7663):311–7.
- 300. Bernstock JD, Bag AK, Fiveash J, Kachurak K, Elsayed G, Chagoya G, et al. Design and Rationale for First-in-Human Phase 1 Immunovirotherapy Clinical Trial of Oncolytic HSV G207 to Treat Malignant Pediatric Cerebellar Brain Tumors. Hum Gene Ther. 2020 Oct 1;31(19–20):1132–9.
- 301. Macedo N, Miller DM, Haq R, Kaufman HL. Clinical landscape of oncolytic virus research in 2020. J Immunother Cancer. 2020 Oct 1;8(2):e001486.

- 302. Bonenfant G, Meng R, Shotwell C, Badu P, Payne AF, Ciota AT, et al. Asian Zika Virus Isolate Significantly Changes the Transcriptional Profile and Alternative RNA Splicing Events in a Neuroblastoma Cell Line. Viruses. 2020 May;12(5):510.
- 303. Babraham Bioinformatics FastQC A Quality Control tool for High Throughput Sequence Data [Internet]. [cited 2023 Mar 29]. Available from: https://www.bioinformatics.babraham.ac.uk/projects/fastqc/
- 304. LaMar D. FastQC. 2015;
- 305. Kim D, Paggi JM, Park C, Bennett C, Salzberg SL. Graph-based genome alignment and genotyping with HISAT2 and HISAT-genotype. Nat Biotechnol. 2019 Aug;37(8):907–15.
- 306. Danecek P, Bonfield JK, Liddle J, Marshall J, Ohan V, Pollard MO, et al. Twelve years of SAMtools and BCFtools. Gigascience. 2021 Feb 16;10(2):giab008.
- 307. Liao Y, Smyth GK, Shi W. featureCounts: an efficient general purpose program for assigning sequence reads to genomic features. Bioinformatics. 2014 Apr 1;30(7):923–30.
- 308. Love MI, Huber W, Anders S. Moderated estimation of fold change and dispersion for RNA-seq data with DESeq2. Genome Biology. 2014 Dec 5;15(12):550.
- 309. Sherman BT, Hao M, Qiu J, Jiao X, Baseler MW, Lane HC, et al. DAVID: a web server for functional enrichment analysis and functional annotation of gene lists (2021 update).

 Nucleic Acids Res. 2022 Mar 23;50(W1):W216-221.
- 310. Huang DW, Sherman BT, Lempicki RA. Systematic and integrative analysis of large gene lists using DAVID bioinformatics resources. Nat Protoc. 2009;4(1):44–57.
- 311. Gene Ontology Consortium. The Gene Ontology resource: enriching a GOld mine. Nucleic Acids Res. 2021 Jan 8;49(D1):D325–34.
- 312. Ashburner M, Ball CA, Blake JA, Botstein D, Butler H, Cherry JM, et al. Gene ontology: tool for the unification of biology. The Gene Ontology Consortium. Nat Genet. 2000 May;25(1):25–9.
- 313. Kanehisa M. Toward understanding the origin and evolution of cellular organisms. Protein Sci. 2019 Nov;28(11):1947–51.

- 314. Kanehisa M, Goto S. KEGG: kyoto encyclopedia of genes and genomes. Nucleic Acids Res. 2000 Jan 1;28(1):27–30.
- 315. Kanehisa M, Furumichi M, Sato Y, Kawashima M, Ishiguro-Watanabe M. KEGG for taxonomy-based analysis of pathways and genomes. Nucleic Acids Res. 2023 Jan 6;51(D1):D587–92.
- 316. Luo W, Pant G, Bhavnasi YK, Blanchard SG Jr, Brouwer C. Pathview Web: user friendly pathway visualization and data integration. Nucleic Acids Research. 2017 July 3;45(W1):W501–8.
- 317. Orchard S, Ammari M, Aranda B, Breuza L, Briganti L, Broackes-Carter F, et al. The MIntAct project—IntAct as a common curation platform for 11 molecular interaction databases.

 Nucleic Acids Res. 2014 Jan 1;42(Database issue):D358–63.
- 318. Scaturro P, Stukalov A, Haas DA, Cortese M, Draganova K, Płaszczyca A, et al. An orthogonal proteomic survey uncovers novel Zika virus host factors. Nature. 2018 Sept;561(7722):253–7.
- 319. Szklarczyk D, Gable AL, Lyon D, Junge A, Wyder S, Huerta-Cepas J, et al. STRING v11: protein-protein association networks with increased coverage, supporting functional discovery in genome-wide experimental datasets. Nucleic Acids Res. 2019 Jan 8;47(D1):D607–13.
- 320. Shannon P, Markiel A, Ozier O, Baliga NS, Wang JT, Ramage D, et al. Cytoscape: a software environment for integrated models of biomolecular interaction networks. Genome Res. 2003 Nov;13(11):2498–504.
- 321. Savidis G, McDougall WM, Meraner P, Perreira JM, Portmann JM, Trincucci G, et al. Identification of Zika Virus and Dengue Virus Dependency Factors using Functional Genomics. Cell Rep. 2016 June 28;16(1):232–46.
- 322. Pereira R, Costa V, Gomes G, Campana P, Pádua R, Barbosa M, et al. Anti-Zika virus activity of plant extracts containing polyphenols and triterpenes on Vero CCL-81 and human neuroblastoma SH-SY5Y cells. Chem Biodivers. 2022 Mar 13;
- 323. Anfasa F, Siegers JY, van der Kroeg M, Mumtaz N, Stalin Raj V, de Vrij FMS, et al. Phenotypic Differences between Asian and African Lineage Zika Viruses in Human Neural Progenitor Cells. mSphere. 2017 Aug;2(4).

- 324. Jorgačevski J, Korva M, Potokar M, Lisjak M, Avšič-Županc T, Zorec R. ZIKV Strains

 Differentially Affect Survival of Human Fetal Astrocytes versus Neurons and Traffic of ZIKVLaden Endocytotic Compartments. Sci Rep. 2019 May 30;9(1):8069.
- 325. Hu H, Zhang W, Huang D, Wang Y, Zhang Y, Yi Y, et al. Clinical characteristics, treatment and prognosis of paediatric patients with metastatic neuroblastoma to the brain. Clinical Neurology and Neurosurgery. 2019 Sept 1;184:105372.
- 326. Wen F, Armstrong N, Hou W, Cruz-Cosme R, Obwolo LA, Ishizuka K, et al. Zika virus increases mind bomb 1 levels, causing degradation of pericentriolar material 1 (PCM1) and dispersion of PCM1-containing granules from the centrosome. J Biol Chem. 2019 Dec 6;294(49):18742–55.
- 327. Gazon H, Barbeau B, Mesnard JM, Peloponese JM. Hijacking of the AP-1 Signaling Pathway during Development of ATL. Frontiers in Microbiology [Internet]. 2018 [cited 2022 Mar 29];8. Available from: https://www.frontiersin.org/article/10.3389/fmicb.2017.02686
- 328. Atsaves V, Leventaki V, Rassidakis GZ, Claret FX. AP-1 Transcription Factors as Regulators of Immune Responses in Cancer. Cancers (Basel). 2019 July 23;11(7):E1037.
- 329. Lima MC, Mendonça LR de, Rezende AM, Carrera RM, Aníbal-Silva CE, Demers M, et al.

 The Transcriptional and Protein Profile From Human Infected Neuroprogenitor Cells Is

 Strongly Correlated to Zika Virus Microcephaly Cytokines Phenotype Evidencing a

 Persistent Inflammation in the CNS. Front Immunol [Internet]. 2019 [cited 2020 July 9];10.

 Available from: https://www.frontiersin.org/articles/10.3389/fimmu.2019.01928/full
- 330. Braz-De-Melo HA, Pasquarelli-do-Nascimento G, Corrêa R, das Neves Almeida R, de Oliveira Santos I, Prado PS, et al. Potential neuroprotective and anti-inflammatory effects provided by omega-3 (DHA) against Zika virus infection in human SH-SY5Y cells. Sci Rep. 2019 Dec 27;9(1):20119.
- 331. Parker JN, Meleth S, Hughes KB, Gillespie GY, Whitley RJ, Markert JM. Enhanced inhibition of syngeneic murine tumors by combinatorial therapy with genetically engineered HSV-1 expressing CCL2 and IL-12. Cancer Gene Ther. 2005 Apr;12(4):359–68.
- 332. Osuna-Ramos JF, Reyes-Ruiz JM, del Ángel RM. The Role of Host Cholesterol During Flavivirus Infection. Front Cell Infect Microbiol. 2018 Nov 2;8:388.

- 333. Raini SK, Takamatsu Y, Dumre SP, Urata S, Mizukami S, Moi ML, et al. The novel therapeutic target and inhibitory effects of PF-429242 against Zika virus infection. Antiviral Res. 2021 Aug;192:105121.
- 334. Weber LW, Boll M, Stampfl A. Maintaining cholesterol homeostasis: Sterol regulatory element-binding proteins. World J Gastroenterol. 2004 Nov 1;10(21):3081–7.
- 335. Sabino C, Basic M, Bender D, Elgner F, Himmelsbach K, Hildt E. Bafilomycin A1 and U18666A Efficiently Impair ZIKV Infection. Viruses. 2019 June 6;11(6):E524.
- 336. Grefhorst A, Elzinga BM, Voshol PJ, Plösch T, Kok T, Bloks VW, et al. Stimulation of lipogenesis by pharmacological activation of the liver X receptor leads to production of large, triglyceride-rich very low density lipoprotein particles. J Biol Chem. 2002 Sept 13;277(37):34182–90.
- 337. Gladwyn-Ng I, Cordón-Barris L, Alfano C, Creppe C, Couderc T, Morelli G, et al. Stress-induced unfolded protein response contributes to Zika virus–associated microcephaly.

 Nat Neurosci. 2018 Jan;21(1):63–71.
- 338. Tan Z, Zhang W, Sun J, Fu Z, Ke X, Zheng C, et al. ZIKV infection activates the IRE1-XBP1 and ATF6 pathways of unfolded protein response in neural cells. J Neuroinflammation [Internet]. 2018 Sept 21 [cited 2020 Apr 30];15. Available from: https://www.ncbi.nlm.nih.gov/pmc/articles/PMC6151056/
- 339. Carr M, Gonzalez G, Martinelli A, Wastika CE, Ito K, Orba Y, et al. Upregulated expression of the antioxidant sestrin 2 identified by transcriptomic analysis of Japanese encephalitis virus-infected SH-SY5Y neuroblastoma cells. Virus Genes. 2019 Oct 1;55(5):630–42.
- 340. Ngo AM, Shurtleff MJ, Popova KD, Kulsuptrakul J, Weissman JS, Puschnik AS. The ER membrane protein complex is required to ensure correct topology and stable expression of flavivirus polyproteins. eLife. 8:e48469.
- 341. Barrows NJ, Anglero-Rodriguez Y, Kim B, Jamison SF, Le Sommer C, McGee CE, et al. Dual roles for the ER membrane protein complex in flavivirus infection: viral entry and protein biogenesis. Sci Rep. 2019 July 4;9(1):9711.
- 342. Lin DL, Inoue T, Chen YJ, Chang A, Tsai B, Tai AW. The ER Membrane Protein Complex Promotes Biogenesis of Dengue and Zika Virus Non-structural Multi-pass Transmembrane Proteins to Support Infection. Cell Reports. 2019 May;27(6):1666-1674.e4.

- 343. Mangieri LR, Mader BJ, Thomas CE, Taylor CA, Luker AM, Tse TE, et al. ATP6V0C Knockdown in Neuroblastoma Cells Alters Autophagy-Lysosome Pathway Function and Metabolism of Proteins that Accumulate in Neurodegenerative Disease. PLOS ONE. 2014 Apr 2;9(4):e93257.
- 344. Owczarek K, Chykunova Y, Jassoy C, Maksym B, Rajfur Z, Pyrc K. Zika virus: mapping and reprogramming the entry. Cell Communication and Signaling. 2019 May 3;17(1):41.
- 345. Han X, Wang J, Yang Y, Qu S, Wan F, Zhang Z, et al. Zika Virus Infection Induced Apoptosis by Modulating the Recruitment and Activation of Proapoptotic Protein Bax. Journal of Virology [Internet]. 2021 Mar 25 [cited 2021 Apr 7];95(8). Available from: https://jvi.asm.org/content/95/8/e01445-20
- 346. Braunger K, Pfeffer S, Shrimal S, Gilmore R, Berninghausen O, Mandon EC, et al. Structural basis for coupling of protein transport and N-glycosylation at the mammalian endoplasmic reticulum. Science. 2018 Apr 13;360(6385):215–9.
- 347. Puschnik AS, Marceau CD, Ooi YS, Majzoub K, Rinis N, Contessa JN, et al. A small molecule oligosaccharyltransferase inhibitor with pan-flaviviral activity. Cell Rep. 2017 Dec 12;21(11):3032–9.
- 348. Monel B, Compton AA, Bruel T, Amraoui S, Burlaud-Gaillard J, Roy N, et al. Zika virus induces massive cytoplasmic vacuolization and paraptosis-like death in infected cells. EMBO J. 2017 June 14;36(12):1653–68.
- 349. Mendonça-Vieira LR de, Aníbal-Silva CE, Menezes-Neto A, Azevedo E de AN, Zanluqui NG, Peron JPS, et al. Reactive Oxygen Species (ROS) Are Not a Key Determinant for Zika Virus-Induced Apoptosis in SH-SY5Y Neuroblastoma Cells. Viruses. 2021 Oct 20;13(11):2111.
- 350. Hughes BW, Addanki KC, Sriskanda AN, McLean E, Bagasra O. Infectivity of Immature Neurons to Zika Virus: A Link to Congenital Zika Syndrome. EBioMedicine. 2016 June 23;10:65–70.
- 351. Hou W, Armstrong N, Obwolo LA, Thomas M, Pang X, Jones KS, et al. Determination of the Cell Permissiveness Spectrum, Mode of RNA Replication, and RNA-Protein Interaction of Zika Virus. BMC Infect Dis [Internet]. 2017 Mar 31 [cited 2020 May 1];17. Available from: https://www.ncbi.nlm.nih.gov/pmc/articles/PMC5374689/

- 352. Castro FL, Geddes VEV, Monteiro FLL, Gonçalves RMDT, Campanati L, Pezzuto P, et al. MicroRNAs 145 and 148a Are Upregulated During Congenital Zika Virus Infection. ASN Neuro. 2019 Jan;11:175909141985098.
- 353. Sánchez-San Martín C, Li T, Bouquet J, Streithorst J, Yu G, Paranjpe A, et al. Differentiation enhances Zika virus infection of neuronal brain cells. Sci Rep [Internet]. 2018 Sept 28 [cited 2020 Apr 30];8. Available from: https://www.ncbi.nlm.nih.gov/pmc/articles/PMC6162312/
- 354. Bos S, Viranaicken W, Turpin J, El-Kalamouni C, Roche M, Krejbich-Trotot P, et al. The structural proteins of epidemic and historical strains of Zika virus differ in their ability to initiate viral infection in human host cells. Virology. 2018 Mar 1;516:265–73.
- 355. Giel-Moloney M, Goncalvez AP, Catalan J, Lecouturier V, Girerd-Chambaz Y, Diaz F, et al. Chimeric yellow fever 17D-Zika virus (ChimeriVax-Zika) as a live-attenuated Zika virus vaccine. Sci Rep [Internet]. 2018 Sept 4 [cited 2020 Apr 30];8. Available from: https://www.ncbi.nlm.nih.gov/pmc/articles/PMC6123396/
- 356. Himmelsbach K, Hildt E. Identification of various cell culture models for the study of Zika virus. World J Virol. 2018 Feb 12;7(1):10–20.
- 357. Alpuche-Lazcano SP, McCullogh CR, Del Corpo O, Rance E, Scarborough RJ, Mouland AJ, et al. Higher Cytopathic Effects of a Zika Virus Brazilian Isolate from Bahia Compared to a Canadian-Imported Thai Strain. Viruses [Internet]. 2018 Jan 27 [cited 2020 Apr 30];10(2). Available from: https://www.ncbi.nlm.nih.gov/pmc/articles/PMC5850360/
- 358. ClinicalTrials.gov [Internet]. 2024 [cited 2024 Aug 28]. Available from: https://clinicaltrials.gov/
- 359. Li H, Saucedo-Cuevas L, Regla-Nava JA, Chai G, Sheets N, Tang W, et al. Zika Virus Infects
 Neural Progenitors in the Adult Mouse Brain and Alters Proliferation. Cell Stem Cell. 2016
 Nov 3;19(5):593–8.
- 360. Quincozes-Santos A, Bobermin LD, Costa NLF, Thomaz NK, Almeida RR de S, Beys-da-Silva WO, et al. The role of glial cells in Zika virus-induced neurodegeneration. Glia. 2023;71(8):1791–803.

- 361. Figueiredo CP, Barros-Aragão FGQ, Neris RLS, Frost PS, Soares C, Souza INO, et al. Zika virus replicates in adult human brain tissue and impairs synapses and memory in mice.

 Nat Commun. 2019 Sept 5;10:3890.
- 362. Sherwood M, Zhou Y, Sui Y, Wang Y, Skipp P, Kaid C, et al. Integrated re-analysis of transcriptomic and proteomic datasets reveals potential mechanisms for Zika viral-based oncolytic therapy in neuroblastoma. F1000Res. 2024 May 21;12:719.
- 363. Ma J, Ramachandran M, Jin C, Quijano-Rubio C, Martikainen M, Yu D, et al.

 Characterization of virus-mediated immunogenic cancer cell death and the consequences for oncolytic virus-based immunotherapy of cancer. Cell Death Dis. 2020 Jan 22;11(1):1–15.
- 364. Lánczky A, Győrffy B. Web-Based Survival Analysis Tool Tailored for Medical Research (KMplot): Development and Implementation. J Med Internet Res. 2021 July 26;23(7):e27633.
- 365. Han Y, Wang Y, Dong X, Sun D, Liu Z, Yue J, et al. TISCH2: expanded datasets and new tools for single-cell transcriptome analyses of the tumor microenvironment. Nucleic Acids Res. 2023 Jan 6;51(D1):D1425–31.
- 366. Riemondy KA, Venkataraman S, Willard N, Nellan A, Sanford B, Griesinger AM, et al. Neoplastic and immune single-cell transcriptomics define subgroup-specific intratumoral heterogeneity of childhood medulloblastoma. Neuro Oncol. 2022 Feb 1;24(2):273–86.
- 367. Subramanian A, Tamayo P, Mootha VK, Mukherjee S, Ebert BL, Gillette MA, et al. Gene set enrichment analysis: a knowledge-based approach for interpreting genome-wide expression profiles. Proc Natl Acad Sci U S A. 2005 Oct 25;102(43):15545–50.
- 368. Cui A, Huang T, Li S, Ma A, Pérez JL, Sander C, et al. Dictionary of immune responses to cytokines at single-cell resolution. Nature. 2024 Jan;625(7994):377–84.
- 369. Kolberg L, Raudvere U, Kuzmin I, Adler P, Vilo J, Peterson H. g:Profiler—interoperable web service for functional enrichment analysis and gene identifier mapping (2023 update).

 Nucleic Acids Research. 2023 July 5;51(W1):W207–12.

- 370. Showalter A, Limaye A, Oyer JL, Igarashi R, Kittipatarin C, Copik AJ, et al. Cytokines in Immunogenic Cell Death: Applications for Cancer Immunotherapy. Cytokine. 2017 June 22;97:123.
- 371. Alim LF, Keane C, Souza-Fonseca-Guimaraes F. Molecular mechanisms of tumour necrosis factor signalling via TNF receptor 1 and TNF receptor 2 in the tumour microenvironment. Current Opinion in Immunology. 2024 Feb 1;86:102409.
- 372. Al-Bahrani M, Asavarut P, Waramit S, Suwan K, Hajitou A. Transmorphic phage-guided systemic delivery of TNFα gene for the treatment of human pediatric medulloblastoma. The FASEB Journal. 2023 June 18;37(7):e23038.
- 373. Dufay N, Reboul A, Touraine-Moulin F, Belin MF, Giraudon P. Soluble Factors, Including TNFα, Secreted by Human T Cells are Both Cytotoxic and Cytostatic for Medulloblastoma Cells. J Neurooncol. 1999 June 1;43(2):115–26.
- 374. Gong B, Guo D, Zheng C, Ma Z, Zhang J, Qu Y, et al. Complement C3a activates astrocytes to promote medulloblastoma progression through TNF-α. Journal of Neuroinflammation. 2022 June 20;19:159.
- 375. Valenzuela-Cardenas M, Gowan C, Dryja P, Bartee MY, Bartee E. TNF blockade enhances the efficacy of myxoma virus-based oncolytic virotherapy. J Immunother Cancer. 2022 May 16;10(5):e004770.
- 376. Christie JD, Appel N, Canter H, Achi JG, Elliott NM, Matos AL de, et al. Systemic delivery of TNF-armed myxoma virus plus immune checkpoint inhibitor eliminates lung metastatic mouse osteosarcoma. Molecular Therapy Oncolytics. 2021 Aug 6;22:539.
- 377. Su Z, Dhusia K, Wu Y. Understanding the functional role of membrane confinements in TNF-mediated signaling by multiscale simulations. Commun Biol. 2022 Mar 11;5(1):1–11.
- 378. Xu H, Cheng M, Chi X, Liu X, Zhou J, Lin T, et al. High-Throughput Screening Identifies

 Mixed-Lineage Kinase 3 as a Key Host Regulatory Factor in Zika Virus Infection. J Virol. 2019

 Sept 15;93(18):e00758-19.
- 379. Meisen WH, Wohleb ES, Jaime-Ramirez AC, Bolyard C, Yoo JY, Russell L, et al. The Impact of Macrophage- and Microglia-Secreted TNFα on Oncolytic HSV-1 Therapy in the Glioblastoma Tumor Microenvironment. Clinical Cancer Research. 2015 July 14;21(14):3274–85.

- 380. Pol JG, Workenhe ST, Konda P, Gujar S, Kroemer G. Cytokines in oncolytic virotherapy. Cytokine Growth Factor Rev. 2020 Dec;56:4–27.
- 381. Castro F, Cardoso AP, Gonçalves RM, Serre K, Oliveira MJ. Interferon-Gamma at the Crossroads of Tumor Immune Surveillance or Evasion. Frontiers in Immunology. 2018 May 4;9:847.
- 382. Hofman L, Lawler SE, Lamfers MLM. The Multifaceted Role of Macrophages in Oncolytic Virotherapy. Viruses. 2021 Aug 9;13(8):1570.
- 383. Chen S, Saeed AFUH, Liu Q, Jiang Q, Xu H, Xiao GG, et al. Macrophages in immunoregulation and therapeutics. Sig Transduct Target Ther. 2023 May 22;8(1):1–35.
- 384. Mantovani A, Allavena P, Marchesi F, Garlanda C. Macrophages as tools and targets in cancer therapy. Nat Rev Drug Discov. 2022 Nov;21(11):799–820.
- 385. Montoya ML, Kasahara N, Okada H. Introduction to immunotherapy for brain tumor patients: challenges and future perspectives. Neuro-Oncology Practice. 2020 Sept 25;7(5):465–76.
- 386. Ghajar-Rahimi G, Kang KD, Totsch SK, Gary S, Rocco A, Blitz S, et al. Clinical Advances in Oncolytic Virotherapy for Pediatric Brain Tumors. Pharmacol Ther. 2022 Nov;239:108193.
- 387. Lin D, Shen Y, Liang T. Oncolytic virotherapy: basic principles, recent advances and future directions. Sig Transduct Target Ther. 2023 Apr 11;8(1):1–29.
- 388. Chen L, Flies DB. Molecular mechanisms of T cell co-stimulation and co-inhibition. Nat Rev Immunol. 2013 Apr;13(4):227–42.
- 389. Nicholas B, Bailey A, Staples KJ, Wilkinson T, Elliott T, Skipp P. Immunopeptidomic analysis of influenza A virus infected human tissues identifies internal proteins as a rich source of HLA ligands. PLOS Pathogens. 2022 Jan 20;18(1):e1009894.
- 390. Subramanian A, Kuehn H, Gould J, Tamayo P, Mesirov JP. GSEA-P: a desktop application for Gene Set Enrichment Analysis. Bioinformatics. 2007 Dec 1;23(23):3251–3.
- 391. Wisniewski JR, Hein MY, Cox J, Mann M. A "proteomic ruler" for protein copy number and concentration estimation without spike-in standards. Mol Cell Proteomics. 2014;13(12):3497–506.

- 392. Jessen LE. PepTools An R-package for making immunoinformatics accessible [Internet]. 2018. Available from: https://github.com/leonjessen/PepTools
- 393. R Core Team. R: A language and environment for statistical computing [Internet]. Vienna, Austria; 2018. Available from: https://www.R-project.org/
- 394. Wickham H, Averick M, Bryan J, Chang W, McGowan LD, François R, et al. Welcome to the tidyverse. Journal of Open Source Software. 2019;4(43):1686.
- 395. Pedersen TL. patchwork: The composer of plots [Internet]. 2019. Available from: https://CRAN.R-project.org/package=patchwork
- 396. Bailey A, Nicholas B, Darley R, Parkinson E, Teo Y, Aleksic M, et al. Characterization of the Class I MHC Peptidome Resulting from DNCB Exposure of HaCaT Cells. Toxicol Sci [Internet]. 2020; Available from: https://www.ncbi.nlm.nih.gov/pubmed/33372950
- 397. Tran NH, Rahman MZ, He L, Xin L, Shan B, Li M. Complete De Novo Assembly of Monoclonal Antibody Sequences. Scientific Reports [Internet]. 2016 Aug 26;6(1). Available from: http://dx.doi.org/10.1038/srep31730
- 398. Andreatta M, Nicastri A, Peng X, Hancock G, Dorrell L, Ternette N, et al. MS-Rescue: A Computational Pipeline to Increase the Quality and Yield of Immunopeptidomics Experiments. PROTEOMICS. 2019;19(4):1800357.
- 399. Bassani-Sternberg M, Gfeller D. Unsupervised HLA Peptidome Deconvolution Improves
 Ligand Prediction Accuracy and Predicts Cooperative Effects in Peptide-HLA Interactions.

 J Immunol. 2016;197(6):2492–9.
- 400. Racle J, Michaux J, Rockinger GA, Arnaud M, Bobisse S, Chong C, et al. Robust prediction of HLA class II epitopes by deep motif deconvolution of immunopeptidomes. Nature Biotechnology. 2019 Nov;37(11):1283–6.
- 401. Nielsen M, Lundegaard C, Worning P, Lauemoller SL, Lamberth K, Buus S, et al. Reliable prediction of T-cell epitopes using neural networks with novel sequence representations. Protein Sci. 2003;12(5):1007–17.
- 402. Andreatta M, Nielsen M. Gapped sequence alignment using artificial neural networks: application to the MHC class I system. Bioinformatics (Oxford, England). 2016 Feb;32(4):511–7.

- 403. Reynisson B, Barra C, Kaabinejadian S, Hildebrand WH, Peters B, Nielsen M. Improved prediction of MHC II antigen presentation through integration and motif deconvolution of mass spectrometry MHC eluted ligand data. Journal of proteome research. 2020 June;19(6):2304–15.
- 404. Calis JJA, Maybeno M, Greenbaum JA, Weiskopf D, De Silva AD, Sette A, et al. Properties of MHC Class I Presented Peptides That Enhance Immunogenicity. PLoS Comput Biol. 2013 Oct 24;9(10):e1003266.
- 405. Marrama D, Chronister WD, Westernberg L, Vita R, Koşaloğlu-Yalçın Z, Sette A, et al. PEPMatch: a tool to identify short peptide sequence matches in large sets of proteins. BMC Bioinformatics. 2023 Dec 18;24(1):485.
- 406. Bui HH, Sidney J, Dinh K, Southwood S, Newman MJ, Sette A. Predicting population coverage of T-cell epitope-based diagnostics and vaccines. BMC Bioinformatics. 2006 Mar 17;7:153.
- 407. Gonzalez-Galarza FF, McCabe A, Santos EJM dos, Jones J, Takeshita L, Ortega-Rivera ND, et al. Allele frequency net database (AFND) 2020 update: gold-standard data classification, open access genotype data and new query tools. Nucleic Acids Research [Internet]. 2019 Nov 13; Available from: http://dx.doi.org/10.1093/nar/gkz1029
- 408. Rock KL, Reits E, Neefjes J. Present Yourself! By MHC Class I and MHC Class II Molecules.

 Trends in Immunology. 2016 Nov 1;37(11):724–37.
- 409. Cornel AM, Mimpen IL, Nierkens S. MHC Class I Downregulation in Cancer: Underlying Mechanisms and Potential Targets for Cancer Immunotherapy. Cancers (Basel). 2020 July 2;12(7):1760.
- 410. Sher AA, Lao YT, Coombs KM. HLA-A, HSPA5, IGFBP5 and PSMA2 Are Restriction Factors for Zika Virus Growth in Astrocytic Cells. Viruses. 2022 Dec 29;15(1):97.
- 411. Marcu A, Schlosser A, Keupp A, Trautwein N, Johann P, Wölfl M, et al. Natural and cryptic peptides dominate the immunopeptidome of atypical teratoid rhabdoid tumors. J Immunother Cancer. 2021 Oct 1;9(10):e003404.
- 412. Crooke SN, Ovsyannikova IG, Kennedy RB, Poland GA. Identification of naturally processed Zika virus peptides by mass spectrometry and validation of memory T cell recall responses in Zika convalescent subjects. PLOS ONE. 2021 June 2;16(6):e0252198.

- 413. Eickhoff CS, Meza KA, Terry FE, Colbert CG, Blazevic A, Gutiérrez AH, et al. Identification of immunodominant T cell epitopes induced by natural Zika virus infection. Front Immunol. 2023;14:1247876.
- 414. Tarbe M, Dong W, Hu G, Xu Y, Sun J, Grayo S, et al. Japanese Encephalitis Virus Vaccination Elicits Cross-Reactive HLA-Class I-Restricted CD8 T Cell Response Against Zika Virus Infection. Front Immunol. 2020 Sept 25;11:577546.
- 415. Súkeníková L, Mallone A, Schreiner B, Ripellino P, Nilsson J, Stoffel M, et al. Autoreactive T cells target peripheral nerves in Guillain–Barré syndrome. Nature. 2024 Feb;626(7997):160–8.
- 416. Marotel M, Hasim MS, Hagerman A, Ardolino M. The two-faces of NK cells in oncolytic virotherapy. Cytokine & Growth Factor Reviews. 2020 Dec 1;56:59–68.
- 417. Polonio CM, da Silva P, Russo FB, Hyppolito BRN, Zanluqui NG, Benazzato C, et al. microRNAs Control Antiviral Immune Response, Cell Death and Chemotaxis Pathways in Human Neuronal Precursor Cells (NPCs) during Zika Virus Infection. Int J Mol Sci. 2022 Sept 7;23(18):10282.
- 418. Fujimura K, Guise AJ, Nakayama T, Schlaffner CN, Meziani A, Kumar M, et al. Integrative systems biology characterizes immune-mediated neurodevelopmental changes in murine Zika virus microcephaly. iScience. 2023 July 21;26(7):106909.
- 419. Dowd KA, DeMaso CR, Pelc RS, Speer SD, Smith ARY, Goo L, et al. Broadly Neutralizing Activity of Zika Virus-Immune Sera Identifies a Single Viral Serotype. Cell Rep. 2016 Aug 9;16(6):1485–91.
- 420. Naiyer MM, Cassidy SA, Magri A, Cowton V, Chen K, Mansour S, et al. KIR2DS2 recognizes conserved peptides derived from viral helicases in the context of HLA-C. Science Immunology. 2017;2(15).
- 421. Herrera BB, Tsai WY, Chang CA, Hamel DJ, Wang WK, Lu Y, et al. Sustained Specific and Cross-Reactive T Cell Responses to Zika and Dengue Virus NS3 in West Africa. J Virol. 2018

 Mar 14;92(7):e01992-17.
- 422. Elong Ngono A, Syed T, Nguyen AV, Regla-Nava JA, Susantono M, Spasova D, et al. CD8+ T cells mediate protection against Zika virus induced by an NS3-based vaccine. Science Advances. 2020 Nov 4;6(45):eabb2154.

- 423. Haque MT, Shah MNA, Paul S, Khan MK, Barua P. Zika viral proteome analysis reveals an epitope cluster within NS3 helicase as a potential vaccine candidate: An in silico study. Informatics in Medicine Unlocked. 2020;21:100434.
- 424. Paul D, Sharif IH, Sayem A, Ahmed H, Saleh MdA, Mahmud S. In silico prediction of a highly immunogenic and conserved epitope against Zika Virus. Informatics in Medicine Unlocked. 2021 Jan 1;24:100613.
- 425. Braz J de M, Batista MV de A. Immunoinformatics-Based Design of Multi-epitope DNA and mRNA Vaccines Against Zika Virus. Bioinform Biol Insights. 2024 Jan 1;18:11779322241257037.
- 426. Antonelli ACB, Almeida VP, de Castro FOF, Silva JM, Pfrimer IAH, Cunha-Neto E, et al. In silico construction of a multiepitope Zika virus vaccine using immunoinformatics tools. Sci Rep. 2022 Jan 7;12(1):53.
- 427. Barker DJ, Maccari G, Georgiou X, Cooper MA, Flicek P, Robinson J, et al. The IPD-IMGT/HLA Database. Nucleic Acids Research. 2023 Jan 6;51(D1):D1053–60.
- 428. Vita R, Blazeska N, Marrama D, IEDB Curation Team Members, Duesing S, Bennett J, et al. The Immune Epitope Database (IEDB): 2024 update. Nucleic Acids Res. 2025 Jan 6;53(D1):D436–43.
- 429. DePeaux K, Delgoffe GM. Integrating innate and adaptive immunity in oncolytic virus therapy. Trends in Cancer. 2024 Feb 1;10(2):135–46.
- 430. Dai L, Xu K, Li J, Huang Q, Song J, Han Y, et al. Protective Zika vaccines engineered to eliminate enhancement of dengue infection via immunodominance switch. Nat Immunol. 2021 Aug;22(8):958–68.
- 431. Jh C, G F, S J. Measurement of cytokine release at the single cell level using the ELISPOT assay. Methods (San Diego, Calif) [Internet]. 2006 Apr [cited 2024 Sept 18];38(4). Available from: https://pubmed.ncbi.nlm.nih.gov/16473524/
- 432. Webb MJ, Sangsuwannukul T, van Vloten J, Evgin L, Kendall B, Tonne J, et al. Expression of tumor antigens within an oncolytic virus enhances the anti-tumor T cell response. Nat Commun. 2024 June 27;15(1):5442.

- 433. Feola S, Russo S, Martins B, Lopes A, Vandermeulen G, Fluhler V, et al. Peptides-Coated Oncolytic Vaccines for Cancer Personalized Medicine. Front Immunol. 2022;13:826164.
- 434. Han Y, Tian X, Zhai J, Zhang Z. Clinical application of immunogenic cell death inducers in cancer immunotherapy: turning cold tumors hot. Front Cell Dev Biol [Internet]. 2024 May 7 [cited 2025 Sept 27];12. Available from: https://www.frontiersin.org/journals/cell-and-developmental-biology/articles/10.3389/fcell.2024.1363121/full
- 435. Bailey S, Jacobs S, Kourti M, Massimino M, Andre N, Doz F, et al. Medulloblastoma therapy: Consensus treatment recommendations from SIOP-Europe and the European Reference Network. EJC Paediatric Oncology. 2025 June 1;5:100205.
- 436. Krystal J, Foster JH. Treatment of High-Risk Neuroblastoma. Children (Basel). 2023 July 28;10(8):1302.
- 437. Dasari S, Tchounwou PB. Cisplatin in cancer therapy: molecular mechanisms of action. Eur J Pharmacol. 2014 Oct 5;740:364–78.
- 438. Li G, Che X, Wang S, Liu D, Xie D, Jiang B, et al. The role of cisplatin in modulating the tumor immune microenvironment and its combination therapy strategies: a new approach to enhance anti-tumor efficacy. Ann Med. 2025;57(1):2447403.
- 439. Leda AR, Bertrand L, Andras IE, El-Hage N, Nair M, Toborek M. Selective Disruption of the Blood-Brain Barrier by Zika Virus. Front Microbiol. 2019;10:2158.
- 440. Hagiwara F, Omata D, Munakata L, Kageyama S, Maruyama K, Kudo N, et al. Brain Delivery of Cisplatin Using Microbubbles in Combination with Ultrasound as an Effective Therapy for Glioblastoma. Pharmaceuticals (Basel). 2023 Nov 13;16(11):1599.
- 441. Michel J, Langstein J, Hofstädter F, Schwarz H. A soluble form of CD137 (ILA/4-1BB), a member of the TNF receptor family, is released by activated lymphocytes and is detectable in sera of patients with rheumatoid arthritis. Eur J Immunol. 1998

 Jan;28(1):290–5.
- 442. Labiano S, Palazón A, Bolaños E, Azpilikueta A, Sánchez-Paulete AR, Morales-Kastresana A, et al. Hypoxia-induced soluble CD137 in malignant cells blocks CD137L-costimulation as an immune escape mechanism. Oncolmmunology. 2016 Jan 2;5(1):e1062967.

- 443. J W, Y W. Role of TNFSF9 bidirectional signal transduction in antitumor immunotherapy.

 European journal of pharmacology [Internet]. 2022 May 8 [cited 2024 May 9];928. Available from: https://pubmed.ncbi.nlm.nih.gov/35714694/
- 444. Voloshin N, Tyurin-Kuzmin P, Karagyaur M, Akopyan Z, Kulebyakin K. Practical Use of Immortalized Cells in Medicine: Current Advances and Future Perspectives. Int J Mol Sci. 2023 Aug 12;24(16):12716.
- 445. Tzec-Interián JA, González-Padilla D, Góngora-Castillo EB. Bioinformatics perspectives on transcriptomics: A comprehensive review of bulk and single-cell RNA sequencing analyses. Quantitative Biology. 2025;13(2):e78.
- 446. Mun DG, Bhat FA, Ding H, Madden BJ, Natesampillai S, Badley AD, et al. Optimizing single cell proteomics using trapped ion mobility spectrometry for label-free experiments.

 Analyst. 2023 July 26;148(15):3466–75.
- 447. Edfors F, Danielsson F, Hallström BM, Käll L, Lundberg E, Pontén F, et al. Gene-specific correlation of RNA and protein levels in human cells and tissues. Mol Syst Biol. 2016 Oct 20;12(10):883.
- 448. Meng X, Liu D, Guan Y. Advances in the application of label-free quantitative proteomics techniques in malignancy research. Biomedical Chromatography. 2023;37(7):e5667.
- 449. Dupree EJ, Jayathirtha M, Yorkey H, Mihasan M, Petre BA, Darie CC. A Critical Review of Bottom-Up Proteomics: The Good, the Bad, and the Future of This Field. Proteomes. 2020 July 6;8(3):14.
- 450. Franco PHC, Zeinert R, Meier-Credo J, Storz G, Langer JD. Detection and quantitation of small proteins using mass spectrometry. Molecular & Cellular Proteomics. 2025 Aug 14;101052.
- 451. Haslam DE, Li J, Dillon ST, Gu X, Cao Y, Zeleznik OA, et al. Stability and reproducibility of proteomic profiles in epidemiological studies: comparing the Olink and SOMAscan platforms. Proteomics. 2022 July;22(13–14):e2100170.
- 452. Norman M, Shami-shah A, D'Amaddio SC, Travis BG, Ter-Ovanesyan D, Dougan TJ, et al. Toward Identification of Markers for Brain-Derived Extracellular Vesicles in Cerebrospinal Fluid: A Large-Scale, Unbiased Analysis Using Proximity Extension Assays. J Extracell Vesicles. 2025 Mar;14(3):e70052.

- 453. Shapiro IE, Bassani-Sternberg M. The impact of immunopeptidomics: From basic research to clinical implementation. Seminars in Immunology. 2023 Mar 1;66:101727.
- 454. Lal S, Carrera D, Phillips JJ, Weiss WA, Raffel C. An oncolytic measles virus-sensitive Group 3 medulloblastoma model in immune-competent mice. Neuro Oncol. 2018 Nov 12;20(12):1606–15.
- 455. Hedberg J, Studebaker A, Smith L, Chen CY, Westfall JJ, Cam M, et al. Oncolytic virus-driven immune remodeling revealed in mouse medulloblastomas at single cell resolution.

 Molecular Therapy Oncolytics. 2023 Sept 21;30:39–55.
- 456. Sherwood M, Mitsugi TG, Kaid C, Coke B, Zatz M, Maringer K, et al. Multi-omics analysis reveals key immunogenic signatures induced by oncolytic Zika virus infection of paediatric brain tumour cells. Sci Rep. 2025 Apr 16;15(1):13090.
- 457. Identification of natural Zika virus peptides presented on the surface of paediatric brain tumour cells by HLA class I | PLOS One [Internet]. [cited 2025 Nov 6]. Available from: https://journals.plos.org/plosone/article?id=10.1371/journal.pone.0335726
- 458. Mitsugi TG, Sherwood M, Jandrey EHF, Assoni AF, Bell J, Coke B, et al. Integrated interactome, proteomic and functional analyses reveal molecular pathways driving L1TD1-induced aggressiveness in CNS embryonal tumor cells. FEBS Letters [Internet]. [cited 2025 Feb 6];n/a(n/a). Available from: https://onlinelibrary.wiley.com/doi/abs/10.1002/1873-3468.70002